Genetic Determinants of Antibiotic Resistance and Susceptibility in Gram-negative Pathogens

By

Ryan David Ward

A dissertation submitted in partial fulfillment of

the requirements for the degree of

Doctor of Philosophy

(Genetics)

at the

UNIVERSITY OF WISCONSIN-MADISON

2024

Date of final oral examination: 12/17/2024

The dissertation is approved by the following members of the Final Oral Committee:

Mark Craven, Professor, Biostatistics and Medical Informatics

Jason Kwan, Associate Professor, Pharmaceutical Sciences

Nicole Perna, Professor, Genetics

Jason Peters, Assistant Professor, Pharmaceutical Sciences

Nathaniel Sharp, Assistant Professor, Genetics

Acknowledgements

I would like to thank my advisor, Dr. Jason Peters, for encouraging intellectual independence and robust scientific discourse throughout my training. His mentorship has been invaluable to my development as a scientist.

I am grateful to my thesis committee members – Dr. Mark Craven, Dr. Jason Kwan, Dr. Nicole Perna, and Dr. Nathaniel Sharp, for their direction.

I am particularly grateful to Dr. Amy Banta, whose mentorship shaped my understanding of bacterial genetics and physiology.

I thank Gerald for his steadfast support and understanding throughout this journey.

I dedicate this thesis to the memory of my mother, whose endless curiosity about the world shaped who I am, and to my father, whose encouragement to persist in her honor made this work possible.

Abstract

Antimicrobial resistance (AMR) in Gram-negative bacteria poses an urgent public health challenge. While traditional approaches have identified essential genes through complete disruption, understanding how partial loss of function affects bacterial survival has remained largely intractable. This thesis applies CRISPR interference (CRISPRi) technology to systematically examine essential gene function in Gram-negative pathogens, focusing on three areas: mapping essential gene vulnerabilities in *Acinetobacter baumannii*, characterizing host-specific essential gene requirements in *Pseudomonas aeruginosa*, and comparing essential gene networks across *Enterobacterales* species.

The systematic analysis identified essential genes and pathways that demonstrate acute sensitivity to knockdown, providing promising therapeutic targets. In *A. baumannii*, this work demonstrated genes and pathways that modulate β-lactam sensitivity, establishing an unexpected link between NADH dehydrogenase activity and polymyxin sensitivity. In *P. aeruginosa*, approaches to overcome infection bottlenecks identified 178 genes with increased vulnerability in the host environment. Comparative analysis of essential gene networks across *Escherichia coli*, *Enterobacter cloacae*, and *Klebsiella pneumoniae* characterized both shared vulnerabilities and species-specific differences in antibiotic response.

These findings challenge binary classifications of gene essentiality and demonstrate that many promising drug targets may have been overlooked by structural approaches like transposon sequencing and gene deletion libraries. By enabling controlled knockdown rather than complete deletion, CRISPRi establishes fundamental patterns of bacterial adaptation and expands opportunities for therapeutic development.

Table of Contents

Table of Figures

Table of Tables

Chapter 1. Introduction

1. Background and Significance

1.1. Public health impact and market failures in combating Gram-negative pathogens

Antimicrobial resistance (AMR) has emerged as a major public health concern, with bacterial AMR directly causing 1.27 million deaths and contributing to 4.95 million deaths globally in 2019 (1). The Gram-negative ESKAPE pathogens (*Enterobacter*, *Klebsiella*, *Acinetobacter*, and *Pseudomonas*) pose particular clinical challenges due to their intrinsically low membrane permeability and multiple resistance mechanisms (2). In the United States, resistant infections add $20 billion in direct healthcare costs and approximately $35 billion in lost productivity annually (3), disproportionately affecting resource-constrained and rural hospitals that struggle to maintain effective infection control programs (4–7).

The economics of antibiotic development has become increasingly unsustainable. Each new antibiotic costs over $1 billion to develop. Yet, annual revenues rarely exceed $100 million (8), due to the restrictive use of novel antibiotics creating an unintended market signals where medically necessary conservation appears as weak demand (9). Traditional small-molecule screening approaches have become stale, with no new antibiotic classes introduced between 1962 and 2000 (10). The cell envelope architecture and resistance mechanisms of Gram-negative bacteria have especially limited drug development progress (11). These pathogens present a particular challenge for traditional drug discovery methods, but functional genomics approaches offer a path to accelerate breakthroughs. High-throughput genetic screens enable systematic identification of both novel antibiotic targets and opportunities for repurposing existing drugs (12), helping to address the unique barriers Gram-negative bacterial physiology poses.

1.2. Genetic foundations for AMR in Gram-negative bacteria

The bacterial cell envelope comprises the outer structures of the cell and serves as the first line of defense against noxious environmental compounds, including antibiotics. Gram-negative bacteria are distinguished from other bacteria by their outer membrane (OM), which provides an additional layer of defense beyond the inner membrane (IM) and thin peptidoglycan cell wall (13). The lipid bilayer of the OM is asymmetrical, containing an inner leaflet of phospholipids on the inside, while the external surface is tightly packed with lipopolysaccharides in most Gram-negatives or lipooligosaccharide in *A. baumannii* (LPS/LOS) (14). The sugar moieties of LPS create a hydrophilic microenvironment on the cell surface that contributes to membrane stability through extensive hydrogen bonding and cation bridging between LPS molecules (15). This organized structure is exceptionally effective at reducing permeability, especially against hydrophobic compounds that can usually diffuse through more typical phospholipid bilayers (16).

This intrinsic impermeability creates a challenge for antibiotic development; while Gram-negative bacteria possess many promising intracellular drug targets [Figure 1], most compounds cannot reach these targets at therapeutically relevant concentrations. The barrier function of the OM is selectively permeable through porins that restrict passage to molecules smaller than approximately 600 Da in *E. coli* (17). This structural constraint leaves a few paths for antibiotic entry. While smaller molecules can pass through porins if they meet the physiochemical criteria for passage, larger antibiotics can either cross the LPS-phospholipid bilayer directly (11) or be transported across the outer membrane (18). For example, while rifampicin effectively inhibits bacterial RNA polymerase in vitro, its large size (822.9 Da) severely limits its utility against Gram-negative pathogens due to poor membrane penetration (19). This limited access to intracellular targets has contributed significantly to the dearth of new

antibiotics effective against Gram-negative infections. The outer membrane itself represents both a barrier and an important antibiotic target.

Figure 1: The Role of Essential Functions in Antibiotics

Major antibiotic classes target essential cellular processes in bacteria (20), including cell wall synthesis (β-lactams, vancomycin), transcription (rifamycins), DNA synthesis (quinolones), protein translation (aminoglycosides, tetracyclines, lincosamides), metabolism (sulfonamides), and outer membrane integrity (polymyxins). The presence of the outer membrane in Gram-negative bacteria creates an additional barrier that many antibiotics must overcome to reach their targets.

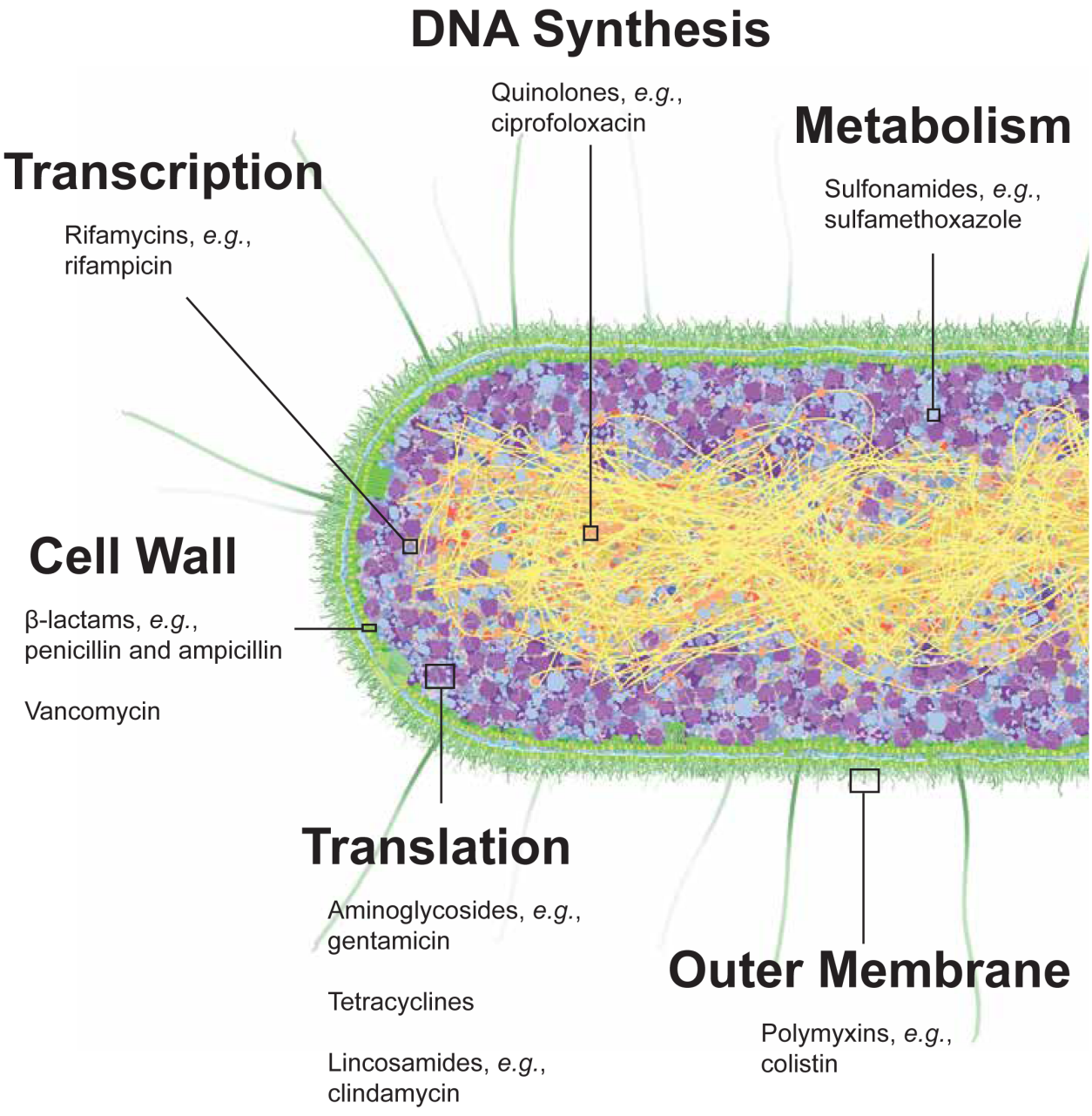

At the core of LPS/LOS structure is lipid A, a conserved phospholipid that anchors LPS/LOS to the outer membrane. The lipid A component usually consists of a *β*-(1→6) glucosamine disaccharide backbone decorated with multiple fatty acid chains and phosphate groups, forming an amphipathic macromolecule contributing to the exceptional outer membrane stability of Gram-negative bacteria (21). The outer membrane provides a protective barrier against toxic compounds and serves as a critical load-bearing component sustaining turgor pressure (22), making this essential structure a vulnerability that certain antibiotics can exploit. Polymyxins (*e.g.,* colistin), take advantage of this vulnerability by directly binding to lipid A, transforming the membrane from a protective barrier into a mechanism for cell death. These "last-resort" antibiotics are thought to kill cells through membrane disruption after binding to lipid A (23). A newly discovered class of antibiotics targets various aspects of outer membrane by trapping LOS in its Lpt membrane transporter (24). However, Gram-negative bacteria can sometimes survive even without these seemingly essential envelope components, as demonstrated by *A. baumannii* strains that strikingly remain viable after complete loss of LOS (25). Though our subsequent work demonstrated that this adaptation comes with significant fitness costs and altered susceptibility to other antibiotics (26).

Bacteria possess intrinsic defense mechanisms beyond membrane barriers, including efflux pumps that actively expel antibiotics from the cell. For example, AbaF in *A. baumannii specifically* contributes to fosfomycin resistance (27). The AcrAB-TolC system in *E. coli*, spanning both inner and outer membranes, expels a wide range of antibiotics and is a key driver of multidrug resistance when upregulated (28). In *P. aeruginosa*, the MexAB-OprM system also expels diverse antibiotics but frequently exhibits increased expression following prolonged antibiotic exposure, further enhancing resistance under stress (29).

Target enzymes can also develop resistance through mutations that prevent antibiotic binding, but these adaptations result in substantial losses in fitness. For example, rifampicin

works by binding to the β-subunit of RNA polymerase, blocking the RNA exit channel and preventing transcript elongation (30). Mutations that alter this binding site confer resistance but create collateral effects – the structural changes that prevent rifampicin binding also alter RNA polymerase's catalytic properties and reduce transcription fidelity (31). These adaptations often have pleiotropic effects beyond the antibiotic target enzyme. In *P. aeruginosa*, RNA polymerase mutations affect metabolic gene expression and alter peptidoglycan precursor levels, leading to unexpected changes in β-lactam susceptibility (*i.e.,* collateral sensitivity (32)) and cell wall function (33). In Gram-positive organisms like MRSA (Methicillin-resistant *Staphylococcus aureus*), low-affinity PBP2a enables continued but compromised cell wall synthesis, where low-affinity PBP2a enables continued but compromised cell wall synthesis (34), these adaptations frequently result in reductions in growth and fitness. These collateral fitness losses help explain why resistant mutations often revert when antibiotics are removed; the metabolic cost of maintaining resistance outweighs its benefit in antibiotic-free environments (35).

In addition to spontaneous adaptations, Gram-negative bacteria frequently use more efficient strategies to acquire resistance. Horizontal gene transfer (HGT) has also transformed environmental bacteria into formidable pathogens (36). Originally an antibiotic-susceptible organism, *A. baumannii* has emerged as a major clinical threat through its exceptional competence to uptake DNA and ability to maintain resistance genes (37). Natural competence enables uptake of resistance islands (*i.e.,* large genomic regions) exceeding 40kb, possessing many resistance genes (38). Mobile genetic elements facilitate the spread of these genes throughout populations (39). One notable example is the acquisition of class D OXA β-lactamases, which spreads on plasmids between strains and has become endemic in healthcare settings (40). Beyond antibiotic resistance, *A. baumannii* possesses persistence traits including desiccation resistance, biofilm formation, and micronutrient acquisition systems (41). This rapid evolution through HGT characterizes Gram-negative ESKAPE pathogens,

where similar mechanisms of DNA uptake, resistance, and persistence have created highly adaptable organisms that present an urgent challenge for antimicrobial therapy.

1.3. Conservation of essential genes and orthology

Essential genes represent the minimal genetic requirements for bacterial survival, forming the foundation of cellular life, and as such make excellent direct targets for antibiotics (42, 43). Strong purifying selection maintains essential gene sequences across bacterial species, even as horizontal gene transfer can rapidly reshape bacterial genomes (44). This evolutionary constraint appears in genes involved in cellular processes where syntenic blocks and sequence homology reflect their essential functions (45, 46). However, this pressure may not be consistent across all essential genes. For example, purifying selection on informational proteins (*i.e.*, involved in transcription, translation, and replication) appears to be influenced by lineage-specific pressures, reducing exchange across species (47). Selection on metabolic proteins appears more uniform, allowing broader functional compatibility, which enables horizontal transfer between bacterial genomes (46).

Sequence-level conservation and protein domain architecture help predict gene function, but predictions become less reliable as evolutionary distance and substitution rates increase between bacterial species and can vary by cellular process (48). Genomic topology also shapes the roles of essential genes in cellular processes by influencing their interactions with other genes (49). Essential genes often co-occur with functionally related genes in operons, either to form proteins for well-defined, static complexes or to participate in linear metabolic and regulatory pathways (50, 51). Comparing genomes as "bags of genes" (52) — measuring shared orthologs—misses important organizational features, particularly co-functional partners that may be distant on the genome or entirely absent in certain species (53). The functional interdependence of these genes, such as their need to form complexes or act sequentially

within pathways, helps explain why certain genes show essential phenotypes that orthology alone cannot predict (51).

2. Methodological Overview

2.1. Approaches to study gene function in bacteria

Antibiotic function relies on targeting essential bacterial genes, but how antibiotics interact with genes remains poorly resolved for many pathogens. Despite exponential growth in genome sequencing since the early 2000s (54), much of the bacterial proteome lacks detailed annotations. In *E. coli* K-12, one of the best-characterized model organisms, functional roles for 20–30% of proteins remain undefined, and annotations often rely on broad, generalized terms like "ATPase" or "transporter" (55, 56). Current annotations of bacterial genes vary widely in their specificity and utility, from broad classifications to more detailed functions (57). Computational approaches using orthology have helped assign these basic functional categories to many genes (58), yet annotations often lack the specificity needed to define their roles in antibiotic resistance and pathogenesis. This challenge is problematic for emerging pathogens, where gene functions may have diverged significantly from well-studied model organisms.

Systematic genetic approaches (*i.e.*, functional genomics) augment computational predictions relying heavily on assumptions and single-gene studies (59). Unlike conventional genetic methods that examine genes individually, functional genomics measures phenotypes of all genes being queried or perturbed under a given condition. This approach moves beyond broad functional classifications to provide direct measurements of gene function in the context of the organism of interest. Because most phenotypes lie on a continuum (*e.g.,* growth rates) rather than existing as a binary, functional genomics captures the full distribution of phenotypic diversity by measuring how each strain responds to different conditions, or in the case of vulnerability studies, by comparing across strains (60). Furthermore, systematic approaches can

reveal emergent properties within cellular systems, especially where unexpected pathways, including complex metabolic processes, may not directly involve specific AMR genes but still contribute to antibiotic resistance in ways not yet fully understood (61). Identifying emergent patterns of gene fitness phenotypes across various conditions also provides stronger evidence for functional relationships between genes than any single phenotype alone (62).

Systematic gene function characterization in bacteria depends on our capacity to link genetic differences to quantifiable phenotypes. Historically, generating null alleles or deleting individual genes has been the basis for functional studies in microbiology (63). Modern molecular genetic tools, such as recombineering systems, ready-to-order oligonucleotides and access to comprehensive genomic data have streamlined the creation of precise genetic mutations in bacteria (64). Building on these gene-by-gene deletion studies, the Keio Collection in *E. coli* K-12 is a landmark example using these approaches, where researchers systematically truncated each non-essential gene and replaced it with a kanamycin resistance cassette (65). However, since each mutation is a constructed through precise molecular steps, scaling this approach even across a relatively small bacterial genome of ~4000 genes is an immense technical undertaking that requires substantial effort and resources to implement systematically (66).

Pooled strategies like transposon sequencing (Tn-seq) address the limitations of scaling single-gene knockouts by enabling genome-wide mutagenesis in a single step (67). In this method, drug resistance cassettes flanked by inverted repeats are cloned alongside a hyperactive transposase into a plasmid and conjugated into a population of cells. The transposase excises the cassette and integrates it randomly throughout the host genome, though with sequence preferences characteristic of each transposase family. This integration disrupts gene function and simultaneously confers antibiotic resistance [Figure 2], allowing only cells containing the randomly inserted marker to survive. The random nature of integration

ensures broad, unbiased genome coverage (68). Since its introduction in 2009, Tn-seq has become the backbone of bacterial high-throughput functional genomics (67). Essential genes are identified by statistical analysis of insertion density across the genome, in which regions with significantly fewer insertions than expected by chance represent genes required for survival under the tested condition (68–70).

Figure 2: Identification of Essential Genes Using Transposon Mutagenesis

Plasmids with Tn*5* expression and a cassette containing an antibiotic resistance marker are introduced into a population of cells. The Tn*5* transposase excises the resistance marker and inserts it into random locations within the host genome, disrupting bacterial genes. Because insertions into essential genes are lethal, such mutants are never recovered. Transformed cells are grown on selective media where only those containing viable insertions survive, allowing essential genes to be identified by their lack of insertions in the surviving population.

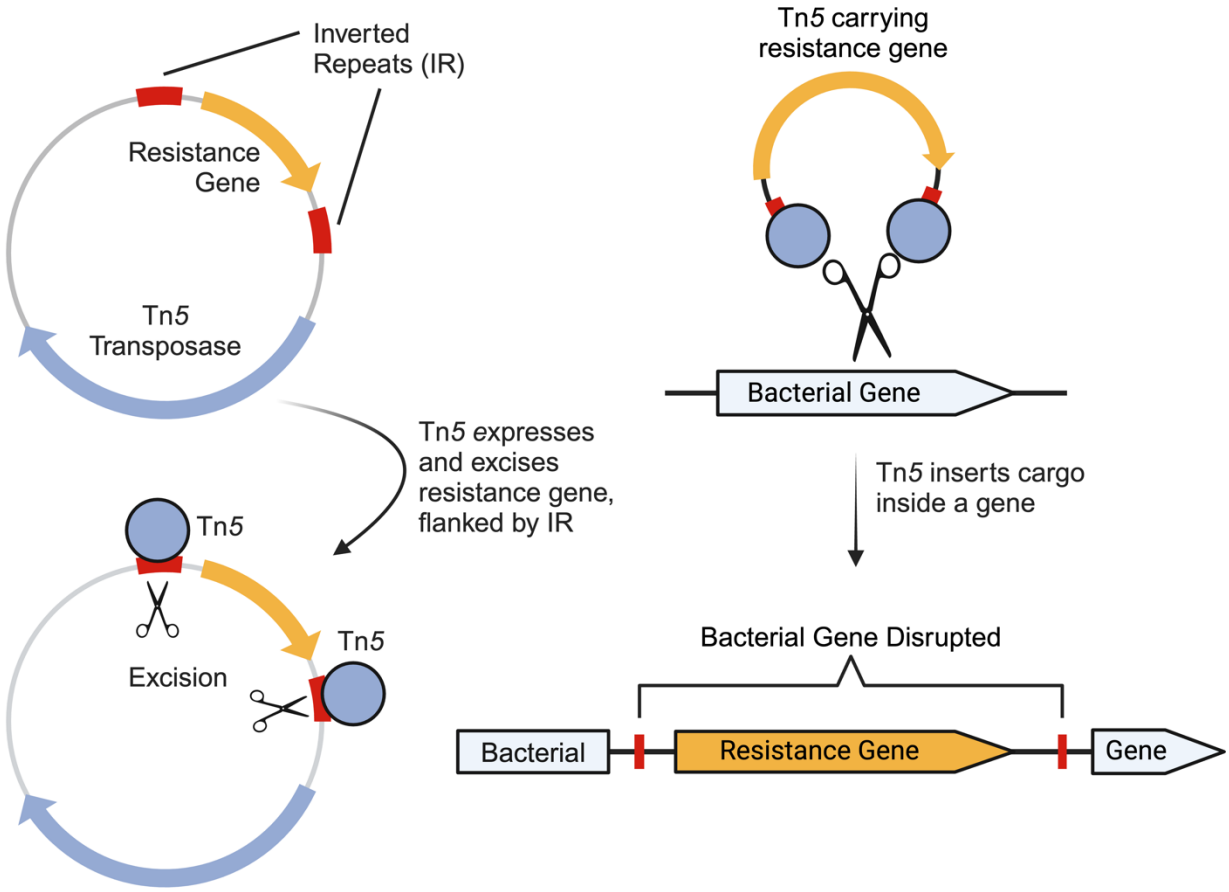

However, Tn-seq has important limitations. Low-density libraries can leave large stretches of DNA without an insert, even when these regions do not contain essential features. More fundamentally, the binary nature of Tn-seq—complete disruption or no effect—hinders its ability to study bacterial physiology. While essential genes can be identified by their absence in Tn-seq datasets, these genes provide no measurable fitness differences between conditions since mutants in these regions are non-viable, with some exceptions (71, 72). Additionally, the permanent nature of transposon insertions prevents analysis of dynamic or condition-dependent phenotypes. Another challenge arises from the strong promoters within transposon resistance cassettes, which can drive expression of downstream genes and complicate experimental interpretation—although this effect has been deliberately exploited to study overexpression phenotypes (73).

CRISPR interference (CRISPRi) addresses these limitations by providing a programmable and scalable approach to gene knockdown rather than knockout. Unlike Tn-seq, which functions as a purely forward genetics tool, CRISPRi allows for targeted (74), tunable (75) suppression of gene expression, making it ideal for studying essential genes and condition-dependent phenotypes. CRISPRi uses a catalytically inactive Cas9 nuclease (dCas9) and a fusion of crRNA and tracrRNA into a single guide RNA (sgRNA) (76) to silence gene expression [Figure 3]. The first 20 nucleotides of the sgRNA, known as the spacer, direct dCas9 to a complementary sequence in target genes (protospacer) with an adjacent PAM (Protospacer Adjacent Motif). Once bound, dCas9 physically blocks either RNA polymerase (RNAP) association with promoter DNA or RNAP elongation throughout the gene body (74), depending on the protospacer location. By offering reversible and gradable control over gene expression, CRISPRi enables nuanced analysis of gene function in ways that Tn-seq cannot.

Figure 3: Mechanism of CRISPRi Gene Knockdown

The catalytically dead Cas9 (dCas9, containing RuvC[D10A] and HNH[H840A] mutations, which jointly confer enzyme inactivation) complexed with a single-guide RNA (sgRNA) binds to complementary DNA sequences containing a PAM (Protospacer Adjacent Motif). When targeted to the non-template strand, the dCas9-sgRNA complex physically impedes RNA polymerase (RNAP) elongation, resulting in transcriptional interference.

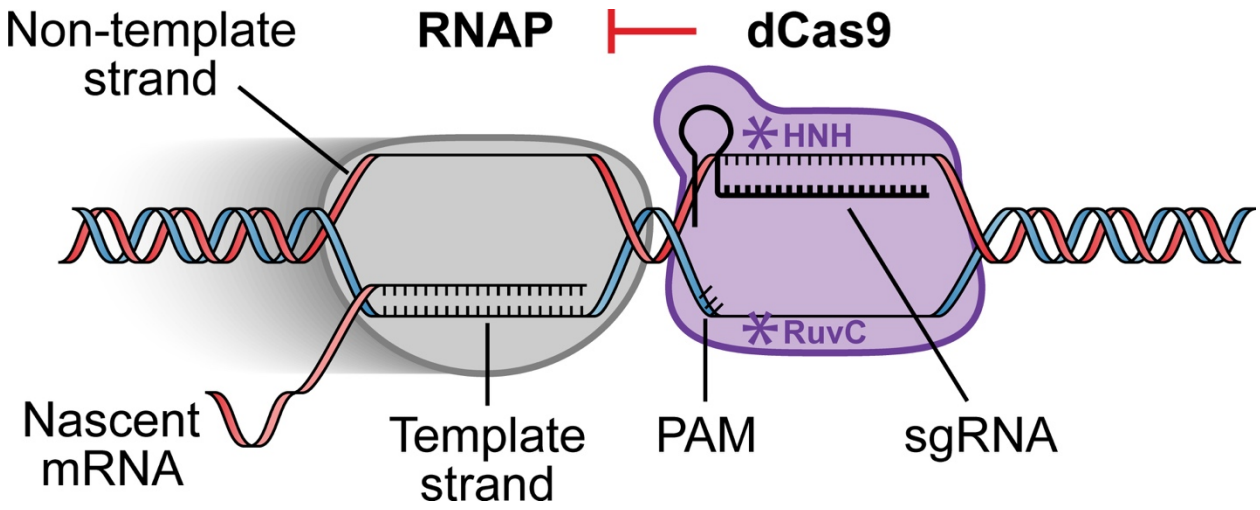

2.2. High-throughput functional genomics

High-throughput functional genomics has revolutionized the study of bacterial genes at scale. Approaches using barcoded libraries—including pooled deletion (77), Tn-seq (68), or CRISPRi, (78) – enable simultaneous measurement of thousands of strains in a single experiment. In contemporary functional genomics libraries, each strain carries a unique DNA identifier, or barcode, which allows systematic tracking of strain abundance in complex populations through genomic DNA sequencing. Barcodes differ depending on the method: deletion junctions in knockout mutants, transposon-genome junctions in Tn-seq libraries, or sgRNA sequences in CRISPRi cassettes. This scalability helps identify genes that are essential or advantageous under specific conditions [Figure 4].

The experimental design considerations for high-throughput screens vary between methods. CRISPRi offers precise control over library composition, allowing researchers to define both the scope (which genes to target) and resolution (how many guides per gene). However, successful CRISPRi screens require an annotated genome for guide design (79), and attention to other technical parameters that affect sensitivity [Table 1]. For instance, antibiotic screens in 384-well plates must balance library diversity against culture volume constraints (i.e., carrying capacity), as both factors affect the detection of drug-gene interactions (80).

Figure 4: Quantitative Fitness Using DNA Barcoding

Genomic DNA is extracted from a pooled population where each strain contains a unique identifying sequence: either an engineered barcode or a strain-specific integration site, such as in Tn-seq. Through amplicon sequencing of these regions, the relative abundance of each strain is measured across n different samples or conditions. This approach is compatible with various genetic perturbation libraries, including gene deletions, CRISPR interference/activation, and randomly generated libraries where the perturbation site itself serves as an identifier. The resulting count matrix enables calculation of both conditional fitness (comparing a strain's abundance across conditions) and relative gene fitness (comparing different strains within a condition). Darker shading in the count summary indicates higher relative abundance of a particular strain.

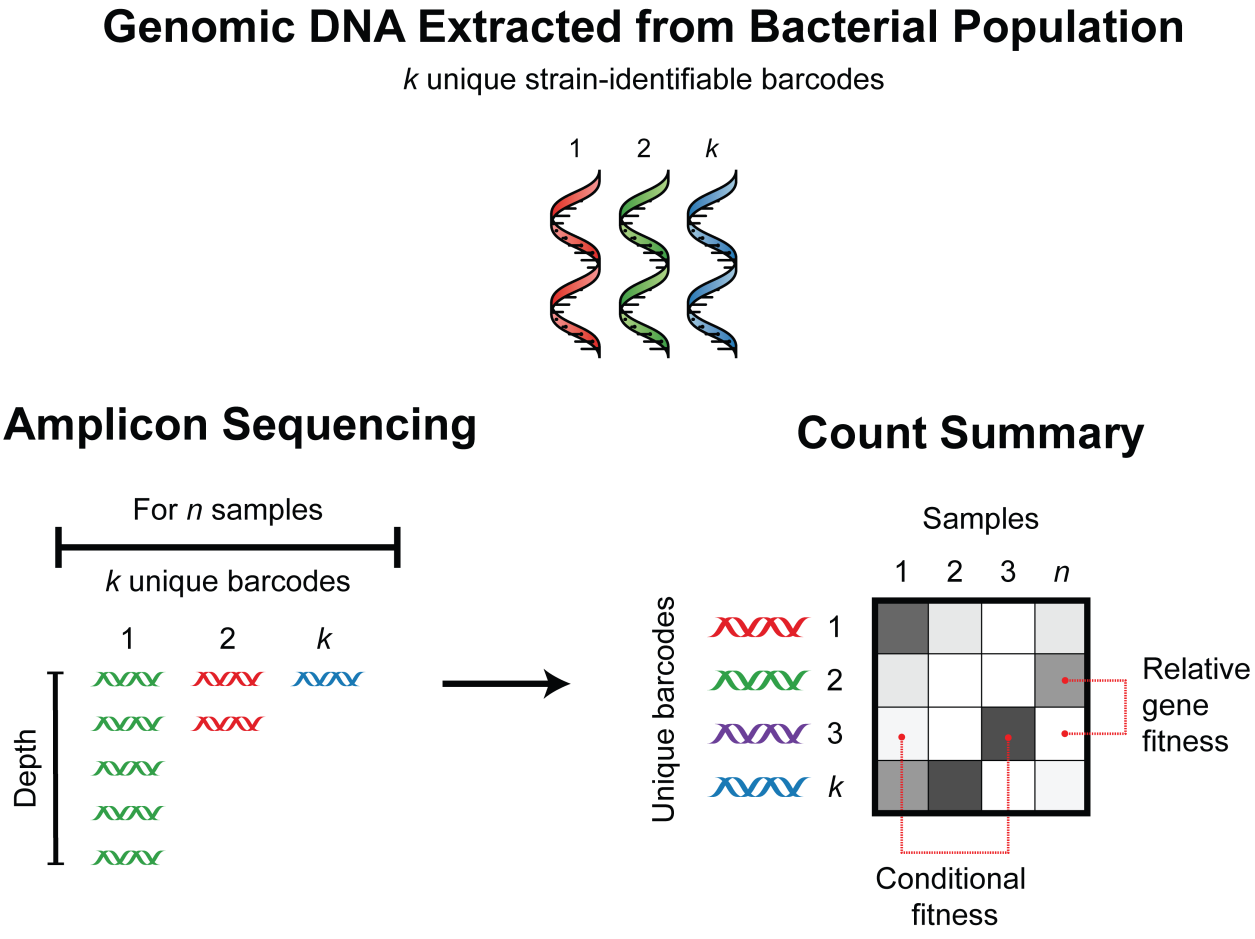

Table 1: Potential Pitfalls in CRISPRi Library Design

Genomic Feature	gRNA Design Challenge	Pitfall Explanation
Genes of unknown function and unannotated regions	Absence of functional annotation hampers gRNA design.	Interference with unknown function genes may yield uninterpretable or misleading phenotypic outcomes (81).
Origin of replication	Targeting *oriC* arrests replication and regulatory protein binding.	Disruption can interfere with the DNA replication, complicating interpretation of the rest of the library (82).
GC content	Regions with extreme GC content can reduce uniqueness and alter binding affinity.	A non-representative GC content can skew binding efficiency, leading to variable knockdown effectiveness or off-target interactions (83).
Regulatory elements (*e.g.,* promoters and terminators)	Regulatory elements can share nucleotide sequences, making them challenging to uniquely target.	Non-specific guide binding or drastic alterations of cellular expression profiles can result in data that is difficult to interpret (84).
Transcription unit	Targeting operons risks polarity (multi-gene perturbation) due to polycistronic mRNA structures.	gRNAs may affect adjacent genes within an operon, making it challenging to ascribe observed effects to the knockdown of a single gene (76).
Overlapping genes	Segments of DNA shared between multiple genes cannot be targeted individually.	Attributing phenotypes to a single gene may not be possible if guides target a common genomic region containing multiple genes (85).
Essential genes	Reduction of expression may be lethal to cells. Sub-maximal knockdown in expression is likely required. (e.g., mismatched guides)	Identifying interactions between gene knockdown and chemical perturbations may not be possible with extreme phenotypic consequences (86).

2.3. CRISPRi technology and application in bacterial genetics research

CRISPRi has become a versatile tool for studying diverse bacterial genomes, for example through Mobile-CRISPRi—a suite of integrating vectors that enables stable chromosomal expression across a wide range of bacterial species (87, 88). Unlike eukaryotic CRISPRi systems that depend on fused silencing domains (89), bacterial implementations achieve robust repression through direct dCas9-sgRNA binding to DNA (74, 87). This mechanism enables targeted genetic analysis but imposes limitations that impact its application. For example, dCas9 binding can block DnaA-mediated DNA unwinding at the origin of replication without generally interfering with DNA replication elsewhere, which doubles as a tool for studying DNA-protein interactions (82). However, transcriptional repression can exhibit polar effects, silencing entire operons (74), and in some bacteria, "reverse polarity" has been observed, where targeting downstream genes reduces upstream expression, with severity varying by species (76, 90–92).

Because CRISPRi works through transcriptional repression rather than DNA disruption, protein levels decrease gradually through dilution during growth (93). In screens, the strength of selective pressure must be carefully tuned – too weak, and subtle phenotypes may be missed – too strong, and only the most extreme outliers will be detected. While inducible promoters provide temporal control over dCas9 expression, constitutive promoters have proven valuable for infection studies where maintaining inducer concentrations is impractical (e.g., due to delivery of inducer inside a host (94)). Additionally, high-level expression of system components can lead to toxicity, either from dCas9 accumulation (95–97) or "bad seed" sgRNAs that broadly off-target multiple genes (91, 98). When targeting essential genes, selective pressure frequently drives suppressor mutations that inactivate the CRISPRi system, enabling escape mutants to outcompete the intended knockdown strain (99).

Mobile-CRISPRi implementations overcome some of these challenges through Tn*7*-mediated site-specific integration downstream of the essential *glmS* gene in Gram-negative bacteria, eliminating the need for antibiotic selection to maintain the CRISPRi system (88). While this strategy is typically benign, it has occasionally been shown to produce organism- and condition-specific effects, such as in *Agrobacterium tumefaciens* (100). For essential genes, additional strategies—such as sgRNA truncations or mismatches—are used to generate predictable reductions in knockdown efficiency [Figure 5], avoiding lethal repression (86, 101, 102). These approaches alongside including non-targeting control guides serve as internal standards, facilitate quantifying strain-level fitness and (86) population-level metrics (*e.g.*, bottlenecks, (103)).

Figure 5: Guide RNA Design Strategies to Tune Knockdown

(A) Perfect match guides bind tightly to the genomic target preventing the initiation or progression of transcription of RNA Polymerase. **(B)** Mismatch guides have intentionally weaker, but predictable binding affinities for their genomic target, stochastically dissociating and occasionally allowing RNA Polymerase to progress resulting in some gene expression. **(C)** Non-targeting guides have no anticipated effect on gene expression.

A. Perfect Match Guide

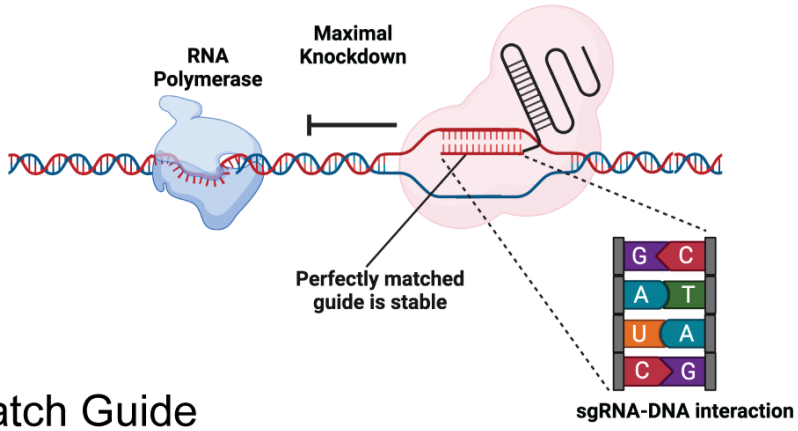

B. Mismatch Guide

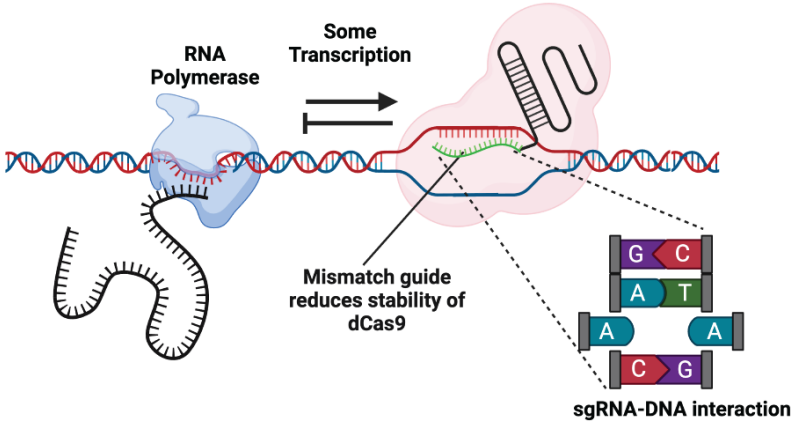

C. Non-targeting Control Guide

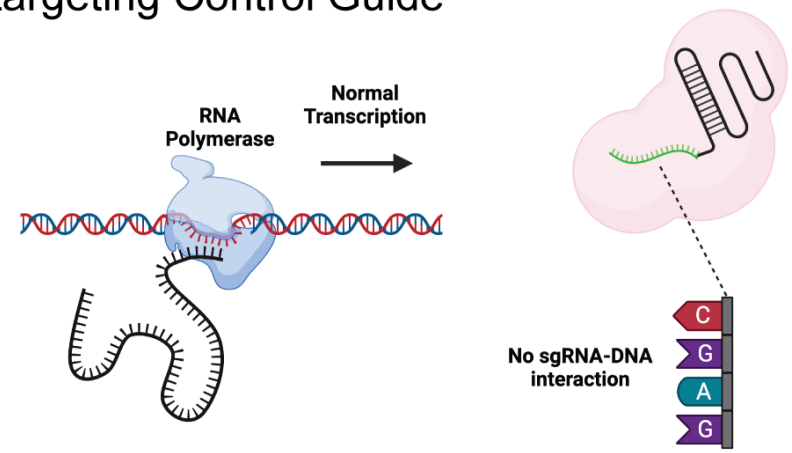

2.4. CRISPRi applications to study AMR in bacteria

Antibiotic resistance demands more effective therapeutic strategies. CRISPRi screens reveal how antibiotics can be optimized through systematic gene perturbation - compounds that hit multiple pathways, like SCH-79797's dual targeting of folate metabolism and membrane integrity, show remarkably low resistance frequencies (104). This principle has guided new therapeutic approaches in *A. baumannii*, where machine learning identified membrane protein inhibitors effective both alone and in combination treatments (105). CRISPRi screening showed these combination effects emerge from specific genetic interactions – strains with reduced expression of an antibiotic's target show severe growth defects, while a second antibiotic can create a synergistic effect when its target lies in the same pathway as the first (106). This genetic interaction principle led to identifying synergistic targets, like the complementary roles of cell wall synthesis and cell division machinery (107). These fitness-based screens provide a systematic foundation for identifying effective drug combinations, even when their precise molecular mechanisms remain unclear.

CRISPRi can aid in identifying antibacterial targets and pathogen vulnerabilities for antibiotic development [Figure 6]. Antibiotics target essential cellular processes, but essential gene function in antibiotic-resistant bacteria remains understudied, limiting drug discovery. These screens are especially useful at defining the cellular roles of essential genes as potential drug targets due to the temporal and titratable components of the system.

Figure 6: Medical Applications of Chemical Genomics with CRISPRi

This schematic illustrates the process of using CRISPRi libraries to identify antimicrobial or toxin targets, revealing chemical-gene fitness patterns through computational analyses. Identified targets, such as gene products or pathways directly inhibited by the antimicrobial, can be used in basic research or further developed for therapeutic or bioproduct applications. Adapted from original artwork by Bill Heelan (93).

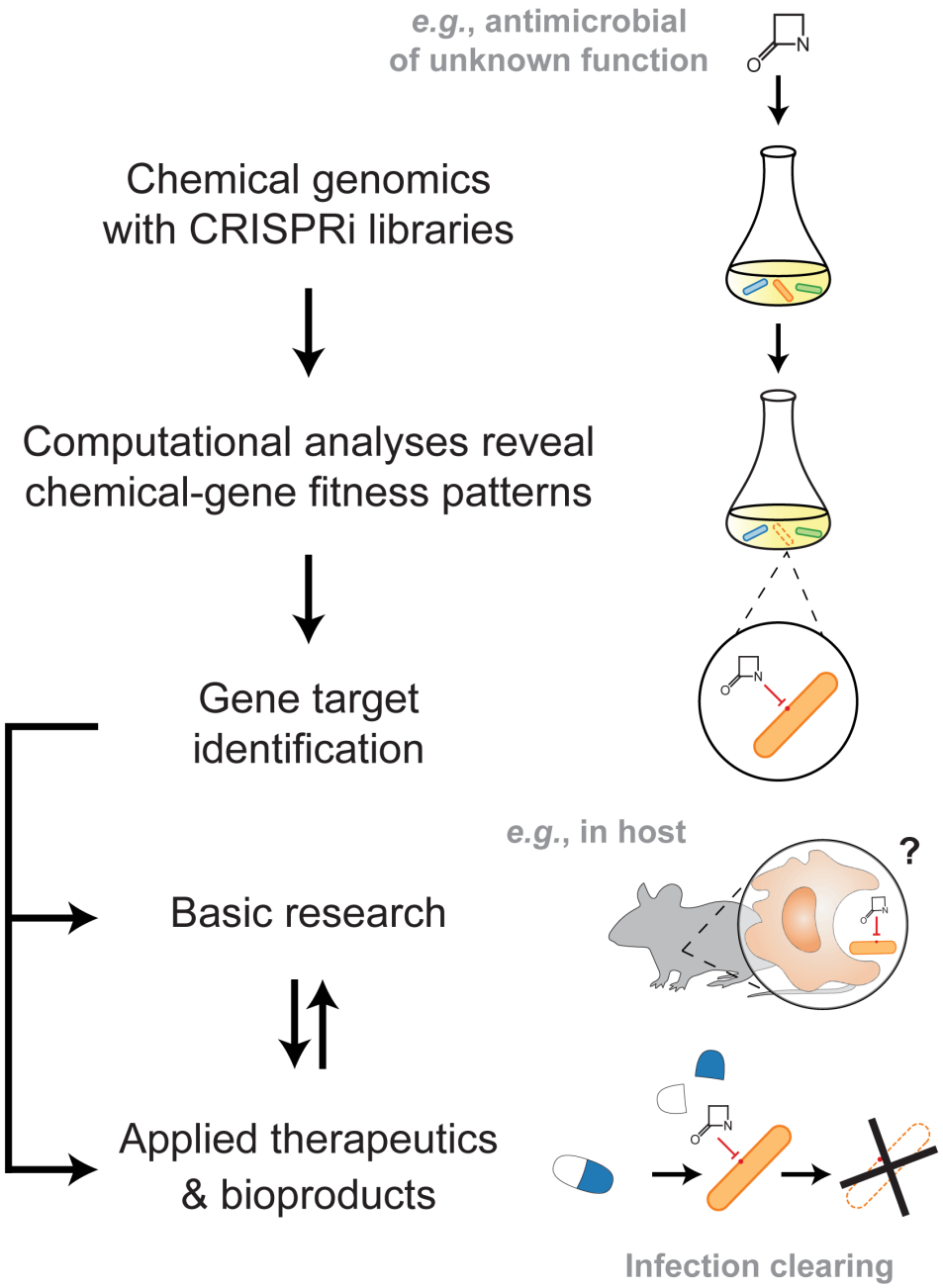

CRISPRi has proven useful to identify vulnerabilities that can be exploited to develop narrow-spectrum antibiotics, which could minimize the widespread killing caused by broad-spectrum drugs that further contribute to AMR (108). For example, in *Streptococcus pneumoniae*, Tn-seq and CRISPRi identified *tarP* and *tarQ* in teichoic acid biosynthesis as potential drug targets (109). In *Acinetobacter baumannii* and *Vibrio cholerae*, CRISPRi screens helped identify weaknesses in processes such as cell division and lipoprotein transport (110, 111). Multiplexed CRISPRi screens have addressed redundant or essential pathways overlooked by traditional knockouts. In *Legionella pneumophila*, repression of effector genes clarified their roles in pathogenesis (112–116). Similarly, genome-wide CRISPRi libraries have identified mechanisms of antibiotic vulnerability and resistance in pathogens like *Mycobacterium tuberculosis*, including cell wall and protein folding pathways as drug targets (60, 117). These results show how CRISPRi can address drug-resistant tuberculosis, where treatment options remain limited (118). Beyond antibiotic resistance, CRISPRi has provided insights into bacterial gene function during infection. In *Pseudomonas aeruginosa* and *Streptococcus pneumoniae*, CRISPRi applied in animal models identified infection-related genes while addressing challenges such as suppressor mutations and bottleneck effects (94, 99, 103, 119).

3. Computational approaches for essential gene analysis

3.1. Comparative functional frameworks for experimental design

Functional genomics screens integrate multiple computational approaches for design and analysis. Hawkins et al. utilized GFP as a species-neutral indicator to quantify gene expression reductions by constructing 30,000 mismatch sgRNAs targeting GFP in *B. subtilis* and *E. coli*. Their approach used FACS and binning to identify sequences with reduced fluorescence and efficacy (86). The identification of consistent guide RNA design rules between organisms separated by over 1.5 billion years of evolution—even before plants and animals split (120)—suggested these principles would extend to pathogenic bacteria. These machine

learning models predict guide RNA efficacy based on sequence features, allowing design of CRISPRi libraries with controlled repression levels, which is required to study essential genes, where complete knockdown causes lethality.

To map essential genes across species, we integrated orthology detection through OrthoFinder (121) with protein interaction networks from STRING-DB (122). This analysis identified both direct sequence conservation and functional pathway conservation, revealing conserved essential gene modules across *A. baumannii* strains 19606, 17978, and AB5075, while extending predictions to *E. cloacae* and *K. pneumoniae*. Anchoring the analysis to experimentally validated essential genes in *E. coli* K-12 strengthened functional assignments for poorly annotated species.

Genomic organization analysis through Mauve alignments identified (123) conserved gene blocks and operons across strains, showing how genomic architecture affects essential gene evolution. This analysis uncovered strain-specific elements like prophages that modulate gene function. For example, synteny analysis revealed the prophage context of GO593_00515, explaining its conditional essentiality. The integration of guide RNA design predictions, orthology mapping, protein networks, and synteny analysis established a framework for both library design and phenotype interpretation.

3.2. Barcode quantification from sequencing data

Quantifying guide RNA barcodes in sequencing data is increasingly complex as library size grows, particularly in mismatch CRISPRi experiments where both perfect matches and mismatches introduce variability in repression levels. Despite its importance, barcode quantification is often oversimplified in published methods. Some approaches rely on aligners like Bowtie2 (103), which are not sensitive to single-nucleotide mismatches, or scripts that have hard-coded junctions or positions (86), making them difficult to reuse between experiments.

Additionally, tools like FASTQC (124), while useful for general quality control (125), fail to assess whether sequencing data sufficiently captures the diversity of the library. Thus, we use heuristic-based approaches (126) to locate barcodes within sequencing reads and ensure library complexity can provide the complexity needed to make meaningful quantifiable inferences in downstream analyses. This method first identifies the offset (o^*), at the position where barcodes most consistently align across reads. This is determined by maximizing the total alignment score:$o^* = \arg\max_o \sum_{i=1}^{n} \mathrm{Valid}(R_i, o) \cdot \mathbb{I}(D > \tau_D)$

where o is a candidate position in the read, $\mathrm{Valid}(R_i, o)$ evaluates whether read R_i contains a valid barcode at position, D is barcode diversity, which is assess as:

$$D = \frac{Unique\ Observed\ Barcodes\ at\ Position\ o^*}{Expected\ Barcodes}$$

where $\mathbb{I}(D > \tau_D)$ evaluates to 1 when τ_D is a threshold that dynamically adjusts based on library size and complexity. If diversity falls below this metric, or if o^* cannot be reliably determined, the dataset is excluded from further analysis.

3.3. Effective population estimates

Population bottlenecks reduce strain diversity and limit the statistical power of functional genomics screens (103, 127). Host immune responses and nutrient limitations create severe population constraints during infection. Even in 2014, bottleneck measurements in *Streptococcus pneumoniae* relied on tracking just three naturally occurring TIGR4 variants (128), while modern pooled screening approaches using thousands of barcoded strains now enable precise measurement of population dynamics during infection (103). To address this, we adapted equations from Krimbas and Tsakas (129), originally developed for estimating effective population size (N_e), and applied the concept of bottleneck size (N_b), as introduced in the Sequence Tag–based Analysis of Microbial Populations (STAMP, (130)).

The non-targeting sgRNA frequency variance ($\hat{F}$) is calculated as:

$$\hat{F} = \frac{1}{k}\sum_{i=1}^{k}\frac{(f_{i,s} - f_{i,0})^2}{f_{i,o}(1 - f_{i,0})}$$

where k is the total number of sgRNAs, $f_{i,o}$ is the frequency of sgRNA i at time 0, and $f_{i,s}$ is the frequency of that sgRNA at timepoint s. Using this variance, we use N_b to estimate N_e as:

$$N_e \approx N_b = \frac{g}{\hat{F} - \frac{1}{S_0} - \frac{1}{S_s}}$$

where g is the average number of generations based on doublings, and S_0 and S_s represent the sample sizes to calculate the sgRNA population composition (130).

Like STAMP, which uses separate molecular barcodes, we utilized 1,000 non-targeting sgRNAs as neutral markers built into the CRISPRi framework itself. These markers provided a baseline for tracking population diversity across timepoints in an experiment, enabling us to monitor and ensure that bottlenecks did not collapse diversity, which would otherwise render targeting sgRNA data unreliable. This approach is particularly useful in host-pathogen studies, where infection dynamics impose severe population constraints. Non-targeting sgRNAs represented the best-case scenario for maintaining strain diversity, allowing us to differentiate true selective pressures from stochastic loss when analyzing fitness effects of guides targeting essential genes.

3.4. Modeling non-linear knockdown-response relationships

Current methods for analyzing essential gene function quantify how bacterial populations change when gene expression is reduced. While RNA-seq analysis tools like edgeR can track the depletion of CRISPRi guide RNAs from a population over time (measuring the rate at which strains expressing specific guides are lost from mixed populations), these linear models fail to

capture non-linear relationships between gene expression and cellular fitness. Studies in *Saccharomyces cerevisiae* demonstrated that each genes exhibit distinct expression-fitness profiles, where some trigger cell death with minimal reduction in expression, yet others maintain cellular function until expression drops below specific thresholds (131). These gene-specific sensitivities and thresholds for inhibition help identify promising antibiotic targets by revealing which genes cannot tolerate even modest reductions in activity.

Essential gene knockdowns often exhibit non-linear phenotypes that cannot be captured by simple models. Hawkins, *et al* (86) designed a massive CRISPRi library of over 300,000 guides targeting GFP in both *B. subtilis* and *E. coli*. By coupling FACS with machine learning, this work established how single-nucleotide sequence variations influenced guide efficacy and provided the first quantitative expression-fitness relationships. Otto, *et al.* (132) employed mismatch CRISPRi in *E. coli* to titrate gene expression, using double-knockdown libraries and RT-qPCR to measure repression levels and fit dose-response curves to quantitatively describe and predict how gene repression differentially impacts the fitness of genes. This approach forms a useful basis for assigning numerical scores to genes that moves beyond the traditional binary classification of "essential". Bosch, *et al.* (60) extended these principles to *M. tuberculosis* and *M. smegmatis*, specifically introducing the term "vulnerability" to describe sigmoidal relationships between gene repression and fitness. This concept, analogous to the enzymological EC_{50}, quantified the effective repression required to achieve a 50-percent change in fitness.

Several gene knockdowns in our antibiotic screens defied standard dose-response modeling, particularly in *A. baumannii* (26). Partial knockdown of *glnS* enhanced bacterial survival up to 4-fold compared to wild-type cells in the presence of imipenem, while knockdown of *nuoB* showed similar enhancement with rifampicin treatment. However, stronger repression of these same genes ultimately killed the cells. These responses differed not only in magnitude

but also changed sign as gene repression increased, exhibiting a biphasic pattern [Figure 7]. Hormetic behavior, where partial gene repression paradoxically increases bacterial fitness in antibiotic conditions, required more sophisticated modeling approaches. We adapted the Brain-Cousens equation, a variation on the logistic model originally developed to describe low-dose stimulation effects in plant herbicide studies (133). By incorporating both stimulatory and inhibitory parameters, this model captures the transition from enhanced growth at low knockdown levels to complete growth inhibition at high knockdown levels, quantified through the hormesis coefficient and EC50-like EK_{50} values (134).

Figure 7: Knockdown-Response Relationships Between Gene Repression and Antibiotic Sensitivity

(**A**) Monophasic response showing continuous fitness decline with increasing knockdown, which fits standard logistic models including the Brain-Cousens Reduced Model. (**B**) Hormetic (biphasic) response where initial gene repression paradoxically increases fitness relative to wild-type before transitioning to declining fitness at higher knockdown levels. Model selection between monotonic and hormetic fits relies on likelihood ratio testing, which accounts for the additional hormesis parameter against the loss of a degree of freedom.

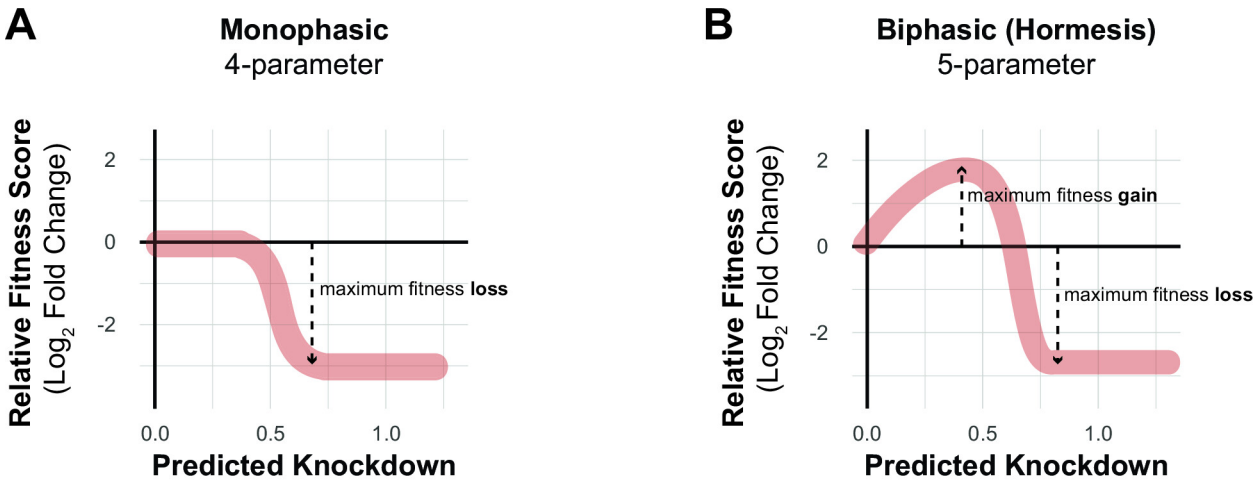

To model this behavior, we use both a full Brain-Cousens model (BC-full), which includes the hormesis parameter (f), and a "reduced" logistic model (BC-reduced), which simplifies the curve by excluding f. The general Brain-Cousens equation is given by:

$$f(x, b, d, e, f) = c + \frac{d - c + f \cdot x}{1 + \exp(\mathrm{b} \cdot \log(x) - \log(e))}$$

Here, x is the dose (*i.e.*, independent variable), b is the slope inflection point, c is lower asymptote (*i.e.*, lowest fitness), d is the upper asymptote (*i.e.*, highest fitness), e is ek_{50} (*i.e.*, half-maximal fitness response to gene knockdown), and f is the hormesis term. Genes were classified as exhibiting hormetic behavior if the BC-full model provided a significantly better fit than the BC-reduced model, as determined by a likelihood ratio test ($p_{LRT} \leq 0.05$) (135). This framework provides a systematic approach for quantifying non-linear dose-response relationships during essential gene knockdowns while being treated with antibiotics.

4. Research Gaps and Objectives

4.1. Thesis Objectives

A fundamental challenge in bacterial genetics has been studying essential genes - those absolutely required for bacterial survival. While transposon sequencing can identify essential genes through regions that cannot tolerate disruption (67–70), understanding how partial loss of essential gene function affects bacterial survival has remained largely intractable. The development of CRISPRi technology represented a breakthrough by enabling controlled reduction of essential gene expression without causing cell death (74, 76). This thesis applies and extends CRISPRi technology to systematically examine essential gene function in Gram-negative pathogens, an approach few laboratories have successfully implemented. The work specifically aims to:

1. Map essential gene vulnerabilities in *A. baumannii* using a tunable CRISPRi system, with special emphasis on genes that alter susceptibility to last-resort antibiotics like carbapenems and polymyxins.

2. Characterize how essential gene requirements change in *P. aeruginosa* during host infection while overcoming traditional bottleneck limitations that have hindered in vivo study.

3. Compare essential gene networks across *Enterobacterales* to identify both shared vulnerabilities and species-specific differences that could inform therapeutic strategies.

This research directly addresses technical limitations that have hindered essential gene study in pathogens. By enabling controlled knockdown rather than complete deletion, CRISPRi allows examination of genes where null mutations are lethal (88). The comparative approach across species reveals how essential pathways have evolved in different bacterial lineages.

4.2. Hypothesis and Research Questions

We hypothesize that essential genes differ in their sensitivity to partial depletion, and that identifying these "vulnerable" genes through CRISPRi will reveal promising therapeutic targets. Further, we predict that comparing depletion phenotypes across multiple pathogens will uncover both conserved vulnerabilities that could serve as broad-spectrum targets and species-specific sensitivities that explain differences in antibiotic susceptibility.

To test these hypotheses, we address several key questions: First, we examine which essential genes show heightened sensitivity to partial knockdown, as these may represent the most promising therapeutic targets. Second, we investigate how the host environment reshapes essential gene requirements during infection, as in vitro studies may miss critical vulnerabilities. Third, we explore how genetic factors enhance or suppress antibiotic activity across bacterial species, potentially revealing new combination therapy strategies. Finally, we assess whether species-specific differences in essential gene networks can explain variations in antibiotic susceptibility, providing insight into why certain species show intrinsic resistance to specific drug classes.

4.3. Subsequent Chapters

This thesis presents three major studies that systematically address these questions. Chapter 2 describes our CRISPRi library targeting 400 essential genes in *A. baumannii*. Our screens linked NADH dehydrogenase activity to polymyxin tolerance and mapped how essential gene knockdown reshapes antibiotic susceptibility. We found an unexpected pattern where moderate repression of certain genes increased antibiotic resistance while complete repression killed cells - the first demonstration of hormesis in this context.

Chapter 3 tackles the technical challenge of studying essential genes during infection. By engineering a *P. aeruginosa* CRISPRi library with 1,000 control guides, we developed tools

to track library bottlenecks during lung infection. The screens revealed metabolic and envelope maintenance genes required specifically in the host environment. Two hits stood out: knockdown of *ispD* or *pgsA* crippled virulence despite minimal effects on growth in culture, validating our approach for finding infection-specific vulnerabilities.

Chapter 4 compares essential gene networks across three *Enterobacterales* species: *E. coli*, *E. cloacae*, and *K. pneumoniae*. While some pathways like cell envelope synthesis showed similar phenotypes, others varied dramatically between species. The Tol-Pal system exemplified this variation – essential in *E. coli* but dispensable in *K. pneumoniae* during carbapenem treatment. Such species-specific differences highlight a key barrier to broad-spectrum drug development.

Chapter 5 outlines key future directions building on the discoveries from our *Enterobacterales* screens. We propose detailed studies of the RNA chaperone *proQ*, whose knockdown dramatically altered antibiotic sensitivity in species-specific ways. To connect our experimental findings to clinical relevance, we will analyze bacterial genome databases like PATRIC and BacWGSTdb, searching for natural variants that mirror the hypomorphic phenotypes we generated through CRISPRi. This database mining will determine whether similar mutations emerge under antibiotic pressure in clinical settings. We also describe planned mechanistic studies of essential genes showing species-specific phenotypes, focusing on how bacteria maintain critical cellular processes when these genes are perturbed. These follow-up experiments aim to define the molecular basis for the varying antibiotic responses we observed between related bacterial species. Finally, we discuss broader applications of our CRISPRi screening approach for studying essential gene networks in other bacterial pathogens.

Chapter 2. Essential Gene Knockdowns Reveal Genetic Vulnerabilities and Antibiotic Sensitivities in *Acinetobacter baumannii*

A version of this chapter has been published (26).

1. Authors

Ryan D. Ward, Jennifer S. Tran, Amy B. Banta, Emily E. Bacon, Warren E. Rose, and

Jason M. Peters

2. Contributions

RDW conducted orthology-based gene selection analyses, developed quantitative frameworks for strain abundance measurements, fitness calculations, pathway enrichment, and drug-gene interaction modeling. RDW executed synergy experiments, selected candidate genes for validation, and generated data visualizations, excluding prophage and membrane analyses.

JST established Mobile-CRISPRi protocols in *A. baumannii*, characterized prophage regulation through growth and expression studies, measured NAD+/NADH ratios, and prepared associated figures.

ABB generated the CRISPRi strain library and performed competition-based fitness measurements and minimum inhibitory concentration determinations.

JMP characterized the novel dCas9 promoter sequence, conducted membrane potential analyses, and prepared the manuscript.

3. Abstract

The emergence of multidrug-resistant Gram-negative bacteria underscores the need to define genetic vulnerabilities that can be therapeutically exploited. The Gram-negative pathogen, *Acinetobacter baumannii*, is considered an urgent threat due to its propensity to evade antibiotic treatments. Essential cellular processes are the target of existing antibiotics and a likely source of new vulnerabilities. Although *A. baumannii* essential genes have been identified by transposon sequencing (Tn-seq), they have not been prioritized by sensitivity to knockdown or antibiotics. Here, we take a systems biology approach to comprehensively characterize *A. baumannii* essential genes using CRISPR interference (CRISPRi). We show that certain essential genes and pathways are acutely sensitive to knockdown, providing a set of vulnerable targets for future therapeutic investigation. Screening our CRISPRi library against last-resort antibiotics uncovered genes and pathways that modulate β-lactam sensitivity, an unexpected link between NADH dehydrogenase activity and growth inhibition by polymyxins, and anticorrelated phenotypes that may explain synergy between polymyxins and rifamycins. Our study demonstrates the power of systematic genetic approaches to identify vulnerabilities in Gram-negative pathogens and uncovers antibiotic-essential gene interactions that better inform combination therapies.

4. Importance

Acinetobacter baumannii is a hospital-acquired pathogen that is resistant to many common antibiotic treatments. To combat resistant *A. baumannii* infections, we need to identify promising therapeutic targets and effective antibiotic combinations. In this study, we comprehensively characterize the genes and pathways that are critical for *A. baumannii* viability. We show that genes involved in aerobic metabolism are central to *A. baumannii* physiology and may represent appealing drug targets. We also find antibiotic-gene interactions that may impact the efficacy of carbapenems, rifamycins, and polymyxins, providing a new window into how

these antibiotics function in mono- and combination therapies. Our studies offer a useful approach for characterizing interactions between drugs and essential genes in pathogens to inform future therapies.

5. Introduction

The rise of antibiotic resistance in Gram-negative pathogens, including *Acinetobacter baumannii*, is a pressing healthcare concern, as many infections become untreatable amid a stalled pipeline for novel therapies (136). *A. baumannii* causes serious infections in hospitalized patients and is considered an urgent threat for its ability to evade killing by last-resort antibiotics (137). It has numerous defenses against antibiotics including a propensity to acquire resistance genes through horizontal transfer (138, 139), low membrane permeability coupled with robust efflux to prevent antibiotics from reaching their cytoplasmic targets (37), and rapid accumulation of resistance mutations (140). Although its unique strengths in resisting antibiotics are well documented, less is known about whether *A. baumannii* carries any unique vulnerabilities that could be therapeutically exploited.

The distinct physiology of *A. baumannii* sets it apart from well-studied, Gram-negative bacteria. Among the Gram-negative ESKAPE pathogens (*i.e., Klebsiella*, *Acinetobacter*, *Pseudomonas*, and *Enterobacter*), *A. baumannii* is the only obligate aerobe, requiring oxidative phosphorylation to generate ATP (141). Further, the outer membrane of *A. baumannii* contains lipooligosaccharide (LOS) rather than lipopolysaccharide (LPS) found in most Gram-negative bacteria (25). LOS and LPS both contain a core lipid A moiety, but LOS lacks the repeating units of O-polysaccharide found in LPS (25). Although LPS is essential for viability in other Gram-negative ESKAPE pathogens, a recent study showed that LOS was dispensable in ~60% of *A. baumannii* strains tested, including contemporary clinical isolates (142). LOS^- strains cannot be targeted by lipid A-binding antibiotics, such as polymyxins, increasing the antibiotic resistance threat posed by *A. baumannii* (143). Finally, *A. baumannii* has numerous genes of

unknown function, including essential genes that are not present in model Gram-negatives or other ESKAPE pathogens (110). These distinctions underscore the importance of examining essential gene phenotypes and antibiotic interactions directly in *A. baumannii*.

Systematic genetic studies of *Acinetobacter* species have provided valuable physiological insights, although *A. baumannii* essential genes have not been comprehensively characterized. Tn-seq studies in *A. baumannii* identified putative essential genes (110, 144), defined phenotypes for previously uncharacterized genes (107), and uncovered the mechanism for strain-specific essentiality of LOS biosynthesis (142). An elegant Tn-seq study of non-pathogenic *Acinetobacter baylyi* monitored depletion of strains with disrupted essential genes following natural transformation (71), but it remains unclear whether those findings are directly applicable to *A. baumannii*.

CRISPR interference (CRISPRi) is the premier genetic tool to define essential gene function and antibiotic-gene interactions in bacteria. This gene knockdown technology uses a programmable, single guide RNA (sgRNA) to direct a catalytically inactive Cas effector protein (typically dCas9) to a target gene for silencing (74, 145). CRISPRi partial knockdowns enable phenotyping of essential genes either by titrating the levels of CRISPRi components using inducible or weak promoters (74, 76, 94), or by modifying the sgRNA to weaken its interaction with target DNA (86, 101, 102) or dCas9 (146). Due to its portability, CRISPRi has proven valuable for phenotyping essential genes in diverse bacteria, including ESKAPE and other pathogens (88, 90, 110). Antibiotic-gene interaction screens using CRISPRi often recover the direct antibiotic target or related pathways among the largest outliers (76, 118). For instance, we previously identified the direct targets of two uncharacterized antibiotics using a *Bacillus subtilis* essential gene CRISPRi library, followed by genetic and biochemical validation of top hits (76). Although CRISPRi has been previously developed in *A. baumannii* by us and others (88, 110), only a handful of essential genes have been phenotyped to date. To systematically probe for

genetic vulnerabilities in *A. baumannii*, we generated and screened a pooled CRISPRi library targeting all putative essential genes [Figure 8A]. We identified essential genes and pathways that are most sensitive to knockdown, thereby prioritizing targets for future drug screens. We further used CRISPRi to define genetic interactions with last-resort antibiotics, finding antibiotic target pathways, obstacles to drug efficacy, and antibiotic-gene phenotypes that that inform synergistic drug combinations.

Figure 8: CRISPRi Screening Overview in *A. baumannii*

(**A**) Design and construction of a Mobile-CRISPRi library targeting all putative essential genes in *A. baumannii* 19606. The library was screened with CRISPRi inducer (1 mM IPTG) to identify genes that are vulnerable to knockdown or with inducer and a sub-MIC concentration of antibiotic to identify antibiotic-gene interactions. (**B-C**) Density plot showing depletion of essential gene targeting sgRNA spacers (perfect match or mismatch) from the library but not depletion of non-targeting control sgRNAs during growth over two time points (T_1 and T_2) (**D**) The population diversity (N_b) of essential gene targeting sgRNAs is reduced relative to controls, indicating that those sgRNAs are depleted during growth. The white horizontal line through the bars indicates a break in the data.

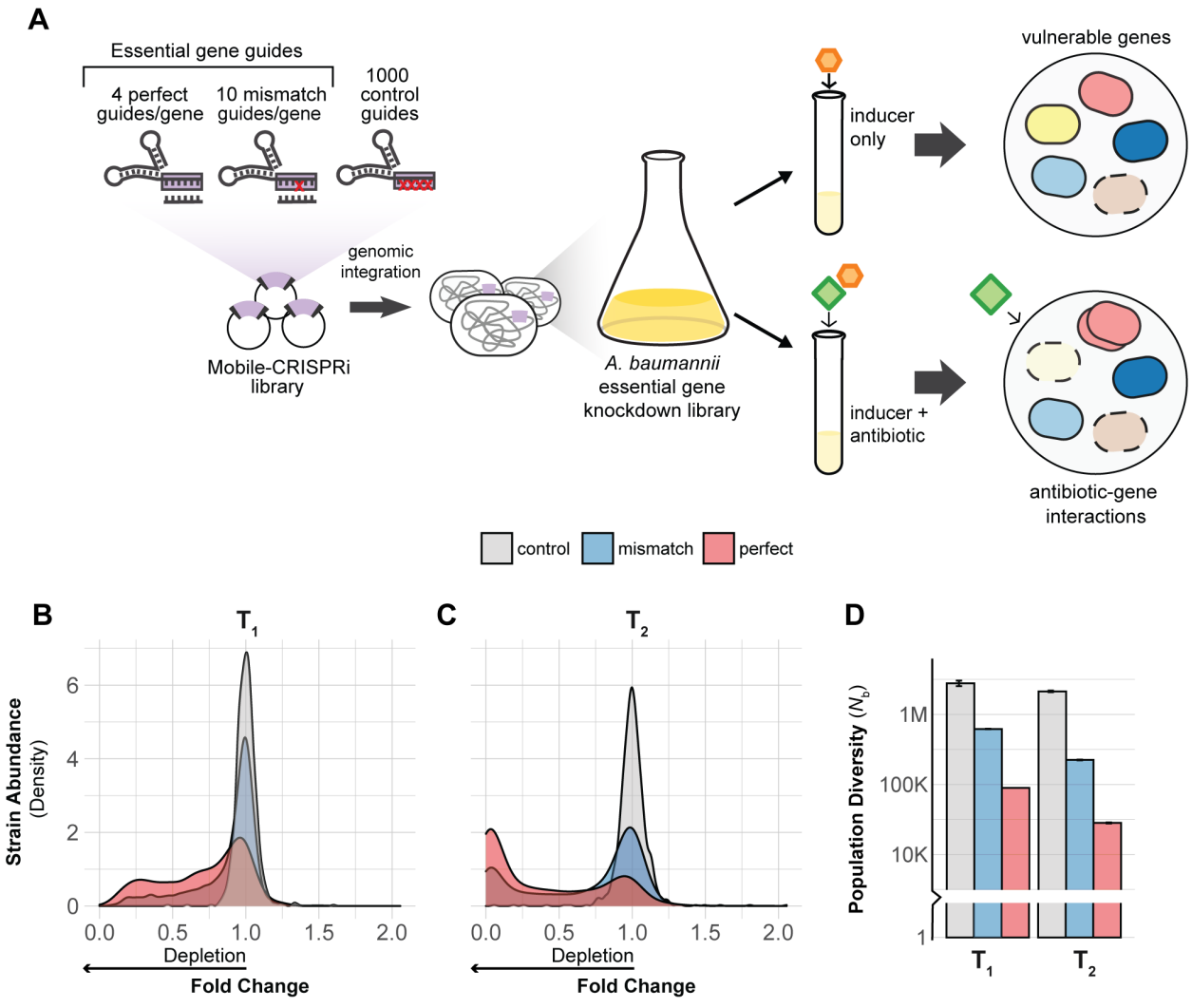

6. Results

6.1. Construction and validation of an *A. baumannii* essential gene CRISPRi library.

We constructed a CRISPRi library targeting all putative essential genes in *A. baumannii* 19606, a strain extensively used to characterize the fundamental biology of *A. baumannii* that is also the type strain for antibiotic susceptibility testing (147). Notably, this strain is viable without LOS (142), allowing us to examine the phenotypic consequences of LOS loss. Developing our library in a susceptible strain made it straightforward to use antibiotics as probes for gene function.

To systematically investigate essential genes, we first optimized CRISPRi in *A. baumannii*, finding that reduced expression of *dcas9* lowered toxicity and still achieved ~20-fold knockdown (Supplementary Methods, [Figure 9A-E, and Tables S1-4]). We next designed and constructed a CRISPRi library targeting all putative essential genes in *A. baumannii*. As the goal of our study was to characterize rather than define essential genes, we used existing Tn-seq data (144) to generate a list of CRISPRi targets we call the "*Ab* essentials" (406 orthologous essential genes total in 19606, [Table 2]). We designed a computationally optimized CRISPRi library targeting the *Ab* essentials that consisted of three types of sgRNAs: 1) perfect match sgRNAs (74) to maximize knockdown (~4/gene), 2) single-base mismatch sgRNAs (86) to create a gradient of partial gene knockdowns (~10/gene), and 3) control sgRNAs that are non-targeting (1000 total). This library was cloned and site-specifically integrated into the 19606 genome using Mobile-CRISPRi [Figure 8A] (88). Illumina sequencing of integrated sgRNA spacers confirmed that our CRISPRi library successfully targeted all the *Ab* essentials (median = 14 guides/gene; [Figure 10A]). Our approach, which includes using multiple sgRNAs per gene and robust statistics, mitigates potential issues with toxic or inactive guides.

Figure 9: Optimization and Characterization of an *A. baumannii* Mobile-CRISPRi System

(**A**) PCR confirmation that Mobile-CRISPRi (MCi) inserted downstream of the *glmS* gene as expected in *A. baumannii*. (**B**) Expression of dCas9 from the $P_{LlacO-1}$ promoter is toxic in *A. baumannii* 19606 (Parent (+*mrfp* guide)), but suppressors can readily be obtained that reduce toxicity (Suppressor (red) and Suppressor (white)). White colony suppressors have reduced toxicity of *dcas9* expression but are still capable of targeting a chromosomal copy of the gene encoding Red Fluorescent Protein (*mrfp*). (**C**) RFP fluorescence of parent ($P_{LlacO-1}$-*dcas9*) and suppressor colonies. Each point is a distinct, single colony. Parent strains likely show intermediate levels of RFP due to the toxic effects of dCas9 expression from $P_{LlacO-1}$. (**D**) White colony suppressors contain a mutation in $P_{LlacO-1}$ that likely reduces its activity; this mutation likely arose from collapse of identical *lac* operator sequences. (**E**) Knockdown quantification of a CRISPRi system that expresses dCas9 from the white suppressor promoter at varying concentrations of inducer (IPTG).

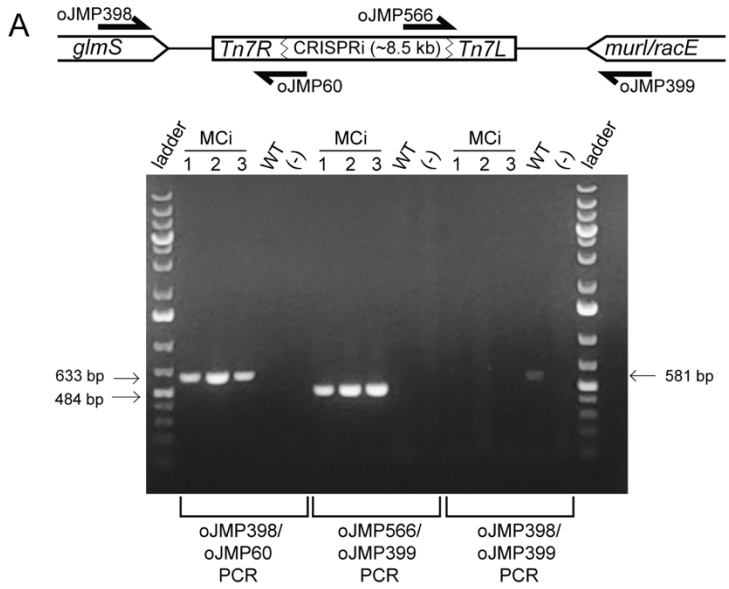
A
oJMP398
oJMP566
glmS
Tn7R
CRISPRi (~8.5 kb)
Tn7L
murI/racE
oJMP60
oJMP399
ladder
MCi
1 2 3
WT
(-)
633 bp
484 bp
581 bp
oJMP398/
oJMP60
PCR
oJMP566/
oJMP399
PCR
oJMP398/
oJMP399
PCR

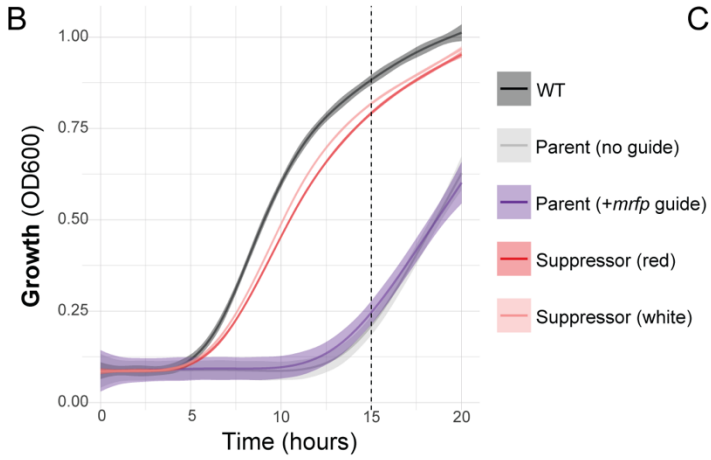
B
Growth (OD600)
Time (hours)
WT
Parent (no guide)
Parent (+mrfp guide)
Suppressor (red)
Suppressor (white)

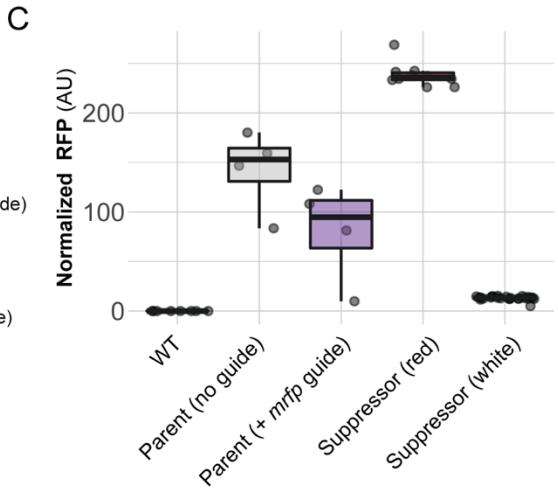
C
Normalized RFP (AU)
WT
Parent (no guide)
Parent (+ mrfp guide)
Suppressor (red)
Suppressor (white)

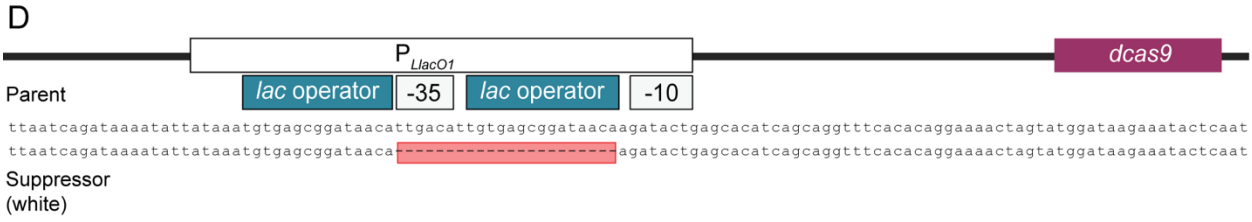
D
P LlacO1
dcas9
Parent
lac operator
-35
lac operator
-10
ttaatcagataaaatattataaatgtgagcggataacattgacattgtgagcggataacaagatactgagcacatcagcaggtttcacacaggaaaactagtatggataagaaatactcaat
ttaatcagataaaatattataaatgtgagcggataaca----------agatactgagcacatcagcaggtttcacacaggaaaactagtatggataagaaatactcaat
Suppressor
(white)

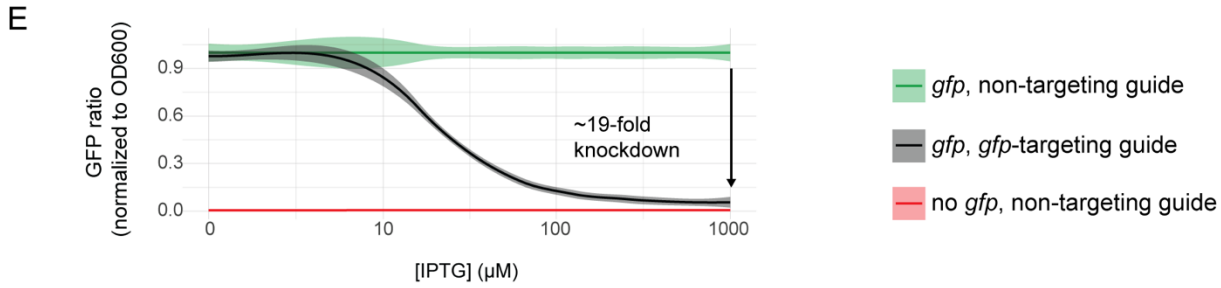
E
GFP ratio
(normalized to OD600)
~19-fold
knockdown
[IPTG] (μM)
gfp, non-targeting guide
gfp, gfp-targeting guide
no gfp, non-targeting guide

Figure 10: Quality Control for The *A. baumannii* Essential Gene CRISPRi Library

(**A**) Histogram of guides/gene in the library. Nearly all genes had 14 guides and the smallest number of guides per gene was 11. Libraries shown here were grown with IPTG to two separate time points (see Methods) and sgRNA spacer depletion was quantified at each time point. Of the 7 genes with less than 14 recovered guides, 4 genes had only 13 (N=3) or 12 (N=1) guides in our initial library design. The other 3 genes likely lost a targeting guide during the library cloning or mating procedures. (**B**) Biological replicates of CRISPRi library experiments showed excellent reproducibility.

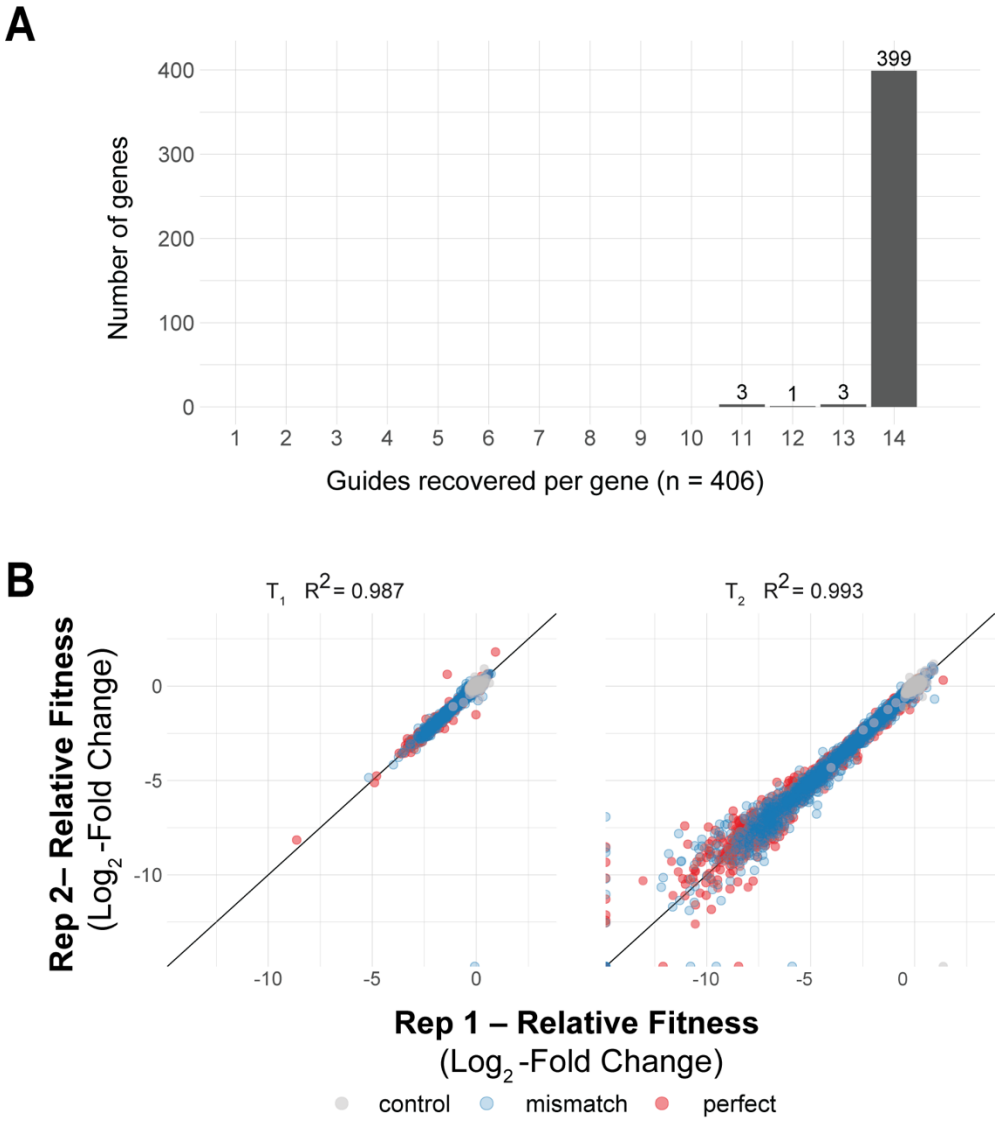

To validate our *A. baumannii* CRISPRi library, we measured the depletion of essential-gene-targeting sgRNAs during pooled growth. We grew the library to exponential phase in rich medium (LB) without induction (T_0), diluted back into fresh medium with saturating IPTG to induce CRISPRi and grew cells for ~7 doublings (T_1), then diluted back a second time in IPTG-containing medium and grew cells for an additional ~7 doublings (T_2). Quantifying strain depletion using $\log_2$ fold change ($\log_2$FC) and population diversity (N_b; (148)) between T_0, T_1, and T_2 ([Figure 8B-D, Figure 10B], [Table 2]) revealed noticeable depletion of essential-gene-targeting sgRNAs by T_1 and substantial depletion by T_2, while control sgRNAs were unaffected. The lack of an induction effect on control strain abundance suggests that toxic guide RNAs such as “bad seeds” (91) are largely absent from our library. Taken together, our CRISPRi library effectively and comprehensively perturbs essential gene functions in *A. baumannii*.

6.2. Identifying *A. baumannii* essential genes and pathways that are sensitive to knockdown.

Essential genes with a strong, negative impact on fitness when knocked down, *i.e.,* “vulnerable" genes, are potential high-value targets for antibiotic development. CRISPRi enables the identification of vulnerable genes by controlling the duration and extent of knockdown (86, 101). To define a set of vulnerable genes, we first quantified depletion of strains containing perfect match guides from the CRISPRi library during growth in rich medium (LB) [Figure 11]. At T_1, 88 genes showed significant depletion ($\log_2$FC<-1 and Stouffer's p<0.05), and by T_2 an additional 192 genes were depleted (280/406 total or 69%; Table 2). Screening our library in antibiotics at sub-MIC (minimal inhibitory concentration) levels recovered phenotypes for 74 for the 126 genes that were non-responsive in rich medium (see below), suggesting that these genes could be involved in antibiotic mode of action [Figure 11B]. The remaining 52 genes that were non-responsive in all our conditions may require additional depletion (86), are false positives from the Tn-seq analysis used to define the *Ab* essentials (144), or are not

essential in 19606. Overall, most *Ab* essentials (354/406 or 87%) showed significant phenotypes in our CRISPRi screens.

Figure 11: Gene-Level Depletion from the CRISPRi Library Under Various Growth Conditions

(**A**) Sankey plot of gene depletion at two time points. Genes are considered vulnerable to knockdown if they were depleted by 2-fold with a Stouffer's *p* value of 0.05 at the time point indicated relative to T_0. (**B**) Sankey plot of gene depletion across any of the conditions assayed in our experiments (IPTG alone, IMI, MER, COL, RIF). Genes are considered responsive if they were depleted by 2-fold with a Stouffer's *p* value of 0.05 at the time point indicated relative to T_0. (**C**) Growth, measured by OD600, over 18 hours for a non-targeting control strain, *lpxC* knockdown strain, and *nuoH* knockdown strain in LB (uninduced, left) or LB with inducer (1 mM IPTG, right).

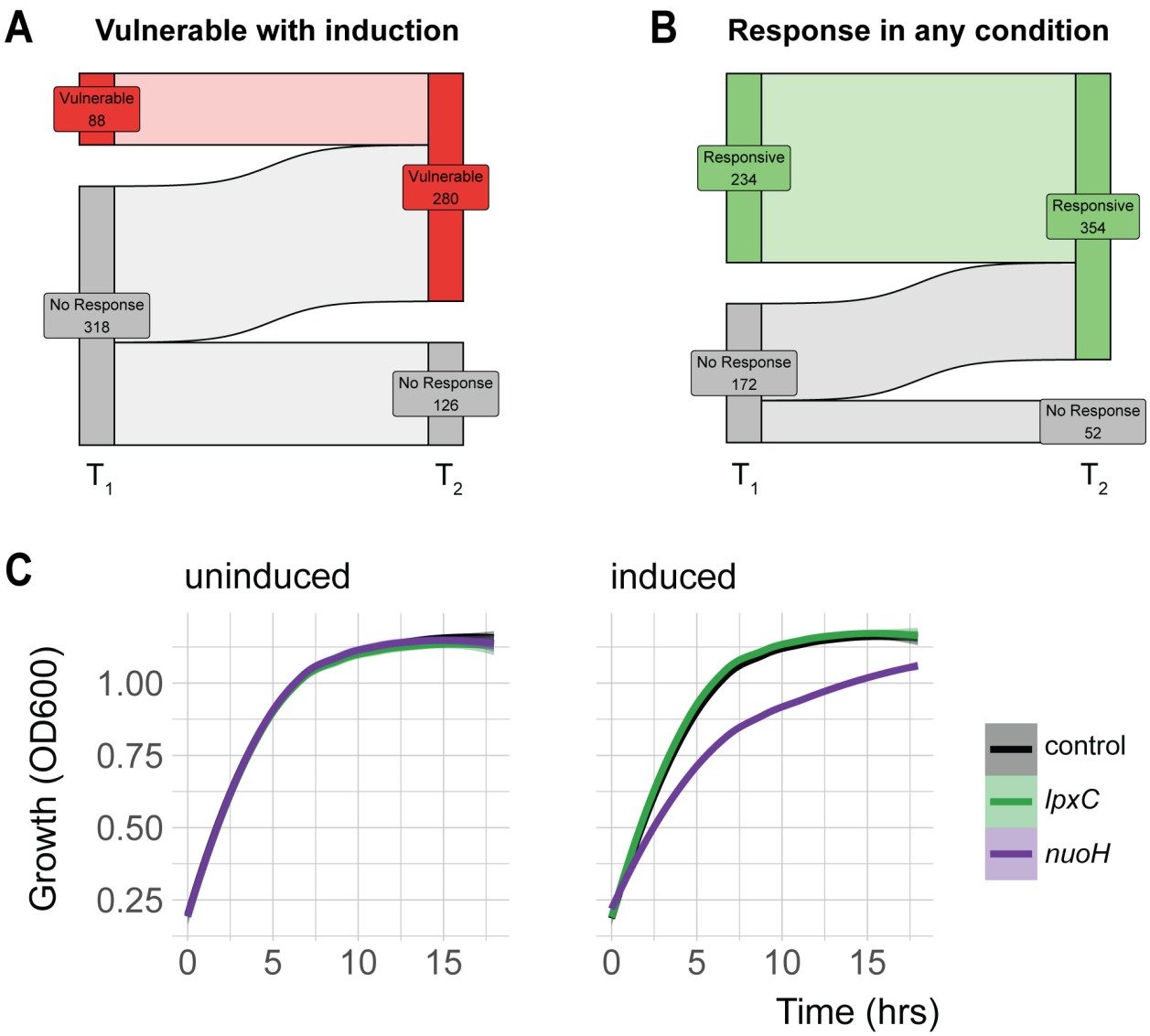

We sought to prioritize target genes and pathways by sensitivity to knockdown. Because CRISPRi knockdown affects transcription units (TUs) that can encode multiple gene products, we assigned essential genes to TUs and then organized the TUs into two groups: those containing only one essential gene and those containing multiple essential genes [Table 2]. We observed that most essential genes fall into one of two groups with respect to TUs: 1) TUs containing only one essential gene, or 2) TUs containing multiple essential genes that participate in the same cellular process; thus, most CRISPRi knockdowns affected single genes or single processes. Next, we ranked TU sensitivity to knockdown by the median log_2FC of perfect match guides targeting essential genes present in the TU [Table 2]. Our measurements of log_2FC are robust; however, we caution that small quantitative differences in gene/TU ranks may not always indicate meaningful variations in vulnerability.

Knockdowns of *murA*, *rpmB*, *aroC* and the poorly characterized gene, GO593_00515 were among the most depleted strains in our CRISPRi library [Figure 12A-B]. These genes represent established as well as underexplored therapeutic targets, and are in TUs containing only one essential gene, allowing straightforward interpretation of phenotypes. The *murA* gene, which encodes the target of fosfomycin (149), is vulnerable to knockdown despite fosfomycin's inefficacy against *A. baumannii* due to efflux by the AbaF pump (27). L28, encoded by *rpmB*, is a bacterium-specific ribosomal protein that is required for assembly of the 70S ribosome in *Escherichia coli* (150, 151), but has no characterized inhibitors to our knowledge. Interestingly, *E. coli* cells with reduced L28 levels accumulate ribosome fragments that can be assembled into translation-competent ribosomes by expressing additional L28 (151), suggesting that L28 could play a role in regulation of ribosome assembly. The *aroC* gene encodes chorismate synthase, a metabolic enzyme genetically upstream of aromatic amino acid and folate biosynthesis. The abundance of aromatic amino acids in LB medium used in our screen suggests that the essential role of *aroC* is likely in folate biosynthesis. Chorismate synthase is essential in several

bacterial species including Gram-positives, such as *B. subtilis* (152), and is vulnerable to knockdown in *Mycobacterium tuberculosis* (60), raising the possibility that *aroC* could be a general, high-value target.

Surprisingly, the most depleted knockdown strain in our library targeted an uncharacterized gene: GO593_00515 [Figure 12A-B]. GO593_00515 is predicted to encode an Arc family transcriptional repressor; Arc repressors have been extensively studied for their role in the Phage P22 life cycle (153). Accordingly, GO593_00515 is located within a predicted prophage in the 19606 genome; this locus is occupied by a similar but distinct prophage in the model resistant strain AB5075 [Figure 13A]. Synteny between the 19606 prophage and P22 suggested a role for GO593_00515 in lysogeny maintenance. Consistent with this hypothesis, we found that GO593_00515 knockdown cells showed little growth 10 hours after dilution into IPTG-containing medium [Figure 13C] and inducing knockdown in growing GO593_00515 CRISPRi cells caused complete lysis occurred within 7 hours [Figure 13B]. We reasoned that if the essential function of GO593_00515 is to repress expression of toxic prophage genes, we could suppress its essentiality by deleting the surrounding prophage genes entirely. Indeed, we recovered prophage deletion strains lacking GO593_00515 after inducing GO593_00515 in the presence of an integrated knockout plasmid [Figure 13C]. Thus, repression of toxic prophage genes is a critical but conditionally essential function in *A. baumannii*. Given the ubiquity of prophages harboring toxic lysis genes (154), we suggest that knockdown of phage repressors could aid in identifying proteins that are exceptional at lysing *A. baumannii*.

Figure 12: *A. baumannii* Genes and Pathways Vulnerable to Knockdown

(**A-B**) Depletion of sgRNAs targeting transcription units (TUs) from the CRISPRi library during growth in inducer over two time points (T_1 and T_2). Vertical dashed lines indicate a two-fold change in relative fitness score, and horizontal dashed lines indicate a Stouffer's *p* value of ≤ 0.05. Stouffer's *p* values were calculated at the TU level by combining the false discovery rates (FDRs) of all individual sgRNAs targeting the TU. TUs related to pathways discussed in the text are colored according to the figure legend and the number of essential genes in a TU is indicated by point size.

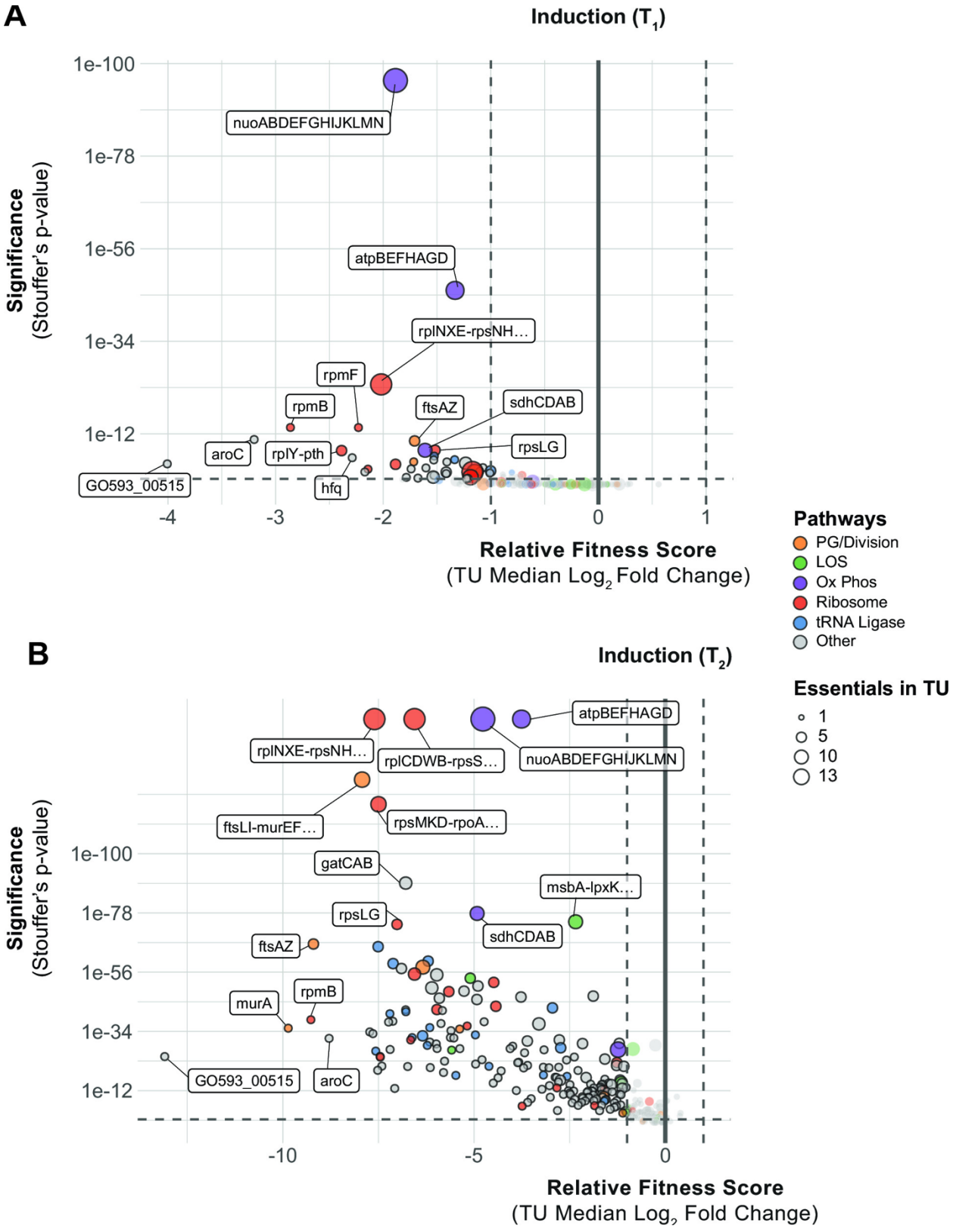
A
Induction (T_1)
Significance
(Stouffer's p-value)
1e-100
1e-78
1e-56
1e-34
1e-12
nuoABDEFGHIJKLMN
atpBEFHAGD
rplNXE-rpsNH…
rpmF
rpmB
ftsAZ
sdhCDAB
rpsLG
aroC
rplY-pth
GO593_00515
hfq
-4
-3
-2
-1
0
1
Relative Fitness Score
(TU Median Log$_2$ Fold Change)
Pathways
PG/Division
LOS
Ox Phos
Ribosome
tRNA Ligase
Other
Essentials in TU
1
5
10
13
B
Induction (T_2)
Significance
(Stouffer's p-value)
1e-100
1e-78
1e-56
1e-34
1e-12
atpBEFHAGD
rplNXE-rpsNH…
rplCDWB-rpsS…
nuoABDEFGHIJKLMN
ftsLI-murEF…
rpsMKD-rpoA…
gatCAB
msbA-lpxK…
rpsLG
sdhCDAB
ftsAZ
murA
rpmB
GO593_00515
aroC
-10
-5
0
Relative Fitness Score
(TU Median Log$_2$ Fold Change)

Figure 13: The GO593_00515 Gene is Conditionally Essential

(A) Mauve alignment of *A. baumannii* 19606 genomic locus containing GO593_00515 (pink) and surrounding prophage (yellow) to 17978 and AB5075. Regions of same color represent alignment between genomes. (B) Cultures seven hours after addition of P1 phage lysate to E. coli MG1655 (left) and addition of inducer (1 mM IPTG) to A. baumannii non-targeting control strain (middle) or GO593_00515 knockdown strain (right). (C) Growth, measured by OD600, over 18 hours for a non-targeting control strain, GO593_00515 knockdown strain, GO593_00515 knockdown strain with single crossover of prophage deletion plasmid (intermediate in construction), and multiple strains of GO593_00515 knockdown with deleted prophage in LB (uninduced, top) or LB with inducer (1 mM IPTG, bottom). (D) Agarose gel electrophoresis of PCR products to confirm prophage deletion using specified primer sets. GeneRuler 1 kb Plus ladder or template genomic DNA are denoted below each lane. PCR products with oJMP1381/1382 for strains with prophage still present suggests prophage excision happens at some frequency in WT.

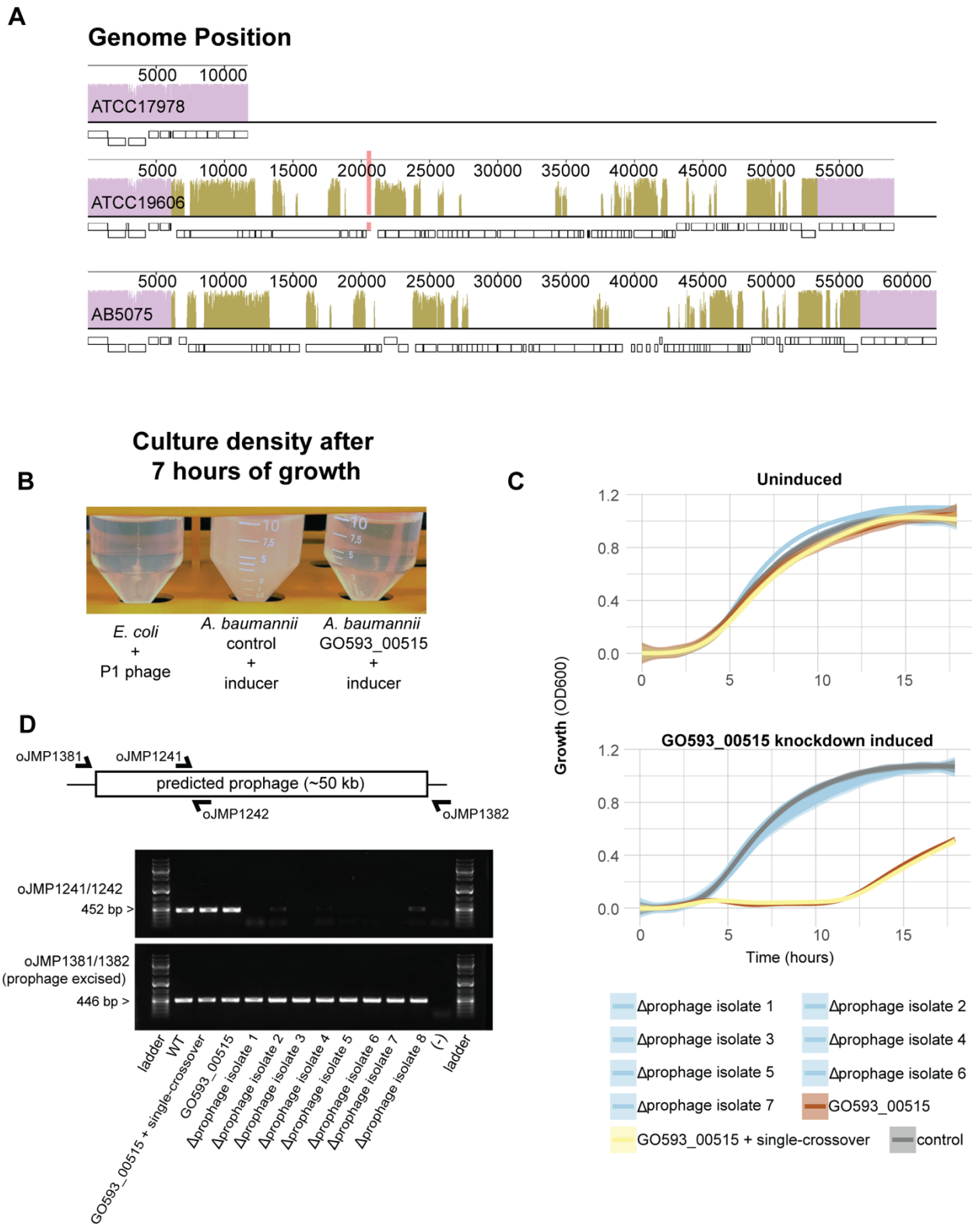
A
Genome Position
ATCC17978
ATCC19606
AB5075
B
Culture density after
7 hours of growth
E. coli
+
P1 phage
A. baumannii
control
+
inducer
A. baumannii
GO593_00515
+
inducer
C
Uninduced
GO593_00515 knockdown induced
Growth (OD600)
Time (hours)
Δprophage isolate 1
Δprophage isolate 2
Δprophage isolate 3
Δprophage isolate 4
Δprophage isolate 5
Δprophage isolate 6
Δprophage isolate 7
GO593_00515
GO593_00515 + single-crossover
control
D
oJMP1381
oJMP1241
predicted prophage (~50 kb)
oJMP1242
oJMP1382
oJMP1241/1242
452 bp >
oJMP1381/1382
(prophage excised)
446 bp >
ladder
WT
GO593_00515 + single-crossover
GO593_00515
Δprophage isolate 1
Δprophage isolate 2
Δprophage isolate 3
Δprophage isolate 4
Δprophage isolate 5
Δprophage isolate 6
Δprophage isolate 7
Δprophage isolate 8
(-)
ladder

Sensitivity to knockdown among groups of genes with related functions provided further insight into *A. baumannii* vulnerabilities. Strong depletion of knockdowns targeting components of the ribosome, peptidoglycan (PG) synthesis, and cell division validated our CRISPRi screen by identifying pathways targeted by clinically relevant antibiotics [Figure 12A-B]. Genes encoding aminoacyl-tRNA synthetases (aaRSs) were functionally enriched among strains with reduced abundance at T_2. Mupirocin, which targets IleRS, is the only inhibitor of a bacterial aaRS used clinically, although other aaRS inhibitors are used to treat infections caused by eukaryotic microbes . aaRSs are currently prioritized as targets for tuberculosis treatment as *M. tuberculosis* aaRS genes are vulnerable to knockdown and a LeuRS/MetRS dual inhibitor is currently undergoing clinical trials (155, 156). Our data demonstrate the vulnerability of aaRS genes in *A. baumannii* and suggest that aaRSs could serve as effective targets. Oxidative phosphorylation (oxphos) genes also stood out by degree of functional depletion in our library as early as T_1 [Figure 12A]. Among the oxphos outliers, genes encoding the NADH dehydrogenase complex I (NDH-1; *nuo* genes) were particularly sensitive to knockdown. This finding highlights the distinct importance of aerobic metabolism in *A. baumannii* compared to other Gram-negative pathogens, such as *E. coli*, where NDH-1 is not essential for viability in aerobic conditions (65).

Ideal antibiotic targets have a tight relationship between target function and fitness such that small perturbations result in a substantial loss of viability. Recent work in model bacteria (86, 101) and *M. tuberculosis* (60) has found that the relationship between knockdown and fitness for essential genes is non-linear and varies by gene or pathway. To examine this phenomenon for *A. baumannii* vulnerable genes, we fit the relationship between gene knockdown (predicted by machine learning (86)) and fitness (log2FC of mismatch guides) to generate "knockdown-response" curves [Figure 14]. We found that vulnerable genes and pathways were highly sensitive to even low levels of knockdown. Knockdown-response curves

allowed us to determine the amount of knockdown required to elicit a half-maximal reduction in fitness (effective knockdown, or EK_{50}) at the gene level. Vulnerable essential genes, such as *murA*, showed a substantial fitness defect at less than half of the maximal knockdown, whereas non-essential genes, such as *lpxA*, showed little fitness defects even at higher levels of knockdown. Other vulnerable genes (*e.g., rpmB*, *aroC*, and GO593_00515) also showed heightened sensitivity to knockdown [Figure 15].

Figure 14: Knockdown-Response Curves Describe Gene Vulnerability

(**A, B**) Knockdown-response curves of the LOS gene *lpxA* and the PG/division gene *murA*. Points are individual mismatch sgRNAs; mismatch sgRNA knockdown was predicted as previously described (19). Colored lines are a 4-parameter logistic fit describing the relationship between relative fitness score and knockdown. The effective knockdown 50 (EK_{50}) is the amount of predicted knockdown needed to achieve a half-maximal effect on relative fitness score. EK_{50}s are depicted as crosshairs.

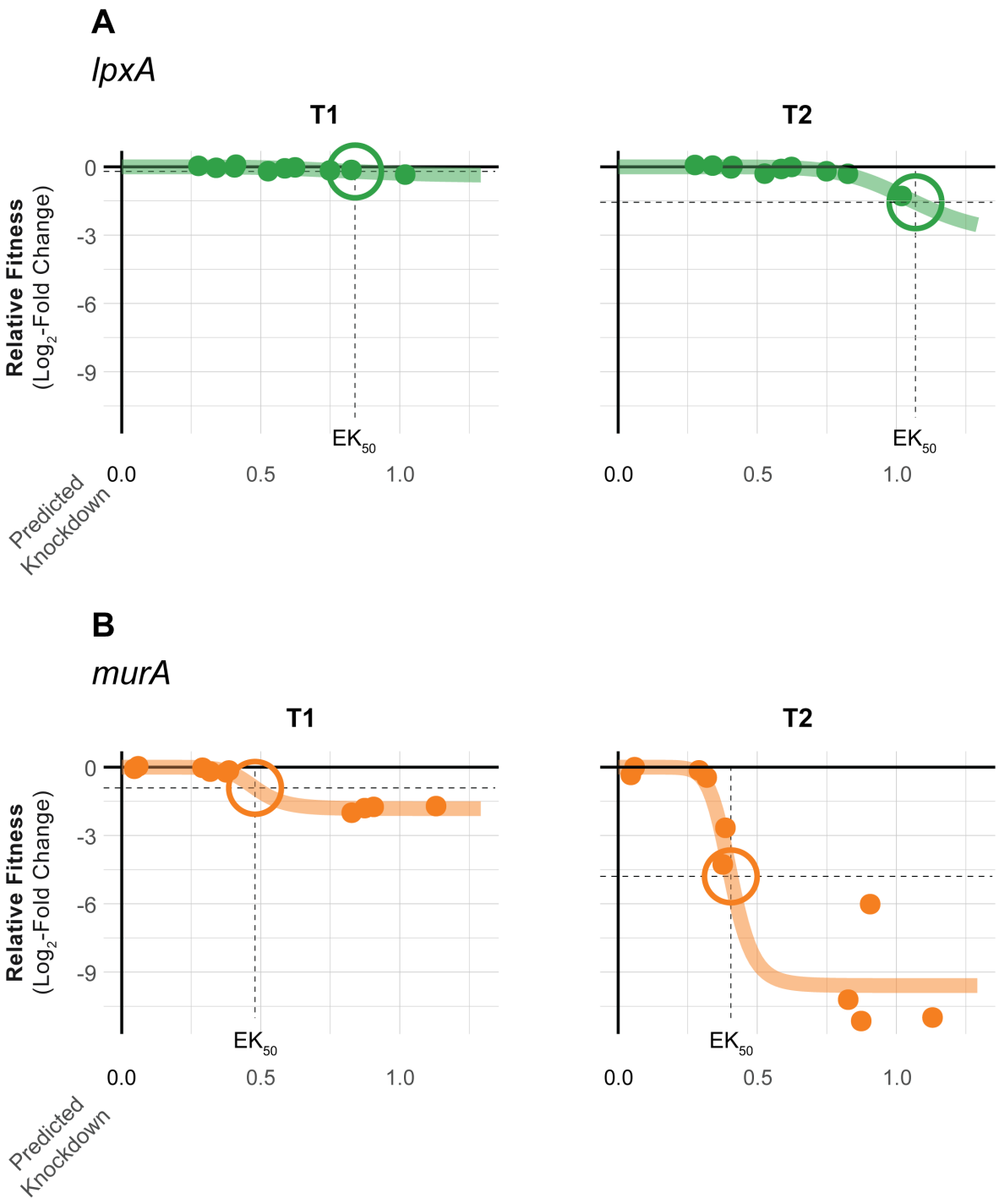
A
lpxA
T1
T2
Relative Fitness
(Log2-Fold Change)
0
-3
-6
-9
EK50
0.0
0.5
1.0
Predicted
Knockdown
B
murA
T1
T2
Relative Fitness
(Log2-Fold Change)
0
-3
-6
-9
EK50
0.0
0.5
1.0
Predicted
Knockdown

Figure 15: Gene-Specific Knockdown-Response Relationships Across Experimental Timepoints

Examples of 4-parameter knockdown-response curves in T_1 and T_2 from genes highlighted in the text. Effective knockdown 50 (EK_{50}) parameters are displayed as crosshairs where the parameter fit resulted in a p value ≤ 0.05. Points are individual sgRNAs.

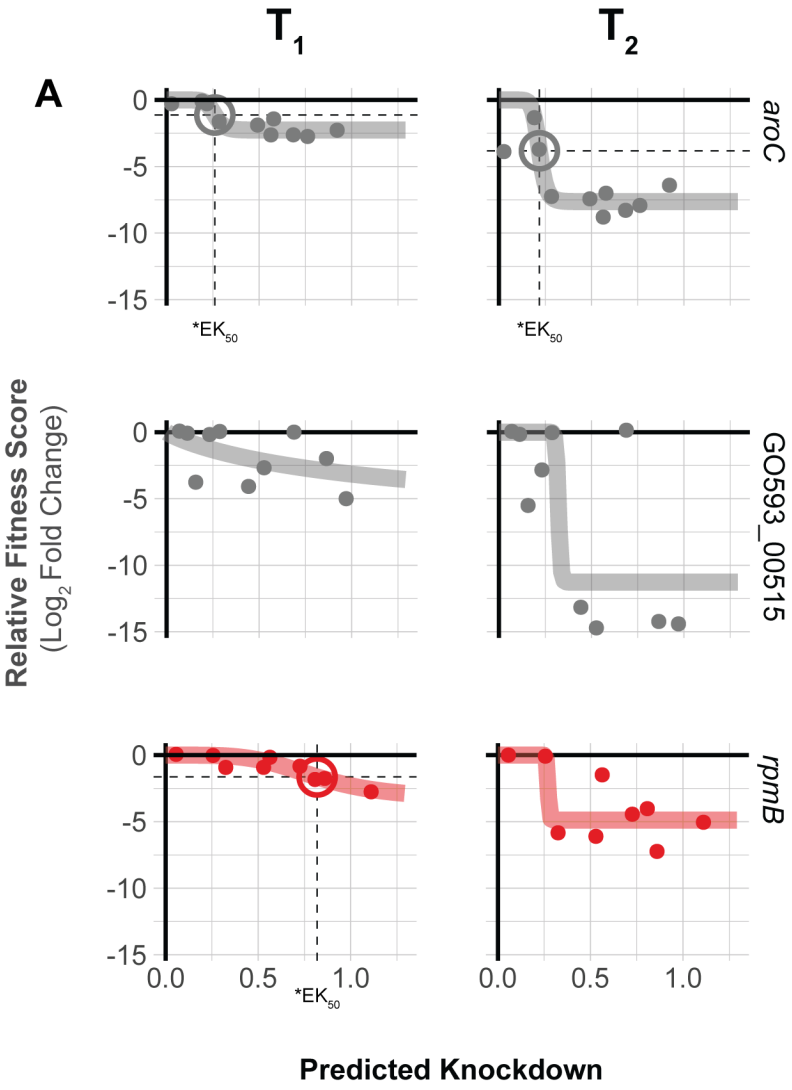

We extended our knockdown-response analysis to the pathway level, finding that pathways with many vulnerable genes (PG/division) required less knockdown, on average, than pathways with few vulnerable genes (LOS) [Figure 16]. Interestingly, although fitness at T_2 was generally lower than T_1 for vulnerable genes, EK_{50} values at both time points were statistically indistinguishable. This demonstrates that even guides with weak knockdown contribute to vulnerability phenotypes and suggests that gene phenotypes occur when a threshold of knockdown is crossed, and that threshold is pathway-dependent in *A. baumannii*.

Figure 16: Knockdown-Response Curves Describe Pathway Vulnerability

(**A, B**) Knockdown response curves for genes in LOS synthesis or PG/division pathways. Points indicate the EK_{50} for individual pathway genes. Boxplots on the y-axis show the distribution of relative fitness scores at EK_{50} for genes in the pathway and boxplots on the x-axis show the distribution of EK_{50} values for genes in the pathway. Statistical significance was assessed using Wilcoxon Rank Sum Test; asterisks indicate $p \leq 0.05$ and ns for not significant.

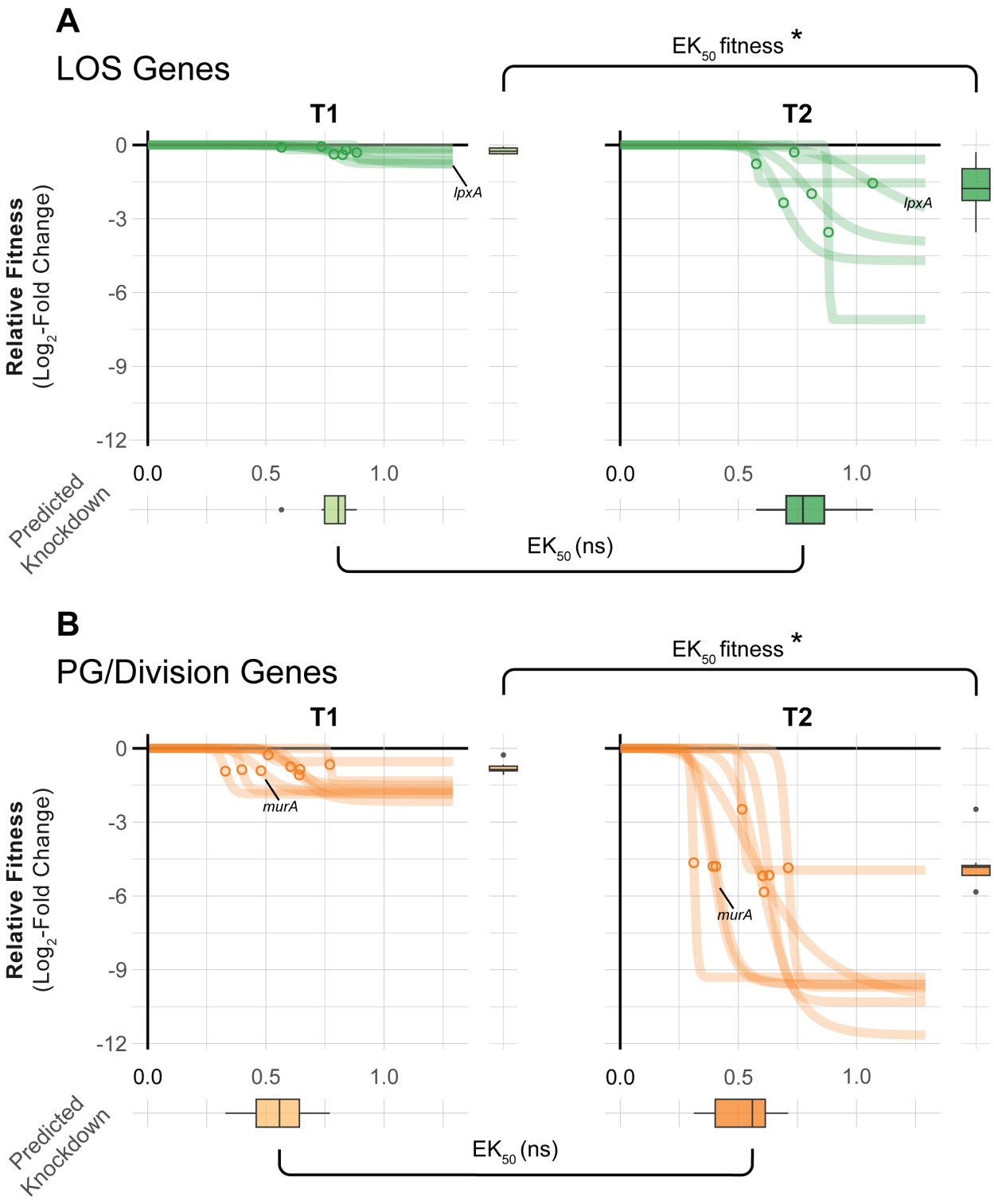
A
LOS Genes
EK50 fitness *
T1
T2
lpxA
lpxA
Relative Fitness
(Log2-Fold Change)
0
-3
-6
-9
-12
0.0
0.5
1.0
Predicted
Knockdown
EK50 (ns)
B
PG/Division Genes
EK50 fitness *
T1
T2
murA
murA
Relative Fitness
(Log2-Fold Change)
0
-3
-6
-9
-12
0.0
0.5
1.0
Predicted
Knockdown
EK50 (ns)

6.3. Essential gene knockdowns that potentiate or mitigate carbapenem sensitivity in *A. baumannii.*

Antibiotic-gene interaction screens have the potential to identify targets that synergize with or antagonize existing therapies. Carbapenems, a class of β-lactam antibiotics, are first-line treatments for *A. baumannii* that block PG synthesis by inhibiting penicillin binding proteins (PBPs) (157). To uncover antibiotic-essential gene interactions that impact sensitivity to carbapenems, we screened our CRISPRi library against sub-MIC concentrations of imipenem (IMI) and meropenem (MER) [Figure 17A, Figure 18A-B]. We found that knockdown of genes involved in cell wall synthesis, including the direct target (*ftsI*, TU: *ftsLI-murEF-mraY*), increased carbapenem sensitivity. Knockdowns of genes required for PG precursor synthesis (*murA*, *dapA*) and translocation (*murJ*) were strongly depleted in both IMI and MER. MurA catalyzes the first committed step of PG synthesis, DapA is part of a pathway that converts L-aspartate to meso-diaminopimelate which is incorporated into PG precursors by MurE, and MurJ, the lipid II flippase, translocates PG precursors from the inside to the outside of the cytoplasmic membrane (158). To validate screen hits, we developed a small-scale version of our initial screen that retains its high sensitivity while reducing pool complexity; this assay uses Next Generation Sequencing to measure competitive fitness between a non-targeting and CRISPRi knockdown strain (*i.e.,* "CoMBaT-seq" or Competition of Multiplexed Barcodes over Time). We validated CoMBaT-seq by recapitulating *murA* vulnerability to knockdown and further sensitivity to IMI [Figure 17B].

Figure 17: Essential Gene Interactions with Carbapenem Antibiotics in *A. baumannii*

(**A**) Boxplots showing the relative fitness scores of selected TUs that interact with imipenem (IMI, 0.09 µg/mL) across the genome at T_1. Points are individual guides in the TU. Boxplots are colored by relevant pathways; light-blue boxplots indicate TUs where tRNA synthetase genes are present with genes in other pathways. (**B-C**) CoMBaT-seq data from a growth competition between either a *murA* or *glnS* knockdown strain and a non-targeting control strain in the presence or absence of IMI (0.09 µg/mL). Only data from the gene targeting strain is depicted as the non-targeting control is the remaining proportion of the population. Points are data from individual experiments (N = 2).

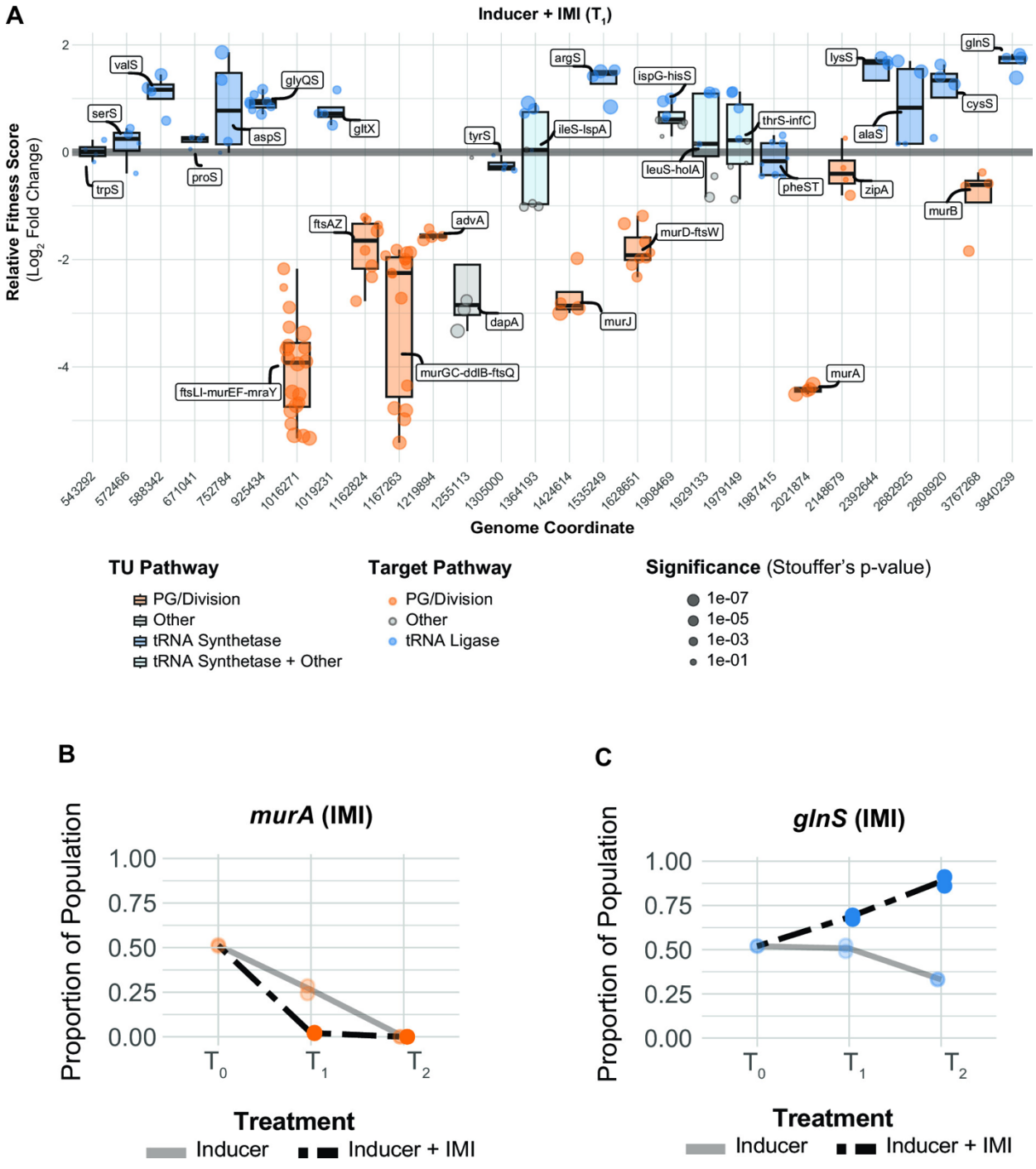
A
Inducer + IMI (T1)
Relative Fitness Score
(Log2 Fold Change)
2
0
-2
-4
valS
serS
trpS
proS
aspS
glyQS
gltX
tyrS
argS
ileS-lspA
ispG-hisS
leuS-holA
thrS-infC
pheST
lysS
alaS
zipA
cysS
glnS
murB
ftsAZ
advA
dapA
murJ
murD-ftsW
murGC-ddlB-ftsQ
ftsLI-murEF-mraY
murA
543292
572466
588342
671041
752784
925434
1016271
1019231
1162824
1167263
1219894
1255113
1305000
1364193
1424614
1535249
1628651
1908469
1929133
1979149
1987415
2021874
2148679
2392644
2682925
2808920
3767268
3840239
Genome Coordinate
TU Pathway
PG/Division
Other
tRNA Synthetase
tRNA Synthetase + Other
Target Pathway
PG/Division
Other
tRNA Ligase
Significance (Stouffer's p-value)
1e-07
1e-05
1e-03
1e-01
B
murA (IMI)
Proportion of Population
1.00
0.75
0.50
0.25
0.00
T0
T1
T2
Treatment
Inducer
Inducer + IMI
C
glnS (IMI)
Proportion of Population
1.00
0.75
0.50
0.25
0.00
T0
T1
T2
Treatment
Inducer
Inducer + IMI

Figure 18: Essential Gene Operon Knockdown Phenotypes in IMI and MER

Imipenem (IMI) (**A**) and meropenem (MER) (**B**). Depletion of sgRNA spacers from the CRISPRi library (relative fitness score) during growth in IPTG at the level of transcription units (TUs). Dashed lines indicate a two-fold loss in relative fitness score and a *p* value of ≤ 0.05. Stouffer's *p* values were calculated at the TU level by aggregating false discovery rates (FDRs) of individual sgRNAs targeting the TU. TUs related to pathways discussed in the text are colored as described in the legend and the number of essential genes in the TU is indicated by point size.

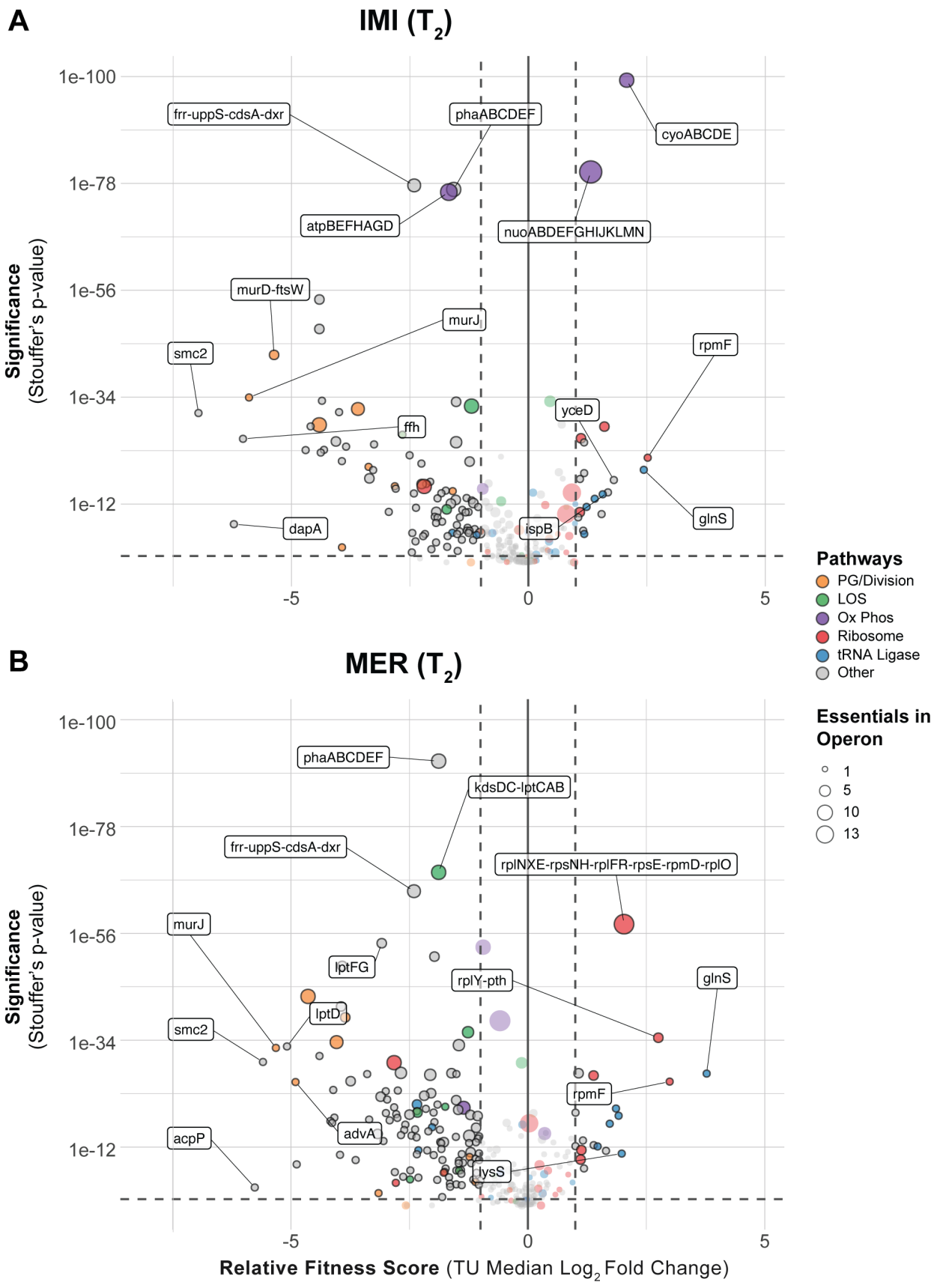
A
IMI (T_2)
1e-100
1e-78
1e-56
1e-34
1e-12
Significance
(Stouffer's p-value)
frr-uppS-cdsA-dxr
phaABCDEF
cyoABCDE
atpBEFHAGD
nuoABDEFGHIJKLMN
murD-ftsW
murJ
smc2
rpmF
yceD
ffh
glnS
dapA
ispB
-5
0
5
B
MER (T_2)
phaABCDEF
kdsDC-lptCAB
frr-uppS-cdsA-dxr
rplNXE-rpsNH-rplFR-rpsE-rpmD-rplO
murJ
lptFG
rplY-pth
glnS
lptD
smc2
rpmF
advA
acpP
lysS
Relative Fitness Score (TU Median Log$_2$ Fold Change)
Pathways
PG/Division
LOS
Ox Phos
Ribosome
tRNA Ligase
Other
Essentials in Operon
1
5
10
13

Because IMI targets cell wall synthesis, reduced growth of gene knockdowns in the same pathway could be considered a “dosing effect” rather than a true synergy. To test for synergy, we performed a checkerboard assay between IMI and fosfomycin. Consistent with our *murA*-IMI interaction, we found that fosfomycin and IMI synergize in *A. baumannii* (FIC<0.5) [Figure 19A], as is the case in other Gram-negative pathogens (*e.g., Pseudomonas aeruginosa* (159)). Although no clinically relevant inhibitors of DapA and MurJ exist, to our knowledge, we speculate that such inhibitors would have the potential to synergize with carbapenems. Intriguingly, knockdowns of *advA*—an Acinetobacter-specific division gene (107)—were also sensitized to carbapenems, raising the possibility of *A. baumannii* targeting combination therapies should inhibitors of AdvA be identified.

Figure 19: Carbapenems are Synergistic with Fosfomycin in *A. baumannii*

2-fold serial dilutions of drugs from minimum inhibitory concentrations (MICs) represented by gray wedges. Wells with red borders show synergy (i.e., no growth & FIC index <0.5).

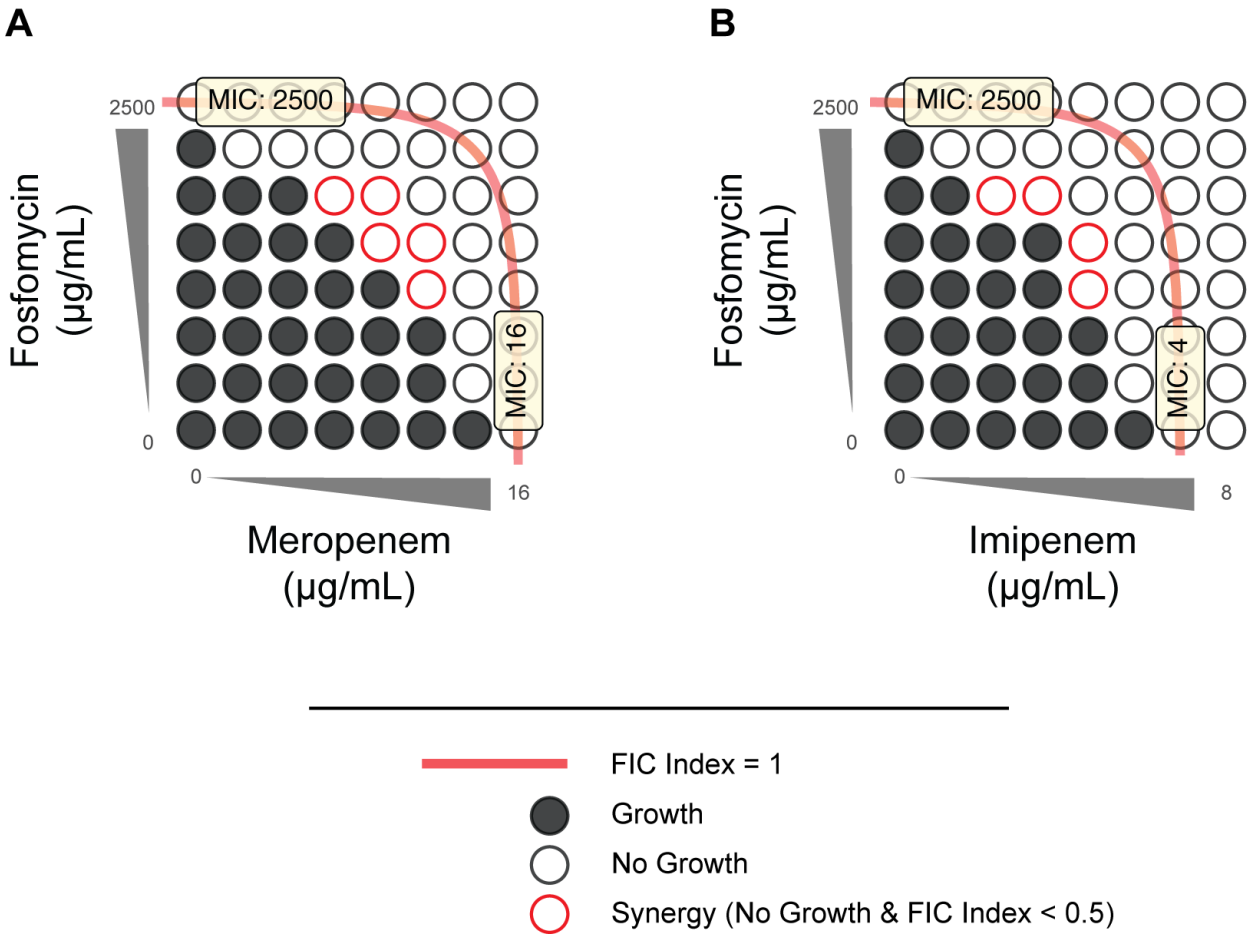

Gene knockdowns that mitigate antibiotic function can reveal routes to resistance or target combinations that result in antagonism and should be avoided therapeutically. Given that increasing carbapenem resistance is an urgent clinical concern for *A. baumannii*, we sought to identify genes and pathways that mitigate the efficacy of IMI and MER. Although previous work suggested that growth rate and β-lactam resistance are linearly related (160, 161), we found only a modest linear relationship growth and IMI/MER resistance across knockdown strains in our library (R2 = 0.005, and 0.007, respectively [Figure 20A-B]). This indicates that slow growing strains of *A. baumannii* are not necessarily more resistant to β-lactam treatment. Instead, we found that specific genetic pathways govern carbapenem resistance. Using gene set enrichment analysis, we identified ribosomal protein genes as a pathway that increases resistance to IMI/MER when perturbed [**IMI**: enrichment score = 4.65, FDR (afc) = 2.12e-06; **MER**: enrichment score = 2.43, FDR (afc) = 0.002], consistent with antagonism between β-lactams and ribosome inhibitors described for other bacteria (162).

aaRS genes also emerged from our enrichment analysis [**IMI**: enrichment score = 4.93, FDR (afc) = 1.04e-06; **MER**: enrichment score = 5.04, FDR (afc) = 1.16e-06], uncovering a connection between tRNA charging and carbapenem resistance, as well as a surprising relationship between knockdown and fitness unique to antagonistic interactions. A subset of aaRS gene knockdowns including *argS*, *lysS*, *valS*, *cysS* and *glnS* showed increased relative fitness in our IMI pooled screen [Figure 17A, Figure 20C]. Although *glnS* resistance to IMI in MIC test strip and growth curve assays was modest [Figure 21], our more sensitive CoMBaT-seq assay showed a clear growth advantage for the *glnS* knockdown when competed against a non-targeting control (in contrast to sensitive knockdowns such as *murA*) [Figure 17B-C].

Figure 20: Essential Gene Knockdown Interactions with Carbapenems

(**A-B**) Scatterplot of mismatch guide relative fitness score (log_2 fold change) in inducer only compared to relative fitness score in imipenem at T_1. Lines represent linear model fits with 95% confidence interval. Guides for genes in PG/division or tRNA ligase pathways are divided into groups using hierarchical clustering based on response to imipenem. Left-hand figures in grayscale indicate trend for all guides; right-hand figures indicate trends for guides for specific pathways. High-response indicates most responsive cluster (greatest absolute log_2-fold changes), low-response indicates other clusters (k=3) in C. (**C**) Hierarchical clustering of tRNA synthetase and PG/division gene knockdowns in response to imipenem (IMI) and meropenem (MER).

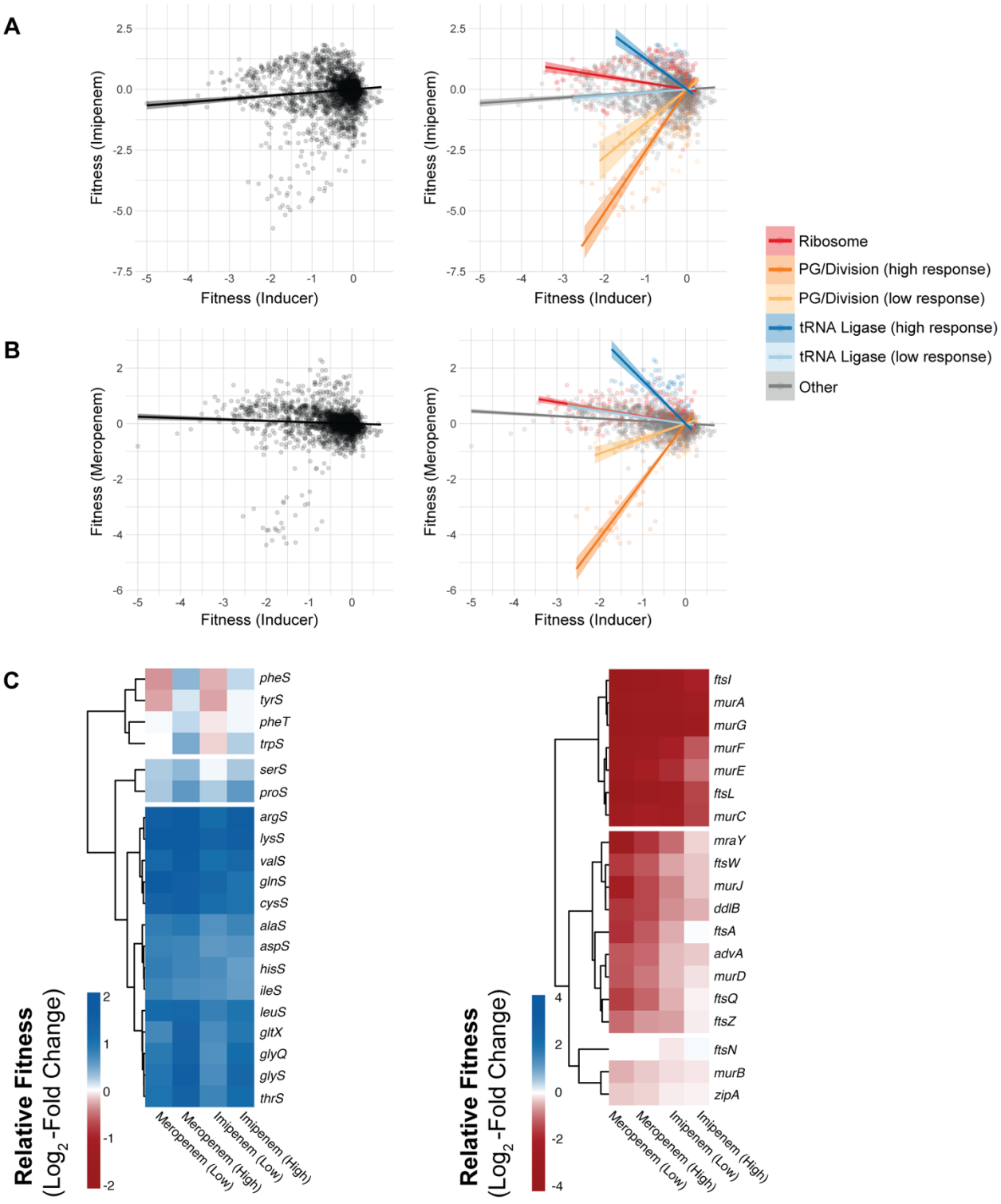
A
B
C
Fitness (Imipenem)
Fitness (Meropenem)
Fitness (Inducer)
Ribosome
PG/Division (high response)
PG/Division (low response)
tRNA Ligase (high response)
tRNA Ligase (low response)
Other
pheS
tyrS
pheT
trpS
serS
proS
argS
lysS
valS
glnS
cysS
alaS
aspS
hisS
ileS
leuS
gltX
glyQ
glyS
thrS
ftsI
murA
murG
murF
murE
ftsL
murC
mraY
ftsW
murJ
ddlB
ftsA
advA
murD
ftsQ
ftsZ
ftsN
murB
zipA
Relative Fitness
(Log2-Fold Change)
Meropenem (Low)
Meropenem (High)
Imipenem (Low)
Imipenem (High)

Figure 21: *glnS* Knockdown Causes a Subtle Change in IMI MIC

Four independently constructed non-targeting (NT) or *glnS* knockdown strains were plated as a lawn on LB + 1mM IPTG and grown in the presence of an IMI MIC test strip. MIC values were read as the concentration line above the intersection between confluent growth and the test strip. The average MICs for NT and *glnS* were 0.6 and 0.9 ng/µL, respectively (p = 0.02, 2 tailed t-test with equal variance).

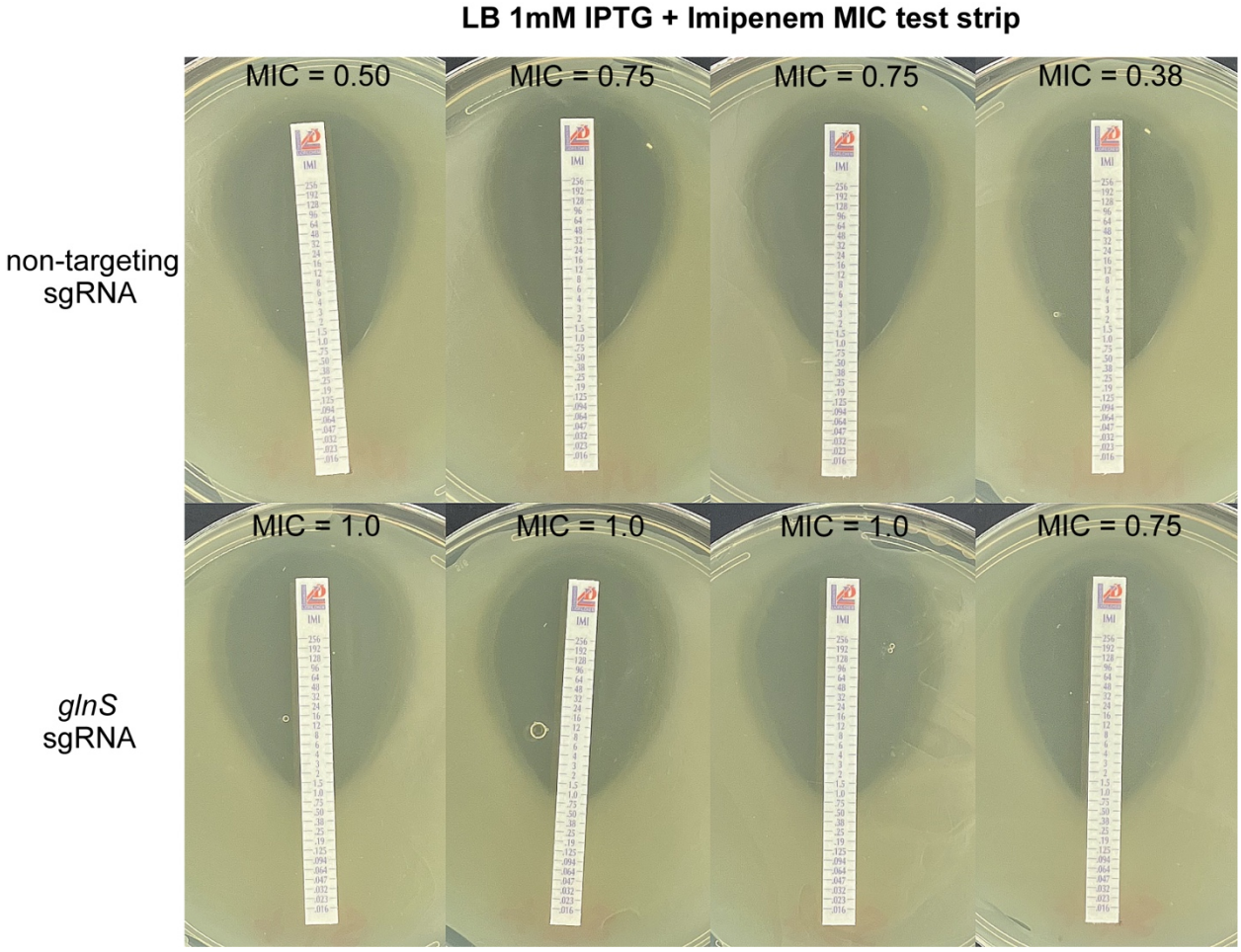

Our observations that the *glnS* knockdown is depleted during growth in rich medium and enriched during growth in IMI implied that the relationship between knockdown and fitness changed across the two conditions. Indeed, a 4-parameter knockdown-response curve fit well to mismatch guides targeting *glnS* without treatment, but poorly to the same guides in IMI treatment [Figure 22A-D, Figure 23A-B]. Remarkably, IMI treated *glnS* knockdown strains showed increased relative fitness as knockdown increased up until a point at the strains lost viability, presumably due to a lack of glutamine tRNA charging. This pattern is reminiscent of a hormetic response in dose-response curves (163) where a low amount of drug produces a positive response that eventually becomes negative at higher doses [Figure 22A-B]. Accordingly, a 5-parameter logistic curve typically used in the context of hormetic responses improved the fit to IMI treated *glnS* mismatch strains but did not improve the fit of untreated strains [Figure 22C-D, Figure 23B]. To test if the hormetic effect we observed between IMI and *glnS* in an antibiotic-gene interaction was relevant to antibiotic-antibiotic interactions, we measured the growth of wild-type *A. baumannii* treated with IMI and the aaRS inhibitor, mupirocin. Consistent with hormesis, IMI antagonized the effect of mupirocin at low concentrations but had no positive impact on growth at higher concentrations [Figure 22E]. Although mupirocin treatment is not clinically relevant for *A. baumannii* due to high-level resistance, our work provides a proof of principle that hormetic effects can be predicted by genetic approaches and influence antibiotic susceptibility.

Figure 22: Knockdown extent affects the sign of antibiotic-gene interactions

(**A-B**) Schematics of idealized dose-response curves showing monotonic or hormetic relationships between dose and response; hormetic responses change the sign of the response depending on dose. (**C-D**) Knockdown-response curves of *glnS* show a nearly monotonic response in the absence of IMI, but a hormetic response in the presence of IMI. (**E**) The interaction between the IleRS tRNA synthetase inhibitor mupirocin (MUP) and IMI shows a hormetic response at intermediate concentrations of IMI.

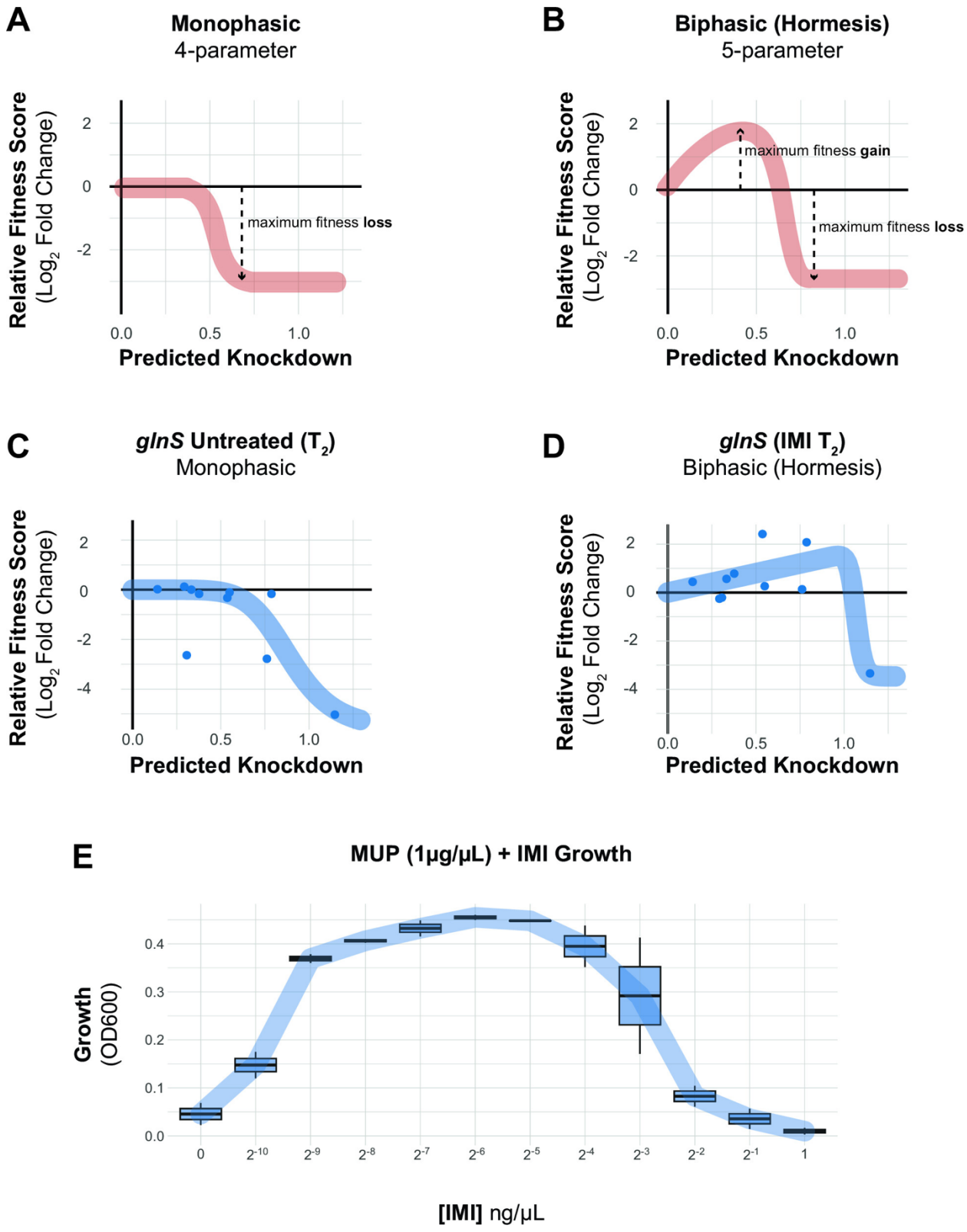
A
Monophasic
4-parameter
Relative Fitness Score
(Log2 Fold Change)
maximum fitness loss
Predicted Knockdown
B
Biphasic (Hormesis)
5-parameter
maximum fitness gain
maximum fitness loss
C
glnS Untreated (T2)
Monophasic
D
glnS (IMI T2)
Biphasic (Hormesis)
E
MUP (1µg/µL) + IMI Growth
Growth
(OD600)
[IMI] ng/µL

Figure 23: Dose-Response Curve Modeling the Fits for *glnS* in IMI

(**A-B**) and *nuoB* in rifampicin (RIF) (**C-D**). Asterisks indicate improvement of the empirical fit from 4-paremeter to 5-parameter, such that the likelihood-ratio test *p* value ≤ 0.05.

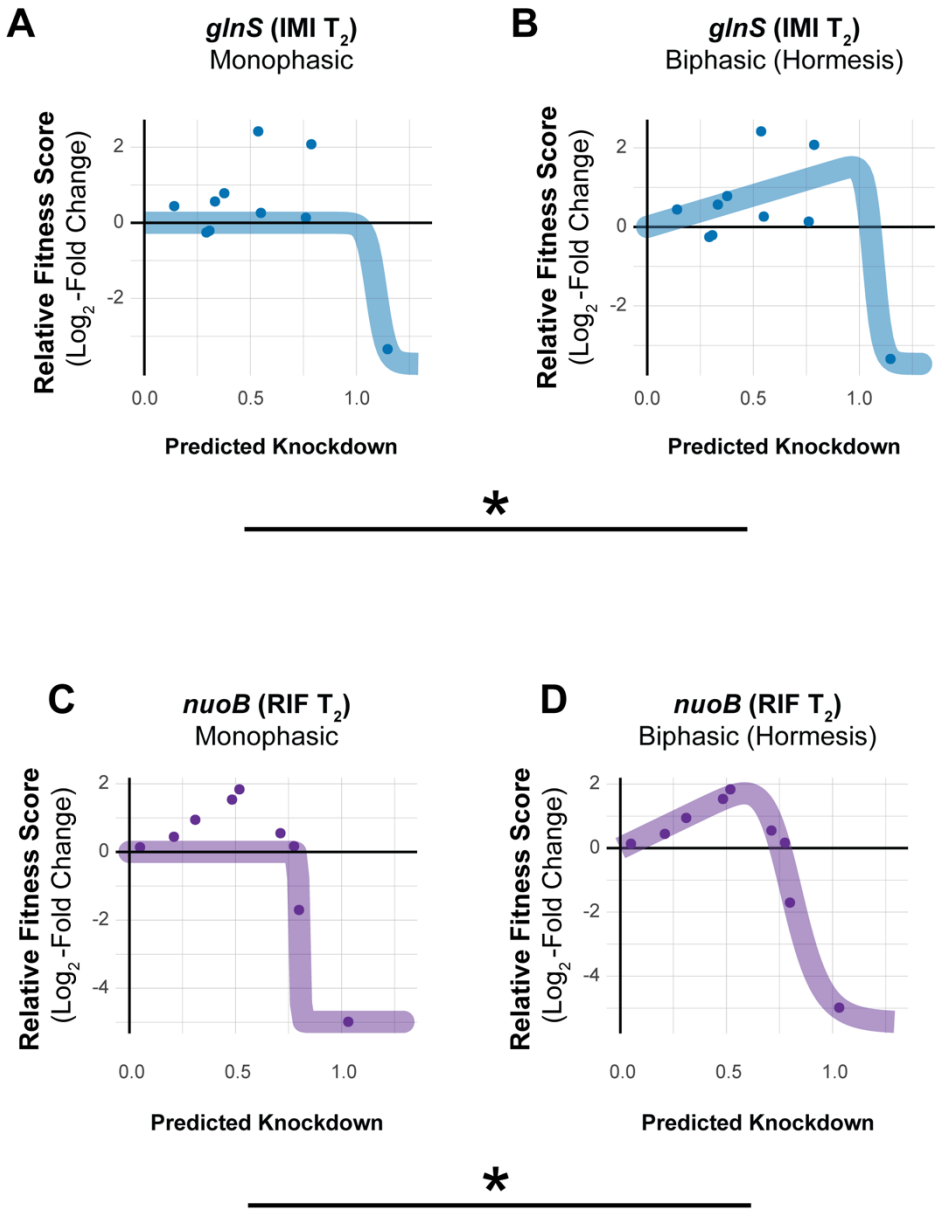

6.4. The synergistic antibiotic pair, colistin and rifampicin, show anticorrelated phenotypes

Antibiotic-gene interaction screens can identify genes and pathways that contribute to drug synergy. Colistin (COL) and rifampicin (RIF) synergistically inhibit *A. baumannii* growth [Figure 24] (164), in part due to permeabilization of the outer membrane by COL (165). To define antibiotic-gene interactions that may inform COL-RIF synergy, we screened our CRISPRi library against COL and RIF individually. We found strong, opposing phenotypes in COL and RIF for genes encoding NDH-1 and LOS biosynthesis genes. COL, a polymyxin class antibiotic, is a last-resort treatment for carbapenem-resistant *A. baumannii* (41). COL binds to the lipid A moiety of LOS and is thought to kill cells by membrane disruption (23); complete loss of LOS results in a >500-fold increase in COL resistance (142). As expected, screening our library against a sub-MIC dose of COL identified LOS synthesis genes as resistant outliers [Figure 25]. Among the most resistant outliers were *lpxC* (TU: *lpxC*) and *lpxA* (TU: *lpxD-fabZ-lpxA*), which encode enzymes that catalyze the first two committed steps in LOS synthesis and are commonly found in selections for COL resistant mutants (142). Genes involved in fatty acid biosynthesis biosynthesis (TU: *fabDG*, TU: *aroQ-accBC*) also showed increased resistance to COL, possibly by limiting the pool of fatty acids available for LOS synthesis [Figure 25]. Surprisingly, knockdown of genes encoding NDH-1 (TU: *nuoABDEFGHIJKLMN*) caused heightened sensitivity to COL in the context of our pooled screen [Figure 25].

Figure 24: COL and RIF are synergistic under our screening conditions in *A. baumannii*

2-fold serial dilutions of drugs from minimum inhibitory concentrations (MICs) represented by gray wedges. Wells with red borders show synergy (*i.e.*, no growth & FIC index <0.5).

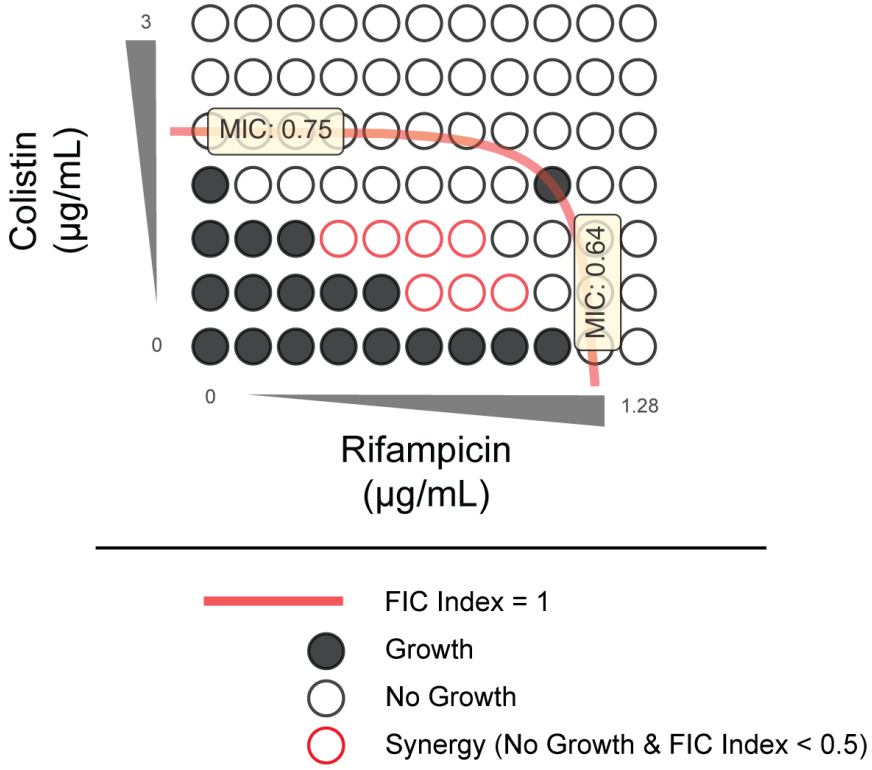

Figure 25: Essential Gene Knockdown Phenotypes in Rifampicin (RIF) versus Colistin (COL)

Depletion of sgRNAs targeting transcription units (TUs) from the CRISPRi library during growth in inducer and RIF or COL at T_2. Vertical dashed lines indicate a two-fold loss in fitness score relative to non-targeting sgRNAs and horizontal dashed lines indicate a Stouffer's *p* value of ≤ 0.05. Stouffer's *p* values were calculated at the TU level by combining the false discovery rates (FDRs) of all individual sgRNAs targeting the TU. TUs related to pathways discussed in the text are colored according to the figure legend and the number of essential genes in a TU is indicated by point size.

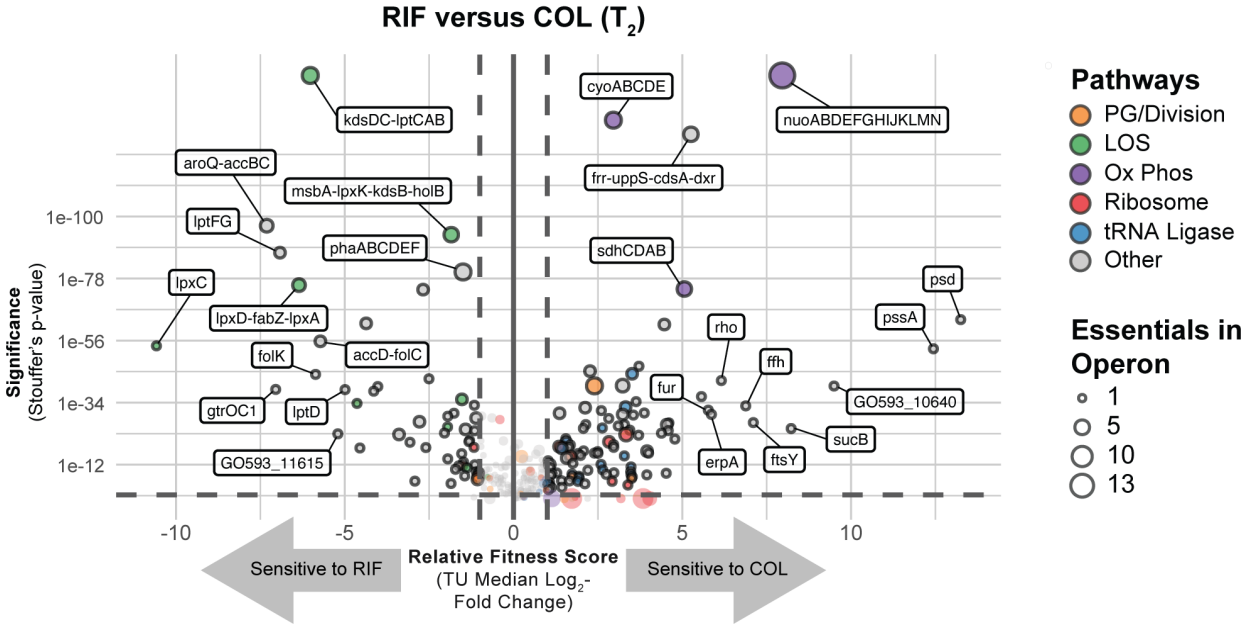

We confirmed the COL sensitivity of a *nuoB* knockdown using our CoMBaT-seq assay [Figure 26A], although MIC test strips showed a more muted effect [Figure 27]. NDH-1 couples conversion of NADH to NAD+ to proton translocation across the inner membrane, but whether the key role for NDH-1 in *A. baumannii* physiology is NAD+ recycling or contributing to membrane potential ($\Delta\psi$) is unknown. To address this issue, we measured the NAD+/NADH ratio and $\Delta\psi$ using an enzyme-coupled luminescence assay (NAD/NADH-Glo) and the membrane potential-sensitive dye Thioflavin T (ThT), respectively [Figure 26B, Figure 28A]. Knockdown of *nuoB* lowered the NAD+/NADH ratio, consistent with reduced conversion of NADH to NAD+ by NDH-1 [Figure 26B]. Unexpectedly, *nuoB* knockdown did not impact $\Delta\psi$, although reduced $\Delta\psi$ in cells treated with the ionophore CCCP was readily apparent in our ThT assay [Figure 28B]. Thus, recycling of NADH to NAD+ for use in the TCA cycle, rather than maintenance of membrane potential, may be the critical cellular role of NDH-1. *A. baumannii* also encodes a non-essential, non-proton pumping NDH-2 enzyme that can be inhibited by COL *in vitro* (166). We speculate that NDH-2 inhibition by COL combined with knockdown of NDH-1 critically reduces cellular NAD+ levels, leading to enhanced sensitivity.

Figure 26: Physiological Characterization of NDH-1 knockdown

(**A**) CoMBaT-seq data from a growth competition between a *nuoB* knockdown strain and a non-targeting control strain in the presence or absence of COL. Only data from the gene targeting strain are depicted as the non-targeting control is the remaining proportion of the population. Points are data from individual experiments (N = 2). (**B**) Measurement of the NAD+/NADH ratio in *nuoB* knockdown and non-targeting cells using the NAD/NADH-Glo assay. An unequal variance t-test was performed and the asterisk indicates that the P-value ≤0.05. (**C and D**) Knockdown-response curves of *nuoB* show a nearly monotonic response in the absence of RIF, but a hormetic response in the presence of RIF. (**E**) CoMBaT-seq data from a growth competition between a *nuoB* knockdown strain and a non-targeting control strain in the presence or absence of RIF. (**F**) Ethidium bromide (EtBr) permeability assay of non-targeting and *nuoB* knockdown strains; *nuoB* knockdowns show decreased access of EtBr to DNA in the cytoplasm.

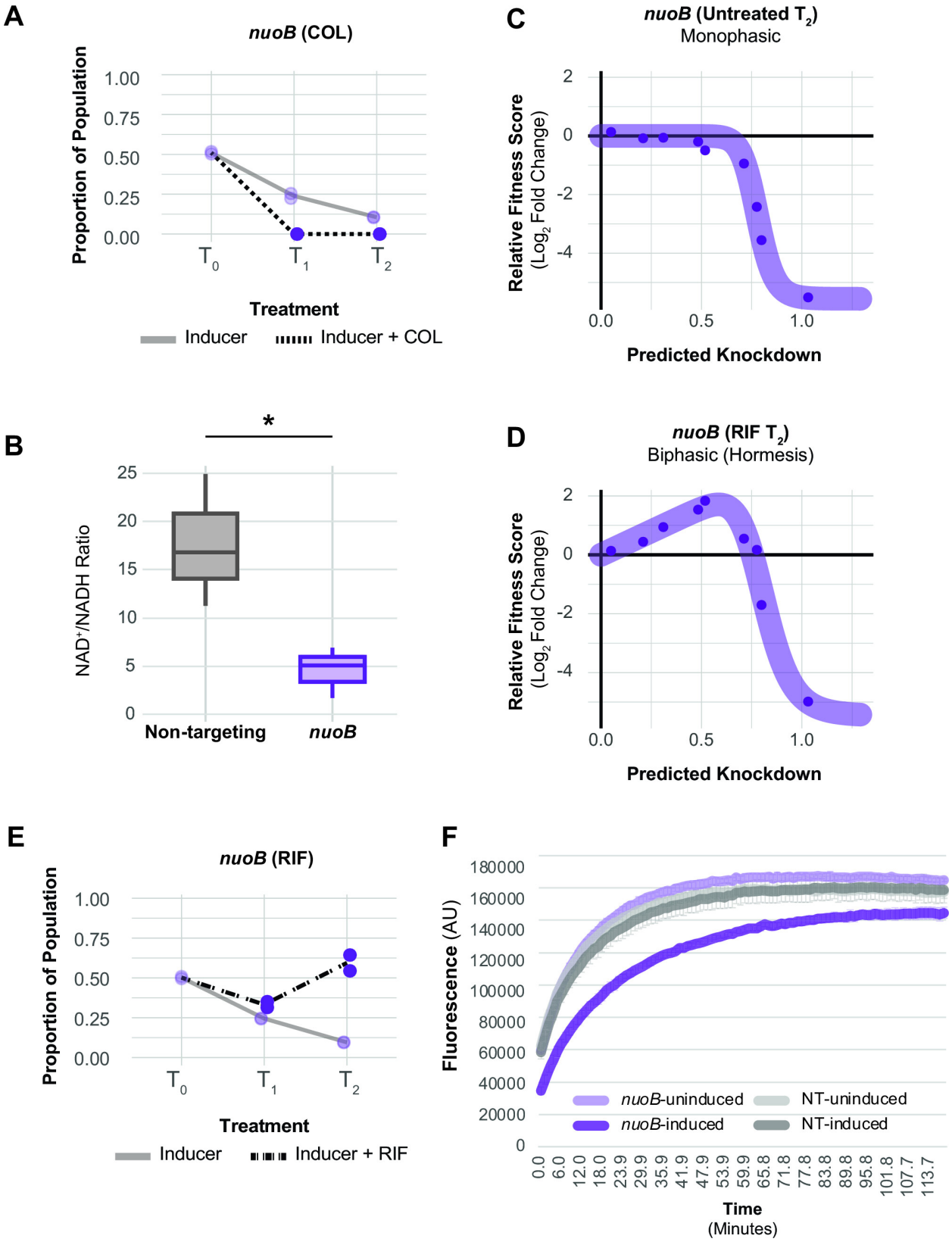
A
nuoB (COL)
Proportion of Population
1.00
0.75
0.50
0.25
0.00
T0
T1
T2
Treatment
Inducer
Inducer + COL
B
*
NAD+/NADH Ratio
25
20
15
10
5
0
Non-targeting
nuoB
C
nuoB (Untreated T2)
Monophasic
Relative Fitness Score
(Log2 Fold Change)
2
0
-2
-4
0.0
0.5
1.0
Predicted Knockdown
D
nuoB (RIF T2)
Biphasic (Hormesis)
Relative Fitness Score
(Log2 Fold Change)
2
0
-2
-4
0.0
0.5
1.0
Predicted Knockdown
E
nuoB (RIF)
Proportion of Population
1.00
0.75
0.50
0.25
0.00
T0
T1
T2
Treatment
Inducer
Inducer + RIF
F
Fluorescence (AU)
180000
160000
140000
120000
100000
80000
60000
40000
20000
0
nuoB-uninduced
nuoB-induced
NT-uninduced
NT-induced
0.0
6.0
12.0
18.0
23.9
29.9
35.9
41.9
47.9
53.9
59.9
65.8
71.8
77.8
83.8
89.8
95.8
101.8
107.7
113.7
Time
(Minutes)

Figure 27: *nuoB* Knockdown Causes a Subtle Change in COL MIC

Four independently constructed non-targeting (NT) or *nuoB* knockdown strains were plated as a lawn on LB + 1mM IPTG and grown in the presence of a COL MIC test strip. MIC values were read as the concentration line above the intersection between confluent growth and the test strip. The average MICs for NT and *nuoB* were 2 and 1.6 ng/μL, respectively (p = 0.02, 2 tailed t-test with equal variance).

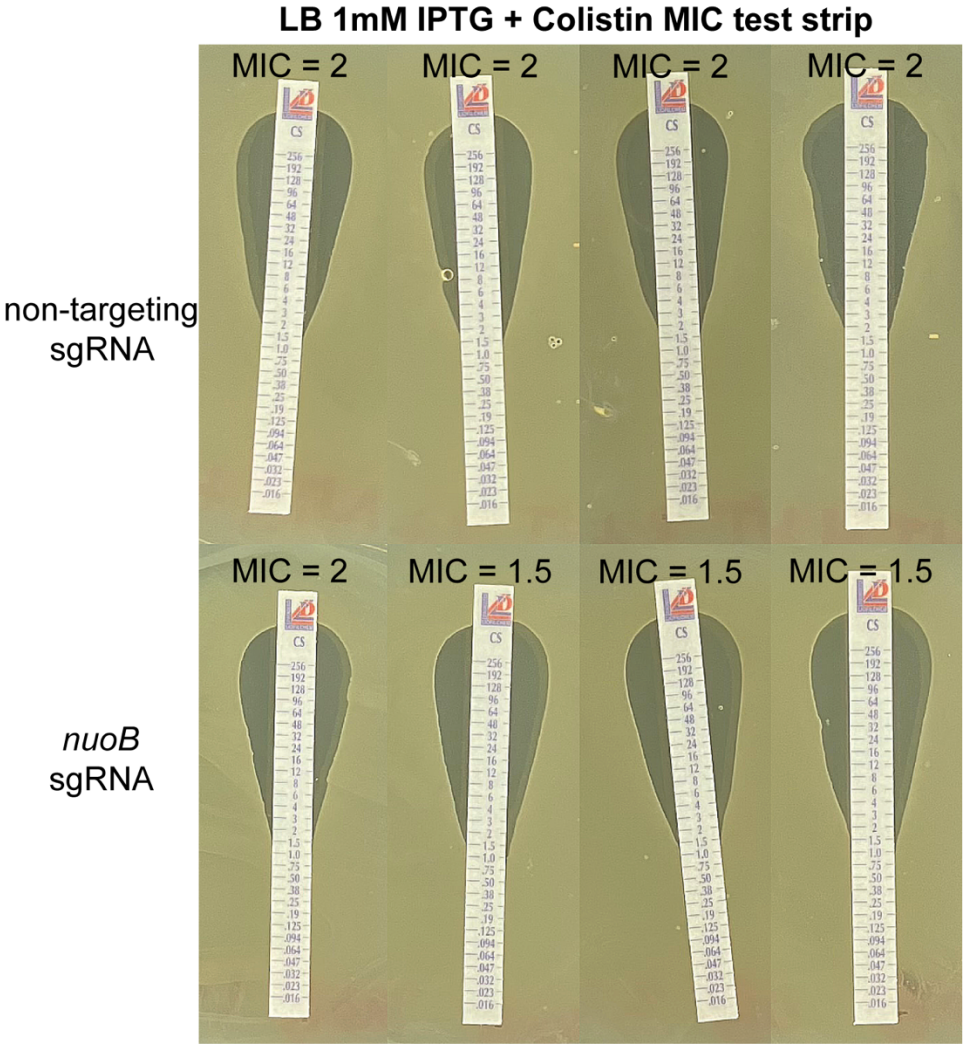

Figure 28: Membrane Potential Analysis in Wild-type and *nuoB* Knockdown Strains

ThT normalized to OD_{600} as a measurement of membrane potential (∆ψ) in non-targeting and *nuoB* knockdown strains. (**A**) and wildtype (**B**). Non-targeting and *nuoB* knockdowns measurements are taken with and without inducer (**A**). Wildtype was treated with CCCP at 0, 4, 6, and 8 ng/µL (**B**).

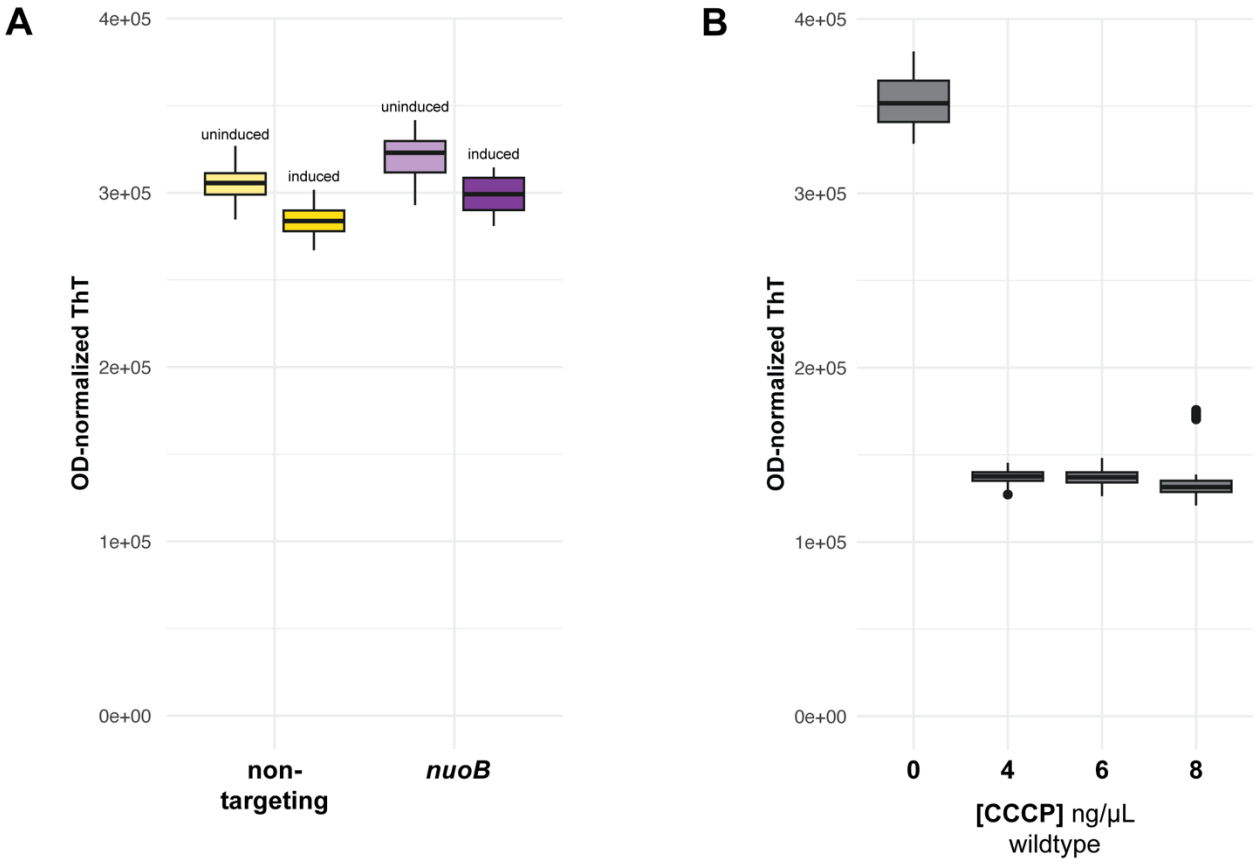

Rifampicin is a relatively large antibiotic (822.9 Da) that targets RNA polymerase (RNAP) in the cytoplasm but is typically avoided for treating Gram-negative infections due to low permeability (19). Consistent with a permeability barrier to rifampicin function (167), we found that knockdown of LOS synthesis and transport genes strongly sensitized cells to rifampicin [enrichment score = 8.83, FDR (afc) = 3.97e-05]. Again, knockdown of genes encoding NDH-1 produced an unexpected phenotype, this time increasing RIF resistance by an unknown mechanism [Figure 25].

To further characterize the NDH-1 RIF resistance phenotype, we examined the knockdown-response curve of *nuoB* with and without RIF treatment. As seen previously with *glnS*, *nuoB* knockdown showed a hormetic response: increasing knockdown of *nuoB* increased relative fitness in RIF until the highest levels of *nuoB* knockdown where growth decreased [Figure 26C-D]. Although MIC changes were modest [Figure 29], our CoMBaT-seq assay showed a clear fitness benefit for *nuoB* knockdown in RIF relative to a non-targeting control [Figure 26E]. We considered that NDH-1 knockdown cells may have reduced permeability, limiting RIF entry into the cytoplasm. To test permeability, we measured uptake of ethidium bromide (EtBr) which fluoresces when bound to DNA in the cytoplasm [Figure 26F]. We found that *nuoB* knockdown cells had a reduced rate of EtBr uptake, demonstrating that cells with reduced NDH-1 activity are less permeable and suggesting a possible mechanism for increased RIF resistance.

Figure 29: *nuoB* Knockdown Causes a Subtle Change in RIF MIC

Four independently constructed non-targeting (NT) or nuoB knockdown strains were plated as a lawn on LB + 1mM IPTG and grown in the presence of a RIF MIC test strip. MIC values were read as the concentration line above the intersection between confluent growth and the test strip. The average MICs for NT and nuoB were 2.25 and 3.25 ng/μL, respectively (p value = 0.03, 2 tailed t-test with equal variance).

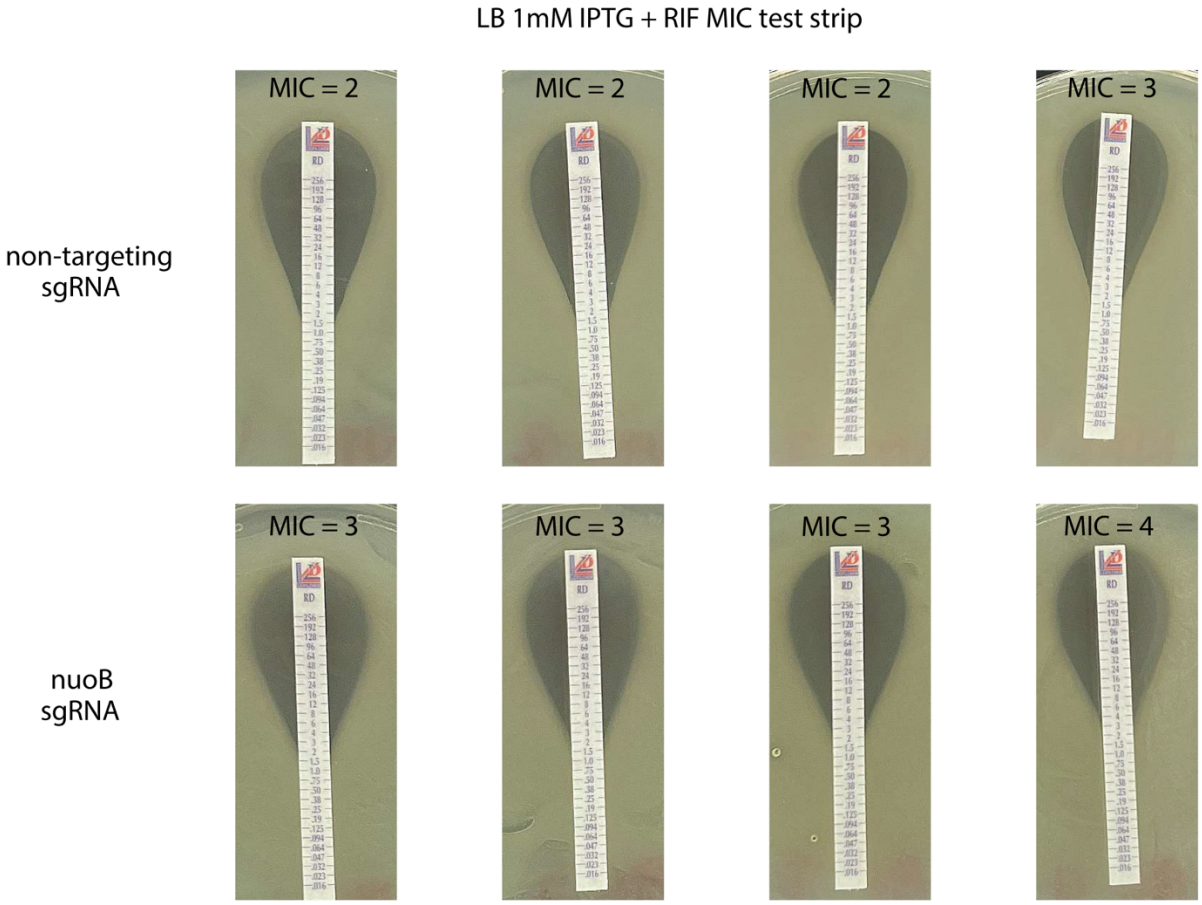

COL and RIF showed the strongest anticorrelated phenotypes in our CRISPRi screen (linear regression, $p<0.001$), with LOS related knockdowns causing resistance to COL and sensitivity to RIF and NDH-1 knockdowns resulting in sensitivity to COL and resistance to RIF [Figure 30]. These anticorrelated phenotypes are consistent with a model in which COL increases the permeability of the outer membrane to RIF (165), but also suggest additional complexities due to *nuo* interactions with COL and RIF. The extent to which NADH-1 modulates COL-RIF synergy will be explored in future studies.

Figure 30: Anticorrelated Gene-Antibiotic Interactions for COL and RIF

Relative fitness score changes for genes encoding NDH-1 or involved in LOS biosynthesis in COL- or RIF-treated conditions relative to untreated.

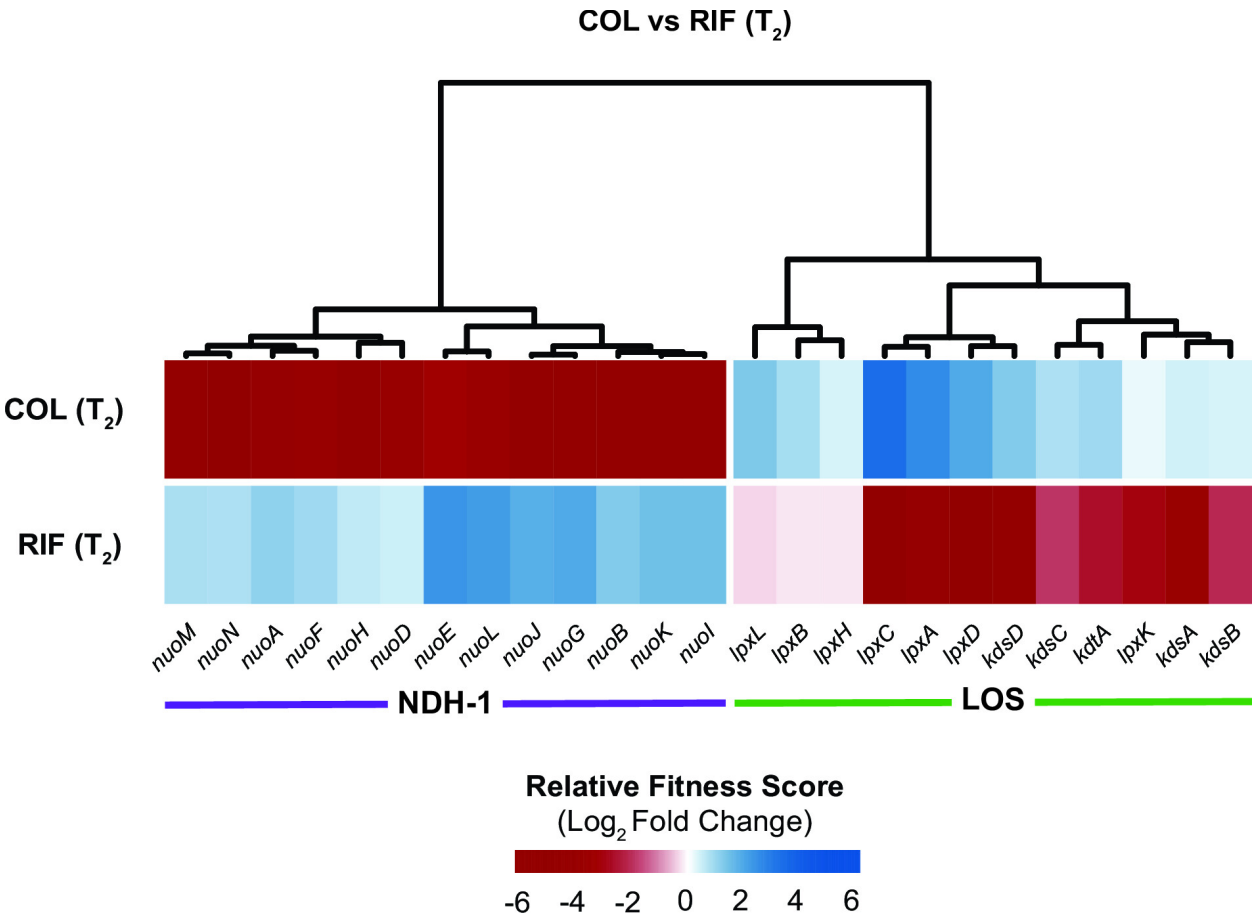

7. Discussion

Bacterial susceptibility to antibiotics is underpinned by species- and condition-specific gene essentiality. The recent lack of innovative treatments for *A. baumannii* and other Gram-negative pathogens can be attributed to our limited knowledge of genetic weaknesses in these bacteria. This work advances our understanding of genetic vulnerabilities in *A. baumannii* by systematically perturbing and phenotyping essential genes. Using CRISPRi to knock down essential gene products, we identified genes that are sensitive to knockdown as well as genes that potentiate or mitigate antibiotic action. Together, these studies define potential targets for antibiotic discovery and provide a genetic approach for understanding synergistic therapies that is broadly applicable.

Our study of essential gene knockdown phenotypes in *A. baumannii* points to both unique and shared genetic vulnerabilities with other bacterial species. Our finding that *A. baumannii* is highly sensitive to depletion of genes encoding NDH-1 highlights a unique weakness in pathogens that are obligate aerobes and a possible therapeutic target. Among the Gram-negative ESKAPE pathogens, only *A. baumannii* is known to require *nuo* genes for aerobic growth in rich medium (168). Recent work from Manoil and colleagues in the non-pathogenic model strain, *Acinetobacter baylyi*, found that genes involved in oxidative phosphorylation were among the first to be depleted from a pool of transposon mutants (71); combining these observations with our CRISPRi results suggests that oxygen-dependent energy production is a physiological linchpin across the *Acinetobacter* genus. Our finding that *A. baumannii* genes involved in PG synthesis and translation are vulnerable to depletion underscores the conserved importance of these pathways across bacterial species (60, 86) and their foundational role as antibiotic targets.

Our finding that knockdown gradients of essential genes treated with antibiotics can mimic hormetic effects seen in dose-response curves (163) has implications for modeling

conditional phenotypes of essential genes and dosing of combination therapies. For most essential genes, complete loss of gene function results in lethality under the majority of conditions. However, our mismatch guide strategy allowed us to examine intermediate levels of essential gene function that may be analogous to partial loss of function alleles found in resistant clinical isolates or adaptive evolution experiments. Partial loss of function mutants can exhibit striking differences in phenotype over a narrow range of function, as we observed with *glnS* and *nuoB* resistance during IMI and RIF treatment, respectively. These hormetic resistance phenotypes fit poorly to established 4-parameter logistic models, emphasizing the importance of considering alternative model parameters and comprehensive statistical approaches when quantifying intricate biological processes. Given our limited set of screening conditions, it is currently unclear how widespread the phenomenon of hormesis is for antibiotic-gene interactions, although we note that clear instances of hormesis were rare in our data. Hormesis in antibiotic interactions may have clinical relevance as well, as doses of combination therapies falling within the concentration window of a hormetic/antagonistic response would be ineffective. Although we could not find further evidence in the *Acinetobacter* literature, certain mutations aaRS genes result in β-lactam resistance in *E. coli* (169), supporting our results. Our ability to predict antagonism between an aaRS inhibitor and carbapenems based on genetic data suggests that screening for antibiotic-gene interactions will have as much value in avoiding antagonisms as it does in identifying potential synergies.

Our data show an unexpected link between NADH dehydrogenase activity and growth inhibition by COL. NDH-1 knockdown strains were highly sensitized to COL in competitive growth assays, but the precise mechanism behind this sensitivity is unclear. Based on our measurements, NDH-1 knockdown primarily affects the ratio of NADH to NAD+ in cells, rather than membrane potential. COL inhibits conversion of NADH to NAD+ by the type II NADH dehydrogenase (NDH-2) in a purified system (166), although at much higher concentrations

than used in our experiments. We speculate that the sensitivity of NDH-1 knockdowns to COL is due insufficient recycling of NAD+, which would be expected to reduce flux through the TCA cycle. In this scenario, CRISPRi knockdown reduces NDH-1 activity while COL inhibits NDH-2 activity, resulting in further skewing of the NADH/NAD+ ratio toward NADH and away from NAD+. Flux through the TCA cycle would be expected to decrease as multiple steps in the cycle require available NAD+ (170, 171). In general, identifying targets that potentiate COL activity may be clinically relevant in the context of combination therapy because toxicity is a major dose-limiting concern of polymyxin antibiotics (172). Employing effective combination treatments using colistin concentrations below toxicity thresholds would greatly improve its clinical utility and safety against *A. baumannii*. Our CRISPRi approach could inform not only combinations with polymyxins, but also other antibiotics which have dose-limiting toxicity concerns that prevent more widespread use.

COL and RIF have been shown to synergistically kill *A. baumannii* and other Gram-negatives (172) in part due to COL disruption of the outer membrane [Vaara:1406489]. The anticorrelated phenotypes we observed in COL and RIF treatment may be relevant to the spectrum of available mutations that allow for the emergence of resistance. For instance, treatment with COL selects for mutations in LOS biosynthesis genes (143), while the loss of LOS promotes permeability to RIF (and other antibiotics (172)). Accordingly, the presence of RIF has been shown to reduce recover of inactivated *lpx* genes in selections for COL resistance (173). Mutations in *nuo* genes are commonly obtained in screens for tobramycin resistance in *P. aeruginosa* (174, 175), supporting a model in which reduced NDH-1 function decreases permeability of the inner membrane to antibiotics. Consistent with this model, we found that EtBr fluorescence, which is often used as a proxy for measuring permeability of small molecules, was decreased in NDH-1 knockdown strains. Mutations in *nuo* can negatively impact other Gram-negative ESKAPE pathogens but are particularly relevant in *A. baumannii* because NDH-1 is

uniquely required for viability. We speculate that anticorrelated phenotypic signatures are predictive of antibiotic synergy in cases where permeability of one antibiotic is enhanced by the second, particularly in the context of bacteria with low permeability such as *A. baumannii* and *P. aeruginosa*. Interrogating a larger chemical genomics dataset with a greater diversity of antibiotics for these organisms will shed light on general rules for antibiotic-gene interactions and their implications for discovering synergy.

Our approach is not without limitations. The high sensitivity of our pooled CRISPRi screens enables us to detect even subtle phenotypes, but these phenotypes may not exceed clinically-relevant thresholds. For instance, we detected several gene-antibiotic interactions with significant pooled phenotypes that resulted in modest MIC changes when assayed in isolation. One challenge with studying essential genes is that excessive knockdown will not only reduce cellular viability but will also select for preexisting suppressors of CRISPRi (often found in the *dcas9* gene (99)). Thus, knockdown levels that enable stable interrogation of essential genes may not be sufficient to push MICs past clinical breakpoints. Nonetheless, our recovery of direct antibiotic targets among the strongest outliers in most CRISPRi screens strongly supports the utility of CRISPRi in elucidating antibiotic function (76, 156). Future work combining CRISPRi with orthogonal essential gene perturbations, such as CRISPR base editing (176), may reveal allele-specific changes in resistance that are often larger in magnitude and more closely reflect resistance mutations found in the clinic. Our work recovered phenotypes for most, but not all the *Ab* essentials. Although we expect some of the non-responsive genes to be false positives from Tn-seq (71), other genes may be non-responsive due to limitations of CRISPRi. For instance, we estimate that our system produces roughly 20-fold knockdown, but variations in guide activity could affect phenotype calls at the margin. Further, TU-level knockdowns could mask phenotypes for some genes, such as eliminating the phenotype of an antitoxin gene in a co-transcribed toxin/antitoxin system.

8. Materials and Methods

8.1. Strains and growth conditions.

Strains are listed in Table 2. Details of strain growth conditions are described in the Supporting Information.

8.2. General molecular biology techniques and plasmid construction.

Plasmids, oligonucleotides and construction listed in Table 2. Details of molecular biology techniques are described in the Supporting Information.

8.3. *A. baumannii* Mobile-CRISPRi system construction.

An *A. baumannii* strain with the Mobile-CRISPRi (MCi) system from pJMP1183 (88) inserted into the att_{Tn7} site (Figure 9A), which constitutively expresses mRFP and has an mRFP-targeting sgRNA, has a growth defect when induced with 1mM IPTG (Figure 9B; “parent”). Strains with suppressors of the growth defect that still maintained a functional CRISPRi system were identified by plating on LB supplemented with 1mM IPTG and selecting white colonies (red colonies would indicate a no longer functional MCi system; Figure 9B-C). gDNA was extracted and mutations in the dCas9 promoter were identified by Sanger sequencing (Figure 9D). The Mobile-CRISPRi plasmid pJMP2748 is a variant of pJMP2754 (Addgene 160666) with the sgRNA promoter derived from pJMP2367 (Addgene 160076) and the dCas9 promoter region amplified from the *A. baumannii* suppressor strain gDNA with oJMP635 and oJMP636. Plasmid pJMP2776, which was used to construct the *A. baumannii* essential gene library and individual sgRNA constructs, was created by removal of the GFP expression cassette from pJMP2748 by digestion with PmeI and re-ligation. This system shows ~20-fold knockdown when targeting the *GFP* gene (Figure 9E). Plasmids were submitted to Addgene.

8.4. *A. baumannii* Mobile-CRISPRi individual gene and gene library construction.

sgRNAs were designed to knockdown essential genes in *A. baumannii* 19606 using a custom python script and Genbank accession #s CP046654.1 and CP046655.1 as detailed in reference (87). Mismatch guides were designed and predicted knockdown was assigned as previously described (19). sgRNA-encoding sequences were cloned between the BsaI sites of Mobile-CRISPRi (MCi) plasmid pJMP2776. Methodology for cloning individual guides was described previously in detail (87). Briefly, two 24-nucleotide (nt) oligonucleotides encoding an sgRNA were designed to overlap such that when annealed, their ends would be complementary to the BsaI-cut ends on the vector.

The pooled essential gene CRISPRi library was constructed by amplification of sgRNA-encoding spacer sequences from a pooled oligonucleotide library followed by ligation into the BsaI-digested MCi plasmid. Specifically, a pool of sgRNA-encoding inserts was generated by PCR amplification with primers oJMP697 and oJMP698 from a 78-nt custom oligonucleotide library (2020-OL-J, Agilent) with the following conditions per 500 µL reaction: 100 µL Q5 buffer, 15 µL GC enhancer, 10 µL 10mM each dNTPs, 25 µL each 10 µM primers oJMP897 and oJMP898, 10 µL 10 nM oligonucleotide library, 5 µL Q5 DNA polymerase, and 310 µL H2O with the following thermocycling parameters: 98°C, 30s; 15 cycles of: 98°C, 15s; 56°C, 15s; 72°C, 15s; 72°C, 10 min; 10°C, hold. Spin-purified PCR products were digested with BsaI-HF-v2 (R3733; NEB) and the size and integrity of full length and digested PCR products were confirmed on a 4% agarose e-gel (Thermo). The BsaI-digested PCR product (without further purification) was ligated into a BsaI-digested MCi plasmid as detailed in (87). The ligation was purified by spot dialysis on a nitrocellulose filter (Millipore VSWP02500) against 0.1 mM Tris, pH 8 buffer for 20 min prior to transformation by electroporation into *E. coli* strain BW25141 (sJMP3053). Cells were plated at a density of ~50,000 cells/plate on 150mm LB-2% agar plates supplemented with carbenicillin. After incubation for 14 h at 37°C, colonies (~900,000 total)

were scraped from the agar plates into LB, pooled, and the plasmid DNA was extracted from ~$1x10^{11}$ cells using a midiprep kit. This pooled Mobile-CRISPRi library was transformed by electroporation into *E. coli* mating strain sJMP3049, plated at a density of ~50,000 cells/plate on 150mm LB-2% agar plates supplemented with carbenicillin and DAP. After incubation for 14 h at 37°C, colonies (~1,000,000 total) were scraped from the agar plates and pooled, the OD_{600} was normalized to 27 in LB with DAP and 15% glycerol and aliquots of the pooled CRISPRi library were stored as strain sJMP2942 at -80°C.

8.5. Transfer of the Mobile-CRISPRi system to the *A. baumannii* chromosome.

The MCi system was transferred to the att_{Tn7} site on the chromosome of *A. baumannii* by quad-parental conjugation of three donor strains—one with a mobilizable plasmid (pTn7C1) encoding Tn7 transposase, another with a conjugal helper plasmid (pEVS74), and a third with a mobilizable plasmid containing a Tn7 transposon encoding the CRISPRi system—and the recipient strain *A. baumannii* 19606. A detailed mating protocol for strains with individual sgRNAs was described previously (87). Briefly, 100 µL of culture of donor and recipient strains were added to 600 µL LB, pelleted at ~8000 x g, washed twice with LB prior to depositing cells on a nitrocellulose filter (Millipore HAWP02500) on an LB plate, and incubated at 37°C, ~5 hr. Cells were removed from the filter by vortexing in 200 µL LB, serially diluted, and grown with selection on LB-gent plates at 37°C.

For pooled library construction, Tn*7* transposase donor (sJMP2644), conjugation helper strain (sJMP2935), and recipient strain (sJMP490) were scraped from LB plates with appropriate selective additives into LB and the OD_{600} was normalized to ~9. An aliquot of sJMP2942 pooled library strain was thawed and diluted to OD_{600} of ~9. Eight mL of each strain was mixed and centrifuged at 8000xg, 10 min. Pelleted cells were resuspended in 4 mL LB, spread on two LB agar plates, and incubated for 5hr at 37°C prior to resuspension in LB + 15% glycerol and storage at -80°C. Aliquots were thawed and serial dilutions were plated on LB

supplemented with gent (150) and LB. Efficiency of trans-conjugation (colony forming units on LB-gent vs. LB) was ~1 in 10^7. The remaining frozen stocks were plated on 150 mm LB plates solidified with 2% agar and supplemented with gent (150) and incubated for 16 h at 37°C. Cells were scraped from plates and resuspended in EZRDM (Teknova) + 25mM succinate + 15% glycerol at OD_{600} = 15 and aliquots were stored at -80°C as strain sJMP2949.

8.6. Library growth experiment.

The *A. baumannii* essential gene CRISPRi library (sJMP2949) was revived by dilution of 50 µL frozen stock (OD_{600} = 15) in 50 mL LB (starting OD_{600} = 0.015) and incubation in 250 mL flasks shaking at 37°C until OD_{600} = 0.2 (~2.5 h) (timepoint = T_0). This culture was diluted to OD_{600} = 0.02 in 4 mL LB with 1mM IPTG and antibiotics (colistin, imipenem, meropenem, rifampicin, and no antibiotic control) in 14 mL snap cap culture tubes (Corning 352059) in duplicate and incubated with shaking for 18 h at 37°C (T_1). These cultures were serially diluted back to OD_{600} = 0.01 into fresh tubes containing the same media and incubated with shaking for 18 h at 37°C again (T_2) for a total of ~10-15 doublings. Cells were pelleted from 1 mL of culture in duplicate at each time point (T_0, T_1, T_2) and stored at -20°C. Final antibiotic concentrations were (in µg/ml): colistin (Sigma C4461): 0.44 and 0.67, imipenem (Sigma I0160): 0.06 and 0.09, meropenem (Sigma 1392454): 0.11 and 0.17, and rifampicin (Sigma R3501): 0.34.

8.7. Sequencing library samples.

DNA was extracted from cell pellets with the DNeasy gDNA extraction kit (Qiagen) according to the manufacturer's protocol, resuspending in a final volume of 100 µL with an average yield of ~50 ng/µL. The sgRNA-encoding region was amplified using Q5 DNA polymerase (NEB) in a 100 µL reaction with 2 µL gDNA (~100 ng) and primers oJMP697 and oJMP698 (nested primers with adapters for index PCR with Illumina TruSeq adapter) according to the manufacturer's protocol using a BioRad C1000 thermocycler with the following program: 98°C, 30s then 16 cycles of: 98°C, 15s; 65°C, 15s; 72°C, 15s. PCR products were purified using

the Monarch PCR and DNA Cleanup and eluted in a final volume of 20 µL for a final concentration of ~20 ng/µL).

Samples were sequenced by the UW-Madison Biotech Center Next Generation Sequencing Core facility. Briefly, PCR products were amplified with nested primers containing i5 and i7 indexes and Illumina TruSeq adapters followed by bead cleanup, quantification, pooling and running on a Novaseq 6000 (150bp paired end reads).

8.8. Library data analysis.

For more information on digital resources and links to custom scripts, see Table 2.

8.9. Counting sgRNA Sequences.

Guides were counted using *seal.sh* script from the *bbtools* package (Release: March 28, 2018). Briefly, paired FASTQ files from amplicon sequencing were aligned in parallel to a reference file corresponding to the guides cloned into the library. Alignment was performed using *k*-mers of 20 nucleotide length—equal to the length of the guide sequence.

8.10. Condition Comparisons – Quantification and Confidence.

Relative fitness scores ($\log_2$ fold change) and confidence intervals were computed using *edgeR*. Briefly, trended dispersion of guides was estimated and imputed into a quasi-likelihood negative binomial log-linear model. Changes in abundance and the corresponding false discovery rates were identified for each guide in each condition individually. Finally, $\log_2$ fold abundance changes were calculated by taking the median guide-level $\log_2$ fold change for perfect match guides; confidence was calculated by computing the Stouffer's *p*-value (*poolr R* package) using FDR for individual guides across genes. Gene functional enrichment was determined using the STRING database (122).

8.11. CoMBaT-seq.

CoMBaT-seq experiments consisted of two competing strains, one containing a non-targeting guide and a second containing a guide targeting a gene of interest. CoMBaT-seq strains were added 1:1 in the presence or absence of the indicated antibiotic and grown as described in “library growth experiment” above. Strain abundance at the end of the experiment was quantified using Nanopore sequencing (performed by Plasmidsaurus or Azenta).

8.12. Knockdown-Response Curves.

Fitting of knockdown response curves is described in detail in the supplemental methods. Briefly, code was adapted from the *drc* (*DoseResponse*) *R* package to generate 4-parameter logistic curves describing the relationship between predicted knockdown (independent) and the $\log_2$ fold change in strain representation (dependent) for all (~10) mismatch guides per gene.

8.13. Supplementary Methods

Strains and growth conditions. *Escherichia coli* and *Acinetobacter baumannii* were grown in Lennox lysogeny broth (LB) (10 g tryptone, 5 g yeast extract, 5 g NaCl per liter; BD 240230) at 37°C in a flask with shaking at 250 rpm, in a culture tube on a roller drum at max speed, in a 96 deep well plate with shaking at 900 rpm, or in a plate reader (Tecan Infinite 200 Pro Mplex) with shaking. Culture medium was solidified with 1.5%-2% agar for growth on plates. Antibiotics were added when necessary: for *E. coli*, 100 µg/mL ampicillin (amp) or carbenicillin (carb), 15 µg/mL gentamicin (gent), or 30 µg/mL kanamycin (kan); and for *A. baumannii*, 150 µg/mL gentamicin (gent) or 60 µg/mL kanamycin (kan). Diaminopimelic acid (DAP) was added at 300 µM to support growth of *E. coli dap*- donor strains. IPTG (isopropyl b-D-1-thiogalactopyranoside) (0 to 1 mM) was added where indicated in the figures or figure legends. Strains were preserved in 15% glycerol at -80°C. *pir*-dependent plasmids were propagated in *E.*

coli strain BW25141 *att*Tn*7*::*acrIIA4* (sJMP3053) for DNA extraction and analysis or in *E. coli* strain WM6026 *att*Tn*7*::*acrIIA4* (sJMP3049) for conjugation.

General molecular biology techniques and plasmid construction. Oligonucleotides were synthesized by Integrated DNA Technologies (Coralville, IA) except the pooled oligonucleotide libraries which were synthesized by Agilent (Santa Clara, CA). Plasmid DNA was purified using the GeneJet plasmid miniprep kit (K0503; Thermo Scientific) or the PureLink HiPure Plasmid Midiprep kit (K210005; Invitrogen). Genomic DNA was purified using the GeneJet genomic DNA purification kit (K0721; Thermo Scientific). DNA fragments were amplified by PCR with Q5 DNA polymerase (M0491; New England Biolabs (NEB)) or OneTaq DNA Polymerase (NEB). DNA was digested with restriction enzymes from NEB. DNA fragments were spin purified using the Monarch PCR & DNA cleanup kit (T1030; NEB) or the DNA Clean & Concentrator kit (D4004; Zymo Research) after digestion or amplification. Linearized plasmids were re-circularized using T4 DNA ligase (M0202; NEB). Plasmids were assembled from restriction enzyme linearized or PCR-amplified vector and PCR products or synthetic DNA fragments using the NEBuilder Hifi DNA assembly kit (E2621; NEB). Individual spacers were cloned into BsaI-digested Mobile-CRISPRi (MCi) plasmids by annealing of two complementary oligonucleotides followed by ligation with T4 DNA ligase (NEB). For additional technical details about cloning individual spacers, see below and reference (87). For details about the pooled CRISPRi library construction, see below. Plasmids were transformed into electrocompetent *E. coli* cells using a Bio-Rad Gene Pulser Xcell on the EC1 setting. Sanger DNA sequencing was performed by Functional Biosciences (Madison, WI). Next Generation Sequencing was performed by the UW-Madison Biotechnology Center Next Generation Sequencing Core using an Illumina NovaSeq 6000.

***E. coli* strain construction.** *E. coli pir*+ cloning (sJMP3053) and mating (sJMP3049) strains expressing the *Listeria monocytogenes* prophage type II-A CRISPR-Cas9 inhibitor protein encoding gene *acrIIA4* (177) were constructed to inhibit dCas9 during Mobile-CRISPRi library construction and conjugation. Additionally, the WT *recA* allele in *E. coli* strain sJMP3049 was replaced with *recA1* to decrease homologous recombination.

Allelic replacement of chromosomal *recA* with *recA1*. An FRT-flanked chloramphenicol resistance (FRT-*cat*-FRT) cassette was inserted on the *E. coli* BW25141 chromosome between *mltB* and *srlA* (closely linked to the *recA1* allele) to facilitate allelic replacement. The FRT-*cat*-FRT cassette was amplified by PCR from plasmid pJMP1356 (88) using primers oJMP211 and oJMP212 (which also have 40 nt homology to the chromosomal insertion site), DpnI digested to destroy the plasmid, and inserted onto the chromosome of strain *E. coli* strain BW25141 (sJMP146) by λ-Red-mediated recombination using pSIM19 (pJMP38) encoding the λ-Red proteins, as previously described (178), resulting in strain sJMP601. The allele was transferred to the *E. coli* WM6026 strain background (sJMP424) by P1–*vir*-mediated transduction, as previously described (179), resulting in strain sJMP604. The *cat* gene was removed by transformation with plasmid pCP20, encoding a constitutively expressed FLP recombinase (pJMP3008), as previously described (180), resulting in strain sJMP624. Identity of the *recA1* allele was confirmed by PCR with flanking primers (oJMP201 and oJMP202) followed by sequencing.

***att*Tn*7*::*acrIIA4* gene insertion.** A plasmid (pJMP3018) bearing a Tn7 transposon encoding the *acrIIA4* gene under the control of a strong constitutive synthetic promoter and a chloramphenicol resistance cassette (FRT-*cat*-FRT) and a plasmid (pJMP442) encoding Tn*7* transposase were co-electroporated into *E. coli* strain BW25113 (sJMP006), using chloramphenicol to select for transposition into the *att*Tn*7* site, resulting in strain sJMP3030. The *att*Tn*7::acrIIA4* allele (Cam^r) was transferred to *E. coli* strain BW25141 or WM6026

expressing *recA* from an unstable mini-F plasmid (sJMP345 or sJMP3040, respectively) by P1–*vir*-mediated transduction, as previously described (179). After serial passaging without selection, the resultant strains after plasmid loss are sJMP3034 or sJMP3043, respectively. The *cat* gene was removed by transformation with a plasmid encoding a constitutively expressed FLP recombinase (pJMP3008), as previously described (180) resulting in final strains sJMP3053 (*E. coli* strain BW25113 expressing *acrIIA4*) and sJMP3049 (*E. coli* strain WM6026 expressing *acrIIA4*).

Growth assay. Growth of *A. baumannii* 19606 WT (sJMP490) and *att*Tn*7*::Mobile-CRISPRi (sJMP6335) in LB with and without 1mM IPTG were compared to assess whether the Mobile-CRISPRi system causes a growth defect. Four individual isolates were grown overnight in 300µL LB in a deep well microtiter plate with shaking at 900rpm. Cultures were diluted 1:1000 in LB or LB + 1mM IPTG and incubated in a plate reader for 16 hr at 37°C with shaking and growth was monitored by measuring OD_{600} every 15 min. This assay was repeated 3 times with 4 independent colonies. Growthcurver (181) was used to compare growth parameters.

Induction assay. Induction of the Mobile-CRISPRi system was assayed by GFP knockdown as described in (87) with adaptations for *A. baumannii*. Briefly, initial cultures (n=4) were grown from single colonies to saturation (18 h) in 300 µL LB + gent in a deep 96-well plate. These cultures were serially diluted 1:10,000 into 300 µL LB medium with no antibiotic and 0 to 1 mM IPTG and grown back to saturation (15 h). Pelleted cells were resuspended in 300µL 1X PBS and 150 µL was transferred to a clear-bottom black microtiter plate and cell density was determined by OD_{600}, and fluorescence was measured by excitation/emission at 482/515 nm using a Tecan Infinite 200 Pro M Plex plate reader. Fluorescence values were normalized to cell density and to measurements from strains not expressing GFP. This assay was repeated 3 times with 4 independent colonies.

Stability assay. Six cultures of *A. baumannii* 19606 *att*Tn*7*::Mobile-CRISPRi (sJMP6335) were serially diluted 1:10^4 in LB (no selection) and grown to saturation. These cultures were passaged every 24 h for 8 days with each passage being ~13 doublings for a total of ~104 doublings. The final culture was serially 1:10 diluted and 3 µL was spotted on plates with and without gent selection. Also, 50µL of culture was streaked on LB to obtain 44 isolated colonies that were then patched on plates with and without gent selection. No difference in plating efficiency or gent resistance was seen indicating that the Mobile-CRISPRi system remains stably incorporated on the *A. baumannii* chromosome for >100 generations even in the absence of selection.

Tn*7* insertion location. Insertion of the CRISPRi expression cassette into the Tn7 att site downstream from *glmS* in *A. baumannii* was confirmed by PCR with primers oJMP60 and oJMP398 (within CRISPRi transposon and upstream of insertion site), oJMP566 and oJMP399 (downstream from insertion site and within the CRISPRi transposon), and oJMP398 and oJMP399 (flanking the insertion site). See Fig S1A.

GO593_00515 knockdown lysis and plaque assay. *A. baumannii* strains with chromosomally located CRISPRi expression cassettes and *E. coli* MG1655 (sJMP163) were grown to saturation in liquid culture medium with or without antibiotic selection, respectively. Cultures were diluted 1:200 into nonselective medium and grown ~4 generations to mid-log. *A. baumannii* cultures were then diluted 1:10 into medium with 1 mM IPTG. P1 lysate was added to sJMP163 cultures as previously described as a lysis positive control (179). *A. baumannii* lysates were collected at 7 hours after induction and filter sterilized. Lysates were spotted on bacterial lawns of *A. baumannii* strain ATCC17978 (sJMP4002) to test for phage activity as previously described (179).

Prophage deletion construction and growth. We hypothesized that gene G0593_00515 is essential because it is repressing expression of toxic gene(s) in the predicted prophage (GenBank CP046654.1; 84,589-131,937). We should, therefore, be able to select for deletion of the prophage in an *A. baumannii* strain with a CRISPRi knockdown of G0593_00515 because that would receive the toxicity. We used a two-step homologous recombination selection/counterselection approach to delete the prophage. First, we assembled homologous regions (~1 kb) upstream and downstream of the prophage (amplified by PCR with oJMP1568/1569 and oJMP1570/1571) adjacently with the AscI-EcoRI fragment of the R6K ori (pir-dependent) plasmid pJMP1183 which also contains kanamycin resistance and mRFP expression cassettes. This plasmid (pJMP4345) was transferred to the chromosome of an *A. baumannii* GO593_00515 CRISPRi knockdown strain (sJMP4341) by conjugation followed by homologous recombination with selection on LB + kan. Red colonies indicate that single-crossover mutants with the plasmid recombined into the genome were selected and grown to saturation in liquid medium. Second, we counter-selected against presence of the prophage by plating on LB with 1 mM IPTG to induce the CRISPR system. The GO593_00515 knockdown has little detectable growth in inducer, so white colonies retaining the ability to grow should be prophage deletions where a second recombination event removed the integrated vector as well as the prophage. Eight individual isolates (strains sJMP4358-4366) were confirmed by PCR with oligos oJMP1241 and oJMP1242 (within GO593_00515) and oJMP1381 and oJMP1382 (flanking prophage).

Prophage deletion/GO593_00515 growth curves. *A. baumannii* strains with chromosomally located CRISPRi expression cassettes with a non-targeting or GO593_00515-targeting guide with and without deleted prophage (sJMP4324, sJMP4341, sJMP4358 and sJMP4360-4365, respectively) were grown to saturation in liquid culture medium with antibiotic selection. The cultures were diluted 1:200 (OD_{600} ~0.02) into nonselective medium with 0 or 1

mM IPTG and grown for 18 hours in a plate reader (Tecan Infinite 200 Pro M Plex) at 37°C with shaking; growth was measured as OD_{600}.

Analysis of growth phenotypes in strains expressing individual sgRNAs. Growth of *A. baumannii* strains with chromosomally located CRISPRi expression cassettes (3-6 individual isolates) was analyzed in a plate reader (Tecan Infinite 200 Pro M Plex at 37°C with orbital shaking) in the presence of IPTG inducer and antibiotics. For strains with sgRNAs targeting *nuoH*, *nuoB*, *lpxC*, and a non-targeting control (sJMP10073, sJMP10074, sJMP10076, and sJMP10081, respectively), after growth to saturation in liquid medium with antibiotic selection, cultures were diluted 1:1000 in media with 0.5 mM IPTG and grown for 18 hours prior to dilution 1:1000 into media with 0.5 mM IPTG plus the following antibiotics (in µg/ml): colistin (2 or 4) or rifampicin (0.48 or 0.96), or no antibiotic control and monitoring of growth for 18 hrs. For strains with sgRNAs targeting *murA*, *glnS*, and a non-targeting control (sJMP10072, sJMP10079, and sJMP10080, respectively), after growth to saturation from individual colonies in liquid medium with antibiotic selection, cultures were diluted 1:200 in media with 1mM IPTG and grown ~4 generations to mid-log phase prior to dilution 1:10 into media with 1mM IPTG plus the following antibiotics (in µg/ml): imipenem (0.09), meropenem (0.17), or no antibiotic control and monitoring of growth for 18 hrs.

Checkerboard assays. Synergistic interactions between antibiotic pairs were evaluated using checkerboard assays in 96-well format. Two-fold serial dilutions of antibiotics were prepared in an 8×8 grid (Corning 3370) at 2× final concentration in LB medium (75 µL/well). For assays with *A. baumannii* 19606 WT (sJMP490), saturated cultures were diluted to OD600 = 0.2 and 75 µL was added to each well (final volume 150 µL, starting OD600 = 0.1). Antibiotic concentration ranges were: fosfomycin (39-2500 µg/mL), imipenem (0.0125-8 µg/mL), and meropenem (0.025-16 µg/mL). For assays with *A. baumannii* Mobile-CRISPRi non-targeting strains (sJMP10081), the final volume was 200 µL containing 1 mM IPTG and antibiotic ranges

of colistin (0.09375-6 μg/mL) and rifampicin (0.0025-2.56 μg/mL). Plates were sealed and incubated at 37°C with shaking (900 rpm for WT, 600 rpm for CRISPRi strains) for 24h. Growth inhibition was defined as OD600 ≤ 10% of the maximum plate value. The fractional inhibitory concentration (FIC) for each antibiotic ($FIC_A$and FIC_B) was calculated as:

$$FIC_A = \frac{[A]_{combo}}{MIC_A}$$

$$FIC_B = \frac{[B]_{combo}}{MIC_B}$$

where $[A]_{combo}$ and $[B]_{combo}$ represent the concentrations of each antibiotic in combination, and MIC_A and MIC_B represent their respective minimum inhibitory concentrations when used alone. The total FIC index was calculated as:

$$FIC_{index} = FIC_A + FIC_B$$

Combinations yielding $FIC_{index} \leq 0.5$ were classified as synergistic, indicating enhanced efficacy of the antibiotics in combination compared to their individual activities.

Imipenem-mupirocin assay. The *A. baumannii* CRISPRi non-targeting strain (sJMP10081) was initially grown overnight on LB agar plates and resuspended into LB containing final concentrations of 1 μg/μL mupirocin or 1 μg/μL mupirocin and two-fold serial dilutions of imipenem (0.0009-1 μg/μL). Cultures were grown to mid-log, diluted to an OD_{600} of ~0.1, and incubated in a plate reader (Tecan Infinite 200 Pro M Plex at 37°C with orbital shaking) for 12 hours before measuring OD_{600}.

Permeability measurements. Strains containing sgRNAs targeting *nuoB* or non-targeting control (sJMP10074 and 10081, respectively) were grown on LB agar plates containing 1mM IPTG overnight. Cell material was scraped off plates, resuspended in equal

volume PBS, and normalized to an OD_{600} of 0.3. Ethidium bromide (EtBr; Bio-Rad #1610433) was added to cell suspensions at a final concentration of 10 ug/mL, and OD_{600} and fluorescence at 545nm excitation/600 emission were read in a plate reader (Tecan Infinite 200 Pro M Plex). Readings occurred in ~1min intervals over the course of ~115 minutes.

NAD+/NADH measurements. Assay was performed with NAD/NADH-Glo™ kit (Promega #G9071). Strains containing sgRNAs targeting *nuoB* or non-targeting control (sJMP10074 and 10081, respectively), inoculated from overnights or resuspended cells, are grown to mid-log in LB. Aliquots of cell cultures are collected and resuspended in PBS, and treated according to manufacturer protocol. Briefly, 100 uL of cell resuspension are treated with equal volume of base solution containing 1% dodecyltrimethylammonium bromide (DTAB) and split into two 50 uL samples for either NAD+ or NADH measurement. NAD+ samples are incubated with 25 uL 0.4N HCl at 60°C for 15 minutes, then neutralized with 25 uL Trizma base. NADH samples are treated with 50 uL HCl/Trizma solution. The prepared NAD/NADH-Glo Detection reagent is added in a 1:1 ratio and incubated for 30-60 minutes. Luminescence is measured using a plate reader (Tecan Infinite 200 Pro M Plex).

Plots. Data were parsed and visualized using the *tidyverse* collection of packages and plotted using *ggplot2* to generate Sankey plots, population bottleneck metrics, volcano plots, and bubble plots. Heatmaps were generated using the *pheatmap R* package. Custom plotting scripts can be found in the project GitHub repo.

Functional enrichments. Functional enrichment analysis was conducted using STRING-db version 11.5. A custom proteome specific to *A. baumannii* ATCC 19606 was uploaded to STRING-db for analysis (Organism ID: STRG0060QIE). Gene knockdowns were ranked based on their relative fitness scores to identify enriched functional categories in each condition. STRING-db parameters for the enrichment were set according to default settings.

Model Selection and Comparison Methodology. We adapted the DRC package in R to analyze mismatch sgRNAs, focusing on parameters such as "shape," "value_min," "value_max," "ek_50," and "hormesis." Our framework extends dose-response relationship analysis by setting parameter constraints, starting values, upper and lower limits. We then compared the Brain-Cousens model with a hormesis parameter (BC-full) to its hormesis-free counterpart, the Log Logistic model (BC-reduced). Using the likelihood ratio test (LRT), genes were evaluated and determined to exhibit biphasic hormetic behavior based on systematic criteria, *i.e*., hormesis fit p-value ≤ 0.5, LRT p-value ≤ 0.5, and with any intermediate fitted value ≥ 1, while terminal phenotype was negative.

Table 2: *A. baumannii* Library Construction and Analysis External Links

Table	URL
Strains	https://github.com/ryandward/acinetobacter_baumannii_CRISPRi_seq/blob/main/Table%20S1%20Strains.md
Plasmids	https://github.com/ryandward/acinetobacter_baumannii_CRISPRi_seq/blob/main/Table%20S2%20Plasmids.md
Oligos	https://github.com/ryandward/acinetobacter_baumannii_CRISPRi_seq/blob/main/Table%20S3%20Oligos.md
Online Resources	https://github.com/ryandward/acinetobacter_baumannii_CRISPRi_seq/blob/main/Table%20S4%20Online%20Resources.md
Guides	https://github.com/ryandward/acinetobacter_baumannii_CRISPRi_seq/blob/main/Table%20S5%20Guides.md
Guides-level Results	https://ryandward.github.io/acinetobacter_baumannii_CRISPRi_seq/Results/guide_level.html
Gene-level Results	https://ryandward.github.io/acinetobacter_baumannii_CRISPRi_seq/Results/gene_level.html
Operon-level Results	https://ryandward.github.io/acinetobacter_baumannii_CRISPRi_seq/Results/transcription_units.html
Operon Annotations	https://github.com/ryandward/acinetobacter_baumannii_CRISPRi_seq/blob/main/Table%20S7%20Operons.md
Ortholog Analysis	https://github.com/ryandward/acinetobacter_baumannii_CRISPRi_seq/blob/main/Table%20S8%20Orthologs.md

Chapter 3. *Pseudomonas aeruginosa* Essential Gene Perturbations that Confer Vulnerability to the Mammalian Host Environment

A version of this work is under review and is currently available on bioRxiv (182).

1. Authors

Neha K. Prasad[†], Ryan D. Ward[†], Michelle A. Yu[†], Michael S. Kwon, Amy B. Banta, Oren S. Rosenberg, Jason M. Peters

[†]These authors contributed equally

2. Contributions

RDW developed comprehensive computational frameworks for population analysis, fitness quantification, and pathway enrichment assessment. RDW identified candidate genes for targeted in vivo validation, generated all figures and figure descriptions, and contributed to manuscript revision.

NKP led experimental design, established the library in *P. aeruginosa*, characterized growth phenotypes, and performed molecular analyses for sequencing preparation.

MAY and MSK executed mouse infection model experiments and associated analyses.

ABB generated the initial CRISPRi strain library in *E. coli*.

OSR secured research funding.

JMP designed the CRISPRi library architecture, prepared the manuscript, and provided additional funding support.

3. Summary:

Multidrug-resistant *Pseudomonas aeruginosa* causes highly morbid infections that are challenging to treat. While antibiotics reduce bacterial populations during infection, the host environment also plays a key role in inhibiting and eliminating pathogens. Identifying genetic targets that create vulnerabilities to the host environment may uncover strategies to synergize with nutrient limitation or inherent immune processes to clear bacterial infections. Here, we screened a partial knockdown library targeting *P. aeruginosa* essential and conditionally essential genes in a murine pneumonia model to identify genes with increased vulnerability in the host environment. We found that partial CRISPR interference (CRISPRi) knockdown of 178 genes showed significant fitness defects in mice relative to axenic culture. We validated two important outliers: *ispD*, encoding a key enzyme in isoprenoid precursor biosynthesis, and *pgsA*, encoding an enzyme involved in phospholipid synthesis that is strongly upregulated in human infections. Partial knockdown of both genes showed decreased virulence in a mouse survival assay but had little impact on *in vitro* growth. The use of CRISPRi screening to uncover genetic vulnerabilities represents a promising strategy to prioritize antibacterial targets that interact with the host environment.

4. Introduction:

Pseudomonas aeruginosa is an environmental bacterium that is a common causative agent of both acute and chronic infections. Due to its inherent resistance to antibiotics and increasing levels of acquired resistance, multidrug-resistant *P. aeruginosa* has been prioritized as a high priority pathogen by the World Health Organization in 2024 (183). While *P. aeruginosa* is estimated to have 321 core essential genes required for growth of multiple strains under multiple culturing conditions (69), only a small fraction of these genes have been targeted for inhibition by small molecule antibiotics in clinical use and clinical development (136).

Although antibiotics are useful for reducing the bacterial burden during infection, their interactions and potential synergy with the native host environment for bacterial clearance are underexploited. It is likely that the extent of target inhibition required for bacterial growth inhibition *in vitro* may exceed that which is needed *in vivo* for specific targets, where the host environment including the immune system mediates clearance of the infection. For example, the synergy of β-lactam antibiotics with host-produced antimicrobial peptides has been shown to reduce the burden of bacteria demonstrating *in vitro* resistance to the β-lactam (184–188). Consequently, target-based whole-cell screens in antibiotic discovery efforts may neglect chemical matter with sufficient *in vivo* efficacy due to poor *in vitro* potency. Comparison of *in vitro* minimal inhibitory concentrations of antibiotics with their associated reduction of bacterial burden during *in vivo* infections is confounded by pharmacokinetic and pharmacodynamic properties of the antibiotic. Thus, a goal of bacterial geneticists has been to substitute chemical inhibition with genetic inhibition, thereby eliminating this confounding effect and expanding the scope of potential antibacterial gene targets to include those without known chemical inhibitors.

For genes that are non-essential *in vitro*, large-scale fitness assessment through transposon insertion sequencing has previously led to the classification of *in vivo* gene essentiality (189). Transposon sequencing of *P. aeruginosa* under various infection conditions has revealed many virulence factors, where gene knockout leads to attenuated virulence of the mutant strain (190). However, anti-virulence interventions have yet to demonstrate clinical efficacy and may not be suitable for people experiencing chronic *P. aeruginosa* lung infections associated with cystic fibrosis, which is often characterized by downregulation or loss-of-function mutations in virulence associated genes (191). Given that complete genetic inhibition strategies cannot be used to probe potential antibiotic targets that are essential *in vitro*, a partial genetic perturbation strategy enables us to probe this valuable category of genes.

Importantly, the notion of essentiality implies a binary effect of genetic inhibition on bacterial fitness, even though intermediary inhibition with chemical drugs indicates that the effect of target inhibition on fitness is, instead, a continuous variable. This gradient is captured by gene vulnerability (192), where partial genetic perturbation of essential genes can confer a quantifiable fitness defect that does not lead to a complete loss of viability. The significance and magnitude of gene vulnerability varies based on culture conditions and can be measured by depletion of the specific mutant from a pooled library (60, 75, 192–194). Essential genes with large *in vivo* vulnerabilities may represent a promising new class of antibacterial targets, since antibiotics must often be administered at high dosages that are capped by dose-limiting adverse effects, and corresponding inhibitors with no *in vitro* efficacy may have been previously overlooked.

Essential genes have been historically difficult to manipulate precisely, as they are requisite for pathogen survival. CRISPR interference (CRISPRi), where a catalytically inactive variant of the Cas9 nuclease (dCas9) sterically hinders RNA polymerase elongation, blocking transcription, is a powerful tool for loss of function screens. We have previously developed Mobile-CRISPRi, a modular and scalable platform to construct knockdown strains in a variety of pathogens (87, 88, 195), which enables us to detect gene vulnerability under *in vitro* and *in vivo* settings.

Previous work phenotyping essential and non-essential genes in mouse models of infection suffered from bottleneck effects or laborious library construction. An inducible CRISPRi screen of genes in the Gram-positive bacterium, *Streptococcus pneumoniae*, in a murine pneumonia model revealed new potential virulence factors and the non-essentiality of a potential antibiotic target that was considered essential *in vitro* (103). However, severe infection-associated bottlenecks limited screen robustness: while 31 genes were identified to have greater *in vivo* vulnerability, knockdown of only one non-essential gene (*purA*) was confirmed to

attenuate virulence. Co-infection with influenza A virus overcame the infection bottleneck allowing for identification of additional virulence-associated genes. A more recent study used an inducible proteolytic degradation library of essential genes in *Mycobacterium tuberculosis* to study antibiotic-essential gene interactions in splenic and pulmonary murine infection model (196). Inducible degradation was achieved by systematically tagging the 3′ ends of essential genes with degradation tags (DAS) and expressing the Clp protease adaptor SspB by feeding mice doxycycline-containing chow. Although this strategy was effective at identifying drug-essential gene synergies, construction of such a library is extremely resource intensive, limiting adoption in other bacteria. Further, some essential genes are recalcitrant to 3′ tagging due to disruption of protein folding. In contrast, the technology and methodology developed in the present study provides a blueprint for overcoming infection bottlenecks that can be readily translated to many other pathogens and infection models.

Here, we developed a partial knockdown strategy that allowed us to probe the vulnerability of essential and conditionally essential *P. aeruginosa* genes *in vivo* [Figure 31]. We generated a pooled CRISPRi library of strains that showed little to no phenotype when grown in rich medium, then screened the library for *in vivo* vulnerability in a murine pneumonia model. Our approach enabled quantification and minimization of experimental bottlenecks by monitoring depletion of non-targeting control single guide RNAs (sgRNAs). We identified dozens of genes that are differentially vulnerable to the host environment, providing a resource for future therapeutic efforts. Finally, we follow up two intriguing hits, *ispD* and *pgsA*, showing that perturbation of these genes outside the pooled context allows for survival of mice that would otherwise succumb to infection with wild-type *P. aeruginosa* at the same dose. The simplicity of our strategy suggests that it will be broadly applicable.

Figure 31: Systematic Identification of Host-Specific Essential Gene Vulnerabilities in *P. aeruginosa*

Overview of the CRISPRi screening approach for identifying in vivo essential genes in *P. aeruginosa* PA14. (A) Essential genes are identified from literature sources based on their necessity for growth in various media, including LB, urine, and sputum, resulting in 526 essential genes. **(B)** A partial knockdown library for PA14 is constructed using Mobile-CRISPRi with a weak constitutive promoter (P_1) to partially inhibit these essential and conditionally essential genes. **(C)** The library is screened for growth effects both in vitro and in a murine pneumonia model, allowing comparison of gene essentiality across different environments. **(D)** Genes that are differentially vulnerable in the host versus LB growth conditions are identified, depicted as a heatmap to illustrate variations in gene vulnerability.

CRISPRi Screening to Identify *In vivo* Vulnerable Essential Genes in *P. aeruginosa*.

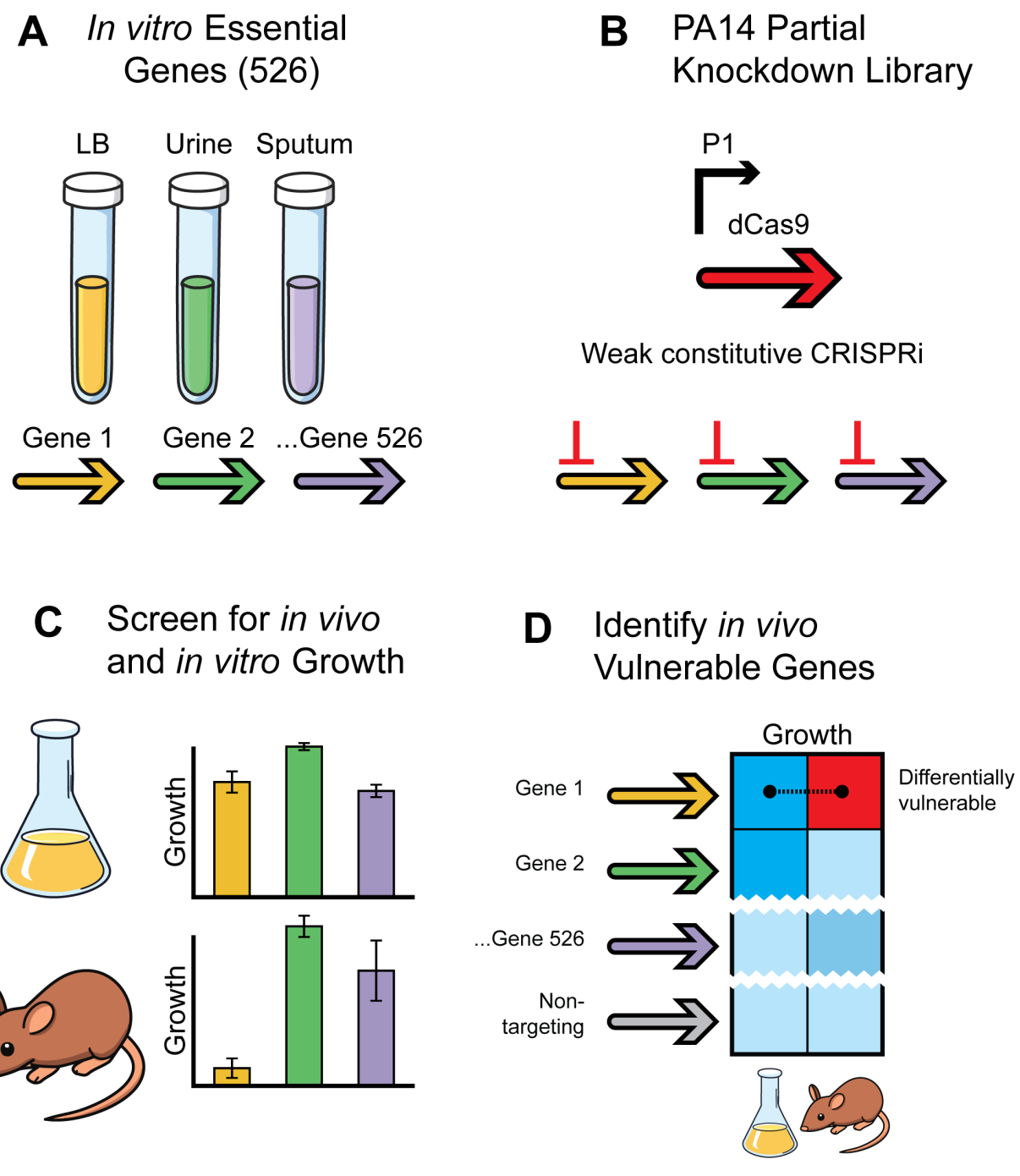

5. Results:

5.1. Pooled Construction of a *P. aeruginosa* Essential Gene Knockdown Library

To mitigate concerns pertaining to the extent and uniformity of gene knockdown when using an inducible CRISPRi promoter in an *in vivo* model, we previously characterized the efficacy of constitutive promoters expressing dCas9 to drive CRISPRi knockdown (87, 88, 195). We elected to use weakest promoter (P_1 resulting in ~10-fold knockdown) for our essential gene knockdown library with the goal of causing a modest perturbation that would show limited fitness effects *in vitro* but potentially large effects *in vivo*.

We selected 526 genes to target in our *P. aeruginosa* PA14 essential gene knockdown library based on a transposon sequencing study that identified the “core” essential genome for *Pseudomonas* (69). Genes that were deemed essential in at least one of the lab- or infection-related growth media (lysogeny broth (LB), minimal medium (M9), synthetic Cystic Fibrosis sputum (SCFM), fetal bovine serum (FBS), and urine) were included in our library design. For each gene in the library, we designed four non-overlapping sgRNA spacers targeting the 5′ end of the coding sequence [Table 4] (87). To assess bottlenecks and control for the effects of CRISPRi knockdown during *in vivo* experiments, we included 1,000 non-targeting sgRNAs in the library as negative controls. Following cloning of the pooled spacer library, CRISPRi vectors were transferred to WT PA14 via triparental mating and were chromosomally integrated into att_{Tn7} site, (87, 195).

We quantified the representation of non-targeting sgRNAs using Illumina next generation sequencing (NGS), finding a normal distribution of spacer counts in the pooled mating strain library and in the pooled PA14 knockdown library (Figure 32). This suggests that there were no substantial technical bottlenecks in construction of the mating strain library for fitness-neutral guides. However, NGS revealed that 10 genes were not detected in the knockdown library after transformation into PA14 (Figure 32), possibly due to excessive knockdown for highly sensitive

genes. Ultimately, the PA14 knockdown library targeted 516 genes represented by at least one sgRNA (Table 3).

Figure 32: Guide RNA Representation Analysis During Library Construction

Density plots showing the distribution of sgRNA counts (Counts per Million) for non-targeting (black) and gene-targeting (red) guides in the *E. coli* mating strain and the PA14 transconjugant.

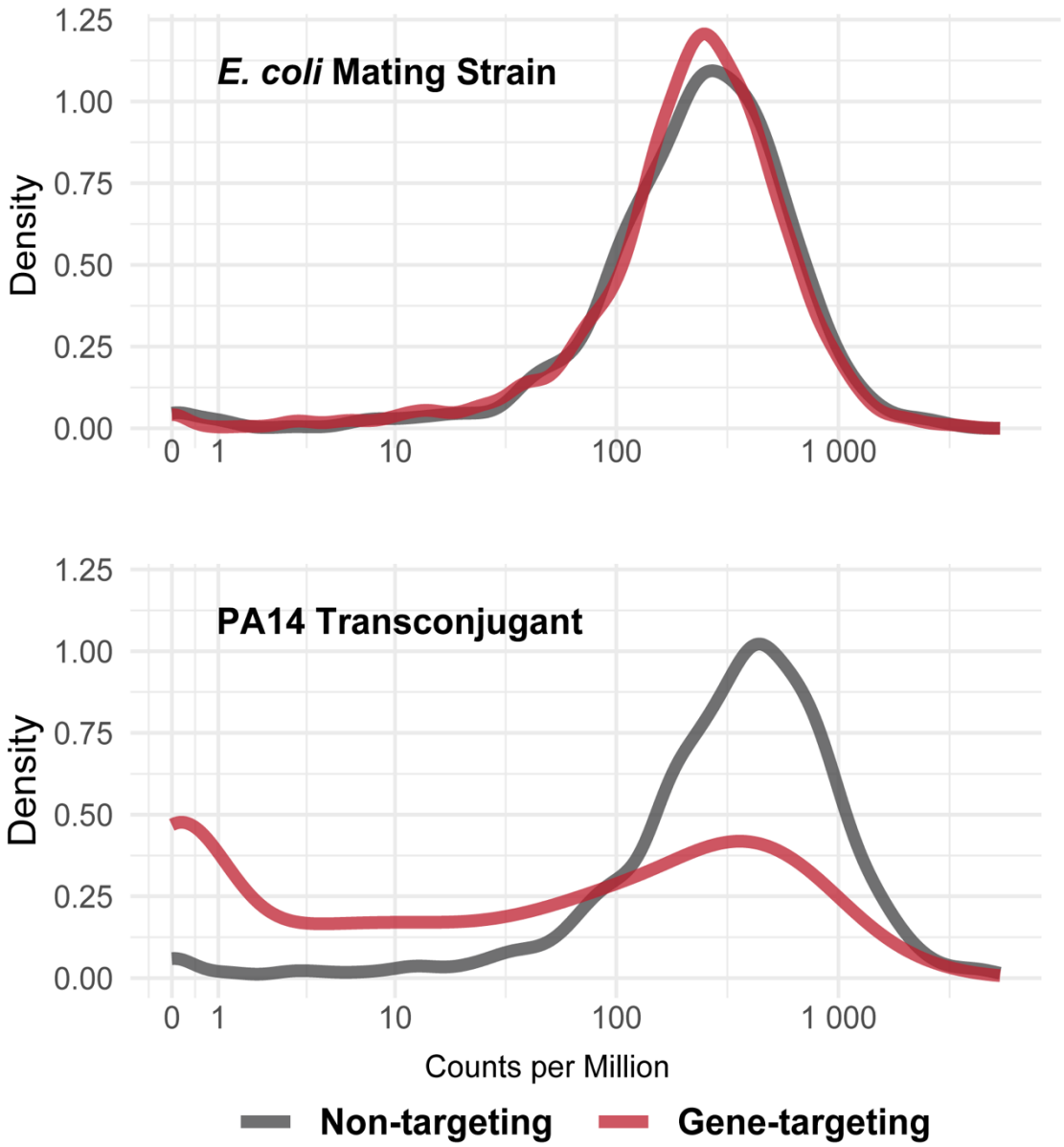

Table 3: *P. aeruginosa* Guide Recovery per Gene in Experimental Conditions

Number of guides recovered in each condition, including *E. coli* donor strain, PA14 transconjugant, LB cultures, and murine infection inocula (high and low dose). Table shows the number of genes with 0, 1, 2, 3, 4, and >0 guides detected in each condition.

		Number of guides per gene					
Sample	**Rep**	**0**	**1**	**2**	**3**	**4**	**>0**
E. coli mating strain	1	0	0	0	14	512	526
PA14 transconjugant	1	10	30	63	125	298	516
Initial inoculum	1	54	82	101	115	174	472
	2	79	104	82	112	149	447
	3	46	73	103	112	192	480
In vitro (LB) 6 generations	1	45	73	102	107	199	481
	2	35	81	103	114	193	491
In vivo (high inoculum)	1	63	98	110	117	138	463
	2	52	88	122	124	140	474
	3	78	100	108	103	137	448
In vivo (low inoculum)	1	102	132	97	107	88	424
	2	99	114	95	105	113	427
	3	203	122	95	75	31	323
	4	80	101	111	105	129	446
	5	84	106	99	93	144	442

5.2. An *in vivo* CRISPRi screen in *P. aeruginosa* murine pneumonia model overcomes infection-associated bottlenecks

Pooled library infections are affected by bottlenecks that can confound the effects of genetic inhibition on measurement of strain loss after infection (103, 130). Bottlenecks can arise from several mechanisms, such as physical barriers to infection, strain loss during inoculation, host clearance pathways as the bacteria transition to invasive disease, or stochastic depletion of mutant strains. Other technical issues with experimental infection models in animals include induction of fatal septic shock with too high of a bacterial inoculum, underrepresentation of the library at time of inoculation or sacrifice, and insufficient duration of infection resulting in too few bacterial doublings–all of which disallow robust detection of strain depletion.

We sought to address these pitfalls in our experimental approach (Figure 33). First, we used direct intratracheal instillation (197), as we reasoned that it would outperform indirect delivery methods (*e.g.,* intranasal instillation) which may generate an additional physical barrier and subsequent strain loss. Second, we minimized the loss of knockdown strains targeting highly vulnerable genes by inoculating mice with a dilution from a thawed glycerol stock, rather than allowing the pooled libraries to grow in axenic culture before inoculation. Third, we amplified sgRNA spacers for library quantification from *P. aeruginosa* colonies that grew after plating lung homogenates to avoid PCR issues that arose from attempting to amplify directly from the lung homogenates (Figure 33B). Finally, as a strategy to distinguish unique vulnerabilities associated with the infection environment from general growth defects conferred by repression of an essential gene, we carried out an *in vitro* screen in parallel to the *in vivo* screen (Figure 33C).

Figure 33: Murine Pneumonia Infection with the PA14 Essential Gene Knockdown Library

(A) Two groups of mice (n=5 per group) were intratracheally instilled with the PA14 knockdown library at high (4.6×10^{11} CFU/animal) or low (4.6×10^{10} CFU/animal) doses to assess infection dynamics. **(B)** After 24 hours of infection, lung homogenates were plated on *Pseudomonas* isolation agar (PIA) containing 30 µg/mL gentamicin. Colonies were harvested after 24 hours, and genomic DNA was extracted for amplicon library preparation and sequencing. **(C)** Concurrently, inoculum samples were cultured in 25 mL of LB medium and grown for six generations before plating on PIA with gentamicin, allowing comparison between in vivo and in vitro growth dynamics.

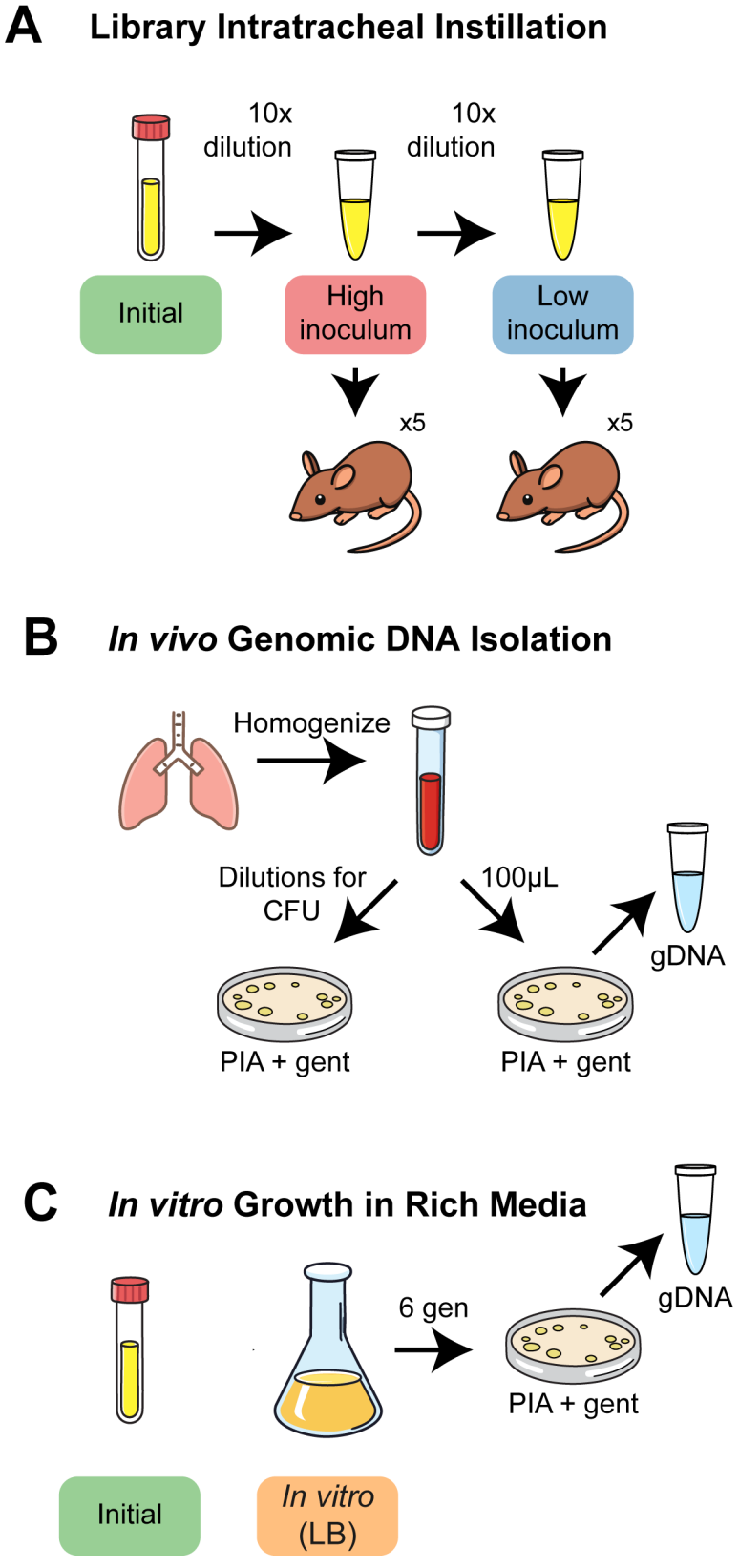
A
Library Intratracheal Instillation
10x dilution
10x dilution
Initial
High inoculum
Low inoculum
x5
x5
B
In vivo Genomic DNA Isolation
Homogenize
Dilutions for CFU
100µL
gDNA
PIA + gent
PIA + gent
C
In vitro Growth in Rich Media
6 gen
gDNA
PIA + gent
Initial
In vitro (LB)

To ensure an appropriate *P. aeruginosa* inoculum for our acute infection experiments, two groups of five mice were intratracheally instilled with approximately 4.6E11 CFU/animal (high inoculum) and 4.6E10 CFU/animal (low inoculum) of the PA14 knockdown library (Figure 33A). This 1-log variation in the bacterial inoculum drastically affected the ability of mice to clear the infection, yielding a screening bottleneck for the low inoculum group. In the low inoculum group, the recovery of animal temperature and weights by the 24-hour time point indicated drastic clearance of infection (Figure 34A). Indeed, the population of negative control sgRNAs was skewed in the lung homogenate samples recovered from this group, suggesting stochastic depletion independent of genetic perturbation (Figure 34B,C). NGS accordingly exposed bottlenecks in the samples recovered from mice infected with the diluted inoculum that prohibited downstream assessment of gene vulnerability.

In contrast, this screening bottleneck was not apparent within the group of mice infected with the more concentrated inoculum. Two of the five mice succumbed to the infection during the 24-hour period, which may be attributable to septic shock, based on the relatively low weight loss coupled with large temperature change in the three surviving mice (Figure 34**A**). In the lung homogenates from the three surviving mice, approximately log-normal distributions of non-targeting controls were recovered, implying the absence of a substantial strain bottleneck (Figure 34B). We evaluated the bottleneck size by calculating the population complexity of the library screened under axenic or *in vivo* conditions, finding that complexity of the non-targeting controls was similar under both conditions. (Figure 34C). The similarity of the distributions between the inoculum and *in vitro* samples suggests that the least fit strains in the PA14 knockdown library had already been depleted during the library construction process (Figure 34B). In contrast, the distribution of gene-targeting sgRNAs is more skewed in the *in vivo* sample, with a larger fraction of sgRNAs showing fewer counts, indicating that the fitness of many knockdown strains is reduced in the infection environment (Figure 34B).

Figure 34: Assessment of Guide RNA Population Maintenance

(A) Individual changes in mouse rectal temperatures and body weights over 24 hours post-infection to assess physiological impacts. Each line represents data from a single animal. **(B)** Distribution of single guide RNA (sgRNA) counts recovered from the inoculum, *in vitro* culture, and lung homogenates from high and low inoculum cohorts, illustrating sgRNA representation across experimental conditions. **(C)** Population bottleneck analysis comparing non-targeting and gene-targeting constructs across *in vitro* growth and both high and low inoculum infection conditions. All plotted data show mean ± SEM, except for panel D, which represents individual animals.

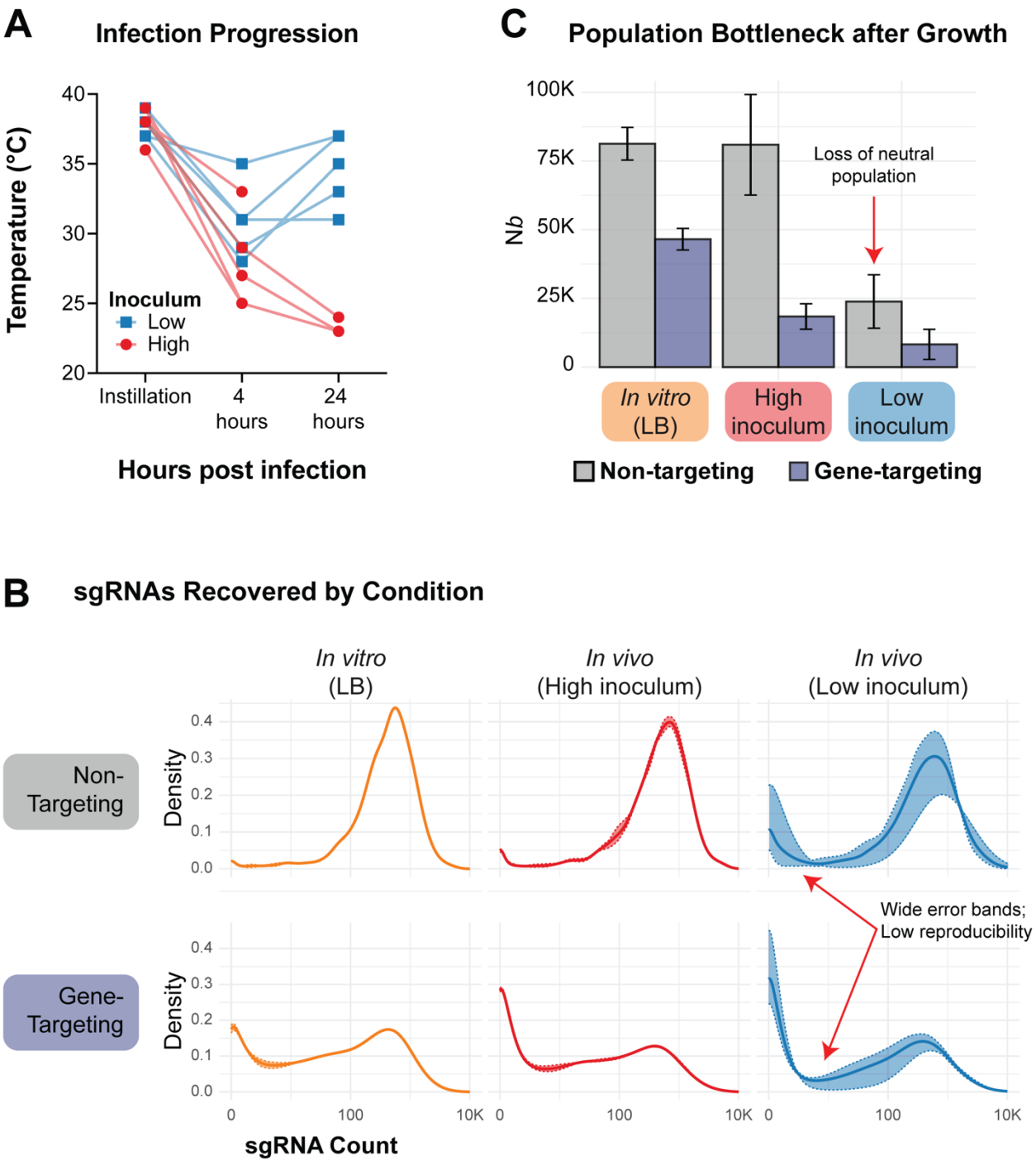
A
Infection Progression
Temperature (°C)
40
35
30
25
20
Inoculum
Low
High
Instillation
4 hours
24 hours
Hours post infection
C
Population Bottleneck after Growth
Nb
100K
75K
50K
25K
0
Loss of neutral population
In vitro (LB)
High inoculum
Low inoculum
Non-targeting
Gene-targeting
B
sgRNAs Recovered by Condition
In vitro (LB)
In vivo (High inoculum)
In vivo (Low inoculum)
Non-Targeting
Gene-Targeting
Density
0.4
0.3
0.2
0.1
0.0
Wide error bands; Low reproducibility
0
100
10K
sgRNA Count

5.3. An *in vivo* CRISPRi Screen Reveals Gene Vulnerability during Murine Pneumonia

In probing the importance of PA14 genes during murine pneumonia infection, we sought to identify hypomorphs with heightened vulnerability to clearance by the host. As the vast majority of genes in the library were targeted by multiple sgRNAs, we calculated the median extent of depletion of the corresponding knockdown strains to determine which essential gene perturbations conferred vulnerability to the mammalian host infection environment relative to nutrient-rich growth medium. Of the 516 genes targeted in the PA14 knockdown library, we were able to calculate changes in relative abundance for 466. Strains corresponding to 178 genes were depleted (Log_2 Fold Change (LFC) < -1, False Discovery Rate (FDR) < 0.05) after 24 hours of growth in the mouse lung compared to cells grown in axenic culture (Figure 35**A,B**). In contrast, no significant *in vitro* vulnerabilities were detected when compared to the distribution of PA14 knockdown library strains in the inoculum, consistent with the idea that knockdown strains with strong negative phenotypes were largely absent from the starting PA14 library. (Figure 35**B**). The lack of detectable genetic vulnerabilities during *in vitro* growth supports the notion that strains in the library inoculum are fit for growth in a nutrition-rich environment.

Figure 35: PA14 Essential Gene Vulnerabilities Identified in *In Vitro* and *In Vivo* Screens

(A) Volcano plots representing changes in strain composition for knockdown strains across two key comparisons: *in vitro* vs. initial (growth effects) and *in vivo* vs. *in vitro* (additional effects in mouse lung environment). Color intensity indicates sgRNA density, with darker colors representing higher density. The y-axis shows FDR (false discovery rate) on an inverted scale, and the x-axis shows the median $\log_2$ fold change for each targeted gene. **(B)** Gene response classification for knockdown strains in *in vitro* and *in vivo* conditions. The Sankey diagram illustrates transitions between response categories: "Vulnerable" (red, FDR ≤ 0.05 and median $\log_2$ fold change < -1), "Resilient" (blue, FDR ≤ 0.05 and median $\log_2$ fold change > 1), and "No Response" (gray, FDR > 0.05). Width of connecting bands indicates the number of genes in each transition. (**C**, **D**) Competitive gene-set enrichment analysis using CAMERA for (**C**) Purine Biosynthesis and (**D**) LPS (Lipopolysaccharide) Biosynthesis & Outer Membrane pathways. Log2 fold change for guides targeting genes in these pathways is shown for *in vitro* vs. initial and *in vivo* vs. *in vitro* comparisons, with FDR values noted below each condition. Boxplots show median (center line), interquartile range (box), and 1.5× interquartile range (whiskers). Individual points represent individual guides, with point size reflecting guide-level significance (FDR). Red lines indicate the significance-weighted median for significantly enriched gene sets (FDR ≤ 0.05).

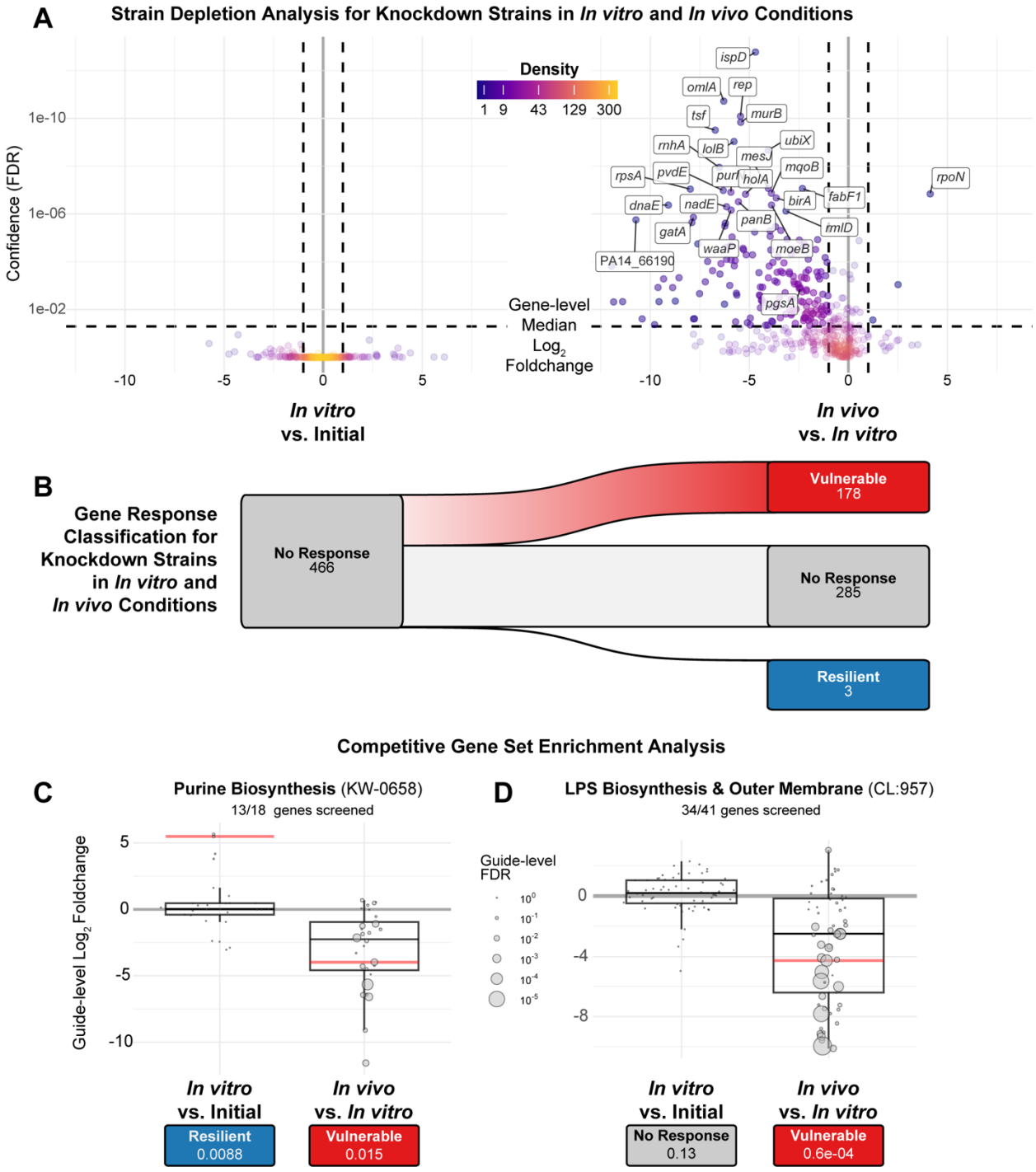
A
Strain Depletion Analysis for Knockdown Strains in In vitro and In vivo Conditions
Density
1 9 43 129 300
Confidence (FDR)
1e-10
1e-06
1e-02
Gene-level Median Log2 Foldchange
-10 -5 0 5
In vitro vs. Initial
In vivo vs. In vitro
ispD
omlA
rep
murB
tsf
rnhA
lolB
ubiX
mesJ
mqoB
rpsA
pvdE
purL
holA
rpoN
dnaE
nadE
birA
fabF1
panB
gatA
rmlD
waaP
moeB
PA14_66190
pgsA
B
Gene Response Classification for Knockdown Strains in In vitro and In vivo Conditions
No Response 466
Vulnerable 178
No Response 285
Resilient 3
Competitive Gene Set Enrichment Analysis
C
Purine Biosynthesis (KW-0658)
13/18 genes screened
Guide-level Log2 Foldchange
5
0
-5
-10
In vitro vs. Initial
In vivo vs. In vitro
Resilient 0.0088
Vulnerable 0.015
D
LPS Biosynthesis & Outer Membrane (CL:957)
34/41 genes screened
Guide-level FDR
10^0
10^-1
10^-2
10^-3
10^-4
10^-5
0
-4
-8
In vitro vs. Initial
In vivo vs. In vitro
No Response 0.13
Vulnerable 0.6e-04

We next investigated *in vivo* vulnerabilities at the pathway level using both gene-level and guide-level analyses. Our initial attempts to aggregate sgRNAs at the gene level failed to identify biological pathways that were enriched for vulnerability in vivo, likely due to increased noise of CRISPRi screening in the host environment relative to axenic culture. To overcome this limitation and better distinguish true signals from noise, we adopted a more nuanced approach. We analyzed all sgRNAs targeting genes within each pathway collectively, effectively increasing the number of measurements we could use to calculate pathway-level statistics. Using this guide-level analysis and competitive gene-set enrichment analysis (CAMERA), we identified several biological pathways that were significantly perturbed and well-represented in the knockdown library—specifically, pathways where at least 70% of the genes were targeted by sgRNAs [Table 4]. Notably, pathways involved in folate biosynthesis (KW-0289) and isoprene biosynthesis (CL:924) exhibited significant *in vivo* vulnerabilities when compared to the *in vitro* baseline, whereas arginine biosynthesis (CL:2388) exhibited *in vivo* resilience [Figure 36]. Additionally, the purine biosynthesis pathway (KW-0658) and the lipopolysaccharide biosynthesis and outer membrane assembly pathway (CL:957) also showed significant depletion *in vivo* (Figure 35**C,D**). This guide-level approach allowed us to detect critical pathways that may not have been identified through traditional gene-level analyses.

Figure 36: Competitive Gene-Set Enrichment Analysis Using CAMERA

(A) Folate biosynthesis (KW-0289, 2/2 genes present), **(B)** Isoprene biosynthesis (CL:924, 5/5 genes present), and **(C)** Arginine biosynthesis (CL:2388, 5/5 genes present) pathways. Log2 fold change for guides targeting genes in these pathways is shown for in vitro vs. initial and in vivo vs. in vitro comparisons, with FDR values noted below each condition. Boxplots represent the distribution of log2 fold changes, and red lines indicate the significance-weighted median for each condition, when the gene-set enrichment is significant (FDR ≤ 0.05). The size of each point reflects guide-level significance (false discovery rate, FDR).

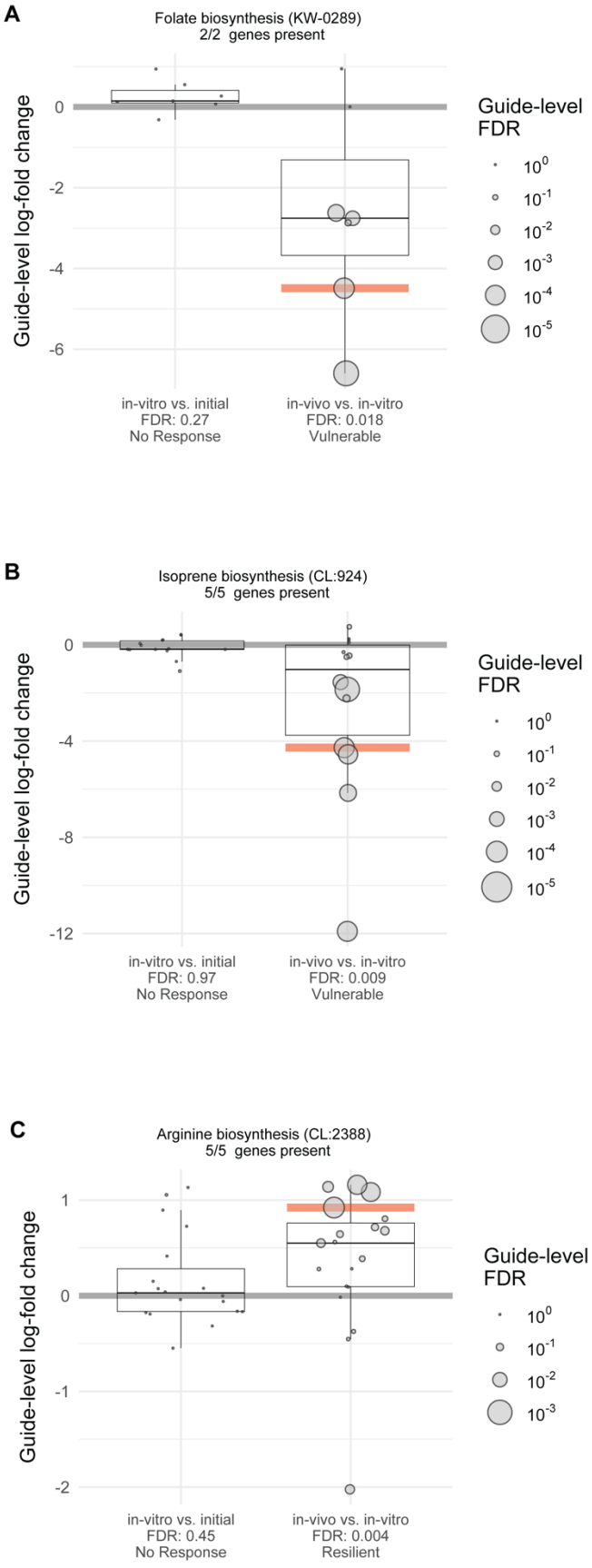
A
Folate biosynthesis (KW-0289)
2/2 genes present
Guide-level log-fold change
0
-2
-4
-6
in-vitro vs. initial
FDR: 0.27
No Response
in-vivo vs. in-vitro
FDR: 0.018
Vulnerable
Guide-level FDR
10^{0}
10^{-1}
10^{-2}
10^{-3}
10^{-4}
10^{-5}
B
Isoprene biosynthesis (CL:924)
5/5 genes present
Guide-level log-fold change
0
-4
-8
-12
in-vitro vs. initial
FDR: 0.97
No Response
in-vivo vs. in-vitro
FDR: 0.009
Vulnerable
Guide-level FDR
10^{0}
10^{-1}
10^{-2}
10^{-3}
10^{-4}
10^{-5}
C
Arginine biosynthesis (CL:2388)
5/5 genes present
Guide-level log-fold change
1
0
-1
-2
in-vitro vs. initial
FDR: 0.45
No Response
in-vivo vs. in-vitro
FDR: 0.004
Resilient
Guide-level FDR
10^{0}
10^{-1}
10^{-2}
10^{-3}

As expected, purine biosynthesis showed significant vulnerability at the pathway level (Figure 35**C**). Previous transposon insertion sequencing (Tn-seq) studies showed that multiple purine biosynthesis genes (*purD*, *purE*, *purF*, *purH*, *purK, purL*, *purN*) are dispensable for growth in rich medium but are required in synthetic sputum (SCFM), whereas *purA* and *purB* are essential in both media (69). A previous study also revealed the essentiality of *purA* in a *S. pneumoniae* murine pneumonia model Exploration of Bacterial Bottlenecks and *Streptococcus pneumoniae*. In our CRISPRi screen, significant gene-level vulnerability was detected for *purA*, *purD*, *purF*, *purL*, *purN*, but not for *purB*, *purK*, *purL*, and *purN*. Given that transposon disruption of *purD*, *purF*, *purL*, and *purN* does not significantly impede bacterial growth in rich media, inhibitors that exploit this *in vivo* vulnerability may not exhibit antibacterial activity in conventional assays, complicating development efforts.

Similarly, CRISPRi knockdown of lipopolysaccharide (LPS) biosynthesis and outer membrane related genes showed significant *in vivo* vulnerability at the pathway level (Figure 35**D**). Tn-seq studies have shown that all seven genes of the LPS transport complex (*lptA*, *lptB, lptC, lptD, lptE, lptF,* and *lptG*) are essential in both rich media and SCFM (69). Specifically, *lptC*, *lptD*, *lptF*, and *lptG* demonstrated significant vulnerability in the mouse lung environment, while *lptA*, *lptB*, and *lptE* did not show this context-specific depletion. In agreement with these findings, a conditional deletion of *lptA* (a.k.a., *lptH*) in PA01 has previously been shown to attenuate virulence in a murine pneumonia model.[24] Partial genetic perturbation allows us to build upon such observations and identify other genes with heightened *in vivo* vulnerability.

The gene encoding the alternative σ factor, RpoN (*rpoN*), is a rare example of a knockdown that decreases *in vivo* vulnerability (Figure 35**B**). RpoN has been shown to regulate virulence pathways (198) and deletion of *rpoN* results in 100-fold less virulence in a mouse thermal injury model (199). However, *P. aeruginosa* commonly evolves *rpoN* loss-of-function mutations during chronic infection of cystic fibrosis patients, suggesting that loss of RpoN

activity may also improve strain fitness in certain contexts (191, 200, 201). Modifications of pathogen-associated molecular patterns (PAMPs), such as those linked to RpoN regulation, enable immune evasion and survival in the infection environment through hindering immune recognition and activation (202, 203). We speculate that virulence-related activities reduced by *rpoN* knockdown are effectively complemented by other strains in the pooled environment, allowing RpoN-deficient cells to escape host clearance mechanisms.

5.4. Validation of Knockdown Vulnerability in Murine Pneumonia Model

Next, we sought to validate hit genes from the pooled screen through assessing survival rates of mice infected with individually constructed knockdowns. Validation with individual knockdown strains could reveal any dependencies of the hypomorphic strain's *in vivo* clearance on the presence of other constituents in the PA14 essential gene knockdown library. For example, deficiencies in one member of the library may only be partially compensated for by other co-infected members of the library in the case of virulence pathways mediated by secreted products, like siderophore production, or community dynamics (204). We pursued two independent strategies to select hypomorphic strains for validation studies: 1) strains that exhibited significantly greater *in vivo* vulnerability than *in vitro* vulnerability; 2) strains corresponding to core essential genes that were previously found to be upregulated during human infection.

Under the first strategy, *ispD* stood out as the most confident hit and was selected for validation studies (**Figure 35B**). As part of the methylerythritol phosphate (MEP) pathway towards the non-mevalonate biosynthesis of isoprenoid precursors, IspD (2-C-methyl-D-erythritol 4-phosphate cytidylyltransferase) catalyzes the formation of 4-diphosphocytidyl-2-C-methyl-D-erythritol. Given most Gram-negative bacterial species use this non-mevalonate pathway whereas humans exclusively use the mevalonate pathway, IspD represents a potential antibacterial target that is currently unexploited in the clinic (205). While fosmidomycin is a

known inhibitor of the MEP pathway through inhibition of IspC (206), few IspD inhibitors with antimicrobial activity have been reported– limited to *Plasmodium falciparum* (207, 208), *Acinetobacter baumannii* (209), and biodefense pathogens *Yersinia pestis* and *Francisella tularensis* (210).

Under the second strategy, *pgsA* stood out as the most confident hit and was selected for validation studies. As part of the selection process, we compared our set of *in vivo* vulnerable genes to a previously published dataset of genes known to be strongly upregulated during human infection (211). Previous studies revealed little overall correlation across the entire genome between transcriptionally important genes, whose expression is affected by a change in the environment, and phenotypically important genes, whose fitness is affected by a change in the environment (212). However, phenotypically and transcriptionally important genes were found to overlap when probing the effects of nutritional stress on metabolic genes (212). We hypothesized that core essential genes that are upregulated during infection will be vulnerable in the host if they cannot be upregulated due to genetic or chemical inhibition, and thus may represent promising antibiotic targets. Based on published datasets, we found that only 4 genes were both “core” essential (69) and significantly upregulated (>2 LFC) during human infection (211): *lptA, lptG, pgsA, cysS*. As previously mentioned, *lptA* and *lptG* are part of the lipopolysaccharide transport system, and a conditional deletion of *lptA* in *P. aeruginosa* has previously been shown to have attenuated virulence in a murine pneumonia model (213). The remaining two genes, *pgsA* and *cysS*, are involved in phospholipid biosynthesis and tRNA aminoacylation, respectively. Of the four genes, only *lptG* and *pgsA* exhibited significant vulnerability when comparing *in vivo* to *in vitro* conditions, indicating specific depletion in response to the mouse lung environment [Table 4]. Since *pgsA* was observed to be the most significantly upregulated of the four during human infections, the corresponding knockdown was chosen for validation studies.

Genetic knockdown mutants of *ispD* and *pgsA*, as well as a control non-targeting strain (NTC), were generated with Mobile-CRISPRi using the same P_1 constitutive promoter from the pooled library. As expected, growth of the *ispD* and *pgsA* partial knockdown mutants in LB media was not substantially different from either WT PA14 or the non-targeting control strain (**Figure 37A**), demonstrating the lack of *in vitro* fitness defects.

Figure 37: Effects of *ispD* and *pgsA* Knockdowns on Virulence and Mouse Thermoregulation

(A) In vitro growth curves of wild-type PA14, non-targeting control (NTC), *ispD* knockdown mutant, and *pgsA* knockdown mutant. Lines represent the mean, and shaded areas represent SEM across biological replicates. **(B, C)** Survival curves of mice infected with wild-type PA14, *pgsA* knockdown, *ispD* knockdown, or NTC mutants. **(D, E)** Changes in body temperature of mice infected with the indicated strains. Lines represent mean values, and shaded areas indicate SEM. **(F, G)** Temperature loss at 20 hours post-infection with the indicated strains. Data are presented as mean ± SEM for 6 to 8 mice per group. Statistical analysis was performed using one-way ANOVA compared to wild type. $^{**}p \leq 0.001$; $^{***}p \leq 0.0001$.

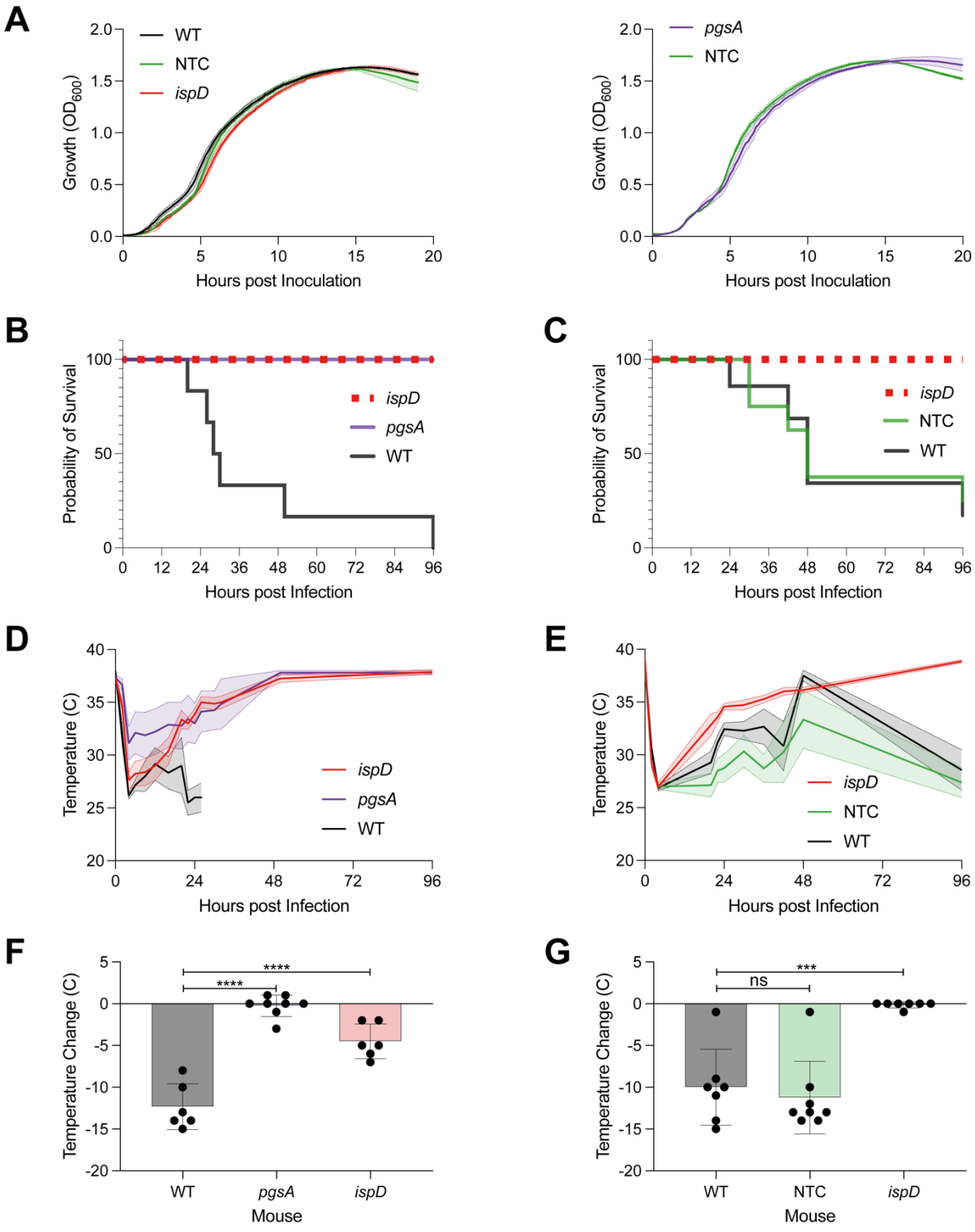
A
WT
NTC
ispD
Growth (OD600)
Hours post Inoculation
pgsA
NTC
Growth (OD600)
Hours post Inoculation
B
Probability of Survival
ispD
pgsA
WT
Hours post Infection
C
Probability of Survival
ispD
NTC
WT
Hours post Infection
D
Temperature (C)
ispD
pgsA
WT
Hours post Infection
E
Temperature (C)
ispD
NTC
WT
Hours post Infection
F
Temperature Change (C)
****
****
WT
pgsA
ispD
Mouse
G
Temperature Change (C)
***
ns
WT
NTC
ispD
Mouse

To validate our screen and confirm that *ispD* and *pgsA* knockdowns were defective for pathogenesis outside of the pooled context, we monitored the survival of mice infected with *ispD* and *pgsA* hypomorphs individually. We intratracheally instilled planktonic monocultures of the *pgsA* and *ispD* knockdown mutants as well as the negative control strain and WT PA14 at 2E6 CFU/animal. Mice infected with the *ispD* and *pgsA* mutants showed 100% survival over 4 days, while the mean survival time of mice infected with WT PA14 or the non-targeting control strain was substantially lower (**Figure 37B, C**). This difference in pathogenicity is also reflected by the observation that mice instilled with *ispD* or *pgsA* knockdown strains more rapidly recovered their body temperature post-infection (**Figure 37D, E**), including a statistically significant difference in temperature loss at the 20-hour time point (**Figure 37F,G**). These findings suggest that partial inhibition of the core essential genes *pgsA* and *ispD* significantly enhances infection clearance *in vivo,* despite the lack of noticeable phenotypic effects *in vitro.*

6. Discussion:

Our pooled *in vivo* CRISPRi screen reveals a heightened vulnerability to the host environment for 178 PA14 genes, providing a genetic resource for promising therapeutic targets. In particular, genetic perturbation of the essential genes *pgsA* and *ispD* did not significantly affect the growth of PA14 in axenic culture, but the same perturbation *in vivo* impeded productive host infection by these mutants. Given that these bacterial genes are required for growth in a mammalian host and are not conserved in humans, they may have high therapeutic potential.

Perturbation of both *pgsA* and *ispD* would both be expected to disrupt envelope functions in *P. aeruginosa*: *pgsA* by affecting phospholipid composition (214) and *ispD* by affecting the levels of isoprenoid precursors available for peptidoglycan synthesis (215). However, the precise mechanisms of how this disruption would cause increased sensitivity *in vivo* are unknown. Connections between bacterial isoprenoids and the human immune system

are well established, suggesting that immune detection could play a role (216). Vγ9/Vδ2 T cells are known to detect (E)-4-Hydroxy-3-methyl-but-2-enyl pyrophosphate (HMB-PP), a MEP pathway intermediate produced by the enzyme IspG (217). This special subset of T cells rapidly responds to the presence of microbes in human blood (216). As IspD lies upstream of IspG in MEP synthesis, the expectation would be that *ispD* knockdown would ultimately produce less HMB-PP and, therefore, reduce stimulation of Vγ9/Vδ2 T cells. Perhaps the potential effects on membrane disruption outweigh any potential immune evasion gained from reducing HMB-PP production. Future work will investigate the impacts of *pgsA* and *ispD* on cell physiology and membrane integrity.

There are limitations to the experimental design of this study. Firstly, the vulnerability profiles are dependent on the extent of knockdown elicited by the P_1 promoter and consistent efficacy across the sgRNAs targeting each gene. Stronger inhibition may reveal vulnerabilities for other genes that were not significantly sensitive to repression driven by P_1 in either *in vitro* or *in vivo* conditions. Conversely, weaker inhibition may alleviate growth-hampering fitness defects that may have led to underrepresentation of essential gene knockdown mutants in the inoculum. Secondly, comparison of *in vitro* fitness defects to *in vivo* fitness defects is inherently affected by the number of doublings that proceed under both conditions. Since the depletion of an unfit strain is expected to increase in magnitude over time, the fitness defect may not be detected if too few doubling times are captured. The *in vitro* 6-generation time point (OD_{600nm} 0.01 to 0.64) was chosen to mimic antibacterial discovery platforms, which typically track bacterial growth from a log-phase culture diluted to 1E5–1E6 CFU/mL until stationary phase. However, *in vivo* generation time likely does not match *in vitro* generation time, further complicating the comparison. Lastly, loss of function hypomorphs generated by gene knockdowns do not precisely mimic the effects of small molecule antibiotics, which may produce effects more like specific genetic alleles (*e.g.,* loss of function in a specific domain or gain of function).

Importantly, the genetic vulnerability insights gleaned in this study may be a proxy for *P. aeruginosa* vulnerability to chemical inhibitors, revealing possible targets for small molecule inhibitors. Partial perturbation of genes corresponding to enzymes with natural substrates is akin to non-competitive chemical inhibition, as target depletion is equivalent to reducing V_{max} while leaving K_m unchanged (218). Furthermore, emerging therapeutic modalities such as CRISPR systems, targeted protein degradation, or antisense technology closely mimic the results of our partial genetic inhibition approach. However, just as the development of non-traditional antibacterials targeting virulence pathways has proven challenging due to the lack of *in vitro* MICs, inhibitors of genes with enhanced *in vivo* vulnerability may face similar barriers to drug development. Developing *in vitro* assays or identifying non-mammalian model organisms that are predictive of exploiting *in vivo* vulnerabilities (219) is critical for capitalizing on this paradigm of target prioritization.

The phenomenon where greater vulnerability is observed *in vivo* than *in vitro* for certain genes suggests that *in vitro* growth inhibitory measurements may undervalue the therapeutic potential of inhibiting these genes *in vivo*. Considering that many small molecule antibiotics have dose-limiting toxicities that have stymied their clinical development (136), the concept of achieving high efficacy of bacterial clearance with a reduced drug dose is especially pertinent.

7. Data and code availability

The DNA sequencing data have been deposited at NCBI BioProject as Database: PRJNA117831. All code is openly available on GitHub ryandward/pseudomonas_analytics.

8. Materials and Methods:

8.1. Strains and Growth Conditions

Escherichia coli and *Pseudomonas aeruginosa* were grown in lysogeny broth (LB), Lennox (BD240230; 10 g tryptone, 5 g yeast extract, 5 g NaCl per liter) at 37°C aerobically in a

flask with shaking at 250 rpm or in a culture tube on a roller drum. For growth on plates, LB was solidified with 1.5-2% agar (BD 214530). Antibiotics were added when necessary: *E. coli* (100 µg/mL ampicillin or carbenicillin, 15 µg/mL gentamicin) and *P. aeruginosa* (30 µg/mL gentamicin). Diaminopimelic acid (DAP) was added at 300 µM to support growth of DAP-auxotrophic *E. coli* strains. All strains were preserved in 15% glycerol at -80°C. Strains are listed in Supplementary Table 4.

8.2. Mobile-CRISPRi Individual Gene and Gene Library Construction

sgRNAs were designed to knockdown essential genes (4 guides/gene plus 1000 non-targeting controls, 3112 total) in *P. aeruginosa* PA14 using a custom python script and *P. aeruginosa* genome sequences; RefSeq accession numbers NC_002516.2 and NC_008463.1 (87). Gene knockdowns included in the library were selected based on essential and conditionally essential genes defined in multiple growth conditions including LB, M9 minimal media, sputum, serum, and urine, with targeted genes [Table 4]. sgRNA-encoding sequences were cloned into Mobile-CRISPRi (MCi) plasmid pJQ47 (pJMP2632, Addgene 134646, which has the sgRNA expression under control of the pTrc promoter and *Homo sapiens* codon-optimized *S. pyogenes* dCas9 expression under control of the Anderson BBa_J23117 weak constitutive promoter (195).

For individual gene construction, the plasmid vector was purified using the Purelink HiPure Plasmid Midiprep kit (Invitrogen K210005) and digested with BsaI-HFv2 (NEB R3733). Two 24-nucleotide oligonucleotides ("top" and "bottom") encoding an sgRNA were designed with appropriate overhangs for Golden Gate Assembly. Oligos (2 µM each) were separately treated with T4 polynucleotide kinase and then annealed in 1X CutSmart buffer (NEB) at 95ºC for 5 min followed by cooling to room temperature. The annealed insert (2 µL of a 1:40 dilution) was ligated into 50 ng BsaI-digested vector using T4 DNA ligase (NEB M0202). Plasmids were transformed into electrocompetent pir+ *E. coli* strain BW25141 and purified using the GeneJet

Plasmid Miniprep kit (Thermo K0503). Following sequence confirmation, plasmids were transformed into electrocompetent pir+ *E. coli* mating strain WM6026.

Pooled CRISPRi plasmid libraries were cloned as described previously with minor modifications (26). A pooled sgRNA library [Table 4] was ordered as single-stranded DNA oligonucleotides (Twist Bioscience) and generated by PCR amplification using Q5 DNA polymerase with the following components per 100 µL reaction: 20 µL Q5 buffer, 3 µL GC enhancer, 2 µL 10mM each dNTPs, 5 µL each 10 µM primers oJMP852 and oJMP853, 2 µL 10 nM oligonucleotide library, and 1 µL Q5 DNA polymerase (NEB M0491). Thermocycling conditions were: 98°C for 30s; 15 cycles of 98°C for 15s, 56°C for 15s, 72°C for 15s; followed by final extension at 72°C for 10 min. PCR products were digested with BsaI-HFv2 and ligated into BsaI-digested MCi plasmid (87). The ligation was purified by spot dialysis on nitrocellulose filter against 0.1 mM Tris, pH 8 buffer for 20 min. The library was transformed into *E. coli* BW25141, achieving approximately 90,000 colonies (~30x coverage) across multiple plates. Colonies were pooled, plasmid DNA extracted, and transformed into WM6026 mating strain, yielding approximately 300,000 colonies (~100x coverage). Library stocks were normalized to OD600 = 8 in LB with DAP and 15% glycerol for storage at -80°C.

8.3. Transfer to *P. aeruginosa* PA14

The Mobile-CRISPRi system was transferred to PA14 through tri-parental mating as described for individual guides and for pooled library construction (26) with minor modifications. Donor strains (*E. coli* WM6026 containing either the CRISPRi plasmid or Tn7 transposase) were grown in LB with ampicillin and DAP, while the PA14 recipient was grown in LB without supplements. Cultures were normalized to OD600 ~3 and mixed in equal proportions (100 µL of each strain for individual constructs; 1.2 mL of each strain for library construction). Mixed cells were spotted onto cellulose filters (13 mm for individual constructs, 25 mm for library; MF-Millipore HAWG01300 or HAWG02500) and incubated at 37°C for 5 hours. Cells were

recovered and plated on selective media (LB with gentamicin, no DAP). For library construction, approximately 240,000 colonies (~80x coverage) were collected. Library stocks were normalized to OD600 = 10 in LB with 15% glycerol for storage at -80°C.

8.4. Mouse infection with pooled Mobile-CRISPRi library

Starting with the resuspension of the glycerol stock in PBS, the inocula were prepared with two serial ten-fold dilutions. The more concentrated of the two inocula was diluted and spread on PIA and PIA + 30 µg/mL gentamicin plates for CFU enumeration. The remaining contents of the glycerol tube were centrifuged, and the pellet was frozen for gDNA extraction.

Pathogen-free male C57BL/6J mice at 8 weeks of age were purchased from Jackson Laboratories. Animal experiments were conducted in accordance with the approval of the Institutional Animal Care and Use Committee (IACUC) at UCSF. A total of 10 mice were anesthetized with isofluorane prior to intratracheal instillation with 50 µL of the *Pseudomonas* knockdown library per an established protocol (22). Animal weights and rectal temperatures were measured at every 6 hours to monitor the course of the infection.

Mice were sacrificed 24 hours post-infection. Lungs were collected in 3 mL of sterile PBS and homogenized by grinding the lung tissue against a cell strainer with the back of a syringe plunger under sterile conditions. 100 µL of lung homogenates were directly plated on 10 PIA + 30 µg/mL gentamicin plates. Then the homogenates were diluted to various degrees in LB media and the same dilution was plated on both PIA and PIA + 30 µg/mL gentamicin plates for CFU enumeration. The plates were incubated for 48 hours prior to harvest. 3-6 mL of LB was used to scrape colonies off PIA + 30 ug/mL gentamicin plates with an L-shaped spreader, and the 10 plates were combined to generate each mouse sample. These cell suspensions were centrifuged and stored at -80 °C prior to gDNA extraction.

8.5. Mouse infection with single strains

In separate experiments, 5 mL ON cultures of *ispD-P$_1$*, *pgsA-P$_1$*, *mrfp-P$_1$*, and WT single-strain knockdown mutants in LB +/- 30 µg/mL gentamicin were grown from glycerol stocks at 37 °C with shaking at 225 rpm. After 16 hours, cultures were diluted 1:100 in 3 mL LB +/- 30 µg/mL gentamicin and were incubated with shaking until OD_{600nm} measured 0.64 (approximately 3 hours). 1 mL of the sub-culture was washed and resuspended in 1 mL PBS. The suspensions were diluted according to predetermined calculations based on OD_{600nm} measurements to yield a target inoculum of 2E6 CFU/animal. Each group contained 6 to 8 C57BL/6 mice at 8 to 12 weeks of age obtained from Jackson Laboratory, and the prior mouse infection protocol was followed. Survival was measured over 96 hours with temperature and weight measured every 6 hours.

8.6. Amplicon library preparation & analysis

Qiagen DNeasy Blood & Tissue kit was used to extract gDNA from samples, and NEBNext Ultra II Q5® Master Mix was used for amplicon library preparation. Custom-made TruSeq primers extend the amplicon to incorporate the i5 and i7 ends, which are recognized by DualSeq primers procured from the Chan-Zuckerburg Biohub. The DualSeq primers are indexed to indicate sample identity and were demultiplexed after NGS. To determine number of reads needed from NGS, the number of unique barcodes was multiplied by a factor of 1,500 (3,112 * 1,500 = ~5,000,000 reads) for robust detection of strain depletion.

8.7. Growth Curves

3 mL LB + 30 µg/mL gentamicin cultures were inoculated with each PA14 strain and incubated at 37 °C with shaking at 225 rpm for 16 hours. Cultures were diluted 1:100 into fresh LB media and 200 µL of the respective cultures was added to each well in a 96-well plate. This plate was covered with an optically clear seal, and a needle was used to poke holes in each of the wells. OD_{600nm} were monitored during incubation in a microplate reader (Synergy H1; BioTek

Instruments, VT) with continuous, fast, double orbital shaking. Samples were blanked with a well containing LB media. Results are representative of three technical replicates and at least two biological replicates.

8.8. Guide RNA Sequence Abundance Analysis

Sequencing data were filtered to include samples with >5 million reads and >85% mapping rate. Analysis was performed using edgeR (v4.2.0) with a quasi-likelihood negative binomial model framework, comparing three conditions: initial inoculum, in vitro growth, and in vivo growth (high-inoculum samples only, due to increased noise in low-inoculum conditions). Control guides served as reference for baseline corrections. For genes with multiple guides, significance estimates were combined using Stouffer's method and effect sizes were summarized using median log-fold changes. Statistical significance was assessed using quasi-likelihood F-tests with FDR correction for multiple comparisons. Data analysis and visualization were performed using R (packages: edgeR v4.2.0, data.table v1.15.4, ggplot2 v3.5.1).

8.9. Population Bottleneck Estimations

Population bottleneck sizes were estimated using frequency-based calculations as described in Abel, et al. (130). Guide frequencies were compared between the initial inoculum and each subsequent condition to estimate the effective population size (*N*b) maintained through each transition. Analysis was performed separately for control and knockdown guides. The average *N*b values were calculated across replicates for each condition, with error bars representing standard error of the mean. This analysis provides quantitative estimates of the population complexity preserved throughout different stages of the experiment.

8.10. Gene-Set Enrichment Analysis

Functional enrichment analysis was performed using predicted genome interactions from STRING-DB (v12.0.2) using the P. aeruginosa UCBPP-PA14 proteome (accessible at

https://version-12-0.string-db.org/organism/STRG0A01FJP). Guide-level differential abundance results were analyzed using camera (limma v3.60.0) to perform competitive gene set testing, with control guides serving as the background set. Gene sets were derived from STRING-DB functional annotations including Gene Ontology terms, protein domains, and pathway annotations. Results were filtered based on false discovery rate (FDR) with enrichment direction and magnitude reported for each significant term.

Table 4: *P. aeruginosa* Library Construction and Analysis External Links

Table	URL
Guide RNA Library	https://github.com/ryandward/pseudomonas_analytics/blob/main/Supplementary%20Tables/Supplementary%20Table%201.xlsx
Guide-level Results (Sheet 1)	https://github.com/ryandward/pseudomonas_analytics/blob/main/Supplementary%20Tables/Supplementary%20Table%202.xlsx
Gene-level Results (Sheet 2)	
Gene-set Enrichment Results	https://github.com/ryandward/pseudomonas_analytics/blob/main/Supplementary%20Tables/Supplementary%20Table%203.xlsx
Strains (Sheet 1)	https://github.com/ryandward/pseudomonas_analytics/blob/main/Supplementary%20Tables/Supplementary%20Table%204.xlsx
Plasmids (Sheet 2)	
Oligonucleotides (Sheet 3)	

Chapter 4. Genetic Determinants of Carbapenem Susceptibility and Resistance in *Enterobacterales*

1. Authors

Ryan D. Ward, Nathan Smith, Luisa Lee, and Jason M. Peters

2. Contributions

RDW conceptualized and executed the experimental framework, performed all molecular cloning and library construction, directed validation experiments, and conducted comprehensive data analysis.

NS and LL conducted bacterial growth measurements.

JMP designed the underlying CRISPRi libraries and provided project funding.

3. Abstract

Infections caused by antibiotic-resistant Enterobacterales species, such as *Escherichia coli*, *Enterobacter cloacae*, and *Klebsiella pneumoniae* are an increasing threat to public health. Few therapeutic options remain for Enterobacterales strains resistant to last-resort antibiotics, such as carbapenems. Thus, approaches that can identify new genetic vulnerabilities in these species or identify mechanisms of resistance could provide much needed therapeutic targets. Here, we use genome-scale CRISPRi (CRISPR interference) knockdown libraries in *E. coli*, *E. cloacae*, and *K. pneumoniae*, to identify genes that are sensitive to depletion (vulnerable) or play roles in susceptibility or resistance to carbapenems. Overall, we find substantial concordance between vulnerable genes in all three species, with notable exceptions in core pathways such as oxidative phosphorylation. Varying susceptibility of *tol-pal* knockdown strains to carbapenems across species points to genetic robustness in systems that promote small molecule efflux and maintain membrane integrity. Knockdowns of the genes encoding the RNA-binding protein ProQ showed also distinct phenotypes across species, suggesting “re-wiring” of RNA regulatory networks over a relatively short evolutionary distance. Genetic interaction

analysis of an *E. coli* Δ*proQ* mutant showed that control of cellular energy systems may underly its carbapenem-resistant phenotype. Our study highlights both consistencies and distinctions between genetic vulnerablities in Enterobacterales that can be used to inform general or species-specific approaches to future therapies.

4. Introduction

Antimicrobial resistance (AMR) poses an urgent public health challenge, with bacterial AMR directly causing 1.27 million deaths and contributing to 4.95 million deaths globally in 2019 (1). The impact extends beyond mortality – in the United States alone, resistant infections add $20 billion in direct healthcare costs and approximately $35 billion in lost productivity annually (3), disproportionately affecting resource-constrained and rural hospitals (4–7). Extended-spectrum β-lactamase (ESBL)-producing *Enterobacterales*, particularly *Escherichia coli*, *Klebsiella pneumoniae*, and *Enterobacter cloacae*, represent a critical subset of this threat due to their intrinsically low membrane permeability and multiple resistance mechanisms (2). The stagnation in antibiotic development – with no new classes introduced between 1962 and 2000 (10) – has made preserving the efficacy of existing last-resort antibiotics like carbapenems increasingly important (157). This economic reality, combined with the increasing prevalence of carbapenem resistance, drives the need to understand how these pathogens evolve and adapt under antibiotic pressure.

Carbapenems, such as imipenem, represent a unique class of β-lactam antibiotics - while extended-spectrum β-lactamases (ESBLs) degrade most β-lactams including third-generation cephalosporins, carbapenems remain effective against ESBL-producing organisms (220). However, carbapenemase genes spread rapidly among Gram-negative pathogens through horizontal gene transfer (221), creating complex fitness landscapes. Though β-lactamase production directly inactivates antibiotics, cellular responses to carbapenem exposure affect multiple pathways. The peptidoglycan synthesis machinery functions within a

network where membrane transport controls antibiotic entry (11), metabolic pathways supply cell wall precursors (158), and stress responses alter gene expression across pathways (32).

The peptidoglycan cell wall serves as both the carbapenem target and shapes resistance evolution. Like other β-lactams, carbapenems block the transpeptidase activity of penicillin-binding proteins (PBPs), preventing crosslinking of new peptidoglycan into the existing matrix (220, 221). Bacteria develop resistance through multiple mechanisms: acquiring carbapenemase genes through horizontal transfer (221), accumulating mutations in cellular pathways (36), and activating stress responses (222). While sequencing identifies acquired resistance genes, mutations have less predictable effects. Many mutations initially reduce protein function and appear deleterious until compensatory changes accumulate under antibiotic pressure (32, 223, 224). The "less is more" evolutionary hypothesis proposes these loss-of-function mutations actively drive adaptation (225). For instance, RNA polymerase mutations in *Pseudomonas aeruginosa* alter peptidoglycan precursor levels, leading to unexpected changes in β-lactam susceptibility (32) and disruptions to cell wall function (33). Similarly, in methicillin-resistant *Staphylococcus aureus* (MRSA), low-affinity PBP2a enables continued but compromised cell wall synthesis (34), these adaptations frequently result in reductions in growth and fitness that drive reversion to wild-type phenotypes in antibiotic-free conditions (35).

Loss-of-function mutations occur through two mechanisms: physical removal through recombination or mobile elements, or deleterious mutations in coding regions (226). Mutations are prevalent in bacterial populations, particularly during range expansions where high mutation rates and genetic drift facilitate the accumulation of deleterious variants, thereby reducing fitness (227). The impact of these mutations varies—some create complete functional knockouts while others retain partial activity through alternative start codons or incomplete disruption of functional domains (228). In pathogenic bacteria, loss-of-function mutations contribute to increased phenotypic diversity and enhanced drug resistance (229), particularly

when they affect genes involved in DNA repair or cellular regulation. For instance, long-term evolution experiments with *Escherichia coli* demonstrated that hypermutability caused by DNA repair mutations accelerates mutation accumulation, enabling rapid adaptation to selective pressures despite the burden of deleterious variants (230). Such dynamics may similarly operate in nosocomial pathogens, where high antibiotic pressures favor temporary hypermutability, potentially shaping resistance development.

CRISPR interference (CRISPRi)-based perturbation extends these natural observations by systematically examining how reduced gene expression affects carbapenem susceptibility. By targeting essential and non-essential genes across multiple *Enterobacterales* species, this approach experimentally models the functional consequences of loss-of-function mutations. Through systematic perturbation of gene expression under antibiotic pressure, this comparative functional genomics work examines how bacteria balance the deleterious effects of essential gene disruption against potential selective advantages.

5. Results

5.1. Construction and validation

To establish CRISPRi systems that were efficacious in *E. coli*, *E. cloacae*, and *K. pneumoniae*, we compared six IPTG-inducible promoters to drive dCas9 expression: PLlacO-1 and five synthetic designs (B, G, I, J, K, (231)). Using GFP knockdown in *E. coli* as our test system, PLlacO-1 showed the strongest repression at 24-fold but exhibited significant leakiness, dropping uninduced GFP to 40% of control levels. Promoter B produced 18-fold knockdown while better maintaining uninduced expression at ~60% of control. Promoter I achieved similar performance with 16-fold repression. We eliminated promoters G, J, and K from consideration due to weak knockdown (12-fold, 8.6-fold, and 2-fold respectively, [Figure 38]). Moving to other species, we tested PLlacO-1, B, and I in both *E. cloacae* and *K. pneumoniae*. *E. cloacae* strains showed tight regulation with promoter B producing 22-fold repression without detectable

leakiness, while promoter I drove even stronger knockdown at 26-fold. In *K. pneumoniae*, promoter I generated 26-fold repression while keeping uninduced expression high at 90% of control. These results led us to choose promoter B for *E. coli* and *E. cloacae* libraries and promoter I for *K. pneumoniae*, balancing maximum knockdown with minimal leaky expression.

Figure 38: Evaluation of CRISPRi Activity Ccross IPTG-Inducible Promoters in Diverse *Enterobacterales* Species

Assessment of promoter performance using three matched reporter constructs [Table 8]. Data is shown on a reverse log scale (y-axis) where 1.0 (dotted line) represents GFP levels in the absence of any guide RNA. All measurements are normalized to the median no-guide control value for each organism (no-guide SEM = 0.01-0.05 across all species). Light colored bars show uninduced GFP levels relative to no-guide control, indicating unintended CRISPRi activity. Dark colored bars of the same hue show induced GFP levels, demonstrating maximal knockdown capability for each promoter. Numbers in the induced bars indicate fold-repression achieved upon induction relative to uninduced samples. Promoters are grouped by organism, with consistent x-axis ordering within each group.

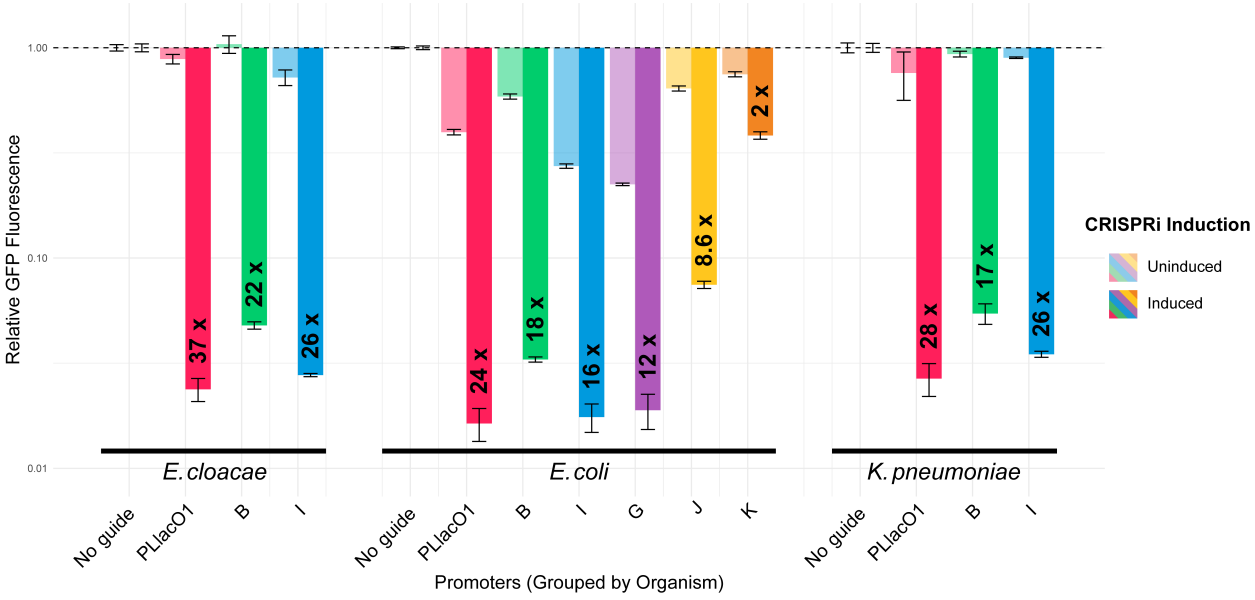

We developed a genome-wide CRISPRi platform to systematically assess gene vulnerabilities under knockdown and antibiotic treatment conditions. The CRISPRi libraries, constructed using Mobile-CRISPRi vectors, were stably integrated into the chromosomes of *E. coli*, *E. cloacae*, and *K. pneumoniae*. Each library consisted of over 20,000 strains per organism, targeting all genes with either perfect match guides (non-essential genes) or perfect and mismatch guides (for putative essential genes) to achieve tunable knockdown. Essential gene targets were selected based on orthology mapping to existing *E . coli* Tn-seq datasets [Figure 39A]. This design enabled us to examine both gene essentiality and the interaction between knockdown and imipenem treatment.

To identify sub-lethal imipenem concentrations that could be used for phenotyping, we evaluated pooled fitness across the entire library in the presence of imipenem in LB (lysogeny broth). Real-time growth kinetics were measured across two-fold dilutions (0.125–32 ng/μL) in a 96-well format, and the experiments were performed in triplicate to ensure reproducibility [Figure 39B]. Consistent trends in growth behavior across replicates indicated predictable population-level responses, with no evidence of unexpected phenomena such as spontaneous mutations leading to resistance. Based on these observations, "low" and "high" imipenem doses were selected qualitatively for each organism, targeting concentrations that produced observable growth inhibition without causing complete population collapse. Growth curves revealed species-specific differences in pooled fitness under uninduced and induced knockdown conditions across these selected concentrations [Figure 39C].

Figure 39: Systematic Approach to Optimize Drug-Gene Interaction Across *Enterobacterales* Using Mobile-CRISPRi

(A) Comprehensive library design and construction strategy. Essential genes were identified through orthology mapping to existing Tn-seq datasets from *E. coli*. A genome-wide CRISPRi library was designed incorporating both perfect match and mismatch guides to achieve tunable knockdown. The library was delivered via Mobile-CRISPRi integration vectors, enabling stable chromosomal insertion across target species. **(B)** High-throughput dose optimization workflow. Drug concentrations were systematically evaluated in 2-fold dilutions (0, 0.125-32 ng/μL) in LB (lysogeny broth) using a 96-well format to identify sub-lethal doses that produced observable growth phenotypes while maintaining cell viability. Selected doses were then grown further in larger culture volumes. **(C)** Species-specific growth responses to antibiotic treatment. Growth curves of *E. cloacae*, *E. coli*, and *K. pneumoniae* under uninduced (blue) and induced (red) conditions across optimized drug concentrations (0, 0.125, 0.25, 0.5, and 1 ng/μL). Bands represent the range across three replicates.

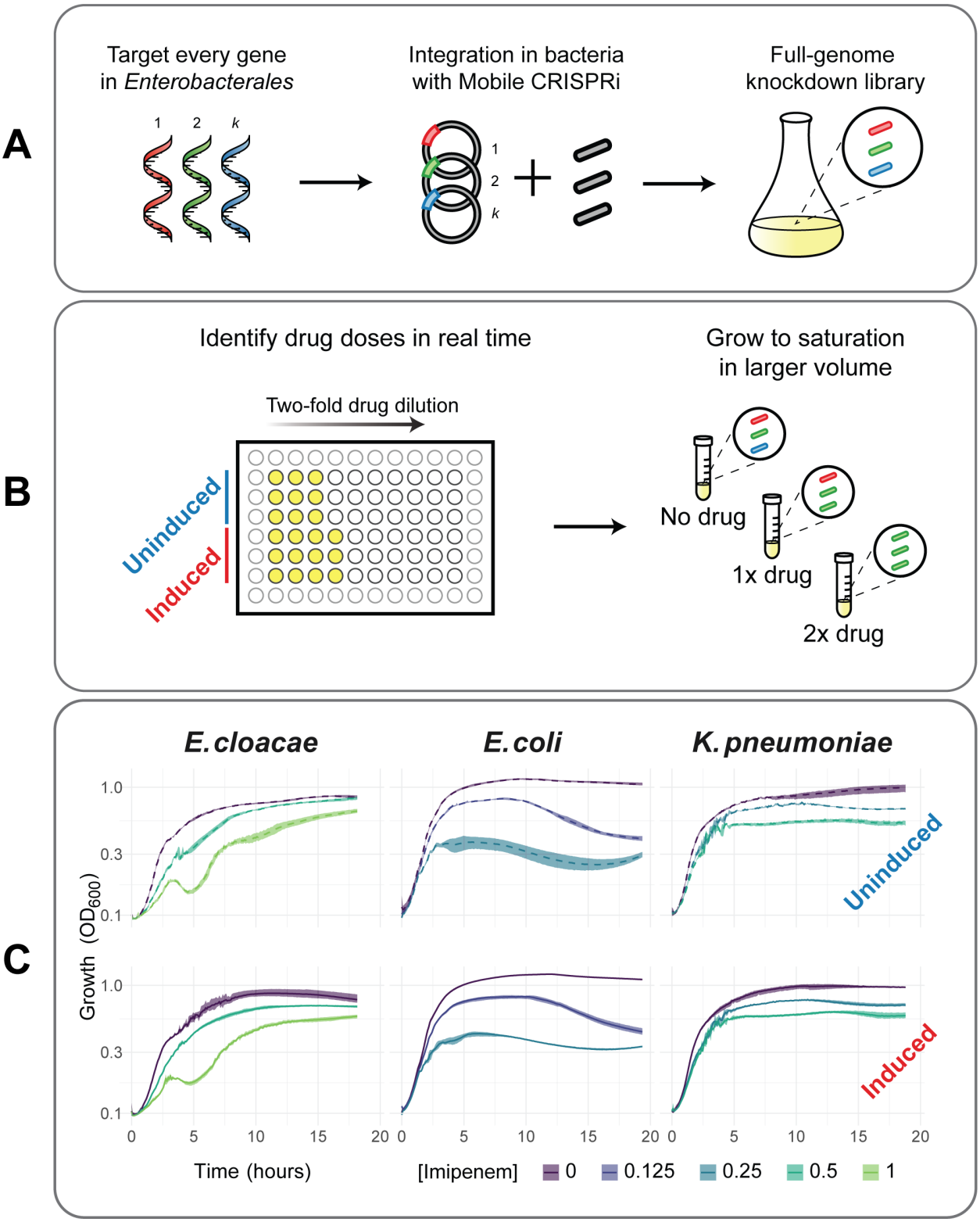
A
Target every gene in Enterobacterales
Integration in bacteria with Mobile CRISPRi
Full-genome knockdown library
1
2
k
B
Identify drug doses in real time
Grow to saturation in larger volume
Two-fold drug dilution
Uninduced
Induced
No drug
1x drug
2x drug
C
E. cloacae
E. coli
K. pneumoniae
Uninduced
Induced
Growth (OD600)
1.0
0.3
0.1
0
5
10
15
20
Time (hours)
[Imipenem]
0
0.125
0.25
0.5
1

Relative fitness score (RFS) was modeled for each strain (i) using:

$$RFS_i = \beta_0 + \beta_{induced,i} + \beta_{1x\ drug} + \beta_{2x\ drug} + \epsilon_i$$

Here, β_0 represents the baseline fitness, $\beta_{induced,i}$captures the fitness impact of inducing knockdown for each strain, $\beta_{1x\ drug}$ and $\beta_{2x\ drug}$ model the effects "low" (1×) and "high" (2×) doses of imipenem, and ϵ_i accounts for residual variability. This equation captures the pooled fitness effects across all strains and conditions, allowing us to model gene vulnerabilities and their interaction with antibiotic pressure.

To evaluate the effectiveness of CRISPRi in identifying essential genes, we compared it against two established *E. coli* genetic resources: the Keio collection of single-gene knockouts (65) and the ultra-dense Tn-seq dataset from Goodall, *et al.* (232). The Keio collection provides direct experimental validation of gene essentiality through systematic deletion attempts. Tn-seq approximates essentiality by measuring the size of insertion-free regions in the genome, with larger gaps suggesting stronger selection against disruption. However, this structural approach can be biased by gene length and local sequence composition. In contrast, CRISPRi directly measures the fitness consequences of reducing gene expression over time (60).

Using receiver operating characteristic (ROC) analysis with the Keio collection as ground truth, we found that CRISPRi achieved an area under the curve (AUC) of 0.89, compared to 0.94 for Tn-seq [Figure 40A]. To understand this difference, we examined the true positive rate (TPR) – the fraction of Keio-validated essential genes correctly identified by each method. The TPR analysis revealed that while Tn-seq excels at identifying completely non-viable mutants, CRISPRi detects a broader range of fitness defects through partial gene repression. To quantify these methodological differences, we developed a ΔTPR metric comparing STRING database pathways (122) assessing CRISPRi and Tn-seq:

$$\Delta TPR^{Pathway} = TPR_i^{CRISPRi} - TPR_i^{TNSeq}$$

Analysis of ΔTPR values revealed major discrepancies between direct fitness measurements by CRISPRi and structural predictions by Tn-seq. Two pathways emerged as the strongest examples: genes encoding the proton-motive force machinery (ΔTPR = -0.81) and NADH dehydrogenase complex I (ΔTPR = -0.64) showed severe pooled growth defects under CRISPRi knockdown despite lacking the large insertion-free regions typically associated with essential genes in Tn-seq data [Figure 40B]. This demonstrates how structural approaches can miss genes where partial loss of function significantly impairs growth even though complete deletion is tolerated. The quantitative nature of these phenotypes matches the mechanism of most antibiotics, which reduce rather than eliminate target protein function, suggesting that CRISPRi can recover gene targets with therapeutic relevance that were missed by other approaches.

Figure 40: Comparison of CRISPRi and Tn-seq Approaches for Identifying Essential Genes in *E. coli*

(A) Receiver operating characteristic (ROC) curves comparing how well CRISPRi (blue) and Tn-seq (red) identify essential genes defined by the Keio collection. The area under the curve (AUC) values indicate that while Tn-seq shows higher concordance with binary essentiality classifications (AUC = 0.94), CRISPRi retains substantial predictive power (AUC = 0.89) despite measuring continuous fitness effects. (B) Vulnerability of *E. coli* genes measured by CRISPRi. The x-axis shows statistical confidence (adjusted *p*-value) while the y-axis shows relative fitness score (RFS, log2 fold change). Points are colored by Keio collection essentiality status. Labeled genes highlight two major functional groups that account for the largest discrepancies between CRISPRi and deletion-based methods: proton motive force-driven plasma membrane ATP synthesis (*atp* genes) and respiratory chain complex I (*nuo* genes).

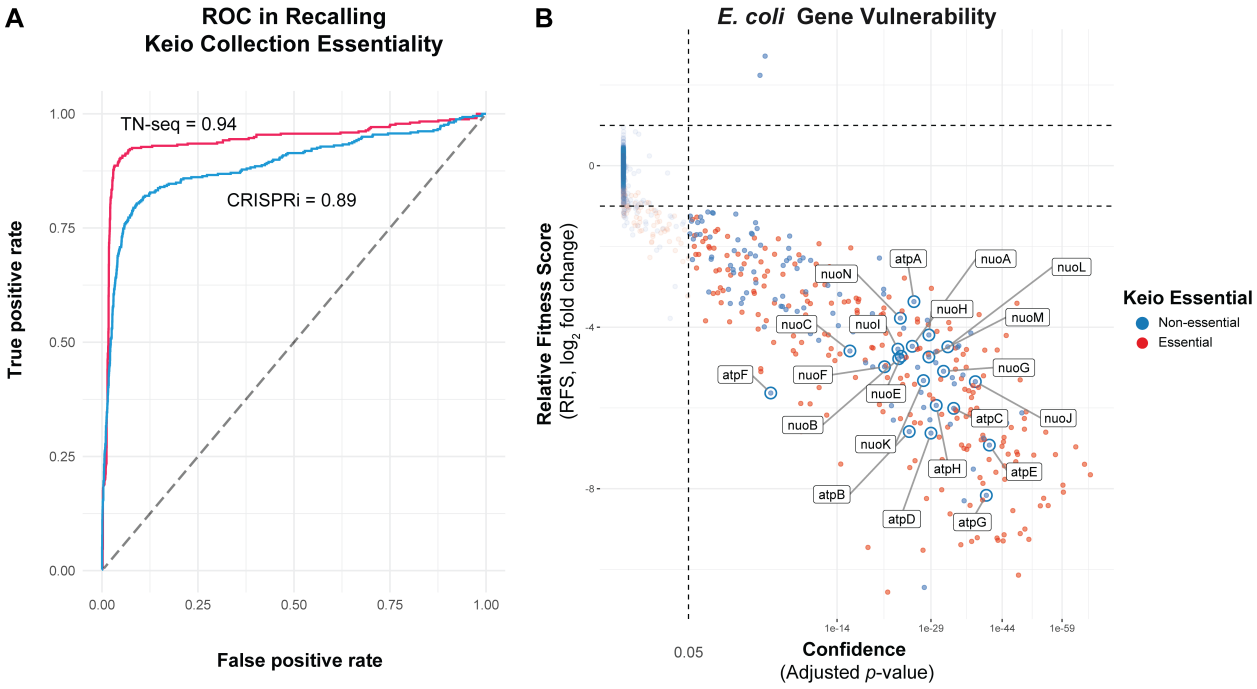

5.2. Genes and pathways that are sensitive to knockdown

Our pathway-level analysis using competitive gene set enrichment analysis (CAMERA) evaluated whether genes in defined functional groups showed coordinated fitness effects compared to the background distribution of all other genes. Four key cellular systems showed significant coordinated depletion across all tested *Enterobacterales* [Table 5, Table 6]. We filtered for pathways containing at least 5 genes where all members displayed consistent phenotypes under CRISPRi induction (gene-level adj.P.Val ≤ 0.05).

The small ribosomal subunit showed the largest sensitivity to perturbation [Figure 41]. The competitive enrichment scores for this pathway spanned from 8.1e-34 in *E. cloacae* to 8.1e-69 in *K. pneumoniae,* indicating strong coordinate depletion of these genes compared to the genomic background. All 24 genes encoding core 30S ribosomal proteins (*rpsABCDEFGHIJKLMNOPQRSTU*) showed strong depletion patterns across species. NADH dehydrogenase perturbation revealed clear species differences. *E. cloacae* showed severe growth defects with a pathway enrichment score of 1.4e-33, while *K. pneumoniae* maintained substantially higher fitness with a score of 1.0e-10. This pattern held across both core complex members (*nuoA-N*) and related oxidoreductases (*fdhF*, *hycF*, *hyfH*, *ndh*). ATP synthase (*atpABCDEFGHI*) and protein secretion machinery (*ffh*, *secGEY*, *ftsY*) showed consistent pathway-level depletion across species (enrichment score ranges 3.9e-32 to 6.5e-21 and 4.6e-22 to 7.5e-31 respectively). Knockdown of lactose utilization genes (*lacYZ*, *ebgA*) increased fitness across species due to reduced IPTG toxicity, demonstrating the expected behavior of our inducible system.

The species-specific patterns of gene sensitivity highlight key differences in how these bacteria maintain core cellular processes. NADH dehydrogenase knockdowns produced similar growth defects in *E. coli* and *E. cloacae*, but *K. pneumoniae* maintained near wild-type growth rates when these genes were targeted. Sec pathway knockdowns (*ffh*, *secGEY*, *ftsY*) severely

reduced growth in all three species, indicating these genes cannot be bypassed through alternative transport mechanisms. These patterns of vulnerability extend beyond binary essentiality, showing how species-specific constraints shape cellular fitness when essential processes are perturbed. Having established these gene-level sensitivities under standard conditions, we next examined how these phenotypes changed under imipenem treatment.

Figure 41: Competitive Gene-Set Enrichment Analysis of Essential Pathways in *Enterobacterales*

Each point represents a guide RNA targeting an essential gene, plotted by its relative fitness score (log2 fold change, y-axis) and statistical confidence (adjusted p-value, x-axis). Points are colored by enriched functional groups from gene ontology analysis [Table 5, Table 6]. Gray points represent guides targeting genes not belonging to significantly enriched pathways. Guides with the strongest phenotypes are labeled. Dashed lines indicate two-fold changes in relative fitness score (RFS, log2FC = ±1). Note that less negative p-values on the x-axis indicate higher statistical confidence.

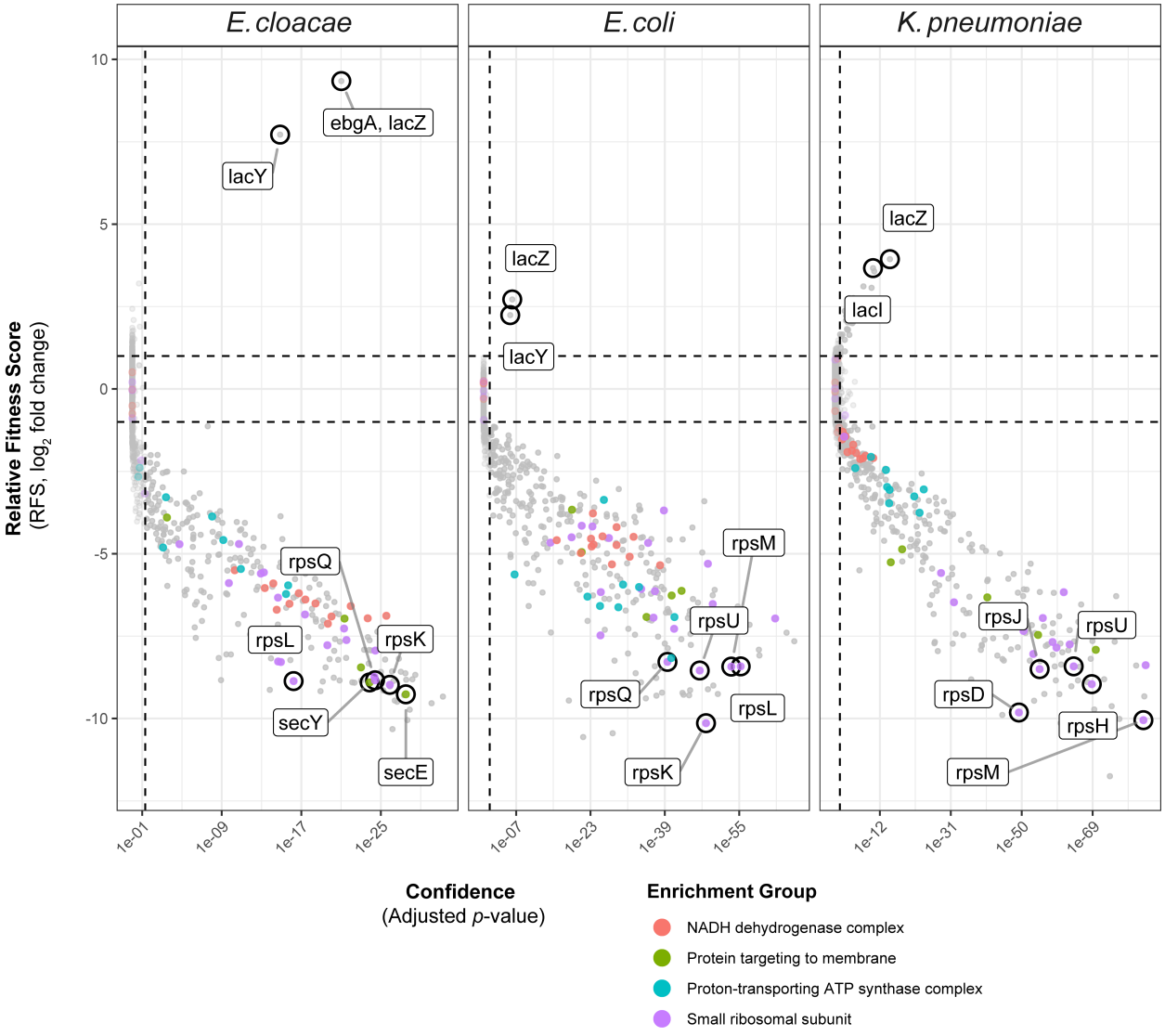

Table 5: Gene Ontology Group Membership

Pathway	GO/GOCC ID	Genes
Protein targeting to membrane	GO:0006612	*ffh, secG, ftsY, secE, secY*
Small ribosomal subunit	GO:0015935	*rpsB, rpsA, raiA, rpsP, rpsU, rpsO, rpsI, rpsG, rpsL, rpsF, rpsR, rpsT, hpf, rpsD, rpsE, rpsH, rpsN, rpsC, rpsS, rpsJ, rpsM, rpsQ, rpsK, sra, rbbA*
NADH dehydrogenase complex	GO:0030964	*fdhF, nuoN, nuoM, nuoL, nuoK, nuoJ, nuoI, nuoH, nuoG, nuoF, nuoE, nuoC, nuoB, nuoA, ndh, hycF, hyfH*
Proton-transporting ATP synthase complex	GOCC:0045259	*atpC, atpD, atpG, atpA, atpH, atpF, atpE, atpB, atpI*

Table 6: CAMERA Enrichment Scores

Pathway	*E. coli*	*E. cloacae*	*K. pneumoniae*
Protein targeting to membrane	4.60E-22	7.50E-31	1.90E-26
Small ribosomal subunit	5.70E-44	8.10E-34	8.10E-69
NADH dehydrogenase complex	1.10E-29	1.40E-33	1.00E-10
Proton-transporting ATP synthase complex	3.90E-32	1.50E-25	6.50E-21

5.3. Differential responses to imipenem treatment

Carbapenem stress demonstrated species-specific envelope maintenance strategies across *Enterobacterales*. To systematically examine these differences, we treated our CRISPRi libraries with sub-MIC concentrations of imipenem and analyzed gene-level and pathway-level responses. β-lactams induce a destructive cycle by blocking the transpeptidase activity of penicillin-binding proteins while allowing continued glycan strand synthesis, leading to accumulation and rapid degradation of uncrosslinked material by lytic transglycosylases (222). This futile cycle particularly impacts envelope integrity through disruption of cell wall assembly and division.

Competitive gene set enrichment analysis (CAMERA) of all Gene Ontology pathways showed that components of the Tol-Pal system (GO:1905153) showed the most extreme variation between species. The Tol-Pal system spans the periplasm, physically connecting the inner membrane proteins TolA/Q/R to the outer membrane-anchored TolB/Pal complex [Figure 42B]. This system maintains envelope integrity through energy-dependent interactions that become especially critical under stress from drugs and detergents (233). Genome architecture analysis showed species-specific variations in the Tol-Pal system [Figure 42C]. In *E. cloacae*, we identified an additional *tolA* fragment downstream of the canonical gene, while in *K. pneumoniae*, another *tolA* fragment was found approximately 1 million base pairs upstream, though sometimes annotated as *tonB*. This dual annotation reflects an underlying structural relationship – TolA and TonB share a conserved fold despite low sequence identity (~20%), organized around key motifs that maintain envelope integrity (234). The conservation of these proteins parallels their roles in essential cellular processes like cell wall assembly and division, where disruption increases susceptibility to β-lactams through effects on peptidoglycan synthesis and turnover (222).

Figure 42: Species-Specific Responses to Imipenem Treatment and Organization of the Tol-Pal System

(A) Changes in Tol-Pal system abundance measured by counts per million (CPM) across three treatment conditions in *E. cloacae*, *E. coli*, and *K. pneumoniae*. Box plots show the distribution of CPM values for Tol-Pal components, with individual points representing biological replicates. FDR values indicate statistical significance of changes between uninduced, induced, and high-dose conditions. **(B)** Schematic representation of the Tol-Pal system spanning the bacterial envelope. TolQ, TolR, and TolA form an inner membrane complex that interacts with the outer membrane-anchored TolB and Pal proteins across the periplasmic space. **(C)** Genomic organization of the Tol-Pal system across species visualized using Clinker. Gray scale indicates sequence identity between homologous genes. In *K. pneumoniae*, an additional gene (VK055_0760) located ~1M nucleotides upstream of the canonical Tol-Pal cluster shares sequence similarity with TolA. Gene sizes and spacing are drawn to scale within the 2.5kb windows shown.

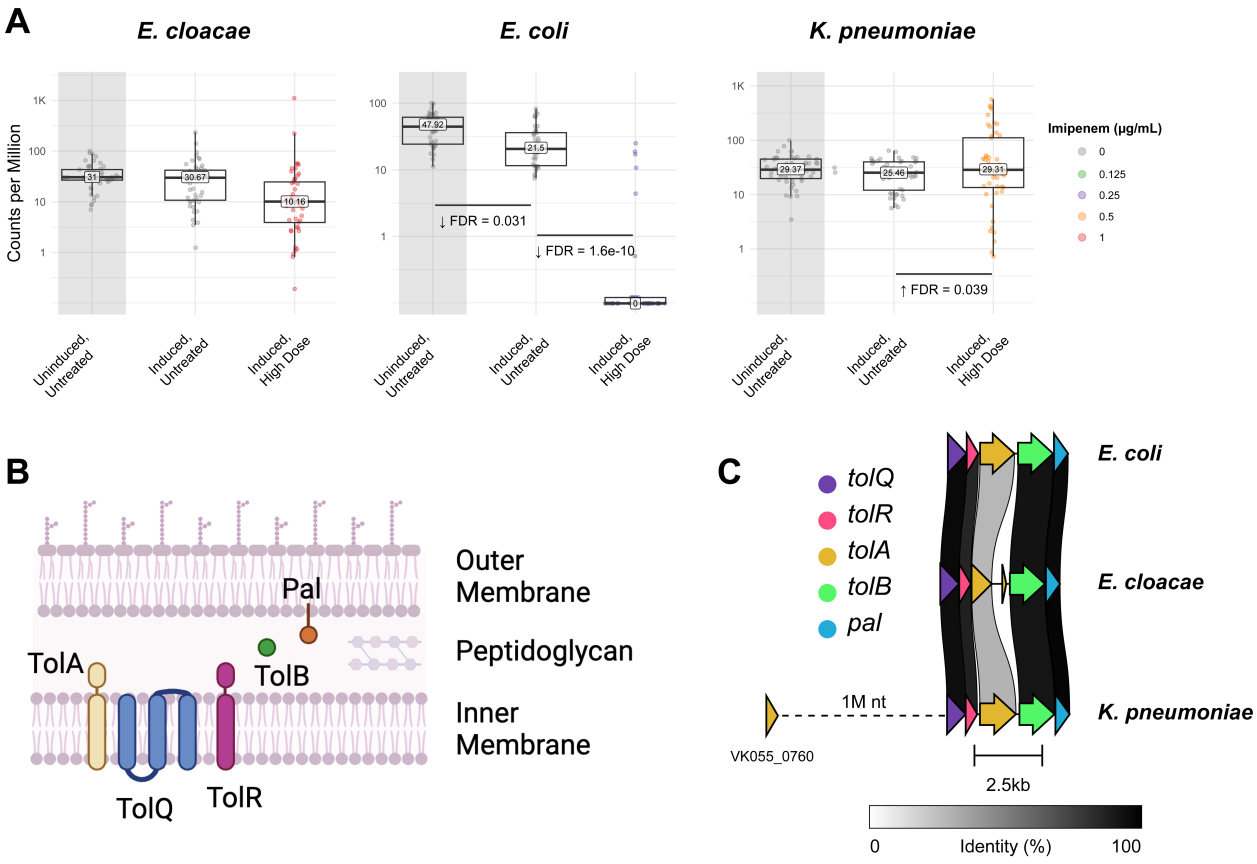

These architectural differences appear to influence species-specific responses to carbapenem stress [Figure 42A]. *K. pneumoniae*, with its additional *tolA* fragment, shows increased fitness under imipenem treatment (CPM increasing from 25.46 to 29.31, FDR = 0.039), while *E. coli* experiences severe depletion (CPM dropping from 47.92 to nearly zero, FDR = 1.6e-10). *E. cloacae* displays an intermediate phenotype with no statistically significant changes in Tol-Pal CPM, suggesting its downstream *tolA* fragment provides partial compensation. The core divisome components further exhibits species-specific stress responses. The ABC transporter FtsX, essential for cell wall hydrolysis during division (235), showed strong depletion across species (RFS < -5) with particularly severe effects in *E. coli* and *K. pneumoniae* (RFS = -12) [Table 7]. Similarly, FtsN, which coordinates septal peptidoglycan synthesis (236), demonstrated consistent depletion, though with greater sensitivity in *E. coli* and *K. pneumoniae* (RFS ≈ -9) compared to *E. cloacae* (RFS = -3).

Knockdown of the RNA chaperone *proQ* produced three distinct species-specific phenotypes, conferring significant fitness advantage in *E. coli* (RFS = 13.0), while compromising fitness in *K. pneumoniae* (RFS = -7.7) and remaining neutral in *E. cloacae* (RFS = 1.2). These divergent responses suggest unexpected plasticity in envelope maintenance systems between species. To better understand these species-specific regulatory networks, we constructed and analyzed libraries in a *proQ* deletion background in *E. coli* to study how envelope integrity is maintained under antibiotic stress.

Table 7: Species-Specific Responses to Imipenem Stress Across Envelope Maintenance Systems

Values represent relative fitness scores (RFS) under imipenem treatment. Bold values indicate significant changes (FDR ≤ 0.05). Multiple values for tolA indicate separate gene copies. Negative values indicate depletion while positive values indicate enrichment in the population.

Pathway/Gene	***E. cloacae***	***E. coli***	***K. pneumoniae***
Tol-Pal System			
tolA	-1.28, 0.239	**-10.0**	0.082, **1.60**
tolB	0.262	**-11.0**	**1.91**
tolQ	0.114	**-10.2**	**2.11**
tolR	-0.768	**-10.4**	**1.25**
pal	0.022	**-9.36**	**1.85**
Cell Division			
ftsE	**-6.02**	**-7.27**	**-11.5**
ftsN	**-2.95**	**-9.73**	**-9.32**
ftsX	**-4.99**	**-11.5**	**-11.6**
ftsZ	-2.25	-2.60	-3.30
LPS Transport			
lptA	-3.62	-2.60	-2.77
lptB	-2.34	**-4.14**	**-3.04**
lptC	-1.27	-3.26	-2.86
lptD	-0.811	**-3.37**	**-4.19**
lptE	-0.183	**-4.39**	**-1.54**
lptF	-1.29	**-3.66**	**-6.07**
lptG	0.06	**-3.05**	**-3.66**
RNA Regulation			
proQ	1.23	**13.0**	**-7.74**

5.4. Full-genome *proQ*-Deletion Background Library Reveals Distinct Essential Gene Vulnerabilities

To systematically examine how ProQ loss affects *E. coli* cellular fitness under carbapenem treatment, we designed a factorial experiment comparing wild-type and Δ*proQ* libraries across three conditions: CRISPRi induction alone, and two doses of imipenem with induction. The response for each gene was derived from a model using edgeR:

$$Y = \beta_0 + \beta_1 X_{WT} + \beta_2 X_{low,WT} + \beta_3 X_{high,WT} + \beta_4 X_{\Delta proQ} + \beta_5 X_{low,\Delta proQ} + \beta_6 X_{high,\Delta proQ} + \epsilon$$

Here, β_0 is the uninduced baseline, and all other terms represent induced conditions by default. The subscripts indicate imipenem concentration (low or high) and strain type (WT or Δ*proQ*). All X terms are binary indicators (0 or 1), and ε represents random error. This model allowed us to isolate strain-specific responses to both knockdown and antibiotic stress. Competitive gene set enrichment analysis (CAMERA) identified two respiratory chain complexes – cytochrome o ubiquinol oxidase (*cyoABCDE*) and NADH:ubiquinone oxidoreductase (*nuoA-N*) – as among the most significantly differentially enriched pathways between strains.

Induction of CRISPRi knockdown reduced fitness of NADH dehydrogenase by 28-fold and cytochrome oxidase by 3.6-fold in wild-type cells [Figure 43]. The Δ*proQ* strain showed reduced sensitivity to knockdown, with only 7.7-fold and 1.2-fold reductions respectively. Imipenem treatment produced opposing effects between strains. At high imipenem concentrations, cytochrome oxidase knockdown strains showed a 52-fold fitness increase in the wild-type background but a 4.5-fold decrease in Δ*proQ*. NADH dehydrogenase displayed a similar pattern at low imipenem concentrations - a 17-fold fitness increase in wild-type reduced to 1.8-fold in Δ*proQ*. β-lactam sensitivity depends on cellular energy state (237), with both respiratory complexes contributing to proton motive force generation. The reversal of imipenem-

induced selection in Δ*proQ* strains points to altered regulation of energy metabolism. ProQ binding studies have identified numerous metabolic transcripts as regulatory targets (238), suggesting direct control of respiratory gene expression.

Figure 43: *proQ* Deletion Alters the Response of Respiratory Complexes to Imipenem Treatment

Fold changes in abundance of **(A)** cytochrome o ubiquinol oxidase (encoded by *cyoABCDE*) and **(B)** NADH:ubiquinone oxidoreductase (encoded by *nuoA-N*) components under CRISPRi induction alone or with low (0.125 µg/mL) or high (0.25 µg/mL) imipenem (IMI) concentrations. Wild-type (WT, green) and Δ*proQ* (purple) strains show distinct patterns of respiratory complex abundance. The y-axis shows fold change (FC) on a log scale relative to uninduced conditions. Individual points represent separate guide RNAs (4 per gene) targeting each gene in the pathway, bars show median values with error bars representing the interquartile range (25th to 75th percentiles). Statistical significance was determined using CAMERA (competitive gene set enrichment analysis); 'ns' indicates conditions where pathway components show no significant coordinated changes compared to baseline (FC = 1, dotted line; FDR > 0.05).

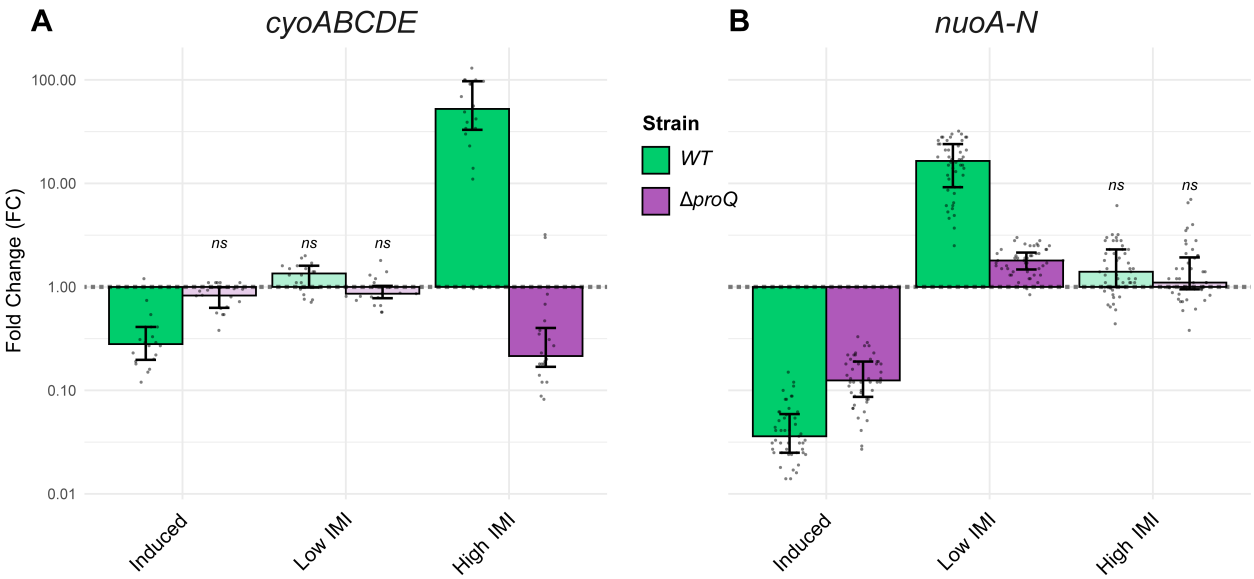

6. Discussion

Our CRISPRi competition screens across three *Enterobacterales* species measured how bacterial populations respond to imipenem treatment when essential genes are partially repressed. While ribosomal and cell envelope gene knockdowns showed similar fitness effects across species, we found unexpected differences in how these bacteria tolerate perturbation of energy metabolism and membrane maintenance pathways. The varying fitness costs of NADH dehydrogenase knockdown between species stand out. *E. coli* and *E. cloacae* populations dropped out rapidly when these genes were targeted, but *K. pneumoniae* maintained competitive growth. These fitness differences align with data showing NADH dehydrogenase affects antibiotic susceptibility through NAD+/NADH ratios rather than membrane potential (26), pointing to fundamental differences in how these species maintain energy balance.

The Tol-Pal system results demonstrate how genome structure shapes bacterial survival strategies. *E. coli* strains carrying Tol-Pal knockdowns were outcompeted under carbapenem stress, while *K. pneumoniae* strains actually increased in frequency. This phenotypic difference aligns with our genomic analyses showing additional *tolA*-like sequences in both *K. pneumoniae* and *E. cloacae*, though these fragments differ between species. While these sequences share orthology with *tolA* based on our Orthofinder analysis, they may represent either partial *tolA* duplications or functionally related envelope maintenance genes like *tonB* (239). The Tol-Pal system helps maintain envelope integrity during both cell elongation and division (240), and our data suggest that *K. pneumoniae* has evolved additional genetic capacity for this essential function. These species-specific differences in envelope maintenance systems help explain varying susceptibility patterns between *Enterobacterales*, though further work is needed to determine the precise molecular mechanisms by which these additional sequences contribute to carbapenem tolerance.

ProQ regulates stress responses differently between bacterial species. In *E. coli*, deletion of proQ completely reversed how respiratory complexes respond to carbapenem treatment; mutants that normally showed reduced fitness in wild-type cells instead grew 52-fold better without ProQ. The opposite occurred in *K. pneumoniae*, where *proQ* knockdown reduced survival under carbapenem stress. Though these species clearly respond differently to loss of ProQ, understanding the mechanism in *K. pneumoniae* will require additional genetic studies. Our findings show how a single RNA regulator can reshape the connection between energy metabolism and antibiotic tolerance.

Our pooled fitness approach demonstrated vulnerabilities that traditional knockout studies have missed. For instance, NADH dehydrogenase knockdown strains showed major competitive disadvantages despite lacking typical essentiality signals in Tn-seq data (232). This discrepancy points to an important limitation in how we traditionally evaluate antibiotic targets. Complete gene deletion may not accurately predict how bacteria respond to the partial inhibition caused by antibiotics (237). The stark fitness defects we observed with partial knockdown suggest that bacteria may have particular difficulty adapting to intermediate states of protein function, even for genes they can theoretically survive without. The extent to which this phenomenon is dependent on direct competition between cells that perturbed/unperturbed for a specific pathway or function (*e.g.*, complex I) is unknown and will be the focus of future research. Cells treated with sub-lethal concentrations of antibiotics often accumulate toxic metabolic intermediaries which may be responsible for some of the depletion phenotypes observed here (241). Regardless of the precise mechanisms at play, the inducible nature of CRISPRi knockdown may better approximate real gene-drug interactions for specific genes or pathways, expanding the set of plausible therapeutic targets.

7. Materials and Methods

A comprehensive wiki containing methods described here is available on Ryan D. Ward's GitHub: https://github.com/ryandward/phylogenetic_CRISPRi/wiki.

7.1. Strains and Growth Conditions

Pooled library strains sJMP5142 (*E. coli*), sJMP5144 (*E. cloacae*), and sJMP5146 (*K. pneumoniae*) were revived from standardized -80°C glycerol stocks (OD600 = 10) by diluting into fresh LB medium to OD600 ~0.02. For antibiotic challenge experiments, a two-fold serial dilution series of imipenem (0.125-32 ng/μL) was prepared in 96-well plates. The libraries were grown in parallel under four conditions: no drug/no induction, no drug/with induction (1 mM IPTG), imipenem/no induction, and imipenem/with induction. Growth was monitored by OD600 measurements using a microplate reader (Tecan Infinite 200 Pro M Plex) with continuous orbital shaking at 37°C. Optical density readings were recorded at 5-minute intervals over 18-24 hours to capture complete growth trajectories. This dual-condition format enabled direct comparison of knockdown effects on antibiotic susceptibility. Competition experiments were performed in biological triplicate using independent library aliquots to account for potential variation in library composition and selection dynamics.

7.2. Essential Gene Identification and Guide RNA Design

Essential genes were identified from the ultra-dense Tn-seq dataset of *E. coli* K-12 (232). Putative essential genes in *E. cloacae* and *K. pneumoniae* were identified through orthology mapping using OrthoFinder v2.5.4 (121) with default parameters. Guide RNAs were designed using custom Python scripts adapted from Hawkins et al. (86) targeting the first 10% of each coding sequence. For each gene, we designed 4 perfect match guides and approximately 10 mismatch guides containing single nucleotide changes predicted to reduce targeting efficiency. Non-targeting control guides (n=1000) were designed to maintain similar

nucleotide composition while avoiding complementarity to target genomes, verified using Bowtie v1 (242).

Guide sequences were synthesized as 78-nucleotide oligonucleotides (Agilent Technologies) containing: 20-nt spacer sequence, constant regions for Gibson assembly, and BsaI restriction sites. The pooled oligonucleotide libraries were amplified using Q5 High-Fidelity DNA Polymerase (NEB) with primers specific to each species. PCR conditions: initial denaturation at 98°C for 30s; 15 cycles of 98°C for 15s, 56°C for 15s, 72°C for 15s; final extension at 72°C for 10 min. Products were purified using DNA Clean & Concentrator columns (Zymo Research) and quantified by Qubit fluorometry prior to cloning into Mobile-CRISPRi vectors as described above.

7.3. Species-Specific CRISPRi Library Development and Construction

Promoter performance was evaluated using a standardized GFP reporter system constructed in pJMP2816. Each promoter variant (PLlacO-1 and synthetic designs B, G, I, J, and K) was cloned upstream of *dcas9* using pJMP2828 (GFP with gmc6 guide RNA) and pJMP2840 (empty vector) as controls. Constructs were transformed into *E. coli* strain BW25141 for cloning (sJMP5058-5075) and WM6026 for conjugation (sJMP5040-5057). GFP fluorescence was measured using a Tecan Infinite 200 Pro M Plex plate reader (excitation/emission: 482/515 nm) after growth in LB medium supplemented with appropriate antibiotics (ampicillin 100 µg/mL, kanamycin 30 µg/mL) and with or without 1 mM IPTG induction. Fluorescence values were normalized to optical density (OD600) and to measurements from strains lacking GFP. Based on these quantitative measurements, promoter B was selected for *E. coli* and *E. cloacae* libraries (18-fold and 22-fold repression respectively), while promoter I was chosen for *K. pneumoniae* (26-fold repression).

For library construction, the Mobile-CRISPRi plasmid backbone containing promoter B (pJMP5135) or promoter I (pJMP5136) was purified using a PureLink HiPure Plasmid Midiprep kit from overnight cultures grown in LB with ampicillin. Plasmid DNA was quantified by Qubit fluorometry, yielding concentrations of 100 ng/µL and 120 ng/µL respectively. The backbones were digested with BsaI-HFv2 in CutSmart buffer for 4 hours at 37°C and purified using a DNA cleanup kit. Guide RNA sequences were amplified from organism-specific oligonucleotide pools using Q5 High-Fidelity DNA Polymerase with primers oJMP1150/1151 (*E. coli*), oJMP1153/1154 (*E. cloacae*), and oJMP1156/1157 (*K. pneumoniae*). PCR conditions were: 98°C for 30s; 15 cycles of 98°C for 15s, 56°C for 15s, 72°C for 15s; followed by 72°C for 10 min. Products were verified on agarose gels to confirm the expected 78 bp size and quantified (25-31 ng/µL).

The amplified guides were digested with BsaI-HFv2 and ligated into the processed vector backbones using T4 DNA ligase in reactions containing 10 mM DTT and 1 mM ATP. After dialysis against 0.1 mM Tris (pH 8.0), ligations were transformed into electrocompetent *E. coli* WM6026 cells and plated on LB agar supplemented with 300 µM diaminopimelic acid (DAP) and 100 µg/mL carbenicillin. This yielded strains sJMP5137 (*E. coli* library, OD600=20), sJMP5138 (*E. cloacae* library, OD600=20), and sJMP5139 (*K. pneumoniae* library, OD600=20) containing the Mobile-CRISPRi plasmid libraries ready for subsequent conjugation into target organisms.

7.4. Library Creation and Transfer

Mobile-CRISPRi plasmids containing promoters optimized for each target organism (promoter B for *E. coli* and *E. cloacae*, promoter I for *K. pneumoniae*) were isolated using a midiprep kit following growth in LB medium supplemented with ampicillin. The plasmids were digested with BsaI-HFv2 in CutSmart buffer for 4 hours at 37°C, followed by purification using a DNA spin column with a maximum loading capacity of 5 µg DNA per column. Target inserts were amplified from synthesized oligonucleotide pools (diluted to 10 nM) using Q5 DNA

polymerase with organism-specific primers under optimized PCR conditions: initial denaturation at 98°C for 30s, followed by 15 cycles of 98°C for 15s, 56°C for 15s, and 72°C for 15s, with a final extension at 72°C for 10 minutes. PCR products were purified and quantified using fluorometry to ensure appropriate DNA concentrations for subsequent steps.

The digested vectors and inserts were combined in a ligation reaction containing T4 DNA ligase buffer supplemented with 10 mM DTT and 1 mM ATP. After 14 hours of ligation at 16°C, the reactions were purified by dialysis against 0.1 mM Tris (pH 8.0) using a nitrocellulose membrane. The ligated libraries were transformed into electrocompetent *E. coli* strain WM6026 cells and plated on LB agar supplemented with 300 µM diaminopimelic acid (DAP) and 100 µg/mL carbenicillin. This yielded approximately 3.6 million colonies for the *E. coli* library, 2.4 million colonies for the *E. cloacae* library, and 1.5 million colonies for the *K. pneumoniae* library. Colonies were harvested by flooding plates with LB medium containing DAP, scraping to collect cells, and storing aliquots in 15% glycerol at -80°C.

Libraries were transferred to target organisms through triparental mating using carefully validated strains. The recipient strains were *E. coli* K-12 MG1655 (sJMP163), *E. cloacae* ATCC 13047 (sJMP269), and *K. pneumoniae* ATCC 43816 KPPR1 (sJMP241). Mating reactions combined normalized cultures (OD600 ≈ 40) of the *E. coli* WM6026 donor carrying the Mobile-CRISPRi library (sJMP5137-5139), a helper strain expressing Tn7 transposase (sJMP469), and the recipient strain in a 2:1:1 ratio. After 2.5 hours of mating at 37°C on non-selective LB agar, cells were collected and stored briefly at -80°C to reduce background growth of untransformed recipients. The libraries were then plated on selective media containing kanamycin to isolate successful transconjugants, yielding final strain collections designated sJMP5142 (*E. coli*), sJMP5144 (*E. cloacae*), and sJMP5146 (*K. pneumoniae*). These final libraries achieved 70-100× coverage of the guide RNA design space, with approximately 1.6 million unique integrants for *E. coli*, 1.9 million for *E. cloacae*, and 2.0 million for *K. pneumoniae*. Colonies were collected

by flooding plates with LB medium, scraping to harvest cells, and storing 96 standardized 1-mL aliquots in 15% glycerol at -80°C for subsequent experiments.

7.5. *proQ* Gene Deletion

The *proQ* deletion strain (sJMP5155) was constructed using λ Red recombineering in *E. coli* MG1655 expressing the pSIM5 temperature-sensitive recombination plasmid (sJMP6963). A FRT-flanked kanamycin resistance cassette was amplified from genomic DNA of a Keio collection strain (sJMP2029, Δ*hfq*::FRT-kan-FRT) using primers oJMP2740 and oJMP2741. The forward primer (oJMP2740) contained 40 bp of homology to the *proQ* 5' region and introduced a TAA stop codon immediately after the start codon, while the reverse primer (oJMP2741) provided 40 bp of homology to the *proQ* 3' region. Both primers included priming sequences for the FRT-kan-FRT cassette. The PCR product was purified and electroporated into cells induced for λ Red expression by heat shock at 42°C for 15 minutes. Recombinants were selected on LB agar supplemented with kanamycin (30 µg/mL) at 37°C. Correct targeting was verified by colony PCR using primers oJMP2731 and oJMP2732, which amplify a region spanning the integration site from -20 bp to +20 bp relative to the *proQ* coding sequence.

For FRT cassette removal, verified recombinants (sJMP5150) were transformed with pCP20 (encoding FLP recombinase) and selected on LB agar with ampicillin (100 µg/mL) at 30°C. Individual colonies were then restreaked on nonselective LB agar and incubated at 42°C to simultaneously resolve the FRT cassette and cure the temperature-sensitive pCP20 plasmid. Resulting colonies were patch-plated to verify sensitivity to both kanamycin and ampicillin, confirming successful marker excision and plasmid loss. The final strain (sJMP5155) was validated by PCR amplification using primers oJMP2731 and oJMP2732, followed by Sanger sequencing to confirm the presence of both the engineered stop codon and the single FRT scar.

7.6. Primers for *proQ* Inactivation and *prc* Promoter Preservation

Targeting Primers for FRT-kan-FRT Cassette Integration. The forward primer oJMP2740 targets the 5' region of *proQ* with the sequence: 5'-GAAA TTTC ATG GAAA ATCA ACCT AAGT TGAA TAGC AGTT AAat tccg ggga tcct gcga cc-3' This primer introduces a strategic mutation converting the third codon from AAA (lysine) to TAA (stop), preserving the first ~10 amino acids of ProQ. The uppercase portion provides homology for recombination, while the lowercase sequence targets the FRT-kan-FRT cassette.

The reverse primer oJMP2741 was positioned to maintain the integrity of the downstream *prc* promoter: 5'-GGAC GTGG CTTG CGTT CGCG GCGC GGTG CGTC TTCT TTCt gtag gctg gagc tgct tcg-3' This primer's homology region (uppercase) terminates approximately 120 bp upstream of the predicted *prc* promoter start site, ensuring its regulatory elements remain intact. The junction sequence was verified to avoid creating inadvertent start codons that could result in translation of the C-terminal portion of ProQ.

Verification Primers for Integration Confirmation. The checking primers oJMP2731 (5'-GCTT GCAA CGAC GGAT TACA-3') and oJMP2732 (5'-ACCG GAAT TTGA TCAG CACG-3') were designed to flank the modification site, enabling verification of both the initial integration and subsequent FRT resolution while confirming preservation of the *prc* promoter region.

7.7. Sequencing and Data Analysis

DNA was extracted from cell pellets with the DNeasy gDNA extraction kit (Qiagen) according to the manufacturer's protocol, resuspending in a final volume of 100 µL with an average yield of ~100 ng/µL. The guide RNA region was amplified using custom primers containing TruSeq adapters. Amplicon libraries were sequenced on an Illumina NovaSeq 6000 platform with 150 bp paired-end reads. Guide RNA counts were quantified using Heuristicount.py, part of the BarCoder Functional Genomics Toolkit – available at

https://github.com/ryandward/barcoder. Relative fitness scores and statistical significance were calculated using edgeR with a quasi-likelihood negative binomial model. Gene set enrichment analysis was performed using competitive gene set testing (CAMERA) against predicted genome interactions from STRING-DB.

7.8. Tol-Pal Operon Conservation Analysis

Genomic sequences for *E. coli* K-12 MG1655 (GCA_000005845.2), *K. pneumoniae* (GCA_000742755.1), and *E. cloacae* (GCA_000025565.1) were analyzed using OrthoFinder (121) to identify Tol-Pal system orthologs. A custom Python script using Biopython extracted genomic regions containing Tol-Pal components using locus tags: *E. coli* (b0737-b0741), *K. pneumoniae* (VK055_1781-1785, VK055_0760), and *E. cloacae* (ECL_02989-02994). Gene cluster alignments and similarity analyses were performed using clinker (243), generating HTML-based visualizations for comparative analysis.

Table 8: *Enterobacterales* Strains and Library Construction

This strain collection starts with initial plasmid construction in *E. coli* BW25141, followed by transfer into conjugation-capable WM6026 donor strains, and finally implementation in target species. Promoter variants (PB, PG, PI, PJ, PK, PLlacO1) are listed sequentially within strain ranges (*e.g.*, sJMP5058-5063 contains promoters PB through PLlacO1 respectively). Each stage maintains this sequential promoter organization: first testing with a GFP reporter system, then adding guide RNA targeting GFP (gmc6), and finally implementing genome-wide guide RNA libraries. The final full-genome knockdown libraries were constructed in three species: *E. coli*, *E. cloacae*, and *K. pneumoniae*.

A. Initial Plasmid Construction

Strain	Background	Promoter	Features	Resistance	Growth Media	Construction
sJMP5058-5063	E. coli BW25141	PB/PG/PI/PJ/PK/PLlacO1	dCas9-GFP	Amp, Kan	LB, Amp, Kan	HiFi assembly into pJMP2816; Electroporation: sJMP5078(1)
sJMP5064-5069	E. coli BW25141	PB/PG/PI/PJ/PK/PLlacO1	dCas9-GFP + gmc6(2)	Amp, Kan	LB, Amp, Kan	HiFi assembly into pJMP2828; Electroporation: sJMP5078(1)
sJMP5070-5075	E. coli BW25141	PB/PG/PI/PJ/PK/PLlacO1	dCas9	Amp, Kan	LB, Amp, Kan	HiFi assembly into pJMP2840; Electroporation: sJMP5078(1)

Notes: (1) sJMP5078: E. coli BW25141 cloning strain, (2) gmc6: CRISPRi guide RNA targeting GFP

B. Conjugation-Capable Donor Strains

Strain	Background	Promoter	Features	Resistance	Growth Media	Construction
sJMP5040-5045	E. coli WM6026	PB/PG/PI/PJ/PK/PLlacO1	dCas9-GFP	Cam, Amp, Kan	LB, Cam, **DAP**, Amp, Kan	Electroporation: pJMP5058-5063 into sJMP5079(3)
sJMP5046-5051	E. coli WM6026	PB/PG/PI/PJ/PK/PLlacO1	dCas9-GFP + gmc6(2)	Cam, Amp, Kan	LB, Cam, **DAP**, Amp, Kan	Electroporation: pJMP5064-5069 into sJMP5079(3)
sJMP5052-5057	E. coli WM6026	PB/PG/PI/PJ/PK/PLlacO1	dCas9	Cam, Amp, Kan	LB, Cam, **DAP**, Amp, Kan	Electroporation: pJMP5070-5075 into sJMP5079(3)

Notes: (1) sJMP5078: E. coli BW25141 cloning strain, (2) gmc6: CRISPRi guide RNA targeting GFP, (3) sJMP5079: E. coli WM6026 DAP auxotroph conjugation strain (Cam, DAP)

C. GFP CRISPRi Activity Test Strains						
Strain	**Background**	**Promoter**	**Features**	**Resistance**	**Growth Media**	**Construction**
***E. coli* Control and Test Strains**						
sJMP5099-5104	E. coli BW25113	PB/PG/PI/PJ/PK/PLlacO1	GFP , attTn7::dCas9	Kan	LB, Kan	Triparental mating: sJMP5040-5045 + sJMP469(4) + sJMP6(5)
sJMP5105-5110	E. coli BW25113	PB/PG/PI/PJ/PK/PLlacO1	GFP , attTn7::dCas9-gmc6(2)	Kan	LB, Kan	Triparental mating: sJMP5046-5051 + sJMP469(4) + sJMP6(5)
sJMP5111-5116	E. coli BW25113	PB/PG/PI/PJ/PK/PLlacO1	attTn7::dCas9	Kan	LB, Kan	Triparental mating: sJMP5052-5057 + sJMP469(4) + sJMP6(5)
***E. cloacae* Control and Test Strains**						
sJMP5117-5119	E. cloacae ATCC 13047	PB/PI/PLlacO1	GFP , attTn7::dCas9	Kan	LB, Kan	Triparental mating: sJMP5040/42/45 + sJMP469(4) + sJMP269(6)
sJMP5120-5122	E. cloacae ATCC 13047	PB/PI/PLlacO1	GFP , attTn7::dCas9-gmc6(2)	Kan	LB, Kan	Triparental mating: sJMP5046/48/51 + sJMP469(4) + sJMP269(6)
sJMP5123-5125	E. cloacae ATCC 13047	PB/PI/PLlacO1	attTn7::dCas9	Kan	LB, Kan	Triparental mating: sJMP5052/54/57 + sJMP469(4) + sJMP269(6)
***K. pneumoniae* Control and Test Strains**						
sJMP5126-5128	K. pneumoniae ATCC 43816	PB/PI/PLlacO1	GFP , attTn7::dCas9	Kan	LB, Kan	Triparental mating: sJMP5040/42/45 + sJMP469(4) + sJMP241(7)
sJMP5129-5131	K. pneumoniae ATCC 43816	PB/PI/PLlacO1	GFP , attTn7::dCas9-gmc6(2)	Kan	LB, Kan	Triparental mating: sJMP5046/48/51 + sJMP469(4) + sJMP241(7)
sJMP5132-5134	K. pneumoniae ATCC 43816	PB/PI/PLlacO1	attTn7::dCas9	Kan	LB, Kan	Triparental mating: sJMP5052/54/57 + sJMP469(4) + sJMP241(7)

Notes: (2) gmc6: CRISPRi guide RNA targeting GFP, (4) sJMP469: E. coli WM6026 carrying Tn7 transposase helper plasmid (Amp), (5) sJMP6: E. coli BW25113 wild-type recipient strain, (6) sJMP269: E. cloacae ATCC 13047 recipient strain, (7) sJMP241: K. pneumoniae ATCC 43816 recipient strain

D. Mobile-CRISPRi Library Construction						
Strain	**Background**	**Promoter**	**Features**	**Resistance**	**Growth Media**	**Construction**
Initial Library Vectors						
sJMP5135-5136	E. coli BW25141	PB/PI dCas9	Cloning vectors	Amp, Kan	LB, Amp, Kan	Electroporation: sJMP5070/5072
Donor Library Strains						
sJMP5137	E. coli WM6026	PB dCas9	E. coli lib (OD600=20)	Amp, Kan	LB, Amp, Kan, **DAP**	Electroporation: E. coli library into pJMP5135
sJMP5138	E. coli WM6026	PB dCas9	E. cloacae lib (OD600=25)	Amp, Kan	LB, Amp, Kan, **DAP**	Electroporation: E. cloacae library into pJMP5135
sJMP5139	E. coli WM6026	PI dCas9	K. pneumoniae lib (OD600=15)	Amp, Kan	LB, Amp, Kan, **DAP**	Electroporation: K. pneumoniae library into pJMP5136
Final Library Strains						
sJMP5142	E. coli MG1655	PB dCas9	attTn7::dCas9-library(8)	Kan	LB, Kan	Triparental mating: sJMP5137 + sJMP469(4) + sJMP163(9)
sJMP5144	E. cloacae ATCC 13047	PB dCas9	attTn7::dCas9-library(8)	Kan	LB, Kan	Triparental mating: sJMP5138 + sJMP469(4) + sJMP269(6)
sJMP5146	K. pneumoniae ATCC 43816	PI dCas9	attTn7::dCas9-library(8)	Kan	LB, Kan	Triparental mating: sJMP5139 + sJMP469(4) + sJMP241(7)
***E. coli proQ* Deletion Series**						
sJMP5153	E. coli MG1655	None	ΔproQ::FRT-Kan-FRT	Kan	LB, Kan	λ Red recombination with pSIM5(10)
sJMP5155	E. coli MG1655	None	ΔproQ::FRT	None	LB	FLP flip-out from sJMP5153
sJMP5161	E. coli MG1655	PB dCas9	ΔproQ::FRT attTn7::dCas9-library(8)	Kan	LB, Kan	Triparental mating: sJMP5137 + sJMP469(4) + sJMP5155

Notes: (4) sJMP469: E. coli WM6026 carrying Tn7 transposase helper plasmid (Amp), (6) sJMP269: E. cloacae ATCC 13047 recipient strain, (7) sJMP241: K. pneumoniae ATCC 43816 recipient strain, (8) Library sizes: E. coli (1.6M CFU), E. cloacae (1.9M CFU), K. pneumoniae (2.0M CFU), (9) sJMP163: E. coli MG1655 wild-type recipient strain, (10) pSIM5: Temperature-sensitive λ Red recombination plasmid

Chapter 5. Conclusions and Future Directions

1. Conclusions

The global rise of antimicrobial resistance has become a defining public health challenge of the 21st century, with a disproportionate burden falling on resource-limited healthcare systems. We investigated essential genes across bacterial pathogens to determine why some infections resist treatment, which is a problem that costs the United States healthcare system over $20 billion annually. Using targeted CRISPRi knockdowns, we mapped how bacteria respond to antibiotics through species-specific genetic interactions that vary between environments. The absence of new antibiotic classes introduced between 1962 and 2000, combined with the rapid evolution of resistance to existing drugs, requires high-throughput approaches to understand bacterial survival mechanisms. Our experiments with essential genes across multiple pathogens demonstrated fundamental biological differences between bacterial species. Single-gene deletion studies have failed to capture the complex relationships between essential cellular processes and antibiotic resistance. The distinct essential gene requirements we measured in each species present unexplored opportunities for species-selective antimicrobial development.

The comparison of essential gene function across *A. baumannii*, *P. aeruginosa*, and multiple *Enterobacterales* species revealed differences in core cellular processes. While pathways like ribosome assembly and cell wall synthesis remained universally essential, energy metabolism and membrane maintenance requirements varied between species. NADH dehydrogenase proved most vulnerable in *A. baumannii*, while *K. pneumoniae* tolerated substantial disruption of this complex. Similar species-specific patterns emerged in membrane maintenance. *E. coli* strains carrying Tol-Pal disruptions rapidly died under carbapenem stress, yet K. *pneumoniae* grew robustly under the same conditions. In *P. aeruginosa*, two metabolic genes showed no growth defects in laboratory conditions but prevented infection in animal

models. The genes, *pgsA* and *ispD*, control basic cellular components – membrane phospholipids and cell wall precursors, respectively. Since *ispD* has no human homolog, these infection-specific essential genes may offer new therapeutic opportunities missed by standard laboratory screens.

Partial inhibition of essential genes *in A. baumannii* produced complex antibiotic responses. In the case of *glnS* and *nuoB*, moderate reduction in gene expression actually increased resistance to imipenem and rifampicin, while strong repression killed cells. CRISPRi-mediated control of essential gene expression measured these intermediate phenotypes that lie between full function and complete deletion. These results motivated experiments testing bacterial responses to different antibiotic concentrations. Our work with sub-lethal imipenem concentrations in *Enterobacterales* showed that antibiotic dose markedly affects the fitness cost of carrying essential gene knockdowns. At low imipenem doses, ribosomal protein knockdowns, NADH dehydrogenase mutants, and ATP synthase deficient strains showed species-specific responses that differed markedly from both untreated and high-dose conditions. These non-linear responses to both gene inhibition and antibiotic treatment suggest that combination therapy outcomes depend heavily on precise dosing – small changes in either drug concentration or target inhibition can produce opposing effects on bacterial survival.

Genomic architecture determined how bacteria maintain essential functions through different evolutionary solutions. Multiple *A. baumannii* clinical isolates, including 17978, 19606, and AB5075, share core essential pathways but exhibit strain-specific differences, particularly in prophage regions where genes like GO593_00515, which were shown to be among the most vulnerable to knockdown. The *Enterobacterales* exhibited more extensive genomic variations affecting essential gene function. *K. pneumoniae* carries additional *tolA*-like sequences absent in *E. coli*, correlating with its enhanced tolerance to Tol-Pal disruption. These sequences shared orthology with *tolA* but may represent either partial duplications or related envelope

maintenance genes. *A. baumannii* demonstrated the most extreme case of envelope adaptation, in which it can survive without lipooligosaccharide entirely. The presence of duplicate genes, mobile elements, and strain-specific genomic architecture demonstrates the plasticity of bacterial essential functions under selective pressure, especially when alternative solutions suffer enormous fitness costs.

2. Future Directions

2.1. ProQ-Mediated Control of Essential Gene Function

The divergent effects of ProQ between bacterial species raise fundamental questions about RNA-based regulation of stress responses. In *E. coli*, ProQ deletion reversed the fitness costs of respiratory chain disruption, while *K. pneumoniae* became more sensitive to the same perturbations without ProQ. This opposite phenotype suggests species-specific RNA regulatory networks, but the molecular mechanisms remain unknown. Our STRING analysis provided initial functional connections between ProQ-affected genes; bacterial genome databases like PATRIC, BacWGSTdb, RegulonDB, and BioCyc represent resources to understand the evolutionary context of ProQ targets. The connection between ProQ and respiratory chain function suggests a role in oxidative stress response, a hypothesis testable through oxidative stress survival experiments and ROS measurements. Clinical isolate collections may also contain natural *proQ* variants that affect antibiotic sensitivity, which would provide a link to bacterial survival during infection.

2.2. Envelope Maintenance and Permeability Adaptations

K. pneumoniae contains additional *tolA*-like sequences absent in *E. coli*, correlating with different responses to Tol-Pal disruption during carbapenem stress. These distinct genetic architectures suggest fundamental differences in envelope maintenance strategies between species. A CoMBaT-seq approach (Competition of Multiplexed Barcodes over Time), which measures strain abundance changes through competitive growth experiments, using

mismatched guides targeting Tol-Pal components across *E. coli*, *K. pneumoniae*, and *E. cloacae* would generate detailed knockdown-response curves. Complementing these knockdowns with targeted overexpression of *tolA*-like sequences, combined with ethidium bromide uptake assays, would establish how gene dosage affects envelope integrity. The presence of multiple *tolA*-like sequences in *K. pneumoniae* is an ideal test case for examining how partial inhibition or overexpression of redundant envelope maintenance genes affects survival. Parallel knockdown gradients across species with different envelope maintenance strategies represents an excellent strategy to identify vulnerabilities in bacterial membrane assembly.

2.3. Host-Pathogen Interactions and Essential Gene Requirements

P. aeruginosa genes *pgsA* and *ispD* became essential only during mouse lung infection, despite minimal growth defects in laboratory media. Either nutritional availability or host factors may trigger these conditional essential gene requirements. A collaboration with an immunology lab could help measure bacterial survival against specific immune components, *e.g.*, neutrophils, antimicrobial peptides, and oxidative stress conditions. CoMBaT-seq screens using isolated neutrophils and defined immune factors represent a focused approach to dissect these host-pathogen interactions. *pgsA* affects bacterial membrane composition through phospholipid synthesis, while *ispD* produces cell wall precursors, both of which could feasibly be targets for immune recognition. Understanding how immune cells detect and respond to these bacterial pathways may identify new antibiotic targets active during infection.

References

1. Murray CJL, Ikuta KS, Sharara F, Swetschinski L, Aguilar GR, Gray A, Han C, Bisignano C, Rao P, Wool E, Johnson SC, Browne AJ, Chipeta MG, Fell F, Hackett S, Haines-Woodhouse G, Hamadani BHK, Kumaran EAP, McManigal B. 2022. Global burden of bacterial antimicrobial resistance in 2019: a systematic analysis. The Lancet 399:629–655.

2. Bassetti M, Garau J. 2021. Current and future perspectives in the treatment of multidrug-resistant Gram-negative infections. J Antimicrob Chemother 76:iv23–iv37.

3. Dadgostar P. 2019. Antimicrobial Resistance: Implications and Costs. Infect Drug Resist 12:3903.

4. Bebell LM, Muiru AN. 2014. Antibiotic use and emerging resistance—how can resource-limited countries turn the tide? Glob Heart 9:347.

5. Brooks K, Eze J, Onalenna O, Rahube TO. 2023. Analysis of antibiotic resistance from a rural community and wastewater contaminated environment linked to human and animal activities. J Hazard Mater Adv 9:100232.

6. Nadimpalli ML, Marks SJ, Montealegre MC, Gilman RH, Pajuelo MJ, Saito M, Tsukayama P, Njenga SM, Kiiru J, Swarthout J, Islam MA, Julian TR, Pickering AJ. 2020. Urban informal settlements as hotspots of antimicrobial resistance and the need to curb environmental transmission. Nat Microbiol 5:787–795.

7. Rural Hospital Closures. Sheps Cent. https://www.shepscenter.unc.edu/programs-projects/rural-health/rural-hospital-closures/. Retrieved 15 November 2024.

8. 2024. A new class of antibiotics is cause for cautious celebration — but the economics must be fixed. Nature 625:7–7.

9. Towse A, Hoyle CK, Goodall J, Hirsch M, Mestre-Ferrandiz J, Rex JH. 2017. Time for a change in how new antibiotics are reimbursed: Development of an insurance framework for funding new antibiotics based on a policy of risk mitigation. Health Policy 121:1025–1030.

10. Silver LL. 2011. Challenges of antibacterial discovery. Clin Microbiol Rev 24:71–109.

11. Zgurskaya HI, López CA, Gnanakaran S. 2015. Permeability Barrier of Gram-Negative Cell Envelopes and Approaches To Bypass It. ACS Infect Dis 1:512–522.

12. Ayon NJ. 2023. High-Throughput Screening of Natural Product and Synthetic Molecule Libraries for Antibacterial Drug Discovery. Metabolites 13:625.

13. Nikaido H. 2003. Molecular basis of bacterial outer membrane permeability revisited. Microbiol Mol Biol Rev MMBR 67:593–656.

14. Saxena D, Maitra R, Bormon R, Czekanska M, Meiers J, Titz A, Verma S, Chopra S. 2023. Tackling the outer membrane: facilitating compound entry into Gram-negative bacterial pathogens. Npj Antimicrob Resist 1:1–22.

15. Rice A, Wereszczynski J. 2018. Atomistic Scale Effects of Lipopolysaccharide Modifications on Bacterial Outer Membrane Defenses. Biophys J 114:1389.

16. Lundstedt E, Kahne D, Ruiz N. 2021. Assembly and Maintenance of Lipids at the Bacterial Outer Membrane. Chem Rev 121:5098–5123.

17. Westfall DA, Krishnamoorthy G, Wolloscheck D, Sarkar R, Zgurskaya HI, Rybenkov VV. 2017. Bifurcation kinetics of drug uptake by Gram-negative bacteria. PLOS ONE 12:e0184671.

18. Dinh T, Paulsen IT, Saier MH. 1994. A family of extracytoplasmic proteins that allow transport of large molecules across the outer membranes of gram-negative bacteria. J Bacteriol 176:3825–3831.

19. Thornsberry C, Hill BC, Swenson JM, McDougal LK. 1983. Rifampin: Spectrum of Antibacterial Activity. Rev Infect Dis 5:S412–S417.

20. PDB-101 RPD. 2019. Antibiotics in Action. https://www.rcsb.org/news/5ccb3021ea7d0653b99c87b2. Retrieved 12 November 2024.

21. Kim S, Patel DS, Park S, Slusky J, Klauda JB, Widmalm G, Im W. 2016. Bilayer Properties of Lipid A from Various Gram-Negative Bacteria. Biophys J 111:1750.

22. Rojas ER, Billings G, Odermatt PD, Auer GK, Zhu L, Miguel A, Chang F, Weibel DB, Theriot JA, Huang KC. 2018. The outer membrane is an essential load-bearing element in Gram-negative bacteria. Nature 559:617–621.

23. Biswas S, Brunel J-M, Dubus J-C, Reynaud-Gaubert M, Rolain J-M. 2012. Colistin: an update on the antibiotic of the 21st century. Expert Rev Anti Infect Ther 10:917–934.

24. Pahil KS, Gilman MSA, Baidin V, Clairfeuille T, Mattei P, Bieniossek C, Dey F, Muri D, Baettig R, Lobritz M, Bradley K, Kruse AC, Kahne D. 2024. A new antibiotic traps lipopolysaccharide in its intermembrane transporter. Nature 625:572–577.

25. Holst O, Molinaro A. 2010. Chapter 3 - Core region and lipid A components of lipopolysaccharides, p. 29–55. *In* Holst, O, Brennan, PJ, Itzstein, M von, Moran, AP (eds.), Microbial Glycobiology. Academic Press, San Diego.

26. Ward RD, Tran JS, Banta AB, Bacon EE, Rose WE, Peters JM. 2024. Essential gene knockdowns reveal genetic vulnerabilities and antibiotic sensitivities in Acinetobacter baumannii. MBio 15:e0205123.

27. Sharma A, Sharma R, Bhattacharyya T, Bhando T, Pathania R. 2017. Fosfomycin resistance in Acinetobacter baumannii is mediated by efflux through a major facilitator superfamily (MFS) transporter-AbaF. J Antimicrob Chemother 72:68–74.

28. Alenazy R. 2022. Drug Efflux Pump Inhibitors: A Promising Approach to Counter Multidrug Resistance in Gram-Negative Pathogens by Targeting AcrB Protein from AcrAB-TolC Multidrug Efflux Pump from Escherichia coli. 9. Biology 11:1328.

29. Morris SJ, Cerceo E. 2020. Trends, Epidemiology, and Management of Multi-Drug Resistant Gram-Negative Bacterial Infections in the Hospitalized Setting. Antibiotics 9.

30. Cutugno L, Cafferty JM, Pané-Farré J, O'Byrne C, Boyd A. 2020. rpoB mutations conferring rifampicin-resistance affect growth, stress response and motility in Vibrio vulnificus. Microbiology 166.

31. Adams RA, Leon G, Miller NM, Reyes SP, Thantrong CH, Thokkadam A, Lemma AS, Sivaloganathan DM, Wan X, Brynildsen MP. 2021. Rifamycin antibiotics and the mechanisms of their failure. J Antibiot (Tokyo) 74.

32. Yekani M, Azargun R, Sharifi S, Nabizadeh E, Nahand JS, Ansari NK, Memar MY, Soki J. 2023. Collateral sensitivity: An evolutionary trade-off between antibiotic resistance mechanisms, attractive for dealing with drug-resistance crisis. Health Sci Rep 6:e1418.

33. Hall AR, Iles J, MacLean RC. 2011. The Fitness Cost of Rifampicin Resistance in*Pseudomonas aeruginosa*Depends on Demand for RNA Polymerase. Genetics 187.

34. Gajdács M. 2019. The Continuing Threat of Methicillin-Resistant Staphylococcus aureus. Antibiotics 8.

35. Dunai A, Spohn R, Farkas Z, Lázár V, Györkei Á, Apjok G, Boross G, Szappanos B, Grézal G, Faragó A, Bodai L, Papp B, Pál C. 2019. Rapid decline of bacterial drug-resistance in an antibiotic-free environment through phenotypic reversion. eLife 8:e47088.

36. Munita JM, Arias CA. 2016. Mechanisms of Antibiotic Resistance. Microbiol Spectr 4:10.1128/microbiolspec.VMBF.

37. Lupo A, Haenni M, Madec J-Y. 2018. Antimicrobial Resistance in Acinetobacter spp. and Pseudomonas spp. Microbiol Spectr 6.

38. Chen C-C, Lin Y-C, Sheng W-H, Chen Y-C, Chang S-C, Hsia K-C, Liao M-H, Li S-Y. 2011. Genome Sequence of a Dominant, Multidrug-Resistant Acinetobacter baumannii Strain, TCDC-AB0715. J Bacteriol 193:2361.

39. Pagano M, Martins AF, Barth AL. 2016. Mobile genetic elements related to carbapenem resistance in Acinetobacter baumannii. Braz J Microbiol Publ Braz Soc Microbiol 47:785–792.

40. Antunes NT, Fisher JF. 2014. Acquired Class D β-Lactamases. Antibiotics 3:398.

41. Harding CM, Hennon SW, Feldman MF. 2018. Uncovering the mechanisms of Acinetobacter baumannii virulence. 2. Nat Rev Microbiol 16:91–102.

42. Fields FR, Lee SW, McConnell MJ. 2016. Using Bacterial Genomes and Essential Genes for the Development of New Antibiotics. Biochem Pharmacol 134:74.

43. Juhas M, Eberl L, Church GM. 2012. Essential genes as antimicrobial targets and cornerstones of synthetic biology. Trends Biotechnol 30:601–607.

44. Daubin V, Szöllősi GJ. 2016. Horizontal Gene Transfer and the History of Life. Cold Spring Harb Perspect Biol 8:a018036.

45. Luo H, Gao F, Lin Y. 2015. Evolutionary conservation analysis between the essential and nonessential genes in bacterial genomes. Sci Rep 5:13210.

46. Przytycka TM, Jothi R, Aravind L, Lipman DJ. 2008. Differences in evolutionary pressure acting within highly conserved ortholog groups. BMC Evol Biol 8:208.

47. Jain R, Rivera MC, Lake JA. 1999. Horizontal gene transfer among genomes: The complexity hypothesis. Proc Natl Acad Sci U S A 96:3801.

48. Koonin EV, Makarova KS, Aravind L. 2001. Horizontal Gene Transfer in Prokaryotes: Quantification and Classification1. Annu Rev Microbiol 55:709–742.

49. Junier I, Hérisson J, Képès F. 2012. Genomic Organization of Evolutionarily Correlated Genes in Bacteria: Limits and Strategies. J Mol Biol 419:369–386.

50. Christen B, Abeliuk E, Collier JM, Kalogeraki VS, Passarelli B, Coller JA, Fero MJ, McAdams HH, Shapiro L. 2011. The essential genome of a bacterium. Mol Syst Biol 7:528.

51. Bratlie MS, Johansen J, Drabløs F. 2010. Relationship between operon preference and functional properties of persistent genes in bacterial genomes. BMC Genomics 11:71.

52. Huynen MA, Bork P. 1998. Measuring genome evolution. Proc Natl Acad Sci 95:5849–5856.

53. Rocha EPC. 2008. The Organization of the Bacterial Genome. Annu Rev Genet 42:211–233.

54. Crécy-lagard V de, Hegedus RA de, Arighi C, Babor J, Bateman A, Blaby I, Blaby-Haas C, Bridge AJ, Burley SK, Cleveland S, Colwell LJ, Conesa A, Dallago C, Danchin A, Waard A de, Deutschbauer A, Dias R, Ding Y, Fang G, Friedberg I, Gerlt J, Goldford J, Gorelik M, Gyori BM, Henry C, Hutinet G, Jaroch M, Karp PD, Kondratova L, Lu Z, Marchler-Bauer A, Martin M-J, McWhite C, Moghe GD, Monaghan P, Morgat A, Mungall CJ, Natale DA, Nelson WC, O'Donoghue S, Orengo C, O'Toole KH, Radivojac P, Reed C, Roberts RJ, Rodionov D, Rodionova IA, Rudolf JD, Saleh L, Sheynkman G, Thibaud-Nissen F, Thomas PD, Uetz P, Vallenet D, Carter EW, Weigele PR, Wood V, Wood-Charlson EM, Xu J. 2022. A roadmap for the functional annotation of protein families: a community perspective. Database J Biol Databases Curation 2022:baac062.

55. Lobb B, Tremblay BJ-M, Moreno-Hagelsieb G, Doxey AC. 2020. An assessment of genome annotation coverage across the bacterial tree of life. Microb Genomics 6:e000341.

56. Wood V, Lock A, Harris MA, Rutherford K, Bähler J, Oliver SG. 2019. Hidden in plain sight: what remains to be discovered in the eukaryotic proteome? Open Biol 9:180241.

57. Vanni C, Schechter MS, Acinas SG, Barberán A, Buttigieg PL, Casamayor EO, Delmont TO, Duarte CM, Eren AM, Finn RD, Kottmann R, Mitchell A, Sánchez P, Siren K, Steinegger M, Gloeckner FO, Fernàndez-Guerra A. 2022. Unifying the known and unknown microbial coding sequence space. eLife 11:e67667.

58. Yu G, Luo W, Fu G, Wang J. 2016. Interspecies gene function prediction using semantic similarity. BMC Syst Biol 10:121.

59. Przybyla L, Gilbert LA. 2022. A new era in functional genomics screens. Nat Rev Genet 23:89–103.

60. Bosch B, DeJesus MA, Poulton NC, Zhang W, Engelhart CA, Zaveri A, Lavalette S, Ruecker N, Trujillo C, Wallach JB, Li S, Ehrt S, Chait BT, Schnappinger D, Rock JM. 2021. Genome-wide gene expression tuning reveals diverse vulnerabilities of M. tuberculosis. Cell 184:4579-4592.e24.

61. Brown ED, Wright GD. 2016. Antibacterial drug discovery in the resistance era. Nature 529:336–343.

62. Cacace E, Kritikos G, Typas A. 2017. Chemical genetics in drug discovery. Curr Opin Syst Biol 4:35–42.

63. Kobras CM, Fenton AK, Sheppard SK. 2021. Next-generation microbiology: from comparative genomics to gene function. Genome Biol 22:123.

64. Thomason LC, Sawitzke JA, Li X, Costantino N, Court DL. 2014. Recombineering: Genetic Engineering in Bacteria Using Homologous Recombination. Curr Protoc Mol Biol 106:1.16.1-1.16.39.

65. Baba T, Ara T, Hasegawa M, Takai Y, Okumura Y, Baba M, Datsenko KA, Tomita M, Wanner BL, Mori H. 2006. Construction of Escherichia coli K-12 in-frame, single-gene knockout mutants: the Keio collection. Mol Syst Biol 2:2006.0008.

66. Tong M, French S, Zahed SSE, Ong W kit, Karp PD, Brown ED. 2020. Gene Dispensability in Escherichia coli Grown in Thirty Different Carbon Environments. mBio 11:e02259.

67. van Opijnen T, Bodi KL, Camilli A. 2009. Tn-seq: high-throughput parallel sequencing for fitness and genetic interaction studies in microorganisms. Nat Methods 6:767–772.

68. Cain AK, Barquist L, Goodman AL, Paulsen IT, Parkhill J, van Opijnen T. 2020. A decade of advances in transposon-insertion sequencing. Nat Rev Genet 21:526–540.

69. Poulsen BE, Yang R, Clatworthy AE, White T, Osmulski SJ, Li L, Penaranda C, Lander ES, Shoresh N, Hung DT. 2019. Defining the core essential genome of Pseudomonas aeruginosa. Proc Natl Acad Sci U S A 116:10072–10080.

70. Rosconi F, Rudmann E, Li J, Surujon D, Anthony J, Frank M, Jones DS, Rock C, Rosch JW, Johnston CD, van Opijnen T. 2022. A bacterial pan-genome makes gene essentiality strain-dependent and evolvable. Nat Microbiol 7:1580–1592.

71. Gallagher LA, Bailey J, Manoil C. 2020. Ranking essential bacterial processes by speed of mutant death. Proc Natl Acad Sci U S A 117:18010–18017.

72. Bailey J, Cass J, Gasper J, Ngo N-D, Wiggins P, Manoil C. 2019. Essential gene deletions producing gigantic bacteria. PLoS Genet 15:e1008195.

73. Santiago M, Matano LM, Moussa SH, Gilmore MS, Walker S, Meredith TC. 2015. A new platform for ultra-high density Staphylococcus aureus transposon libraries. BMC Genomics 16:252.

74. Qi LS, Larson MH, Gilbert LA, Doudna JA, Weissman JS, Arkin AP, Lim WA. 2013. Repurposing CRISPR as an RNA-guided platform for sequence-specific control of gene expression. Cell 152:1173–1183.

75. Hawkins JS, Silvis MR, Koo B-M, Peters JM, Jost M, Hearne CC, Weissman JS, Todor H, Gross CA. 2019. Modulated efficacy CRISPRi reveals evolutionary conservation of essential gene expression-fitness relationships in bacteria. bioRxiv 805333.

76. Peters JM, Colavin A, Shi H, Czarny TL, Larson MH, Wong S, Hawkins JS, Lu CHS, Koo B-M, Marta E, Shiver AL, Whitehead EH, Weissman JS, Brown ED, Qi LS, Huang KC, Gross CA. 2016. A Comprehensive, CRISPR-based Functional Analysis of Essential Genes in Bacteria. Cell 165:1493–1506.

77. Goodall ECA, Morris FC, McKeand SA, Sullivan R, Warner IA, Sheehan E, Boelter G, Icke C, Cunningham AF, Cole JA, Banzhaf M, Bryant JA, Henderson IR. 2022. LI-Detector: a Method for Curating Ordered Gene-Replacement Libraries. Microbiol Spectr 10:e00833-22.

78. de Bakker V, Liu X, Bravo AM, Veening J-W. 2022. CRISPRi-seq for genome-wide fitness quantification in bacteria. Nat Protoc 17:252–281.

79. Wang T, Guan C, Guo J, Liu B, Wu Y, Xie Z, Zhang C, Xing X-H. 2018. Pooled CRISPR interference screening enables genome-scale functional genomics study in bacteria with superior performance. 1. Nat Commun 9:2475.

80. Zhang R, Xu W, Shao S, Wang Q. 2021. Gene Silencing Through CRISPR Interference in Bacteria: Current Advances and Future Prospects. Front Microbiol 12:635227.

81. Todor H, Silvis MR, Osadnik H, Gross CA. 2021. Bacterial CRISPR screens for gene function. Curr Opin Microbiol 59:102–109.

82. Wiktor J, Lesterlin C, Sherratt DJ, Dekker C. 2016. CRISPR-mediated control of the bacterial initiation of replication. Nucleic Acids Res 44:3801–3810.

83. Javaid N, Choi S. 2021. CRISPR/Cas System and Factors Affecting Its Precision and Efficiency. Front Cell Dev Biol 9:761709.

84. Akinci E, Hamilton MC, Khowpinitchai B, Sherwood RI. 2021. Using CRISPR to understand and manipulate gene regulation. Dev Camb Engl 148:dev182667.

85. Fonseca MM, Harris DJ, Posada D. 2013. Origin and Length Distribution of Unidirectional Prokaryotic Overlapping Genes. G3 GenesGenomesGenetics 4:19.

86. Hawkins JS, Silvis MR, Koo B-M, Peters JM, Osadnik H, Jost M, Hearne CC, Weissman JS, Todor H, Gross CA. 2020. Mismatch-CRISPRi Reveals the Co-varying Expression-Fitness Relationships of Essential Genes in Escherichia coli and Bacillus subtilis. Cell Syst https://doi.org/10.1016/j.cels.2020.09.009.

87. Banta AB, Ward RD, Tran JS, Bacon EE, Peters JM. 2020. Programmable Gene Knockdown in Diverse Bacteria Using Mobile-CRISPRi. Curr Protoc Microbiol 59:e130.

88. Peters JM, Koo B-M, Patino R, Heussler GE, Hearne CC, Qu J, Inclan YF, Hawkins JS, Lu CHS, Silvis MR, Harden MM, Osadnik H, Peters JE, Engel JN, Dutton RJ, Grossman AD, Gross CA, Rosenberg OS. 2019. Enabling genetic analysis of diverse bacteria with Mobile-CRISPRi. Nat Microbiol 4:244–250.

89. Gilbert LA, Larson MH, Morsut L, Liu Z, Brar GA, Torres SE, Stern-Ginossar N, Brandman O, Whitehead EH, Doudna JA, Lim WA, Weissman JS, Qi LS. 2013. CRISPR-mediated modular RNA-guided regulation of transcription in eukaryotes. Cell 154:442–451.

90. Rock JM, Hopkins FF, Chavez A, Diallo M, Chase MR, Gerrick ER, Pritchard JR, Church GM, Rubin EJ, Sassetti CM, Schnappinger D, Fortune SM. 2017. Programmable transcriptional repression in mycobacteria using an orthogonal CRISPR interference platform. Nat Microbiol 2:16274.

91. Cui L, Vigouroux A, Rousset F, Varet H, Khanna V, Bikard D. 2018. A CRISPRi screen in E. coli reveals sequence-specific toxicity of dCas9. 1. Nat Commun 9:1912.

92. Enright AL, Banta AB, Ward RD, Rivera Vazquez J, Felczak MM, Wolfe MB, TerAvest MA, Amador-Noguez D, Peters JM. 2023. The genetics of aerotolerant growth in an alphaproteobacterium with a naturally reduced genome. mBio e0148723.

93. Enright AL, Heelan WJ, Ward RD, Peters JM. 2024. CRISPRi functional genomics in bacteria and its application to medical and industrial research. Microbiol Mol Biol Rev MMBR 88:e0017022.

94. Qu J, Prasad NK, Yu MA, Chen S, Lyden A, Herrera N, Silvis MR, Crawford E, Looney MR, Peters JM, Rosenberg OS. 2019. Modulating pathogenesis with Mobile-CRISPRi. J Bacteriol https://doi.org/10.1128/JB.00304-19.

95. Cho S, Choe D, Lee E, Kim SC, Palsson B, Cho B-K. 2018. High-Level dCas9 Expression Induces Abnormal Cell Morphology in Escherichia coli. ACS Synth Biol 7:1085–1094.

96. Lee YJ, Hoynes-O'Connor A, Leong MC, Moon TS. 2016. Programmable control of bacterial gene expression with the combined CRISPR and antisense RNA system. Nucleic Acids Res 44:2462–2473.

97. Zhang S, Voigt CA. 2018. Engineered dCas9 with reduced toxicity in bacteria: implications for genetic circuit design. Nucleic Acids Res 46:11115–11125.

98. Rostain W, Grebert T, Vyhovskyi D, Pizarro PT, Tshinsele-Van Bellingen G, Cui L, Bikard D. 2023. Cas9 off-target binding to the promoter of bacterial genes leads to silencing and toxicity. Nucleic Acids Res 51:3485–3496.

99. Zhao H, Sun Y, Peters JM, Gross CA, Garner EC, Helmann JD. 2016. Depletion of Undecaprenyl Pyrophosphate Phosphatases Disrupts Cell Envelope Biogenesis in Bacillus subtilis. J Bacteriol 198:2925–2935.

100. Figueroa-Cuilan W, Daniel JJ, Howell M, Sulaiman A, Brown PJB. 2016. Mini-Tn7 Insertion in an Artificial attTn7 Site Enables Depletion of the Essential Master Regulator CtrA in the Phytopathogen Agrobacterium tumefaciens. Appl Env Microbiol 82:5015–5025.

101. Mathis AD, Otto RM, Reynolds KA. 2021. A simplified strategy for titrating gene expression reveals new relationships between genotype, environment, and bacterial growth. Nucleic Acids Res 49:e6.

102. Vigouroux A, Oldewurtel E, Cui L, Bikard D, Teeffelen S van. 2018. Tuning dCas9's ability to block transcription enables robust, noiseless knockdown of bacterial genes. Mol Syst Biol 14:e7899.

103. Liu X, Kimmey JM, Matarazzo L, de Bakker V, Van Maele L, Sirard J-C, Nizet V, Veening J-W. 2021. Exploration of Bacterial Bottlenecks and Streptococcus pneumoniae Pathogenesis by CRISPRi-Seq. Cell Host Microbe 29:107-120.e6.

104. Martin JK, Sheehan JP, Bratton BP, Moore GM, Mateus A, Li SH-J, Kim H, Rabinowitz JD, Typas A, Savitski MM, Wilson MZ, Gitai Z. 2020. A Dual-Mechanism Antibiotic Kills Gram-Negative Bacteria and Avoids Drug Resistance. Cell 181:1518-1532.e14.

105. Liu G, Catacutan DB, Rathod K, Swanson K, Jin W, Mohammed JC, Chiappino-Pepe A, Syed SA, Fragis M, Rachwalski K, Magolan J, Surette MG, Coombes BK, Jaakkola T, Barzilay R, Collins JJ, Stokes JM. 2023. Deep learning-guided discovery of an antibiotic targeting Acinetobacter baumannii. Nat Chem Biol 19:1342–1350.

106. Ward RD, Tran JS, Banta AB, Bacon EE, Rose WE, Peters JM. 2023. Essential Gene Knockdowns Reveal Genetic Vulnerabilities and Antibiotic Sensitivities in Acinetobacter baumannii. BioRxiv Prepr Serv Biol 2023.08.02.551708.

107. Geisinger E, Mortman NJ, Dai Y, Cokol M, Syal S, Farinha A, Fisher DG, Tang AY, Lazinski DW, Wood S, Anthony J, van Opijnen T, Isberg RR. 2020. Antibiotic susceptibility signatures identify potential antimicrobial targets in the Acinetobacter baumannii cell envelope. Nat Commun 11:4522.

108. Khurana MP, Curran-Sebastian J, Bhatt S, Knight GM. 2024. Modelling the implementation of narrow versus broader spectrum antibiotics in the empiric treatment of E. coli bacteraemia. Sci Rep 14:16986.

109. Liu X, Gallay C, Kjos M, Domenech A, Slager J, van Kessel SP, Knoops K, Sorg RA, Zhang J, Veening J. 2017. High-throughput CRISPRi phenotyping identifies new essential genes in Streptococcus pneumoniae. Mol Syst Biol 13.

110. Bai J, Dai Y, Farinha A, Tang AY, Syal S, Vargas-Cuebas G, van Opijnen T, Isberg RR, Geisinger E. 2021. Essential Gene Analysis in Acinetobacter baumannii by High-Density Transposon Mutagenesis and CRISPR Interference. J Bacteriol 203:e0056520.

111. Caro F, Place NM, Mekalanos JJ. 2019. Analysis of lipoprotein transport depletion in Vibrio cholerae using CRISPRi. Proc Natl Acad Sci U S A 116:17013–17022.

112. Luo Z-Q, Isberg RR. 2004. Multiple substrates of the Legionella pneumophila Dot/Icm system identified by interbacterial protein transfer. Proc Natl Acad Sci U S A 101:841–846.

113. Burstein D, Zusman T, Degtyar E, Viner R, Segal G, Pupko T. 2009. Genome-scale identification of Legionella pneumophila effectors using a machine learning approach. PLoS Pathog 5:e1000508.

114. Zhu W, Banga S, Tan Y, Zheng C, Stephenson R, Gately J, Luo Z-Q. 2011. Comprehensive identification of protein substrates of the Dot/Icm type IV transporter of Legionella pneumophila. PloS One 6:e17638.

115. Lifshitz Z, Burstein D, Peeri M, Zusman T, Schwartz K, Shuman HA, Pupko T, Segal G. 2013. Computational modeling and experimental validation of the Legionella and Coxiella virulence-related type-IVB secretion signal. Proc Natl Acad Sci U S A 110:E707-715.

116. Wexler M, Zusman T, Linsky M, Lifshitz Z, Segal G. 2022. The Legionella genus core effectors display functional conservation among orthologs by themselves or combined with an accessory protein. Curr Res Microb Sci 3:100105.

117. McNeil MB, Keighley LM, Cook JR, Cheung C-Y, Cook GM. 2021. CRISPR interference identifies vulnerable cellular pathways with bactericidal phenotypes in Mycobacterium tuberculosis. Mol Microbiol 116:1033–1043.

118. Li S, Poulton NC, Chang JS, Azadian ZA, DeJesus MA, Ruecker N, Zimmerman MD, Eckartt KA, Bosch B, Engelhart CA, Sullivan DF, Gengenbacher M, Dartois VA, Schnappinger D, Rock JM. 2022. CRISPRi chemical genetics and comparative genomics identify genes mediating drug potency in Mycobacterium tuberculosis. 6. Nat Microbiol 7:766–779.

119. Rousset F, Cui L, Siouve E, Becavin C, Depardieu F, Bikard D. 2018. Genome-wide CRISPR-dCas9 screens in E. coli identify essential genes and phage host factors. PLoS Genet 14:e1007749.

120. Condon C. 2003. RNA Processing and Degradation in Bacillus subtilis. Microbiol Mol Biol Rev 67:157–174.

121. Emms DM, Kelly S. 2019. OrthoFinder: phylogenetic orthology inference for comparative genomics. Genome Biol 20:238.

122. Szklarczyk D, Kirsch R, Koutrouli M, Nastou K, Mehryary F, Hachilif R, Gable AL, Fang T, Doncheva NT, Pyysalo S, Bork P, Jensen LJ, von Mering C. 2023. The STRING database in 2023: protein-protein association networks and functional enrichment analyses for any sequenced genome of interest. Nucleic Acids Res 51:D638–D646.

123. Darling ACE, Mau B, Blattner FR, Perna NT. 2004. Mauve: multiple alignment of conserved genomic sequence with rearrangements. Genome Res 14:1394–1403.

124. Babraham Bioinformatics - FastQC A Quality Control tool for High Throughput Sequence Data. https://www.bioinformatics.babraham.ac.uk/projects/fastqc/. Retrieved 19 November 2024.

125. Leggett RM, Ramirez-Gonzalez RH, Clavijo BJ, Waite D, Davey RP. 2013. Sequencing quality assessment tools to enable data-driven informatics for high throughput genomics. Front Genet 4:288.

126. Ward RD. 2024. ryandward/barcoder. Python.

127. Bock C, Datlinger P, Chardon F, Coelho MA, Dong MB, Lawson KA, Lu T, Maroc L, Norman TM, Song B, Stanley G, Chen S, Garnett M, Li W, Moffat J, Qi LS, Shapiro RS, Shendure J, Weissman JS, Zhuang X. 2022. High-content CRISPR screening. Nat Rev Methods Primer 2:1–23.

128. Gerlini A, Colomba L, Furi L, Braccini T, Manso AS, Pammolli A, Wang B, Vivi A, Tassini M, van Rooijen N, Pozzi G, Ricci S, Andrew PW, Koedel U, Moxon ER, Oggioni MR. 2014. The Role of Host and Microbial Factors in the Pathogenesis of Pneumococcal Bacteraemia Arising from a Single Bacterial Cell Bottleneck. PLoS Pathog 10:e1004026.

129. Krimbas CB, Tsakas S. 1971. THE GENETICS OF DACUS OLEAE. V. CHANGES OF ESTERASE POLYMORPHISM IN A NATURAL POPULATION FOLLOWING INSECTICIDE CONTROL—SELECTION OR DRIFT?1. Evolution 25:454–460.

130. Abel S, Abel zur Wiesch P, Chang H-H, Davis BM, Lipsitch M, Waldor MK. 2015. Sequence tag-based analysis of microbial population dynamics. Nat Methods 12:223–6, 3 p following 226.

131. Essential gene disruptions reveal complex relationships between phenotypic robustness, pleiotropy, and fitness | Molecular Systems Biology. https://www.embopress.org/doi/full/10.15252/msb.20145264. Retrieved 25 November 2024.

132. Otto RM, Turska-Nowak A, Brown PM, Reynolds KA. 2024. A continuous epistasis model for predicting growth rate given combinatorial variation in gene expression and environment. Cell Syst 15:134-148.e7.

133. Brain P, Cousens R. 1989. An equation to describe dose responses where there is stimulation of growth at low doses. Weed Res 29:93–96.

134. Mattson MP. 2007. Hormesis Defined. Ageing Res Rev 7:1.

135. Lewis F, Butler A, Gilbert L. 2011. A unified approach to model selection using the likelihood ratio test. Methods Ecol Evol 2:155–162.

136. Prasad NK, Seiple IB, Cirz RT, Rosenberg OS. 2022. Leaks in the pipeline: A failure analysis of Gram-negative antibiotic development from 2010 to 2020. Antimicrob Agents Chemother 66:e0005422.

137. Centers for Disease Control and Prevention (U.S.). 2019. Antibiotic resistance threats in the United States, 2019. Centers for Disease Control and Prevention (U.S.).

138. Poirel L, Naas T, Nordmann P. 2010. Diversity, epidemiology, and genetics of class D beta-lactamases. Antimicrob Agents Chemother 54:24–38.

139. Héritier C, Poirel L, Lambert T, Nordmann P. 2005. Contribution of acquired carbapenem-hydrolyzing oxacillinases to carbapenem resistance in Acinetobacter baumannii. Antimicrob Agents Chemother 49:3198–3202.

140. Valentine SC, Contreras D, Tan S, Real LJ, Chu S, Xu HH. 2008. Phenotypic and molecular characterization of Acinetobacter baumannii clinical isolates from nosocomial outbreaks in Los Angeles County, California. J Clin Microbiol 46:2499–2507.

141. Zhao J, Zhu Y, Han J, Lin Y-W, Aichem M, Wang J, Chen K, Velkov T, Schreiber F, Li J. 2020. Genome-Scale Metabolic Modeling Reveals Metabolic Alterations of Multidrug-Resistant Acinetobacter baumannii in a Murine Bloodstream Infection Model. Microorganisms 8:E1793.

142. Boll JM, Crofts AA, Peters K, Cattoir V, Vollmer W, Davies BW, Trent MS. 2016. A penicillin-binding protein inhibits selection of colistin-resistant, lipooligosaccharide-deficient Acinetobacter baumannii. Proc Natl Acad Sci U S A 113:E6228–E6237.

143. Moffatt JH, Harper M, Harrison P, Hale JDF, Vinogradov E, Seemann T, Henry R, Crane B, St Michael F, Cox AD, Adler B, Nation RL, Li J, Boyce JD. 2010. Colistin resistance in Acinetobacter baumannii is mediated by complete loss of lipopolysaccharide production. Antimicrob Agents Chemother 54:4971–4977.

144. Gallagher LA, Ramage E, Weiss EJ, Radey M, Hayden HS, Held KG, Huse HK, Zurawski DV, Brittnacher MJ, Manoil C. 2015. Resources for Genetic and Genomic Analysis of Emerging Pathogen Acinetobacter baumannii. J Bacteriol 197:2027–2035.

145. Bikard D, Jiang W, Samai P, Hochschild A, Zhang F, Marraffini LA. 2013. Programmable repression and activation of bacterial gene expression using an engineered CRISPR-Cas system. Nucleic Acids Res gkt520.

146. Byun G, Yang J, Seo SW. 2023. CRISPRi-mediated tunable control of gene expression level with engineered single-guide RNA in Escherichia coli. Nucleic Acids Res 51:4650–4659.

147. Tsubouchi T, Suzuki M, Niki M, Oinuma K-I, Niki M, Kakeya H, Kaneko Y. 2020. Complete Genome Sequence of Acinetobacter baumannii ATCC 19606T, a Model Strain of Pathogenic Bacteria Causing Nosocomial Infection. Microbiol Resour Announc 9:e00289-20.

148. Hullahalli K, Pritchard JR, Waldor MK. 2021. Refined Quantification of Infection Bottlenecks and Pathogen Dissemination with STAMPR. mSystems 6:e0088721.

149. Silver LL. 2017. Fosfomycin: Mechanism and Resistance. Cold Spring Harb Perspect Med 7:a025262.

150. Maguire BA, Wild DG. 1997. The roles of proteins L28 and L33 in the assembly and function of Escherichia coli ribosomes in vivo. Mol Microbiol 23:237–245.

151. Maguire BA, Wild DG. 1997. Mutations in the rpmBG operon of Escherichia coli that affect ribosome assembly. J Bacteriol 179:2486–2493.

152. Koo B-M, Kritikos G, Farelli JD, Todor H, Tong K, Kimsey H, Wapinski I, Galardini M, Cabal A, Peters JM, Hachmann A-B, Rudner DZ, Allen KN, Typas A, Gross CA. 2017. Construction and Analysis of Two Genome-Scale Deletion Libraries for Bacillus subtilis. Cell Syst 4:291-305.e7.

153. Sauer RT, Krovatin W, DeAnda J, Youderian P, Susskind MM. 1983. Primary structure of the immI immunity region of bacteriophage P22. J Mol Biol 168:699–713.

154. Young R. 2014. Phage lysis: three steps, three choices, one outcome. J Microbiol Seoul Korea 52:243–258.

155. Volynets GP, Usenko MO, Gudzera OI, Starosyla SA, Balanda AO, Syniugin AR, Gorbatiuk OB, Prykhod'ko AO, Bdzhola VG, Yarmoluk SM, Tukalo MA. 2022. Identification of dual-targeted Mycobacterium tuberculosis aminoacyl-tRNA synthetase inhibitors using machine learning. Future Med Chem 14:1223–1237.

156. Johnson RA, Chan AN, Ward RD, McGlade CA, Hatfield BM, Peters JM, Li B. 2021. Inhibition of Isoleucyl-tRNA Synthetase by the Hybrid Antibiotic Thiomarinol. J Am Chem Soc 143:12003–12013.

157. Papp-Wallace KM, Endimiani A, Taracila MA, Bonomo RA. 2011. Carbapenems: Past, Present, and Future ▿. Antimicrob Agents Chemother 55:4943–4960.

158. Kouidmi I, Levesque RC, Paradis-Bleau C. 2014. The biology of Mur ligases as an antibacterial target. Mol Microbiol 94:242–253.

159. Falagas ME, Kastoris AC, Karageorgopoulos DE, Rafailidis PI. 2009. Fosfomycin for the treatment of infections caused by multidrug-resistant non-fermenting Gram-negative bacilli: a systematic review of microbiological, animal and clinical studies. Int J Antimicrob Agents 34:111–120.

160. Lee AJ, Wang S, Meredith HR, Zhuang B, Dai Z, You L. 2018. Robust, linear correlations between growth rates and β-lactam–mediated lysis rates. Proc Natl Acad Sci 115:4069–4074.

161. Tuomanen E, Cozens R, Tosch W, Zak O, Tomasz A. 1986. The rate of killing of Escherichia coli by beta-lactam antibiotics is strictly proportional to the rate of bacterial growth. J Gen Microbiol 132:1297–1304.

162. Mathies AW, Leedom JM, Ivler D, Wehrle PF, Portnoy B. 1967. Antibiotic antagonism in bacterial meningitis. Antimicrob Agents Chemother 7:218–224.

163. Calabrese EJ, Mattson MP. 2017. How does hormesis impact biology, toxicology, and medicine? 1. Npj Aging Mech Dis 3:1–8.

164. Hogg GM, Barr JG, Webb CH. 1998. In-vitro activity of the combination of colistin and rifampicin against multidrug-resistant strains of Acinetobacter baumannii. J Antimicrob Chemother 41:494–495.

165. Vaara M. 1992. Agents that increase the permeability of the outer membrane. Microbiol Rev 56:395–411.

166. Deris ZZ, Akter J, Sivanesan S, Roberts KD, Thompson PE, Nation RL, Li J, Velkov T. 2014. A secondary mode of action of polymyxins against Gram-negative bacteria involves the inhibition of NADH-quinone oxidoreductase activity. 2. J Antibiot (Tokyo) 67:147–151.

167. The firA gene of Escherichia coli encodes UDP-3-O-(R-3-hydroxymyristoyl)-glucosamine N-acyltransferase. The third step of endotoxin biosynthesis - PubMed. https://pubmed.ncbi.nlm.nih.gov/8366125/. Retrieved 26 October 2022.

168. Luo H, Lin Y, Liu T, Lai F-L, Zhang C-T, Gao F, Zhang R. 2021. DEG 15, an update of the Database of Essential Genes that includes built-in analysis tools. Nucleic Acids Res 49:D677–D686.

169. Vinella D, Joseleau-Petit D, Thévenet D, Bouloc P, D'Ari R. 1993. Penicillin-binding protein 2 inactivation in Escherichia coli results in cell division inhibition, which is relieved by FtsZ overexpression. J Bacteriol 175:6704–6710.

170. Hards K, Adolph C, Harold LK, McNeil MB, Cheung C-Y, Jinich A, Rhee KY, Cook GM. 2020. Two for the price of one: Attacking the energetic-metabolic hub of mycobacteria to produce new chemotherapeutic agents. Prog Biophys Mol Biol 152:35–44.

171. Vilchèze C, Weisbrod TR, Chen B, Kremer L, Hazbón MH, Wang F, Alland D, Sacchettini JC, Jacobs WR. 2005. Altered NADH/NAD+ Ratio Mediates Coresistance to Isoniazid and Ethionamide in Mycobacteria. Antimicrob Agents Chemother 49:708–720.

172. MacNair CR, Stokes JM, Carfrae LA, Fiebig-Comyn AA, Coombes BK, Mulvey MR, Brown ED. 2018. Overcoming mcr-1 mediated colistin resistance with colistin in combination with other antibiotics. 1. Nat Commun 9:458.

173. Olmeda-López H, Corral-Lugo A, McConnell MJ. 2021. Effect of Subinhibitory Concentrations of Antibiotics and Disinfectants on ISAba-Mediated Inactivation of Lipooligosaccharide Biosynthesis Genes in Acinetobacter baumannii. 10. Antibiotics 10:1259.

174. Schurek KN, Marr AK, Taylor PK, Wiegand I, Semenec L, Khaira BK, Hancock REW. 2008. Novel Genetic Determinants of Low-Level Aminoglycoside Resistance in *Pseudomonas aeruginosa*. Antimicrob Agents Chemother 52:4213–4219.

175. Santi I, Manfredi P, Maffei E, Egli A, Jenal U. 2021. Evolution of Antibiotic Tolerance Shapes Resistance Development in Chronic Pseudomonas aeruginosa Infections 12:17.

176. Shelake RM, Pramanik D, Kim J-Y. 2023. Improved Dual Base Editor Systems (iACBEs) for Simultaneous Conversion of Adenine and Cytosine in the Bacterium Escherichia coli. mBio 14:e02296-22.

177. Rauch BJ, Silvis MR, Hultquist JF, Waters CS, McGregor MJ, Krogan NJ, Bondy-Denomy J. 2017. Inhibition of CRISPR-Cas9 with Bacteriophage Proteins. Cell 168:150-158.e10.

178. Thomason LC, Sawitzke JA, Li X, Costantino N, Court DL. 2014. Recombineering: genetic engineering in bacteria using homologous recombination. Curr Protoc Mol Biol 106:1.16.1-39.

179. Thomason LC, Costantino N, Court DL. 2007. E. coli genome manipulation by P1 transduction. Curr Protoc Mol Biol Chapter 1:1.17.1-1.17.8.

180. Cherepanov PP, Wackernagel W. 1995. Gene disruption in Escherichia coli: TcR and KmR cassettes with the option of Flp-catalyzed excision of the antibiotic-resistance determinant. Gene 158:9–14.

181. Sprouffske K, Wagner A. 2016. Growthcurver: an R package for obtaining interpretable metrics from microbial growth curves. BMC Bioinformatics 17:172.

182. Prasad NK, Ward RD, Yu MA, Kwon MS, Banta AB, Rosenberg OS, Peters JM. 2024. Pseudomonas aeruginosa essential gene perturbations that confer vulnerability to the mammalian host environment. bioRxiv https://doi.org/10.1101/2024.11.05.622029.

183. 2024. WHO bacterial priority pathogens list, 2024: Bacterial pathogens of public health importance to guide research, development and strategies to prevent and control antimicrobial resistance. World Health Organization.

184. Kristian SA, Timmer AM, Liu GY, Lauth X, Sal-Man N, Rosenfeld Y, Shai Y, Gallo RL, Nizet V. 2007. Impairment of innate immune killing mechanisms by bacteriostatic antibiotics. FASEB J 21:1107–1116.

185. Dhand A, Bayer AS, Pogliano J, Yang S-J, Bolaris M, Nizet V, Wang G, Sakoulas G. 2011. Use of antistaphylococcal beta-lactams to increase daptomycin activity in eradicating persistent bacteremia due to methicillin-resistant Staphylococcus aureus: role of enhanced daptomycin binding. Clin Infect Dis 53:158–163.

186. Sakoulas G, Bayer AS, Pogliano J, Tsuji BT, Yang S-J, Mishra NN, Nizet V, Yeaman MR, Moise PA. 2012. Ampicillin enhances daptomycin- and cationic host defense peptide-mediated killing of ampicillin- and vancomycin-resistant Enterococcus faecium. Antimicrob Agents Chemother 56:838–844.

187. Dhand A, Sakoulas G. 2014. Daptomycin in combination with other antibiotics for the treatment of complicated methicillin-resistant Staphylococcus aureus bacteremia. Clin Ther 36:1303–1316.

188. Sakoulas G, Nonejuie P, Kullar R, Pogliano J, Rybak MJ, Nizet V. 2015. Examining the use of ceftaroline in the treatment of Streptococcus pneumoniae meningitis with reference to human cathelicidin LL-37. Antimicrob Agents Chemother 59:2428–2431.

189. van Opijnen T, Camilli A. 2012. A fine scale phenotype-genotype virulence map of a bacterial pathogen. Genome Res 22:2541–2551.

190. Skurnik D, Roux D, Aschard H, Cattoir V, Yoder-Himes D, Lory S, Pier GB. 2013. A comprehensive analysis of in vitro and in vivo genetic fitness of Pseudomonas aeruginosa using high-throughput sequencing of transposon libraries. PLoS Pathog 9:e1003582.

191. Smith EE, Buckley DG, Wu Z, Saenphimmachak C, Hoffman LR, D'Argenio DA, Miller SI, Ramsey BW, Speert DP, Moskowitz SM, Burns JL, Kaul R, Olson MV. 2006. Genetic adaptation by Pseudomonas aeruginosa to the airways of cystic fibrosis patients. Proc Natl Acad Sci U A 103:8487–8492.

192. Wei J-R, Krishnamoorthy V, Murphy K, Kim J-H, Schnappinger D, Alber T, Sassetti CM, Rhee KY, Rubin EJ. 2011. Depletion of antibiotic targets has widely varying effects on growth. Proc Natl Acad Sci U A 108:4176–4181.

193. Jost M, Santos DA, Saunders RA, Horlbeck MA, Hawkins JS, Scaria SM, Norman TM, Hussmann JA, Liem CR, Gross CA, Weissman JS. 2020. Titrating gene expression using libraries of systematically attenuated CRISPR guide RNAs. Nat Biotechnol 38:355–364.

194. Keren L, Hausser J, Lotan-Pompan M, Vainberg Slutskin I, Alisar H, Kaminski S, Weinberger A, Alon U, Milo R, Segal E. 2016. Massively parallel interrogation of the effects of gene expression levels on fitness. Cell 166:1282-1294.e18.

195. Qu J, Prasad NK, Yu MA, Chen S, Lyden A, Herrera N, Silvis MR, Crawford E, Looney MR, Peters JM, Rosenberg OS. 2019. Modulating pathogenesis with Mobile-CRISPRi. J Bacteriol 201.

196. Oluoch PO, Koh E-I, Proulx MK, Reames CJ, Papavinasasundaram KG, Murphy KC, Zimmerman MD, Dartois V, Sassetti CM. 2024. Chemical genetic interactions elucidate pathways controlling tuberculosis antibiotic efficacy during infection. bioRxivorg 2024.09.04.609063.

197. Ortiz-Muñoz G, Looney MR. 2015. Non-invasive intratracheal instillation in mice. Bio Protoc 5.

198. Lloyd MG, Lundgren BR, Hall CW, Gagnon LB-P, Mah T-F, Moffat JF, Nomura CT. 2017. Targeting the alternative sigma factor RpoN to combat virulence in Pseudomonas aeruginosa. Sci Rep 7:12615.

199. Hendrickson EL, Plotnikova J, Mahajan-Miklos S, Rahme LG, Ausubel FM. 2001. Differential roles of the Pseudomonas aeruginosa PA14 rpoN gene in pathogenicity in plants, nematodes, insects, and mice. J Bacteriol 183:7126–7134.

200. Jeukens J, Boyle B, Kukavica-Ibrulj I, Ouellet MM, Aaron SD, Charette SJ, Fothergill JL, Tucker NP, Winstanley C, Levesque RC. 2014. Comparative genomics of isolates of a Pseudomonas aeruginosa epidemic strain associated with chronic lung infections of cystic fibrosis patients. PLoS One 9:e87611.

201. Marvig RL, Dolce D, Sommer LM, Petersen B, Ciofu O, Campana S, Molin S, Taccetti G, Johansen HK. 2015. Within-host microevolution of Pseudomonas aeruginosa in Italian cystic fibrosis patients. BMC Microbiol 15:218.

202. Cigana C, Curcurù L, Leone MR, Ieranò T, Lorè NI, Bianconi I, Silipo A, Cozzolino F, Lanzetta R, Molinaro A, Bernardini ML, Bragonzi A. 2009. Pseudomonas aeruginosa exploits lipid A and muropeptides modification as a strategy to lower innate immunity during cystic fibrosis lung infection. PLoS One 4:e8439.

203. Amiel E, Lovewell RR, O'Toole GA, Hogan DA, Berwin B. 2010. Pseudomonas aeruginosa evasion of phagocytosis is mediated by loss of swimming motility and is independent of flagellum expression. Infect Immun 78:2937–2945.

204. Griffin AS, West SA, Buckling A. 2004. Cooperation and competition in pathogenic bacteria. Nature 430:1024–1027.

205. Masini T, Hirsch AKH. 2014. Development of inhibitors of the 2C-methyl-D-erythritol 4-phosphate (MEP) pathway enzymes as potential anti-infective agents. J Med Chem 57:9740–9763.

206. Knak T, Abdullaziz MA, Höfmann S, Alves Avelar LA, Klein S, Martin M, Fischer M, Tanaka N, Kurz T. 2022. Over 40 years of fosmidomycin drug research: A comprehensive review and future opportunities. Pharm Basel 15:1553.

207. Diamanti E, Hamed MM, Lacour A, Bravo P, Illarionov B, Fischer M, Rottmann M, Witschel M, Hirsch AKH. 2022. Targeting the IspD enzyme in the MEP pathway: Identification of a novel fragment class. ChemMedChem 17:e202100679.

208. Ghavami M, Merino EF, Yao Z-K, Elahi R, Simpson ME, Fernández-Murga ML, Butler JH, Casasanta MA, Krai PM, Totrov MM, Slade DJ, Carlier PR, Cassera MB. 2018. Biological studies and target engagement of the 2- C-methyl-d-erythritol 4-phosphate cytidylyltransferase (IspD)-targeting antimalarial agent (1 R,3 S)-MMV008138 and analogs. ACS Infect Dis 4:549–559.

209. Chen X, Zhao H, Wang C, Hamed M, Shang Q, Yang Y, Diao X, Sun X, Hu W, Jiang X, Zhang Y, Hirsch AKH, Wu D, Zhuang J. 2024. Two natural compounds as potential inhibitors against the Helicobacter pylori and Acinetobacter baumannii IspD enzymes. Int J Antimicrob Agents 63:107160.

210. Haymond A, Dowdy T, Johny C, Johnson C, Ball H, Dailey A, Schweibenz B, Villarroel K, Young R, Mantooth CJ, Patel T, Bases J, Dowd CS, Couch RD. 2018. A high-throughput screening campaign to identify inhibitors of DXP reductoisomerase (IspC) and MEP cytidylyltransferase (IspD). Anal Biochem 542:63–75.

211. Cornforth DM, Dees JL, Ibberson CB, Huse HK, Mathiesen IH, Kirketerp-Møller K, Wolcott RD, Rumbaugh KP, Bjarnsholt T, Whiteley M. 2018. Pseudomonas aeruginosa transcriptome during human infection. Proc Natl Acad Sci U A 115:E5125–E5134.

212. Jensen PA, Zhu Z, van Opijnen T. 2017. Antibiotics disrupt coordination between transcriptional and phenotypic stress responses in pathogenic bacteria. Cell Rep 20:1705–1716.

213. Fernández-Piñar R, Lo Sciuto A, Rossi A, Ranucci S, Bragonzi A, Imperi F. 2015. In vitro and in vivo screening for novel essential cell-envelope proteins in Pseudomonas aeruginosa. Sci Rep 5:17593.

214. Kikuchi S, Shibuya I, Matsumoto K. 2000. Viability of an Escherichia coli pgsA null mutant lacking detectable phosphatidylglycerol and cardiolipin. J Bacteriol 182:371–376.

215. Heuston S, Begley M, Gahan CGM, Hill C. 2012. Isoprenoid biosynthesis in bacterial pathogens. Microbiology 158:1389–1401.

216. Eberl M, Roberts GW, Meuter S, Williams JD, Topley N, Moser B. 2009. A rapid crosstalk of human gammadelta T cells and monocytes drives the acute inflammation in bacterial infections. PLoS Pathog 5:e1000308.

217. Fox DT, Poulter CD. 2002. Synthesis of (E)-4-hydroxydimethylallyl diphosphate. An intermediate in the methyl erythritol phosphate branch of the isoprenoid pathway. J Org Chem 67:5009–5010.

218. Ramachandran V, Singh R, Yang X, Tunduguru R, Mohapatra S, Khandelwal S, Patel S, Datta S. 2013. Genetic and chemical knockdown: a complementary strategy for evaluating an anti-infective target. Adv Appl Bioinform Chem 6:1–13.

219. Benghezal M, Adam E, Lucas A, Burn C, Orchard MG, Deuschel C, Valentino E, Braillard S, Paccaud J-P, Cosson P. 2007. Inhibitors of bacterial virulence identified in a surrogate host model. Cell Microbiol 9:1336–1342.

220. Meletis G. 2016. Carbapenem resistance: overview of the problem and future perspectives. Ther Adv Infect Dis 3:15–21.

221. Jacobs LMC, Consol P, Chen Y. 2024. Drug Discovery in the Field of β-Lactams: An Academic Perspective. Antibiotics 13:59.

222. Lai GC, Cho H, Bernhardt TG. 2017. The mecillinam resistome reveals a role for peptidoglycan endopeptidases in stimulating cell wall synthesis in Escherichia coli. PLOS Genet 13:e1006934.

223. Camps M, Herman A, Loh E, Loeb LA. 2007. Genetic Constraints on Protein Evolution. Crit Rev Biochem Mol Biol 42:10.1080/10409230701597642.

224. Rajer F, Sandegren L. 2022. The Role of Antibiotic Resistance Genes in the Fitness Cost of Multiresistance Plasmids. mBio 13:e0355221.

225. Olson MV. 1999. When less is more: gene loss as an engine of evolutionary change. Am J Hum Genet 64:18–23.

226. Albalat R, Cañestro C. 2016. Evolution by gene loss. Nat Rev Genet 17:379–391.

227. Bosshard L, Dupanloup I, Tenaillon O, Bruggmann R, Ackermann M, Peischl S, Excoffier L. 2017. Accumulation of Deleterious Mutations During Bacterial Range Expansions. Genetics 207:669–684.

228. Xu Y-C, Guo Y-L. 2020. Less Is More, Natural Loss-of-Function Mutation Is a Strategy for Adaptation. Plant Commun 1:100103.

229. Billmyre RB, Clancey SA, Heitman J. 2017. Natural mismatch repair mutations mediate phenotypic diversity and drug resistance in Cryptococcus deuterogattii. eLife 6:e28802.

230. Tenaillon O, Barrick JE, Ribeck N, Deatherage DE, Blanchard JL, Dasgupta A, Wu GC, Wielgoss S, Cruveiller S, Médigue C, Schneider D, Lenski RE. 2016. Tempo and mode of genome evolution in a 50,000-generation experiment. Nature 536:165–170.

231. Banta AB, Enright AL, Siletti C, Peters JM. 2020. A High-Efficacy CRISPR Interference System for Gene Function Discovery in Zymomonas mobilis. Appl Environ Microbiol 86:e01621-20.

232. Goodall ECA, Robinson A, Johnston IG, Jabbari S, Turner KA, Cunningham AF, Lund PA, Cole JA, Henderson IR. 2018. The Essential Genome of Escherichia coli K-12. mBio 9.

233. Gerding MA, Ogata Y, Pecora ND, Niki H, de Boer PAJ. 2007. The trans-envelope Tol–Pal complex is part of the cell division machinery and required for proper outer-membrane invagination during cell constriction in E. coli. Mol Microbiol 63:1008–1025.

234. Keller KL, Brinkman KK, Larsen RA. 2007. TonB/TolA amino-terminal domain modeling. Methods Enzymol 423:134–148.

235. Schmidt KL, Peterson ND, Kustusch RJ, Wissel MC, Graham B, Phillips GJ, Weiss DS. 2004. A Predicted ABC Transporter, FtsEX, Is Needed for Cell Division in Escherichia coli. J Bacteriol 186:785–793.

236. Britton BM, Yovanno RA, Costa SF, McCausland J, Lau AY, Xiao J, Hensel Z. 2023. Conformational changes in the essential E. coli septal cell wall synthesis complex suggest an activation mechanism. Nat Commun 14:4585.

237. Lobritz MA, Belenky P, Porter CBM, Gutierrez A, Yang JH, Schwarz EG, Dwyer DJ, Khalil AS, Collins JJ. 2015. Antibiotic efficacy is linked to bacterial cellular respiration. Proc Natl Acad Sci 112:8173–8180.

238. Holmqvist E, Li L, Bischler T, Barquist L, Vogel J. 2018. Global Maps of ProQ Binding In Vivo Reveal Target Recognition via RNA Structure and Stability Control at mRNA 3’ Ends. Mol Cell 70:971-982.e6.

239. Lloubès R, Cascales E, Walburger A, Bouveret E, Lazdunski C, Bernadac A, Journet L. 2001. The Tol-Pal proteins of the *Escherichia coli* cell envelope: an energized system required for outer membrane integrity? Res Microbiol 152:523–529.

240. Park S, Cho H. 2022. The Tol-Pal System Plays an Important Role in Maintaining Cell Integrity During Elongation in Escherichia coli. Front Microbiol 13:891926.

241. Belenky P, Ye JD, Porter CBM, Cohen NR, Lobritz MA, Ferrante T, Jain S, Korry BJ, Schwarz EG, Walker GC, Collins JJ. 2015. Bactericidal Antibiotics Induce Toxic Metabolic Perturbations that Lead to Cellular Damage. Cell Rep 13:968–980.

242. Langmead B. 2010. Aligning short sequencing reads with Bowtie. Curr Protoc Bioinforma Ed Board Andreas Baxevanis Al CHAPTER:Unit-11.7.

243. Gilchrist CLM, Chooi Y-H. 2021. clinker & clustermap.js: automatic generation of gene cluster comparison figures. Bioinformatics 37:2473–2475.